Copy 537

~~CONFIDENTIAL~~ NASA TM X-820

NASA TM X-820

GPO PRICE $ ________

OTS PRICE(S) $ ________

Hard copy (HC) ________

Microfiche (MF) ________

~~GROUP 4 Downgraded at 3 year intervals; declassified after 12 years~~

TECHNICAL MEMORANDUM

X-820

INVESTIGATION OF THE AERODYNAMIC CHARACTERISTICS OF A 0.02-SCALE MODEL OF THE X-15 AIRPLANE AT MACH NUMBERS OF 2.96, 3.96, AND 4.65 AT HIGH ANGLES OF ATTACK

By Royce L. McKinney and Julia A. Lancaster

Langley Research Center
Langley Station, Hampton, Va.

NATIONAL AERONAUTICS AND SPACE ADMINISTRATION

WASHINGTON June 1963

~~CONFIDENTIAL~~

[redacted]

NATIONAL AERONAUTICS AND SPACE ADMINISTRATION

TECHNICAL MEMORANDUM X-820

INVESTIGATION OF THE AERODYNAMIC CHARACTERISTICS OF A 0.02-SCALE MODEL OF THE X-15 AIRPLANE AT MACH NUMBERS OF 2.96, 3.96, AND 4.65 AT HIGH ANGLES OF ATTACK*

By Royce L. McKinney and Julia A. Lancaster

SUMMARY

23925

An investigation has been made in the Langley Unitary Plan wind tunnel to determine the longitudinal and lateral aerodynamic characteristics of a 0.02-scale model of the X-15 airplane at angles of attack from -5° to 45°. The investigation was made at Mach numbers of 2.96, 3.96, and 4.65 at Reynolds numbers, based on the wing mean geometric chord, of 0.55×10^6, 0.60×10^6, and 0.84×10^6, respectively. Results are presented and summarized with only a limited analysis.

INTRODUCTION

The scheduled flight program of the X-15 research aircraft includes high-speed flights at approximately constant altitude and also flights along ballistic trajectories to high altitudes. In order to avoid the high dynamic pressures and associated high aerodynamic heating rates, it was contemplated that the high-speed flights and recovery from ballistic trajectories would be made at extremely high altitudes. The lift coefficients and lift-drag ratios necessary for the lower altitude maneuvers are obtainable at angles of attack less than 25°, and the aerodynamic characteristics of the X-15 at angles of attack below 25° are presented in reference 1. The purpose of the present investigation was to determine the aerodynamic characteristics of the X-15 at angles of attack beyond 25° with particular emphasis on the lateral and directional stability derivatives and the maximum trimmed angles of attack. The range of this investigation was extended below an angle of attack of 25° in order to provide a comparison with previous results. The present configuration is identical to that of reference 1 with the exception of the addition of retracted landing skids on the bottom of the side fairings between the horizontal stabilizers and the fuselage. The data are presented with only a limited analysis inasmuch as the data contained in this report have been used in analyses such as the one presented in reference 2.

---

*Title, Unclassified.

[redacted]

[redacted]

SYMBOLS

The longitudinal stability characteristics of the model are referred to the stability system of axes, and the lateral stability characteristics are referred to the body system of axes. The systems of axes used and the positive directions of the forces, moments, and angles are shown in figure 1. The forces and moments are presented about a point located on the plane of symmetry at 0.20 mean geometric chord. The symbols used are defined as follows:

b	span
$\bar{c}$	mean geometric chord
C_D'	drag coefficient, Drag/qS
C_L	lift coefficient, Lift/qS
C_m	pitching-moment coefficient, Pitching moment/$qS\bar{c}$
C_{m_O}	zero-lift pitching-moment coefficient
C_l	rolling-moment coefficient, Rolling moment/qSb
C_n	yawing-moment coefficient, Yawing moment/qSb
C_Y	side-force coefficient, Side force/qS
C_{l_β}	effective dihedral parameter, $\partial C_l/\partial\beta$
C_{n_β}	directional stability parameter, $\partial C_n/\partial\beta$
C_{Y_β}	side-force parameter, $\partial C_Y/\partial\beta$
M	free-stream Mach number
q	free-stream dynamic pressure
S	wing area
α	angle of attack referred to fuselage reference line, deg
β	angle of sideslip referred to model plane of symmetry, deg
δ_V	deflection of movable portions of vertical stabilizer

[redacted]

[redacted]

δ_{V_U} deflection of movable portion of upper vertical stabilizer, positive with trailing edge left, deg

δ_{V_J} deflection of movable jettisonable portion of lower vertical stabilizer, positive with trailing edge left, deg

δ_H deflection of horizontal stabilizers

$\delta_{H_L}, \delta_{H_R}$ deflection of left and right horizontal stabilizers, respectively, positive with trailing edge down, deg

δ_S deflection of speed brakes

δ_{S_U} deflection of both upper speed brakes, positive with trailing edge outboard, deg

δ_{S_B} deflection of both lower speed brakes, positive with trailing edge outboard, deg

δ_{S_R} deflection of speed brakes on right side of upper and lower vertical stabilizers, left speed brakes closed, positive with trailing edge right, deg

Configuration component designations:

W wing

F fuselage

H horizontal stabilizers

V vertical stabilizers without jettisonable portion

J jettisonable portion of lower vertical stabilizer

APPARATUS AND MODEL

Tunnel

The investigation was conducted in the high Mach number test section of the Langley Unitary Plan wind tunnel, which is a variable-pressure continuous-flow tunnel. The nozzle leading to the test section is of the asymmetric sliding-block type which permits continuous variation of test-section Mach number from 2.30 to 4.65.

[redacted]

[redacted]

Model

Photographs of the model are presented in figure 2. Model details and geometry are presented in table I and figure 3. The model has a wing with a 25.64° sweepback of the quarter-chord line, an aspect ratio of 2.50°, a taper ratio of 0.20°, a dihedral of 0°, and a modified NACA 66-005 airfoil section. Roll and pitch control are provided by differential and/or simultaneous deflection of the all-moving horizontal stabilizers. Directional control is obtained from deflection of the movable portions of the upper and lower vertical stabilizers. The horizontal stabilizer has a 45.00° sweepback of the quarter-chord line, an aspect ratio of 2.834, a taper ratio of 0.2061, a dihedral of -15.000°, and a modified NACA 66-005 airfoil section. The upper portion of the vertical stabilizer shown in figure 3(b) has a sweepback of 23.413° at the quarter-chord line, an aspect ratio of 0.5158, a taper ratio of 0.741, and a 10° wedge airfoil section. The lower portion of the vertical stabilizer, shown in figure 3(b), has a sweepback of 23.413° at the quarter-chord line, an aspect ratio of 0.429, a taper ratio of 0.788, and a 10° wedge airfoil section.

The speed brakes are formed by wedges which simulate hinged panels of the surface of the upper and lower vertical stabilizers. The speed brakes extend vertically over the complete width of the fixed portions of the vertical stabilizers and cover approximately one-third of the horizontal length forward from the trailing edges. Wedges simulating the speed brakes open 25° and 35° were used.

Forces and moments were measured by an internal, six-component, strain-gage balance. This balance was supported by a sting attached to a special angle-of-attack sector which provided an angle-of-attack range of -5° to 50°. This sector was supported by the main support system which allowed sideslip concurrently with variable angle of attack.

TESTS

Tests were made through an angle-of-attack range from approximately -5° to 45° at angles of sideslip of -5° and 0°. Sideslip tests were made at angles of attack of about 21° to 38° through a sideslip range from approximately -10° to 4°.

Reynolds numbers, based on the mean geometric chord of the wing, were 0.55×10^6, 0.60×10^6, and 0.84×10^6 at the test Mach numbers of 2.96, 3.96, and 4.65, respectively. The dewpoint temperature, measured at stagnation pressure, was maintained below -30° F in order to assure negligible condensation effects.

CORRECTIONS AND ACCURACY

Angles of attack and sideslip have been corrected for the deflection of the model support system caused by aerodynamic forces and moments. Angle of attack

[redacted]

has also been corrected for the flow angularity which exists in the vertical plane of the test section. This flow angularity was determined by testing the model both upright and inverted.

Balance chamber pressure and base pressure were measured and the drag data were corrected to correspond to a chamber and base pressure equal to free-stream static pressure.

The maximum deviation of local Mach number from the value presented is about ±0.015.

Based on pretest calibration, balance accuracies, and repeatability, the force and moment coefficients and angles are estimated to be within the following limits:

C_L	±0.03
C_D'	±0.02
C_m	±0.02
C_l	±0.001
C_n	±0.003
C_Y	±0.01
α, deg	±0.10
β, deg	±0.10

PRESENTATION OF RESULTS

The results of the investigation are presented in the following figures:

[redacted]

SUMMARY OF RESULTS

Longitudinal Characteristics

All the configurations tested indicated static longitudinal stability for trimmed conditions over the entire Mach number range. However, most of the pitch data at Mach numbers of 3.96 and 4.65 exhibit marked nonlinearities at low angles of attack. (For example, see fig. 6(b).) This effect, as noted in reference 3, is probably the result of wing-wake impingement on the horizontal stabilizers. The basic configuration can be trimmed to a maximum angle of attack of about 33° with a pitch-control deflection of -45°. (See fig. 20.) Speed-brake deflection causes a negative trim change and a reduction in the maximum attainable α_{trim}. (See fig. 15(c), for example.) Use of the horizontal tail for lateral control also causes a longitudinal trim change (fig. 19), since only one surface was deflected from the 35° pitch-control position with which the roll-control configuration is compared.

Lateral and Directional Characteristics

Positive roll-control effectiveness is exhibited at all Mach numbers throughout the angle-of-attack range with the exception that at $\alpha = 0^{\circ}$, the wing-wake impingement on the horizontal tail reduces roll-control effectiveness to zero at the two higher test Mach numbers. (See fig. 28.) Favorable yawing moment due to roll control is exhibited at all Mach numbers and angles of attack. (See fig. 28.) Positive directional control is available throughout the angle-of-attack and Mach number ranges either from deflection of both the upper and lower vertical tails or from asymmetric deflection of the speed brakes (fig. 29).

The data presented in figures 30 to 34 were calculated from tests made at $\beta = 0^{\circ}$ and $\beta = -5^{\circ}$. The configurations with the jettisonable portion of the lower vertical tail removed indicate a generally progressive decrease in $C_{n_{\beta}}$ with increasing angle of attack (fig. 32). With the addition of the lower portion of the vertical tail, the directional stability is significantly increased, particularly at the higher angles of attack. However, the addition of the lower vertical tail also provides a large increment in $C_{l_{\beta}}$ which generally changes the effective dihedral from positive to negative. Deflection of the speed brakes increases the effectiveness of the vertical tail and results in a substantial increase in $C_{n_{\beta}}$ except at the higher angles of attack (fig. 30).

Langley Research Center,
National Aeronautics and Space Administration,
Langley Station, Hampton, Va., March 19, 1963.

[redacted]

REFERENCES

1. Franklin, Arthur E., and Lust, Robert M.: Investigation of the Aerodynamic Characteristics of a 0.067-Scale Model of the X-15 Airplane (Configuration 3) at Mach Numbers of 2.29, 2.98, and 4.65. NASA TM X-38, 1959.

2. Petersen, Forrest S., Rediess, Herman A., and Weil, Joseph: Lateral-Directional Control Characteristics of the X-15 Airplane. NASA TM X-726, 1962.

3. Penland, Jim A., and Fetterman, David E., Jr.: Static Longitudinal, Directional, and Lateral Stability and Control Data at a Mach Number of 6.83 of the Final Configuration of the X-15 Research Airplane. NASA TM X-236, 1960.

[redacted]

[redacted]

TABLE I.- GEOMETRIC CHARACTERISTICS OF MODEL

Wing:	
Area, total, sq in.	11.520
Area, exposed, sq in.	6.050
Span, in.	5.366
Aspect ratio	2.500
Root chord, fuselage center line, in.	3.578
Root chord, exposed, in.	2.64
Tip chord, in.	0.716
Mean geometric chord, in.	2.465
Sweepback angles, deg:	
Leading edge	36.75
25-percent-chord line	25.64
Trailing edge	17.74
Taper ratio	0.200
Dihedral angle, deg	0
Incidence angle, deg	0
Airfoil section, parallel to fuselage center line	Modified NACA 66-005
Leading-edge radius, in.:	
Tip	0.008
Fuselage-line chord	0.014
Horizontal tail:	
Area, exposed, sq in.	2.878
Semispan (panel span), in.	1.330
Aspect ratio of exposed area	1.229
Taper ratio of exposed area	0.328
Root chord, exposed, in.	1.658
Tip chord, in.	0.506
Mean geometric chord of exposed area, in.	1.184
Sweepback angles, deg:	
Leading edge	50.58
25-percent-chord line	45.00
Trailing edge	19.28
Dihedral, deg	-15.000
Airfoil section, parallel to fuselage center line	Modified NACA 66-005
Leading-edge radius, in.:	
Tip	0.005
Fuselage-line chord	0.010
Upper vertical tail:	
Area, exposed, sq in.	2.356
Span, in.	1.10
Aspect ratio of exposed area	0.516
Taper ratio of exposed area	0.738
Root chord, fuselage surface line, in.	2.450
Tip chord, in.	1.81
Mean geometric chord of exposed area, in.	2.148
Sweepback angles, deg:	
Leading edge	30.000
25-percent-chord line	23.413
Trailing edge	0
Airfoil section, parallel to fuselage center line	10° full wedge
Leading-edge radius, in.	0.010
Control surface:	
Area, sq in.	1.521
Root chord, in.	2.250
Mean geometric chord, in.	2.039
Lower vertical tail:	
Area, exposed, sq in.	1.982
Span, exposed, in.:	
Maximum	0.920
Minimum	0.880
Average	0.900
Aspect ratio of exposed area	0.427
Taper ratio of exposed area	0.783
Root chord, in.	2.450
Tip chord, in.	1.919
Mean geometric chord of exposed area, in.	2.200
Sweepback angles, deg:	
Leading edge	30.000
25-percent-chord line	23.413
Trailing edge	0
Airfoil section, parallel to fuselage center line	10° full wedge
Leading-edge radius, in.	0.010
Control surface:	
Area, sq in.	1.149
Root chord, in.	2.250
Mean geometric chord, in.	2.093
Fuselage:	
Length, in.	11.76
Maximum diameter, in.	1.12
Maximum width including side fairings, in.	1.76
Fineness ratio, ratio of length to body diameter	10.50
Base diameter, in.	0.960

[redacted]

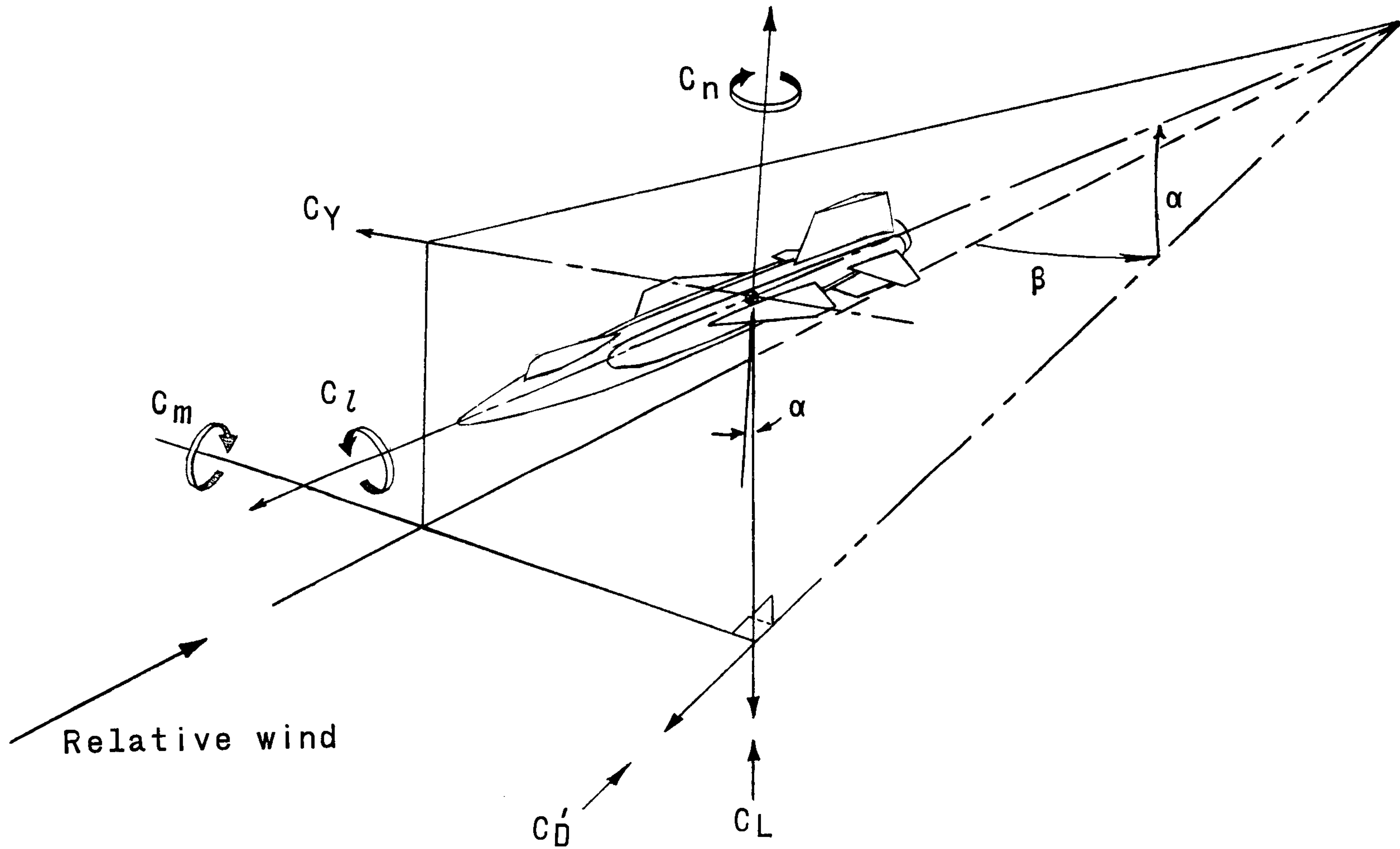

(a) Stability axes.

Figure 1.- Reference axes. Positive directions of forces, moments, and angles are indicated.

[redacted]

[redacted]

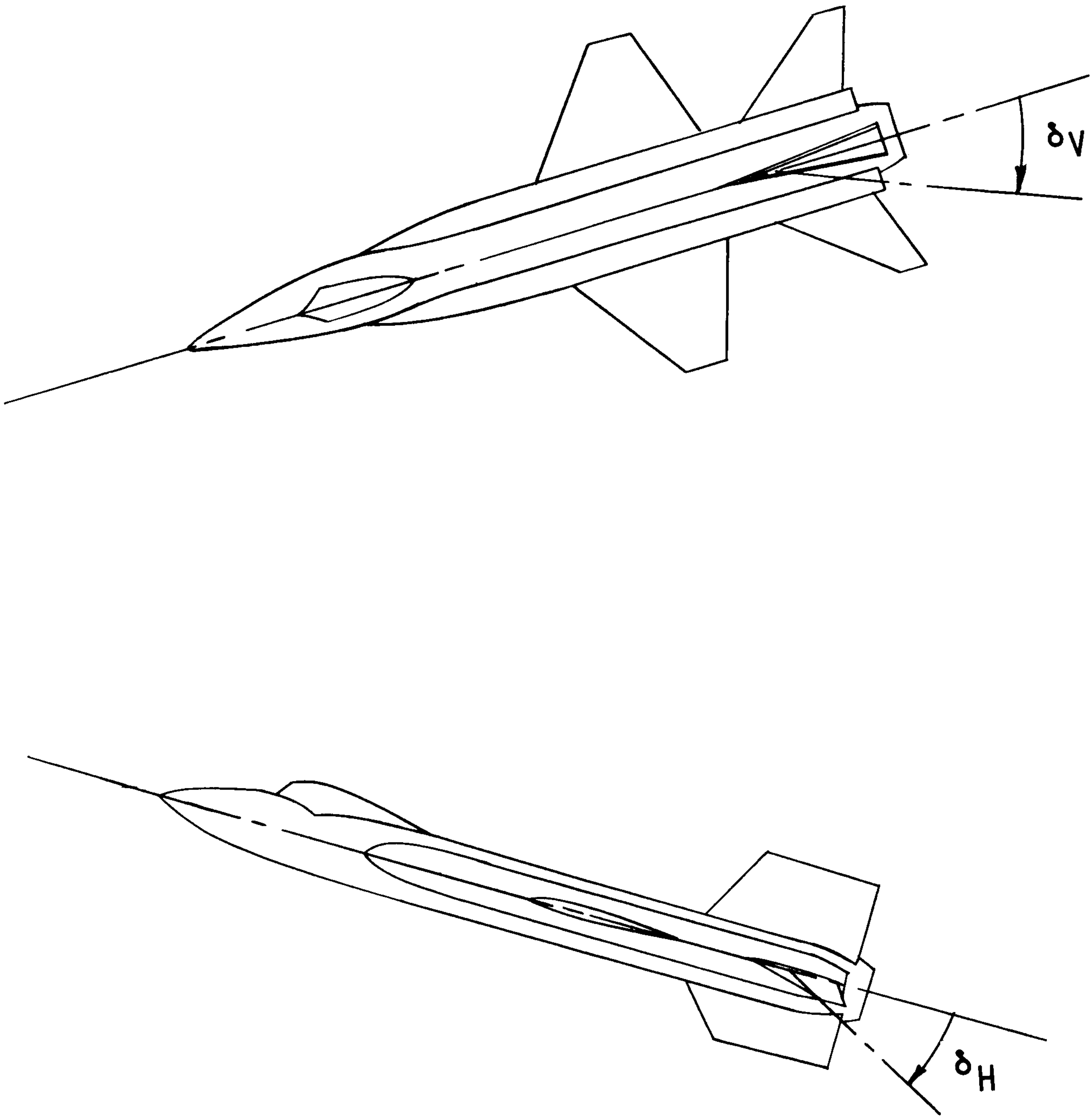

(b) Vertical- and horizontal-stabilizer deflections.

Figure 1.- Concluded.

[redacted]

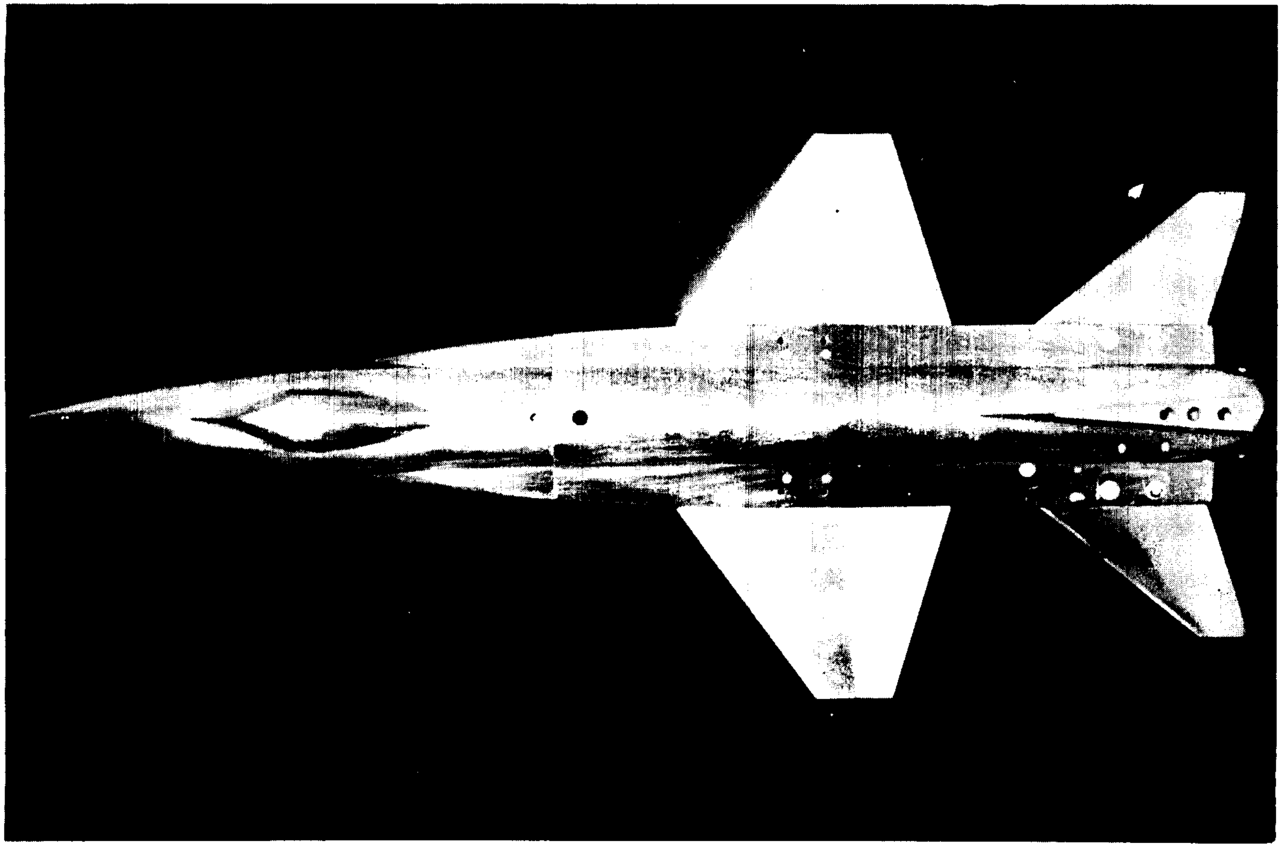

(a) Top view. L-63-84

Figure 2.- Photographs of model.

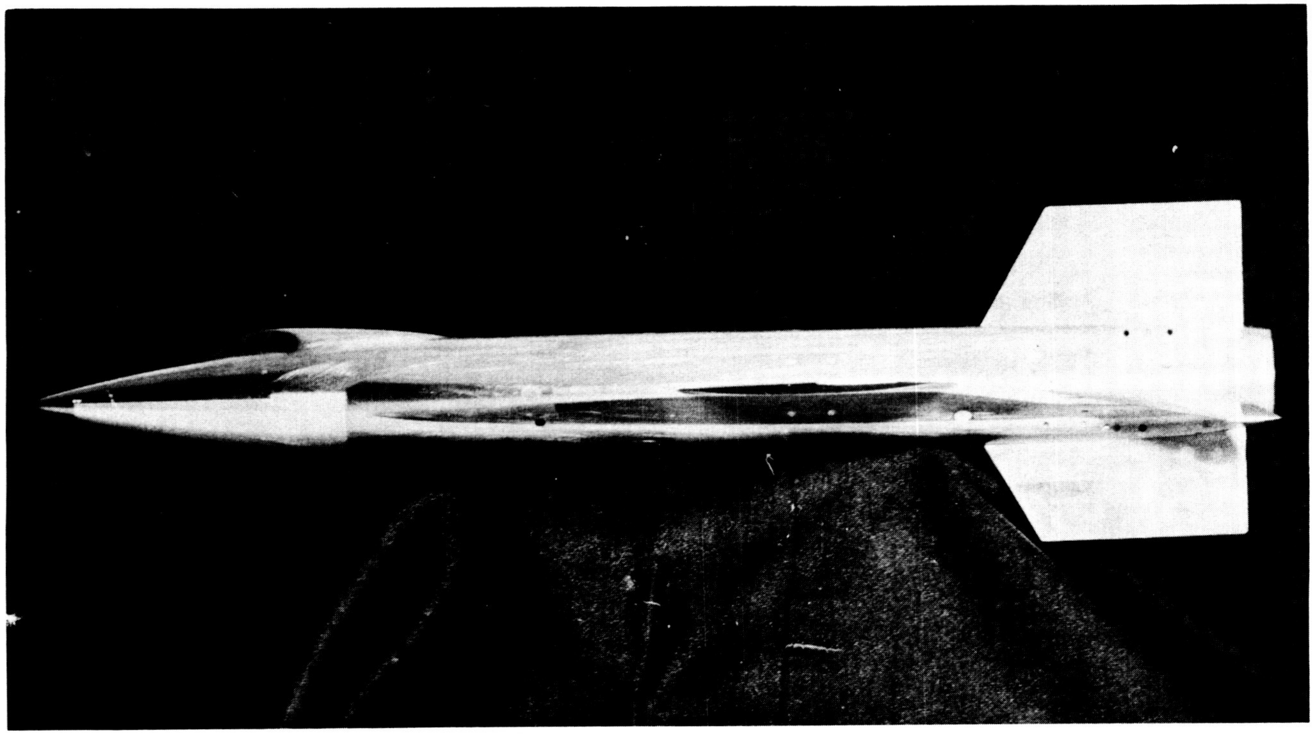

(b) Side view.　　L-63-85

Figure 2.- Continued.

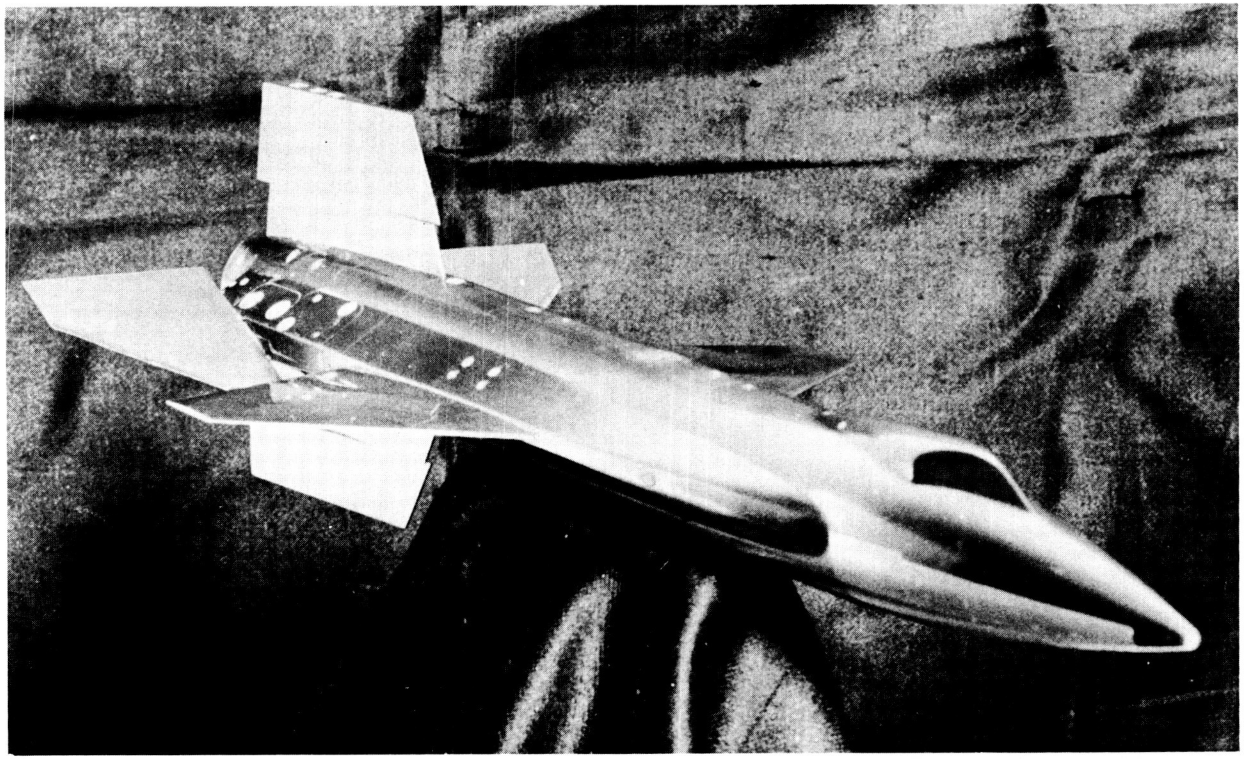

(c) Front quarter view showing deflection of control surfaces. L-63-86

Figure 2.- Continued.

[redacted]

[redacted]

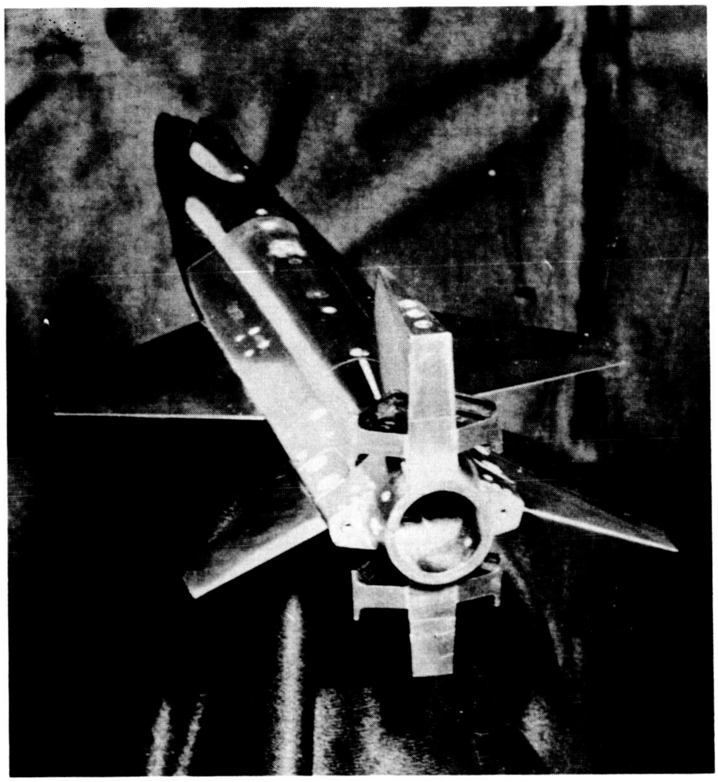

L-63-87

(d) Rear view showing wedges used to simulate speed-brake deflections.

Figure 2.- Concluded.

[redacted]

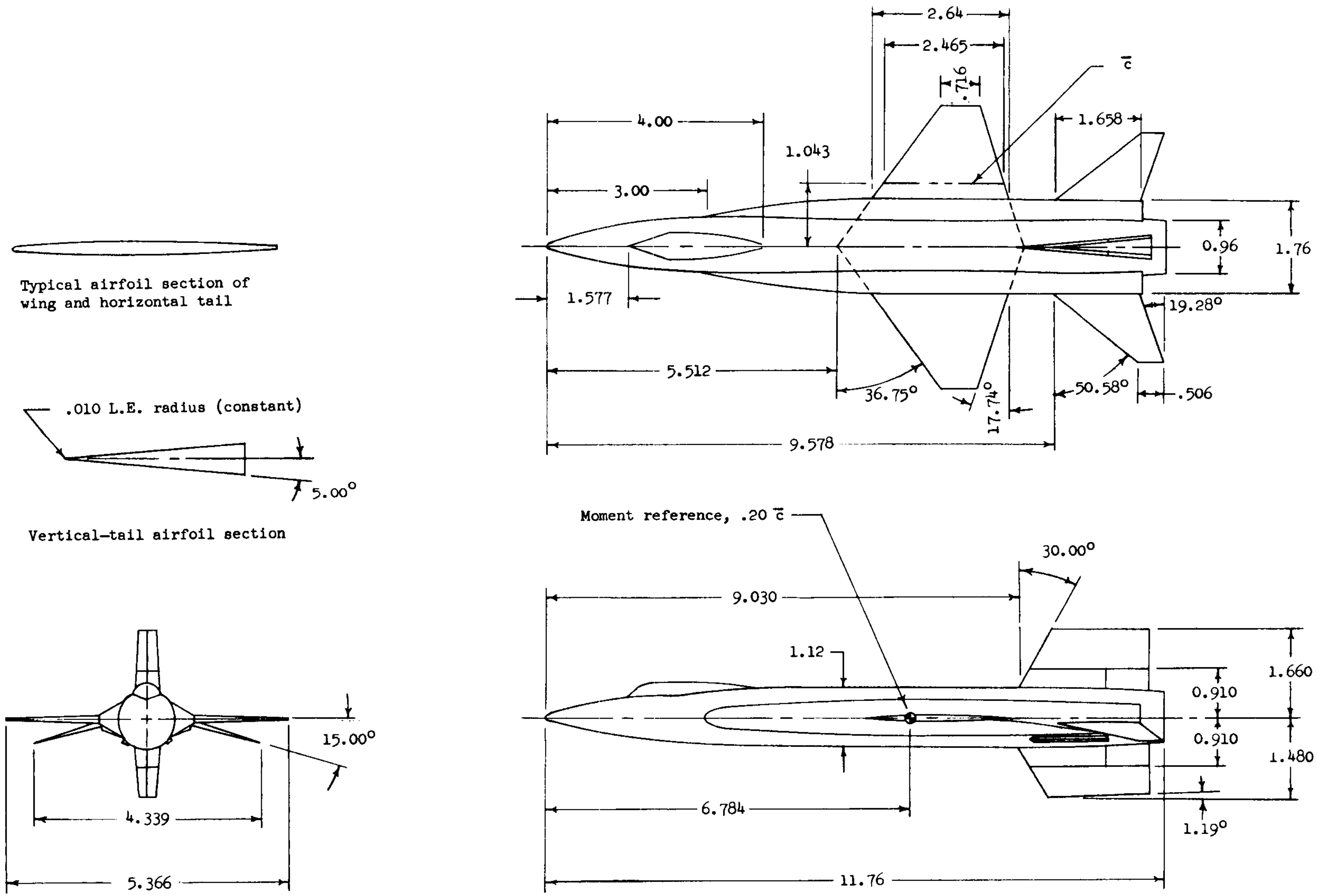

(a) Complete model.

Figure 3.- Details of the force model. All dimensions are in inches unless otherwise noted.

[redacted]

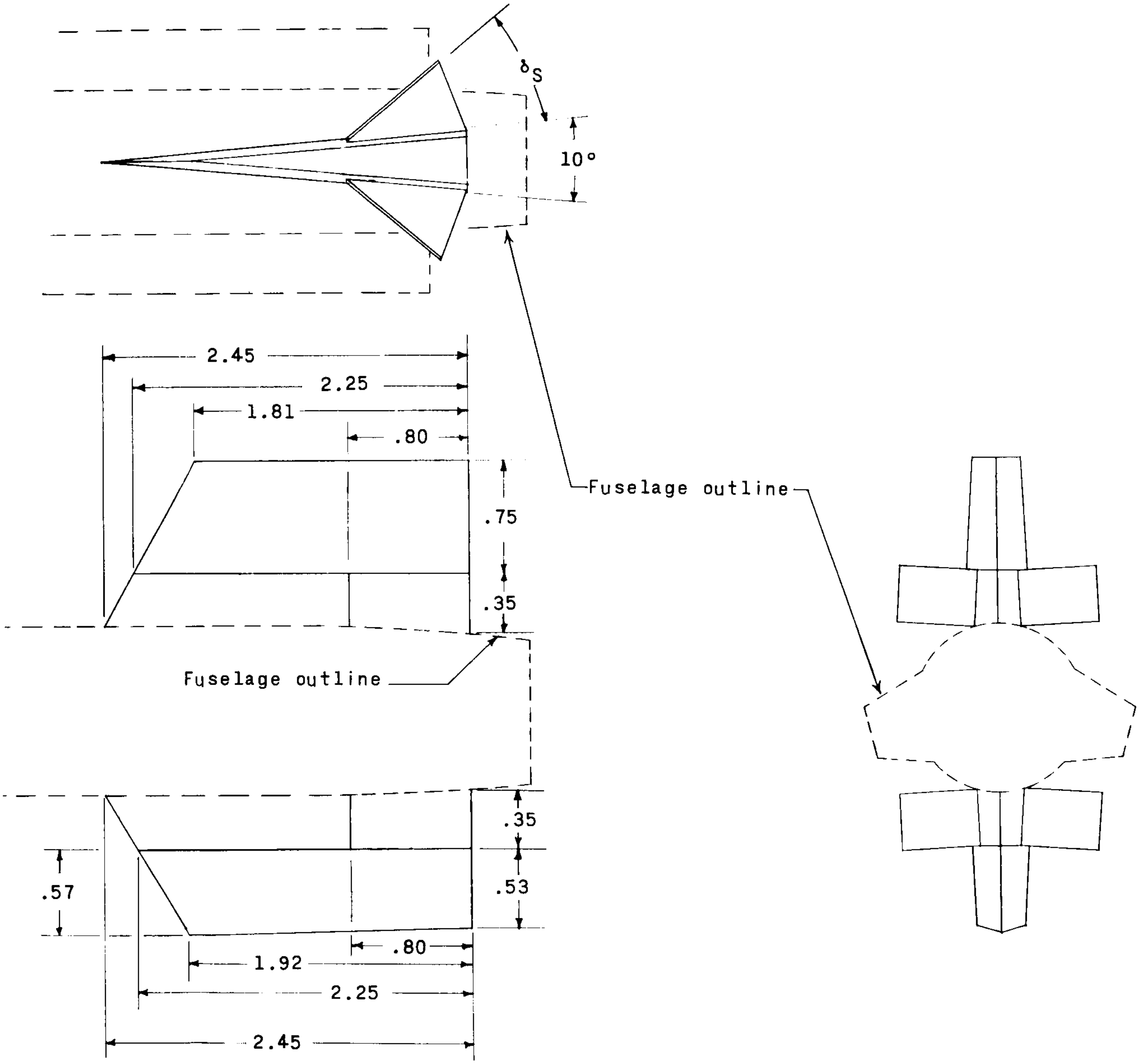

(b) Details of vertical stabilizers and speed brakes.

Figure 3.- Concluded.

[redacted]

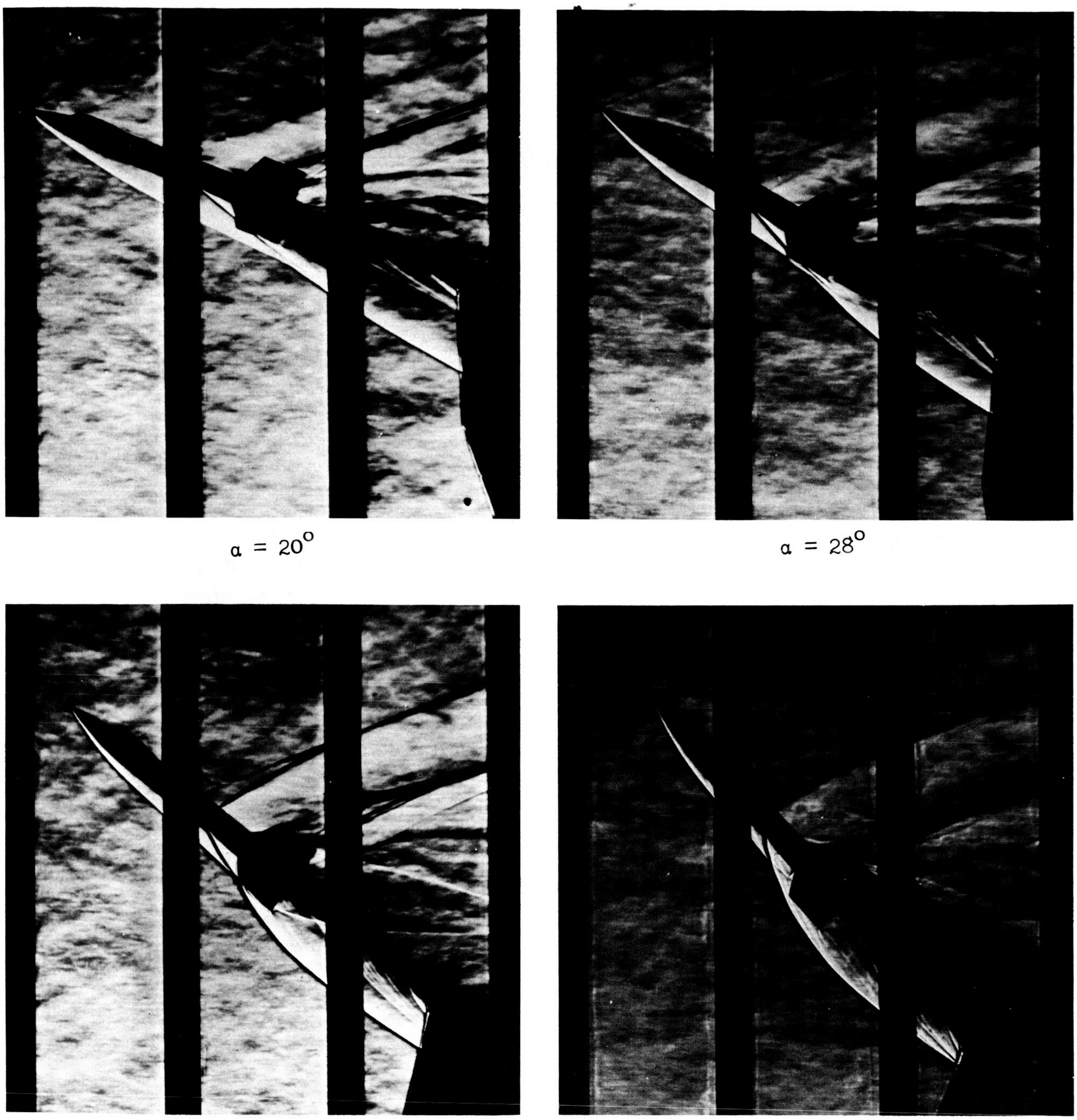

$\alpha = 20^{\circ}$ $\alpha = 28^{\circ}$

$\alpha = 36^{\circ}$ $\alpha = 44^{\circ}$

(a) M = 2.96. L-63-88

Figure 4.- Schlieren photographs of complete model.

[redacted]

[redacted]

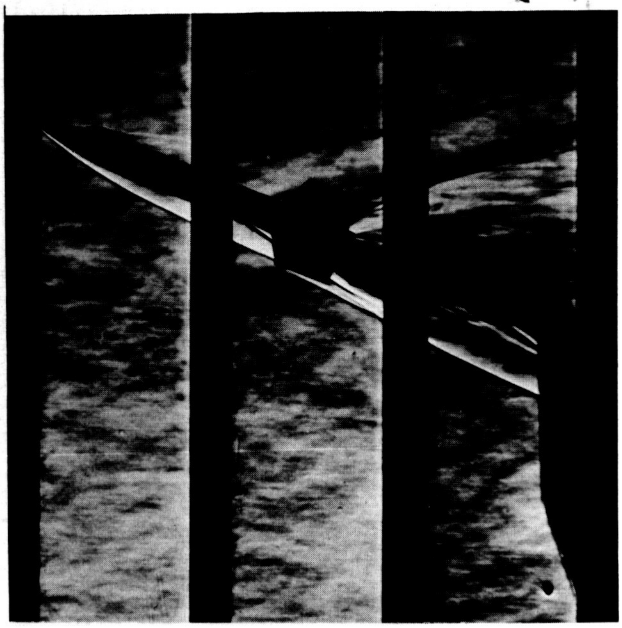

$\alpha = 20^{\circ}$

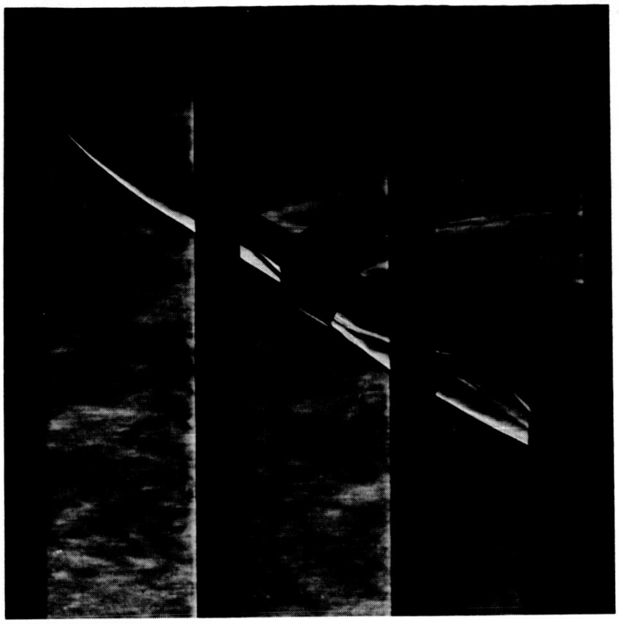

$\alpha = 28^{\circ}$

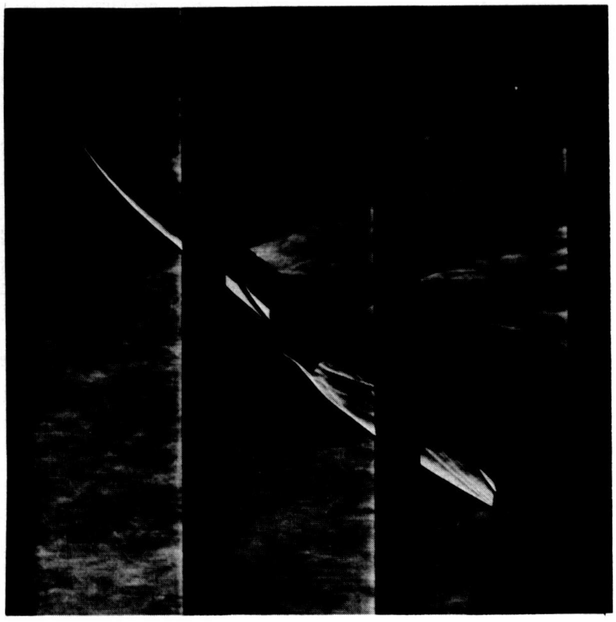

$\alpha = 36^{\circ}$

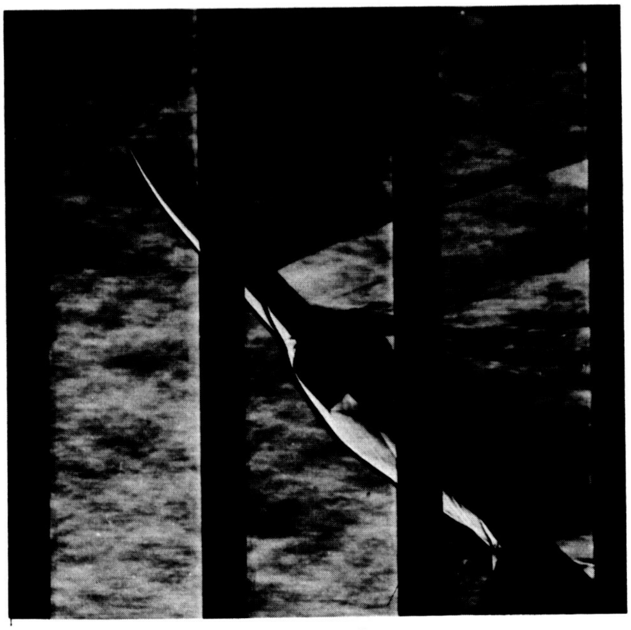

$\alpha = 44^{\circ}$

(b) $M = 3.96$. L-63-89

Figure 4.- Continued.

[redacted]

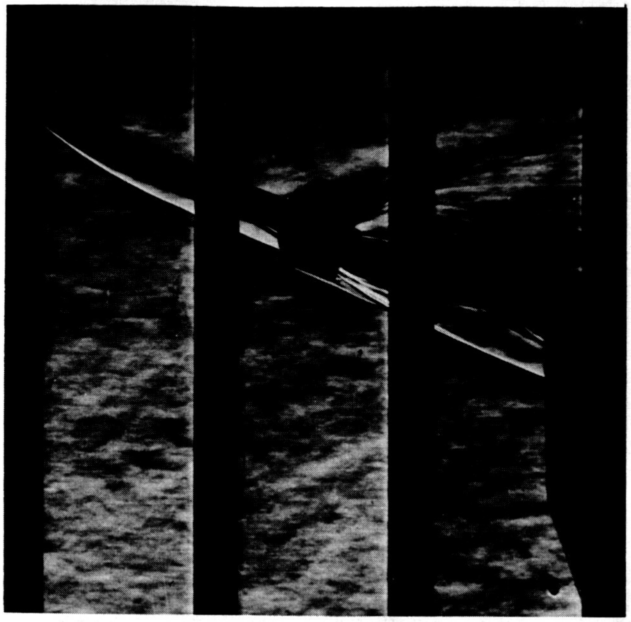

$\alpha = 20^{\circ}$

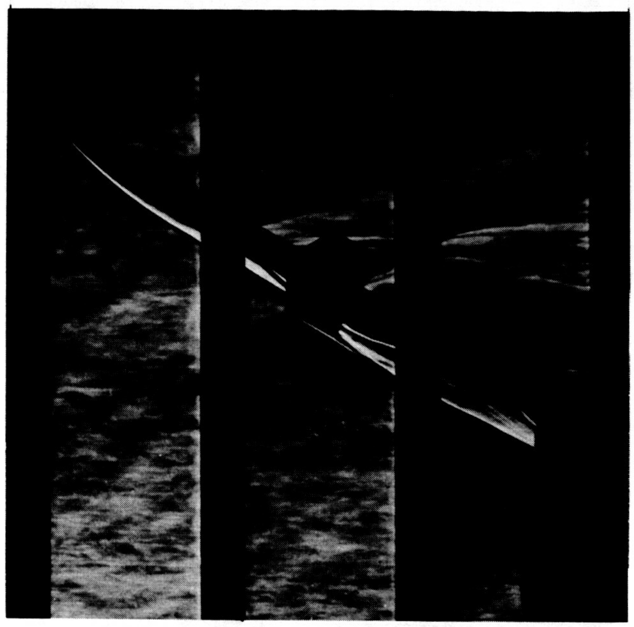

$\alpha = 28^{\circ}$

$\alpha = 36^{\circ}$

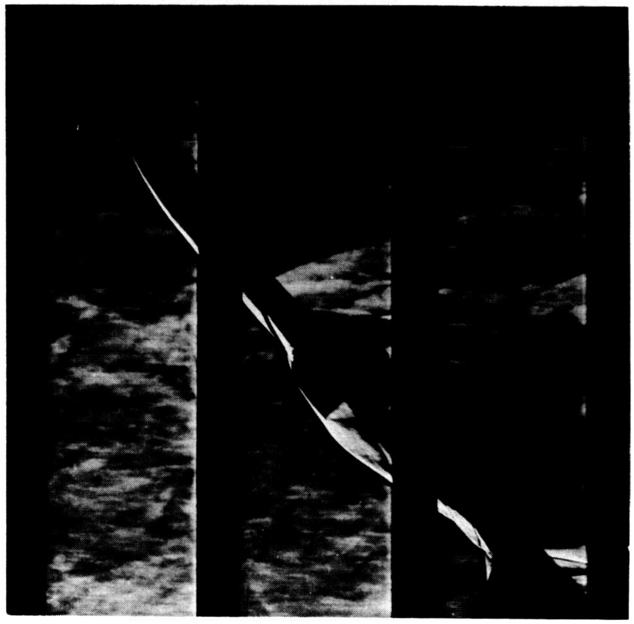

$\alpha = 44^{\circ}$

(c) $M = 4.65$. L-63-90

Figure 4.- Concluded.

[redacted]

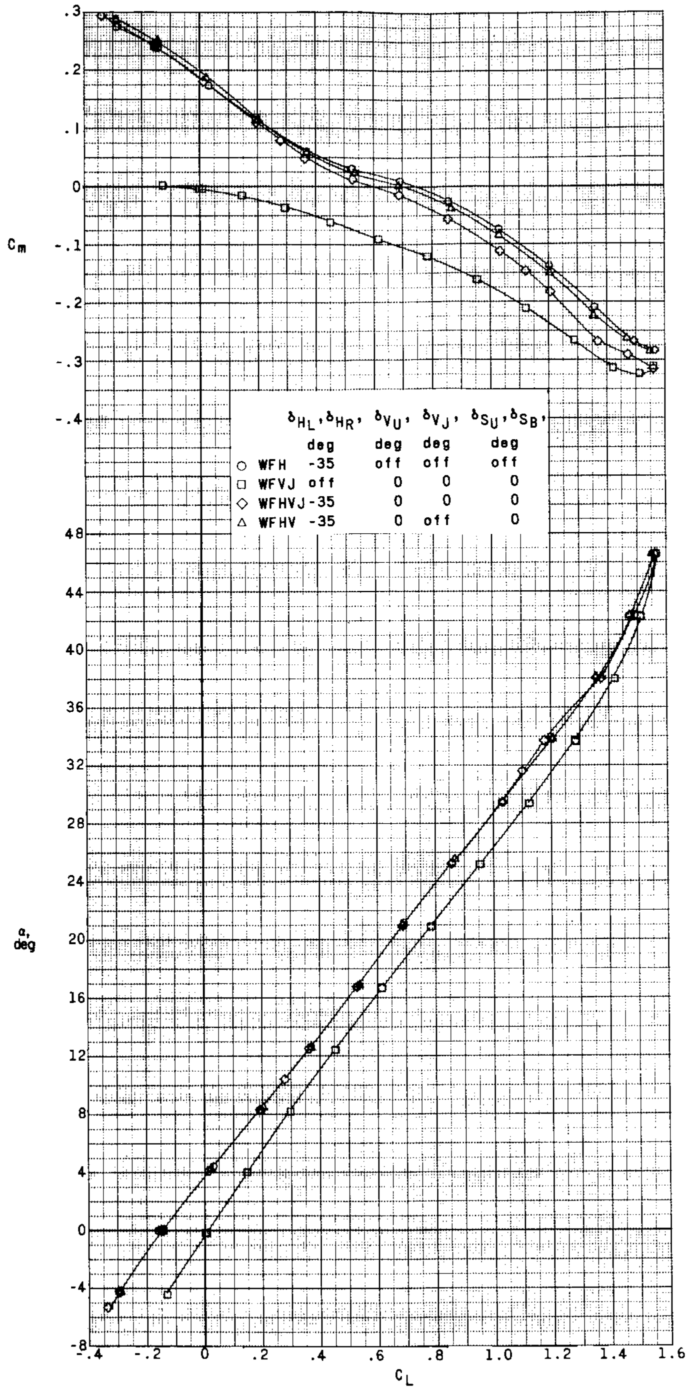

(a) M = 2.96.

Figure 5.- Effect of various configuration components on aerodynamic characteristics in pitch. $\beta = 0^{\circ}$.

[redacted]

DEC[redacted]IED

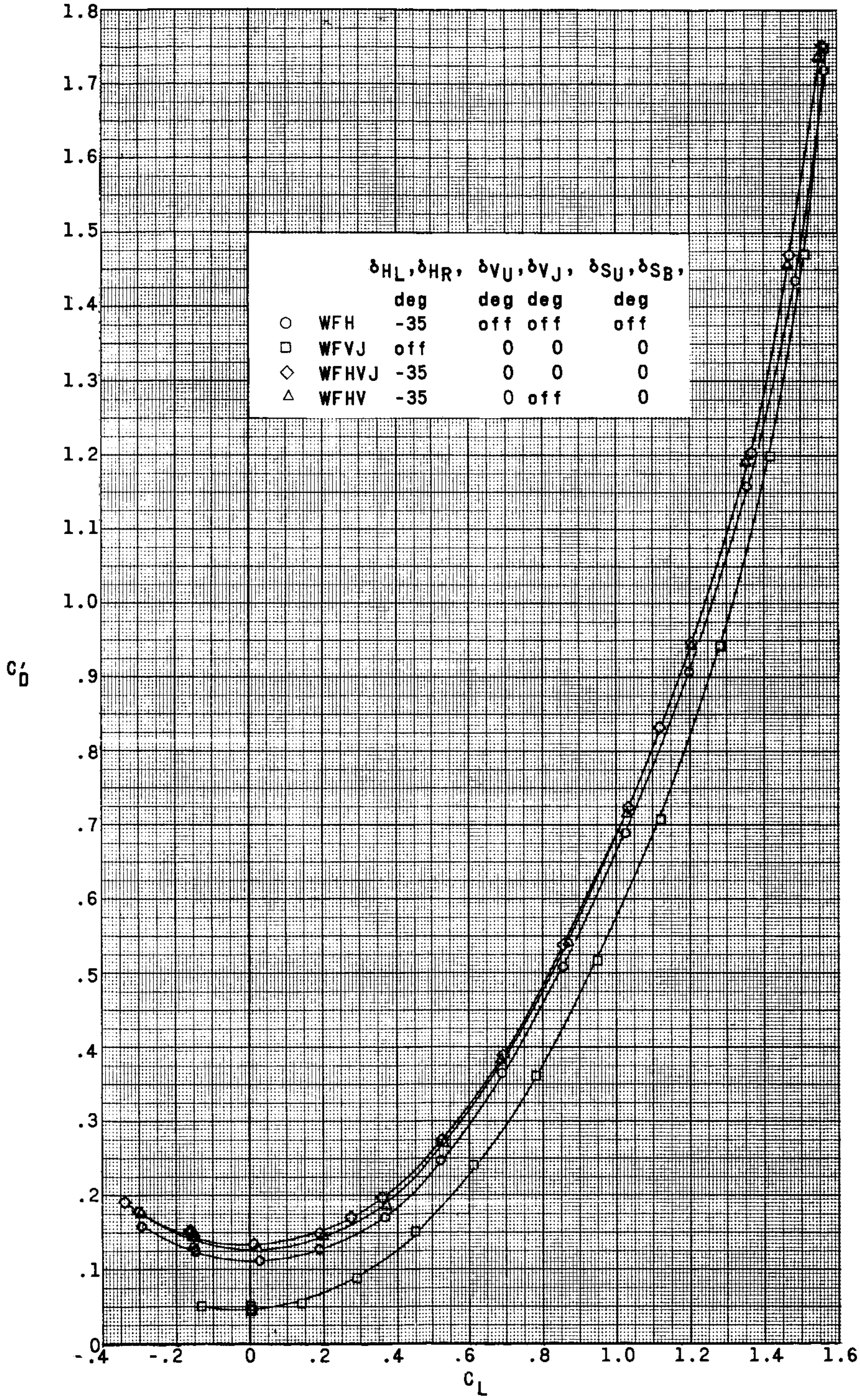

(a) Concluded.

Figure 5.- Continued.

[redacted]

[redacted]

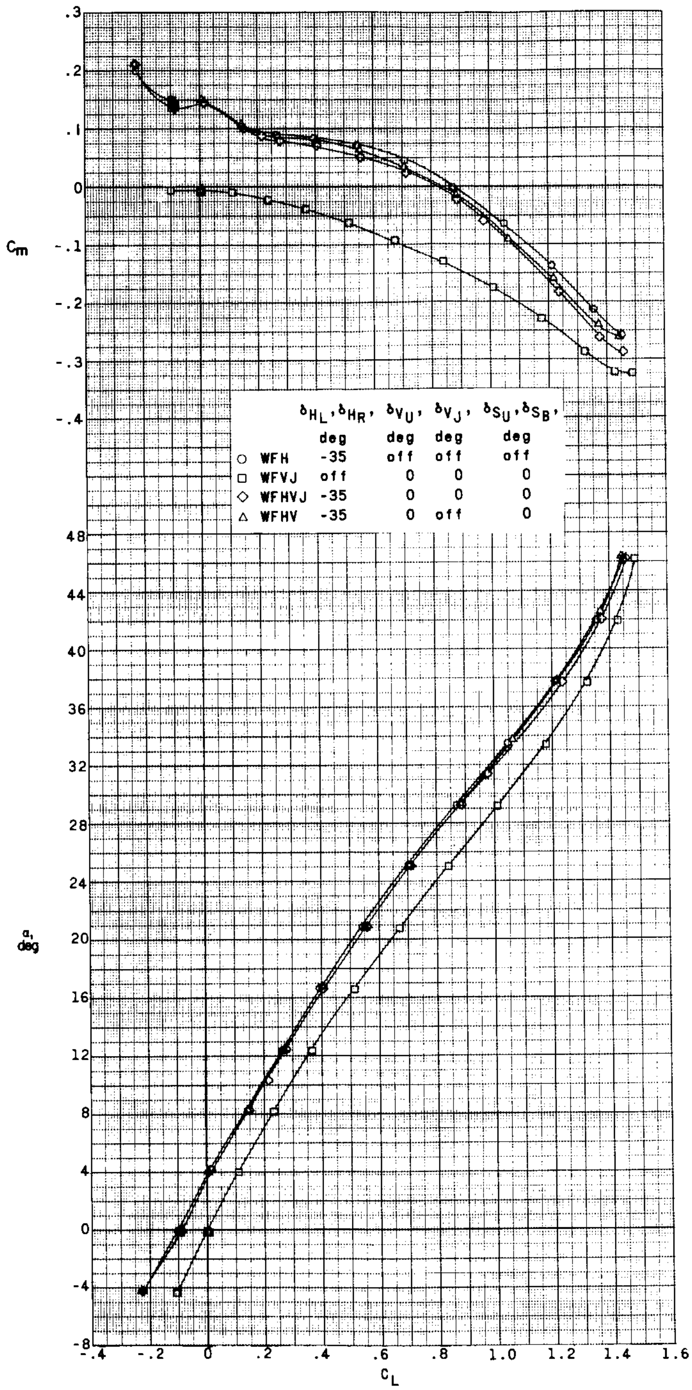

(b) M = 3.96.

Figure 5.- Continued.

[redacted]

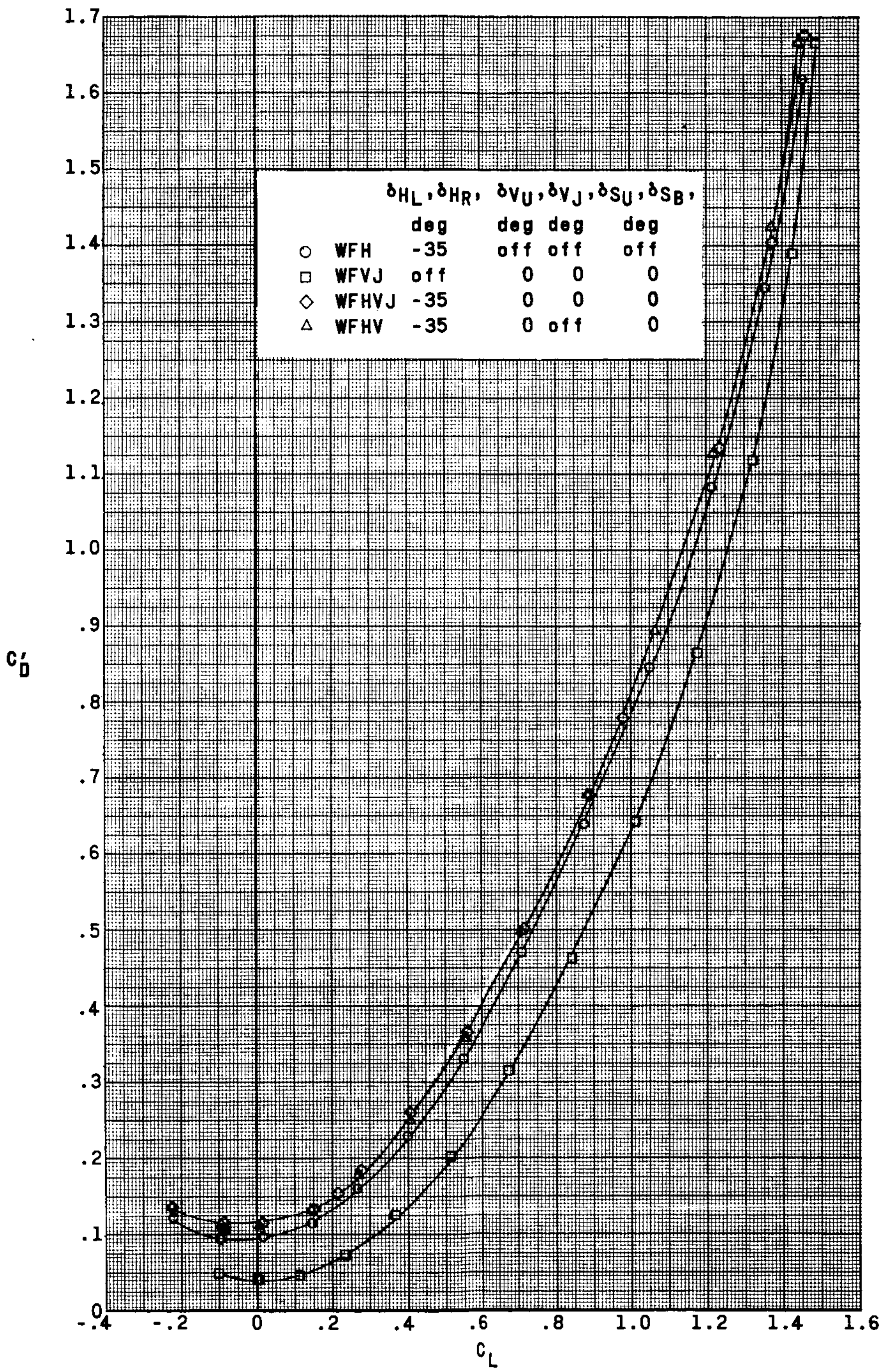

(b) Concluded.

Figure 5.- Continued.

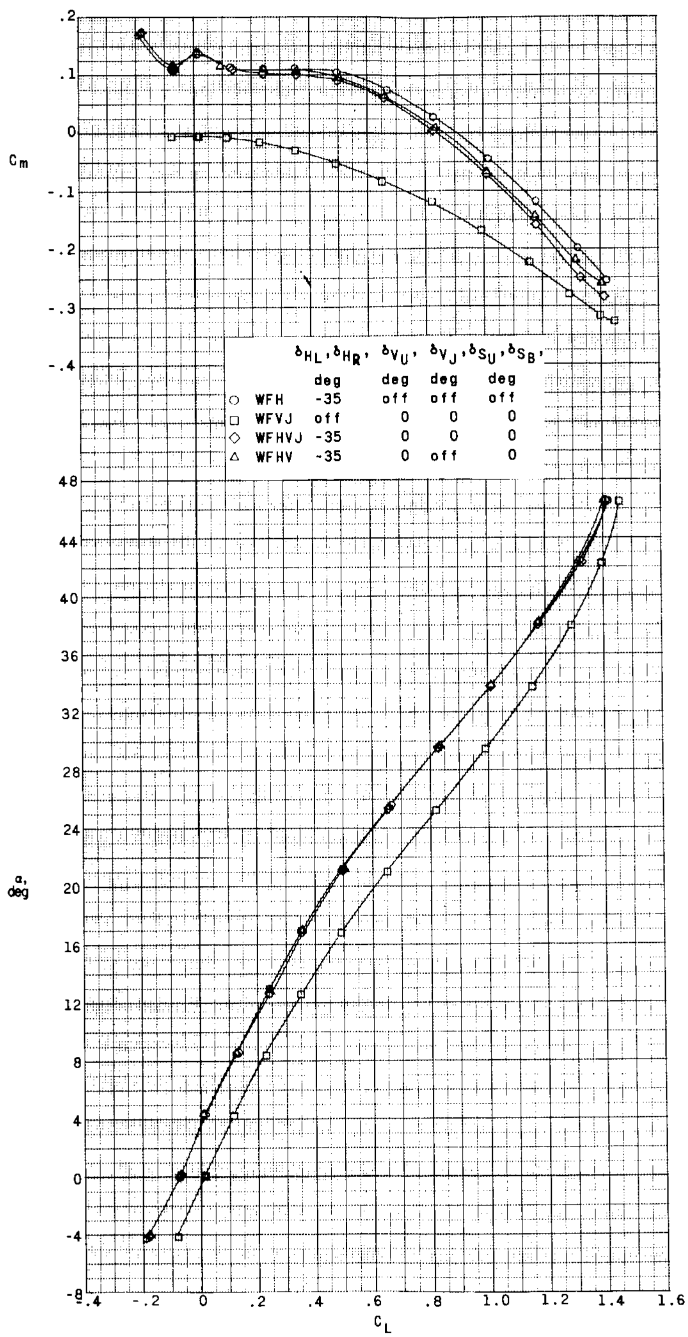

(c) M = 4.65.

Figure 5.- Continued.

[redacted]

DE[redacted]FIED

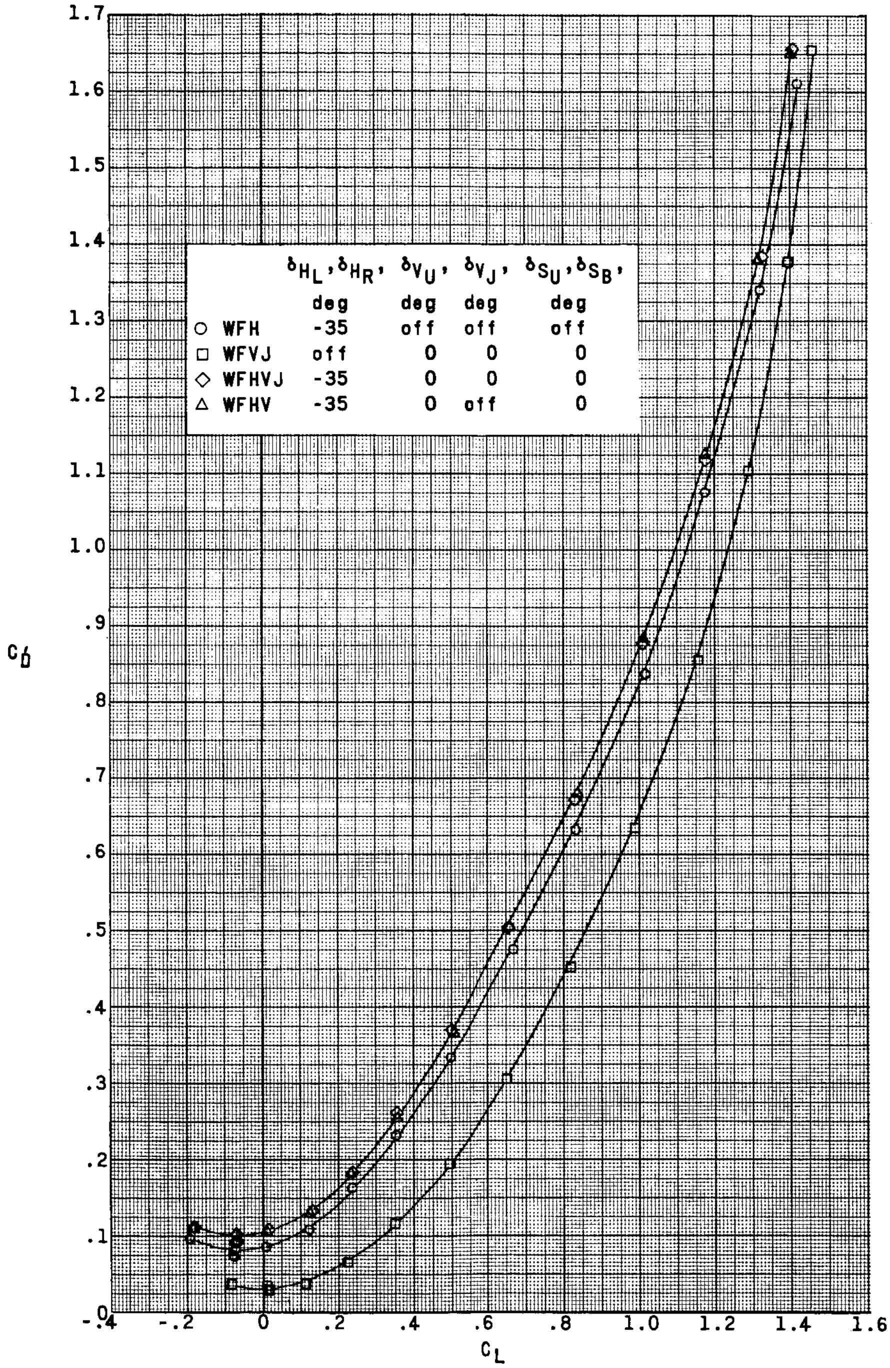

(c) Concluded.

Figure 5.- Concluded.

[redacted]

[redacted]

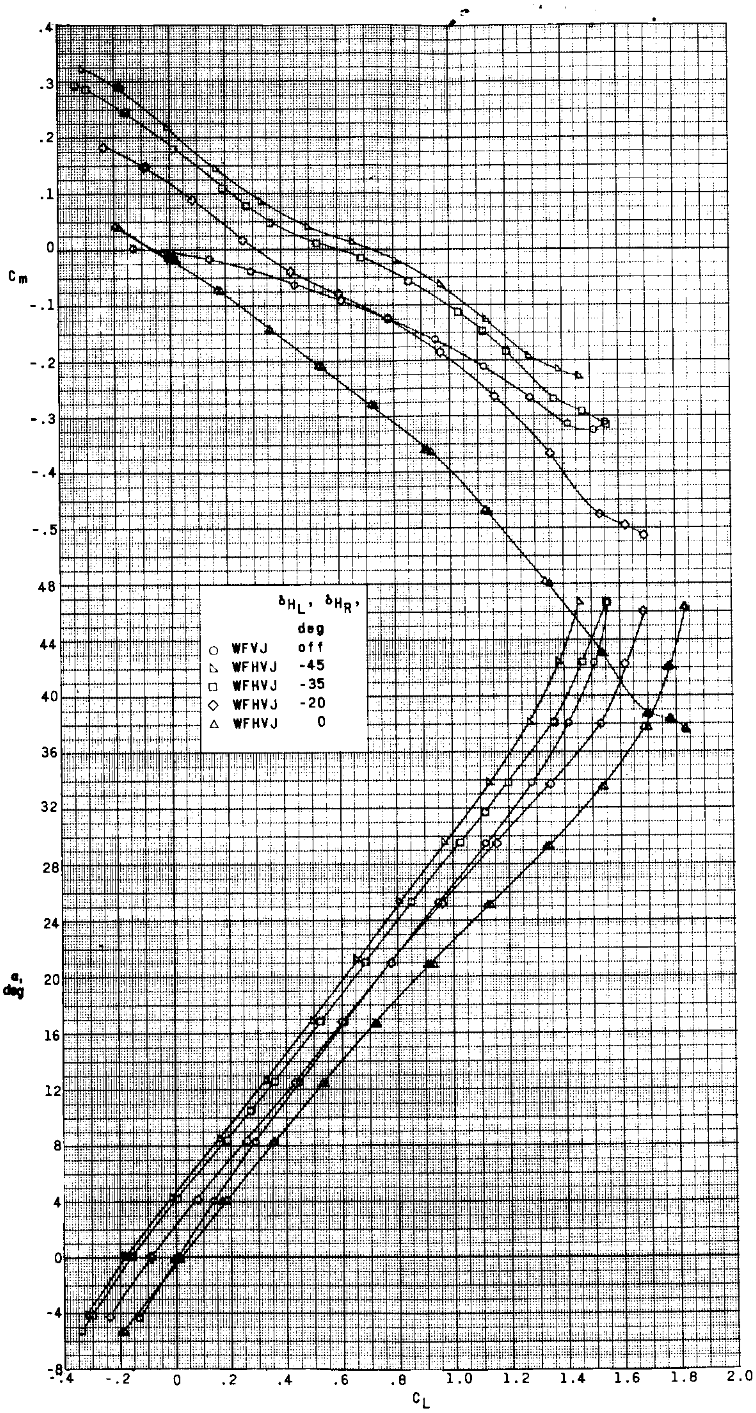

(a) M = 2.96.

Figure 6.- Effect of pitch-control deflections on aerodynamic characteristics in pitch. $\beta = 0^{\circ}$; $\delta_{V_U} = \delta_{V_J} = 0^{\circ}$; speed brakes retracted.

[redacted]

DE[redacted]FIED

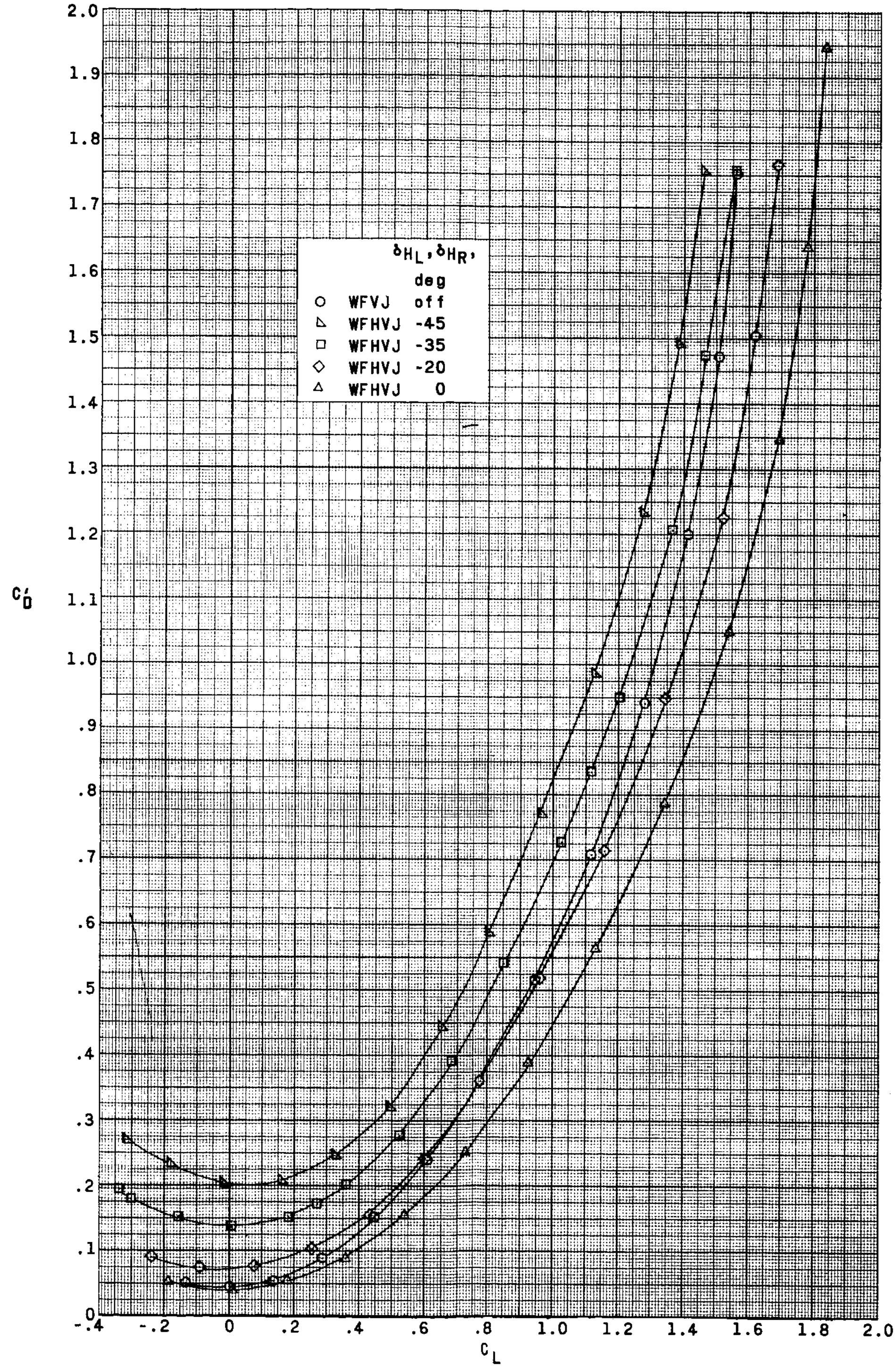

(a) Concluded.

Figure 6.- Continued.

[redacted]

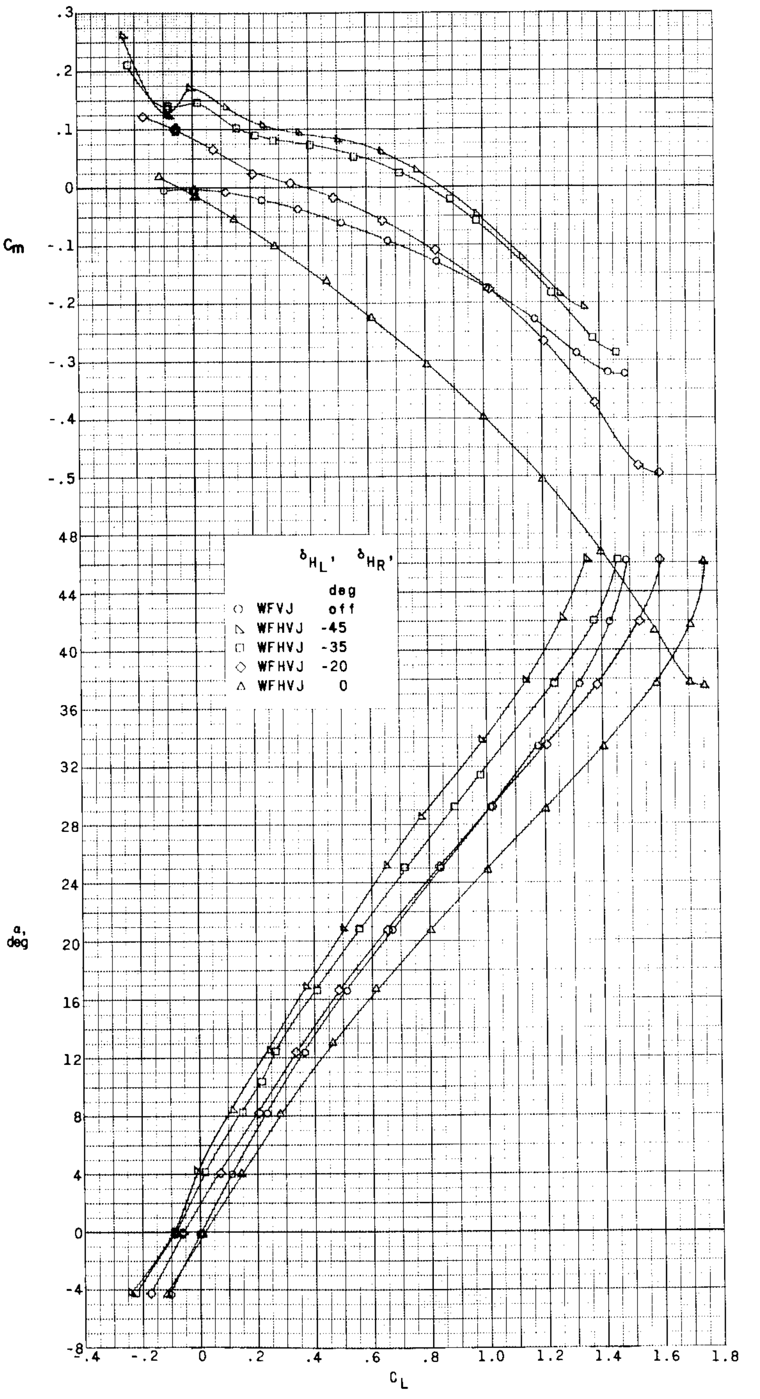

(b) M = 3.96.

Figure 6.- Continued.

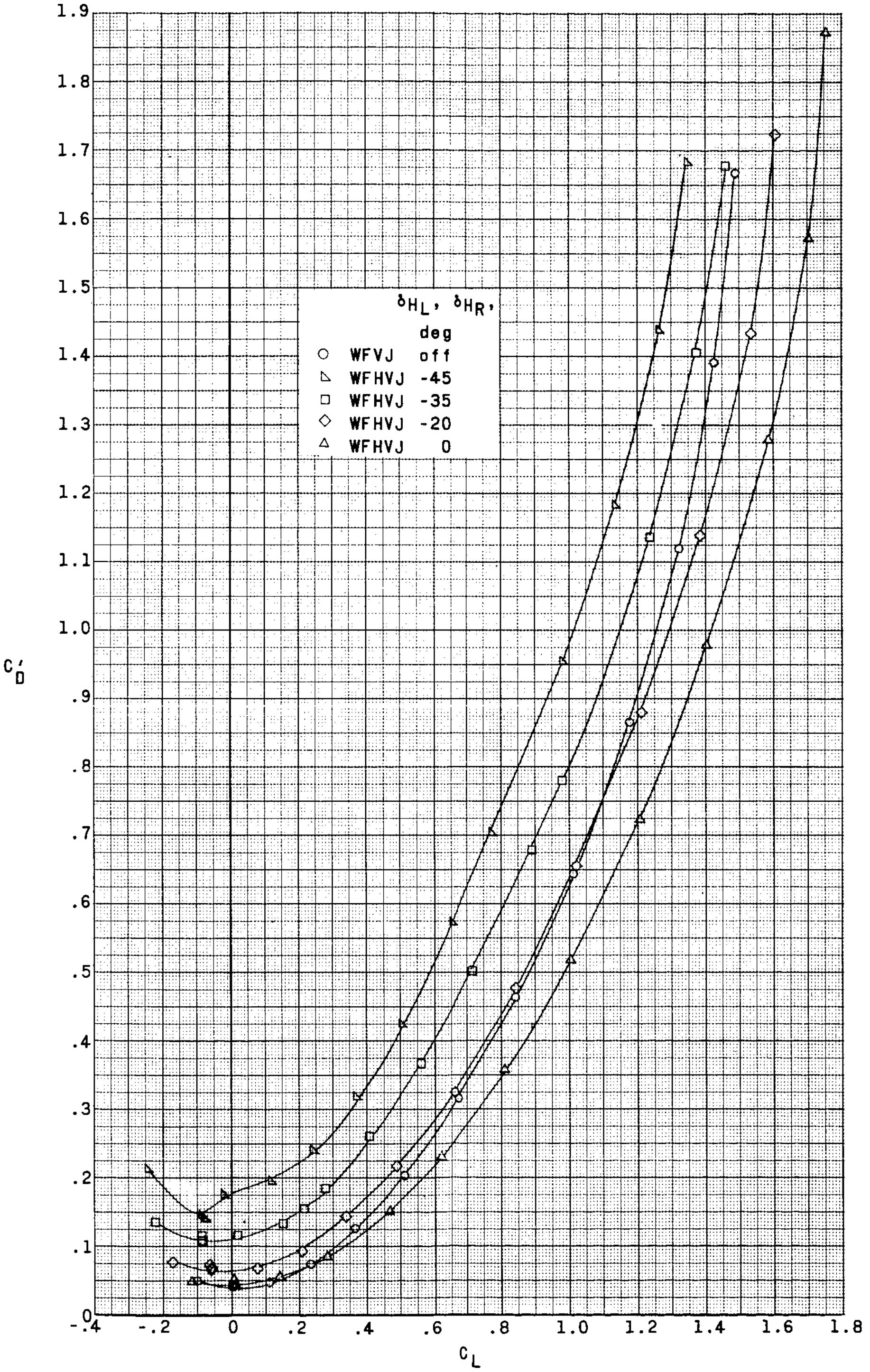

(b) Concluded.

Figure 6.- Continued.

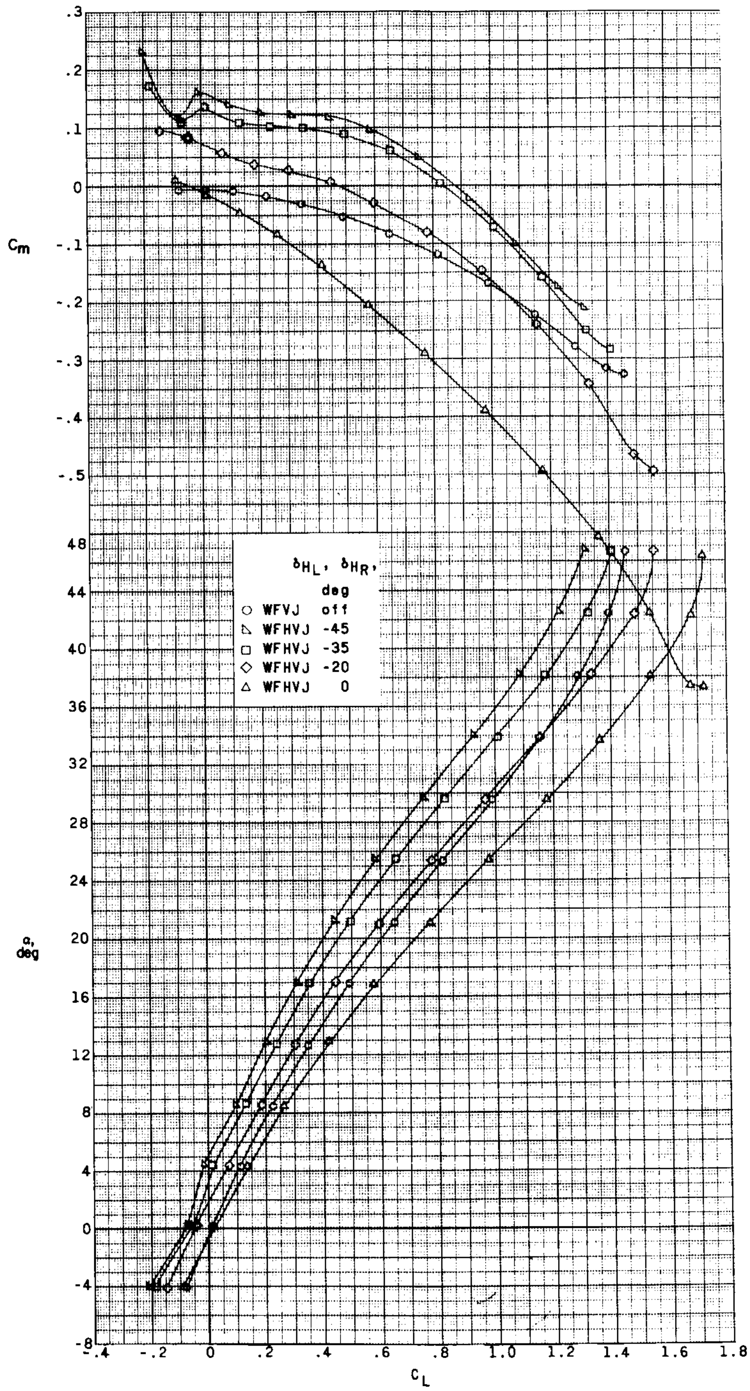

(c) M = 4.65.

Figure 6.- Continued.

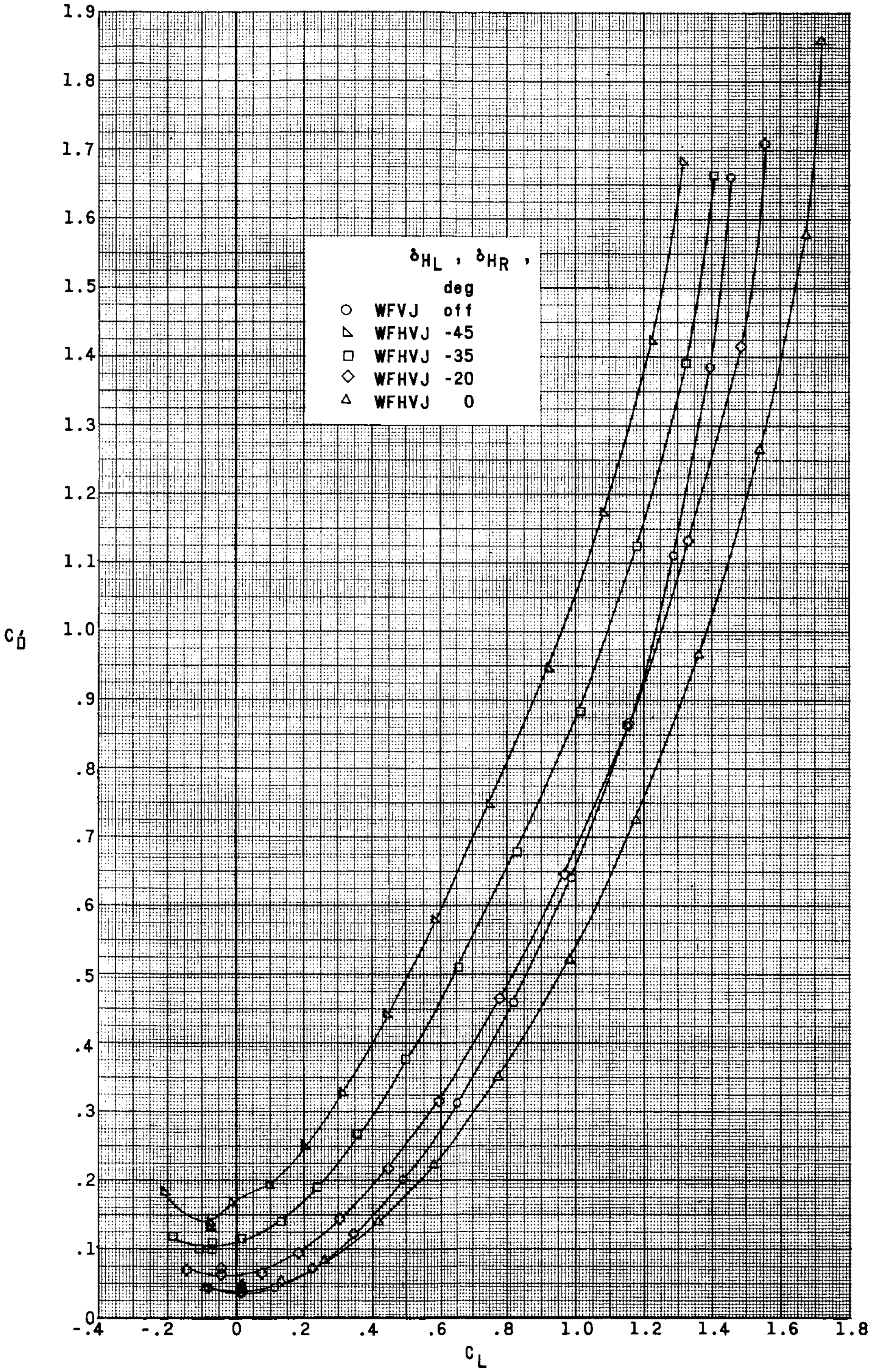

(c) Concluded.

Figure 6.- Concluded.

[redacted]

[redacted]

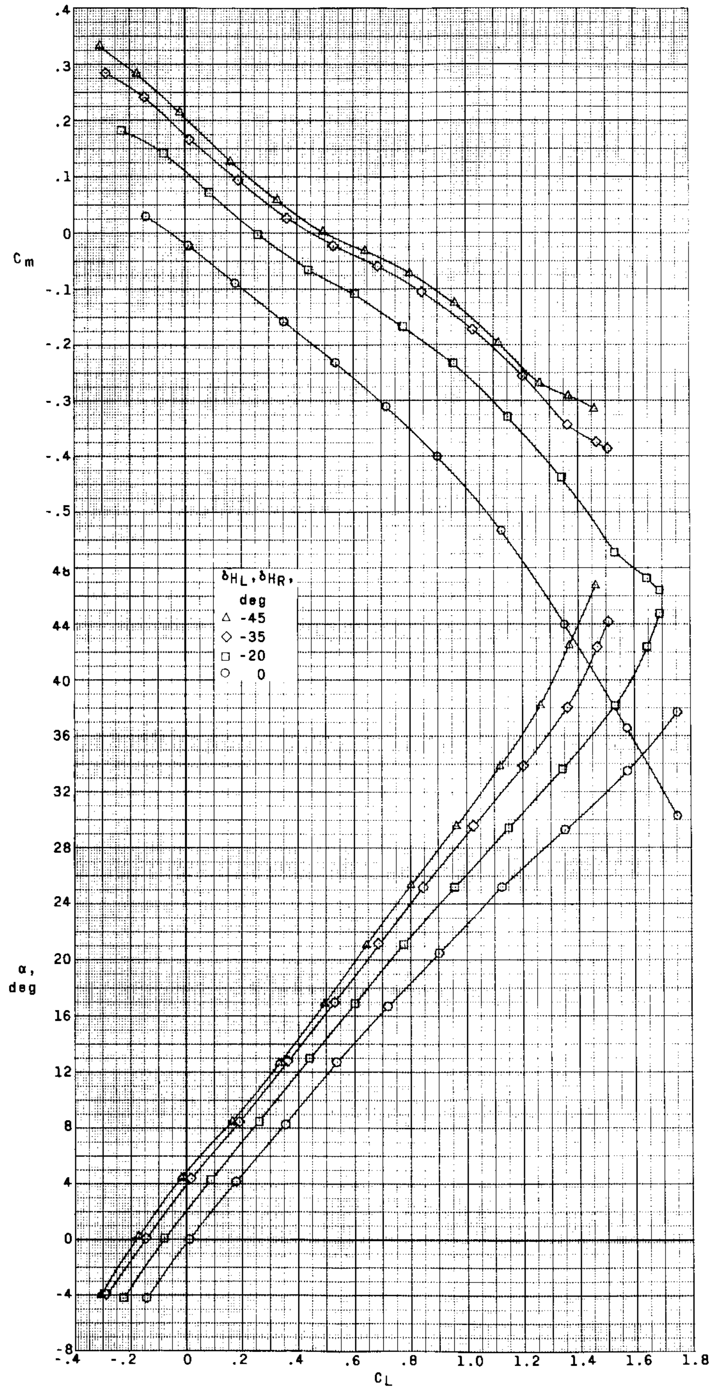

(a) M = 2.96.

Figure 7.- Effect of pitch-control deflections on aerodynamic characteristics in pitch. $\beta = 0^\circ$; $\delta_{V_U} = \delta_{V_J} = 0^\circ$; $\delta_{S_U} = \delta_{S_B} = 35^\circ$; WFHVJ.

[redacted]

DE[redacted]IFIED

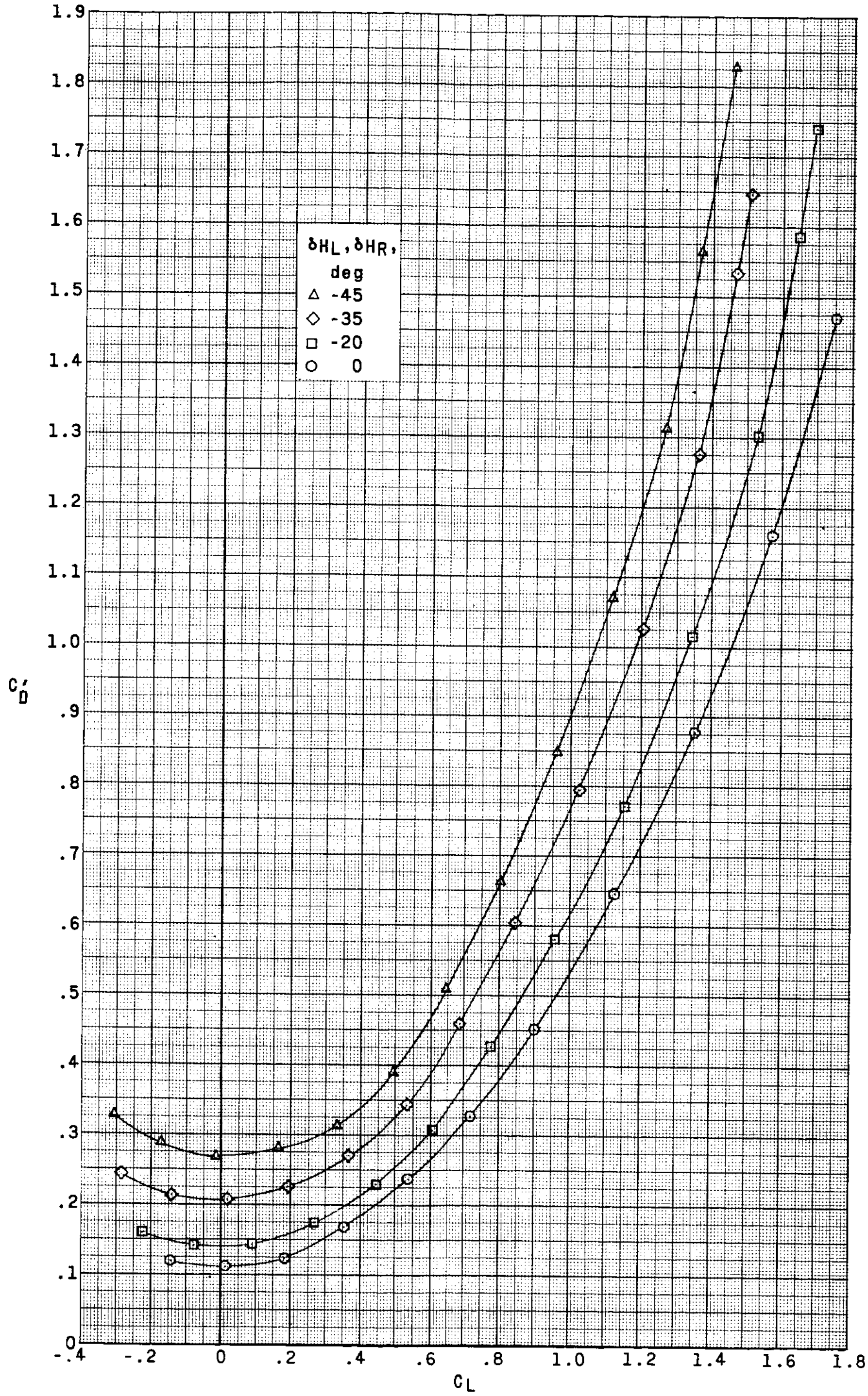

(a) Concluded.

Figure 7.- Continued.

[redacted]

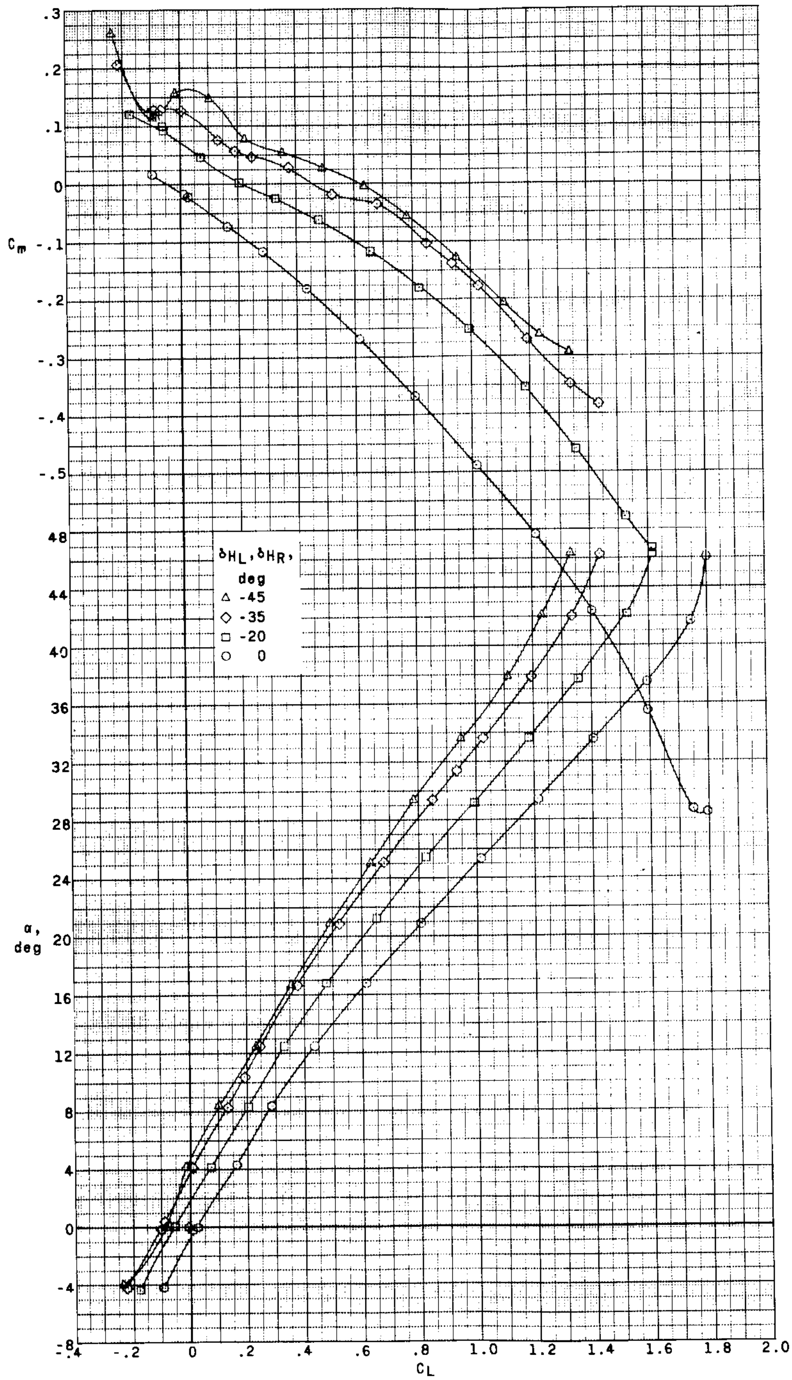

(b) M = 3.96.

Figure 7.- Continued.

[redacted]

DE[redacted]FIED

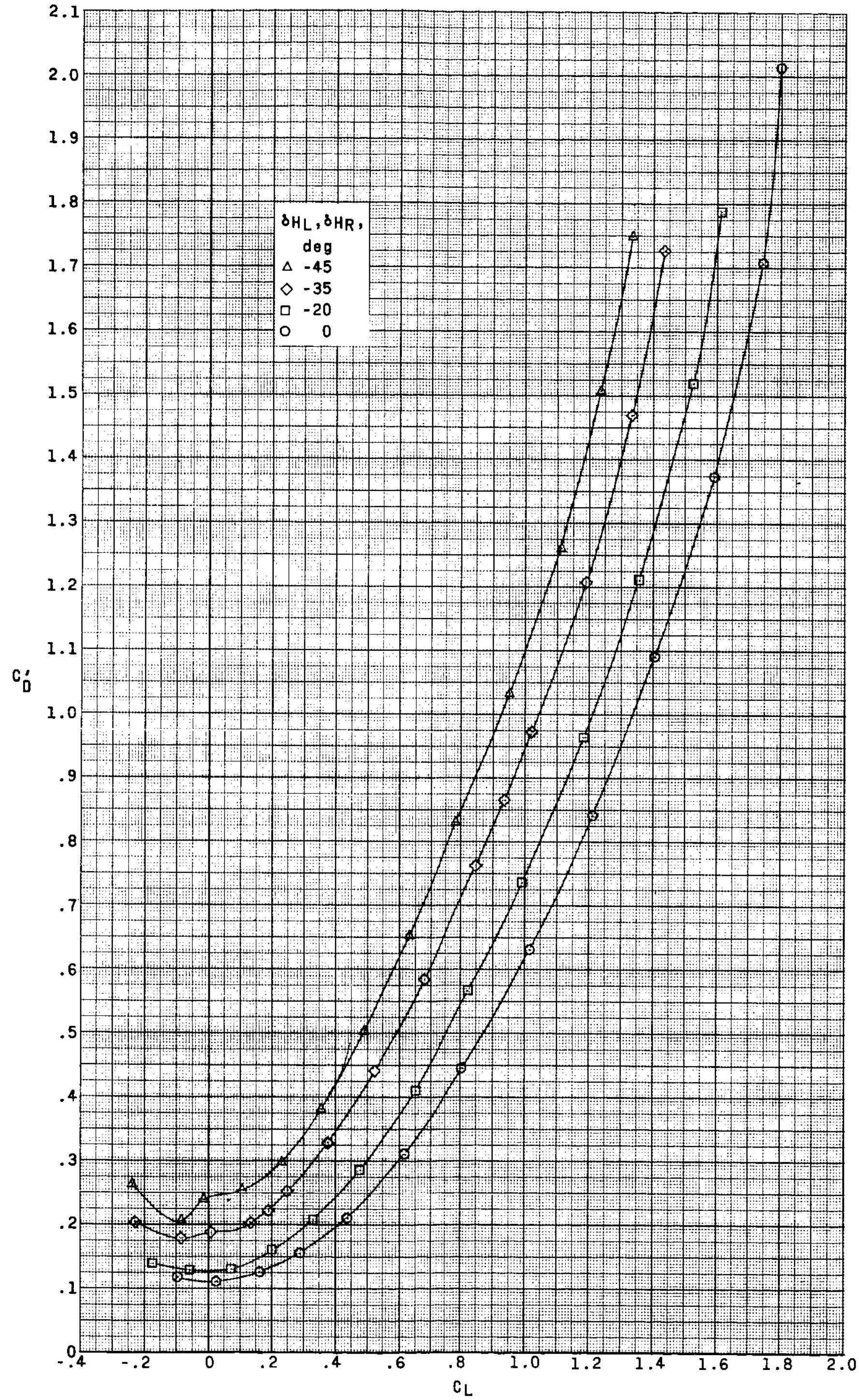

(b) Concluded.

Figure 7.- Continued.

[redacted]

[redacted]

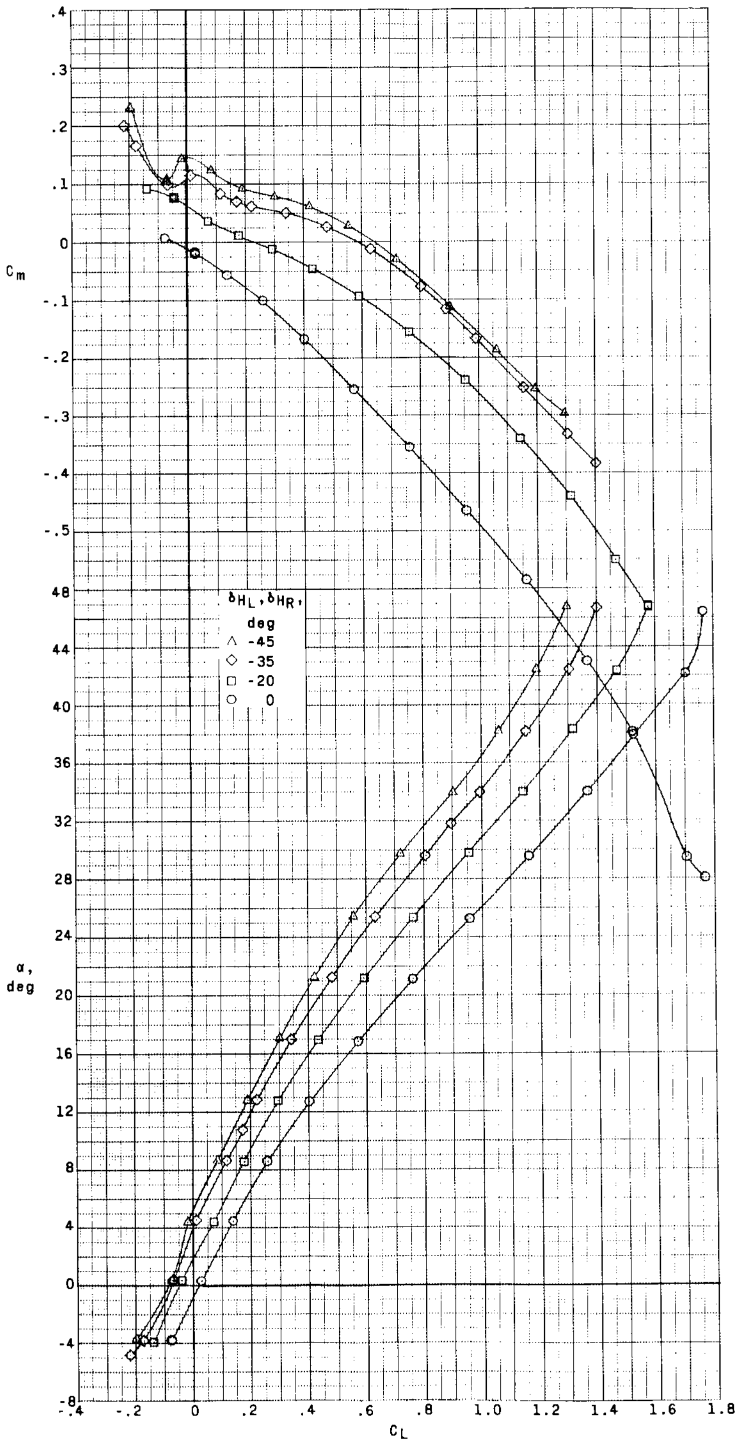

(c) M = 4.65.

Figure 7.- Continued.

[redacted]

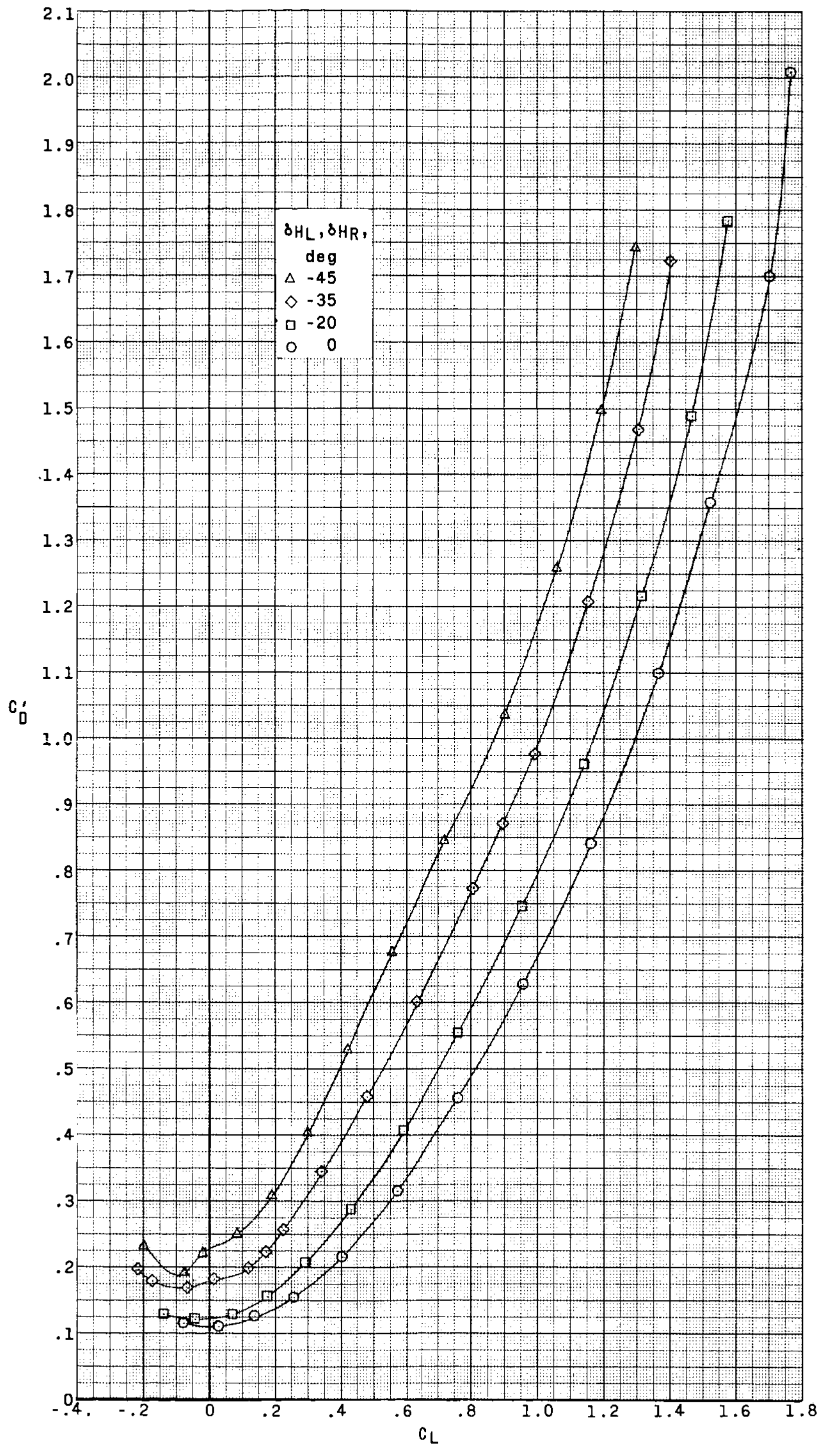

(c) Concluded.

Figure 7.- Concluded.

[redacted]

[redacted]

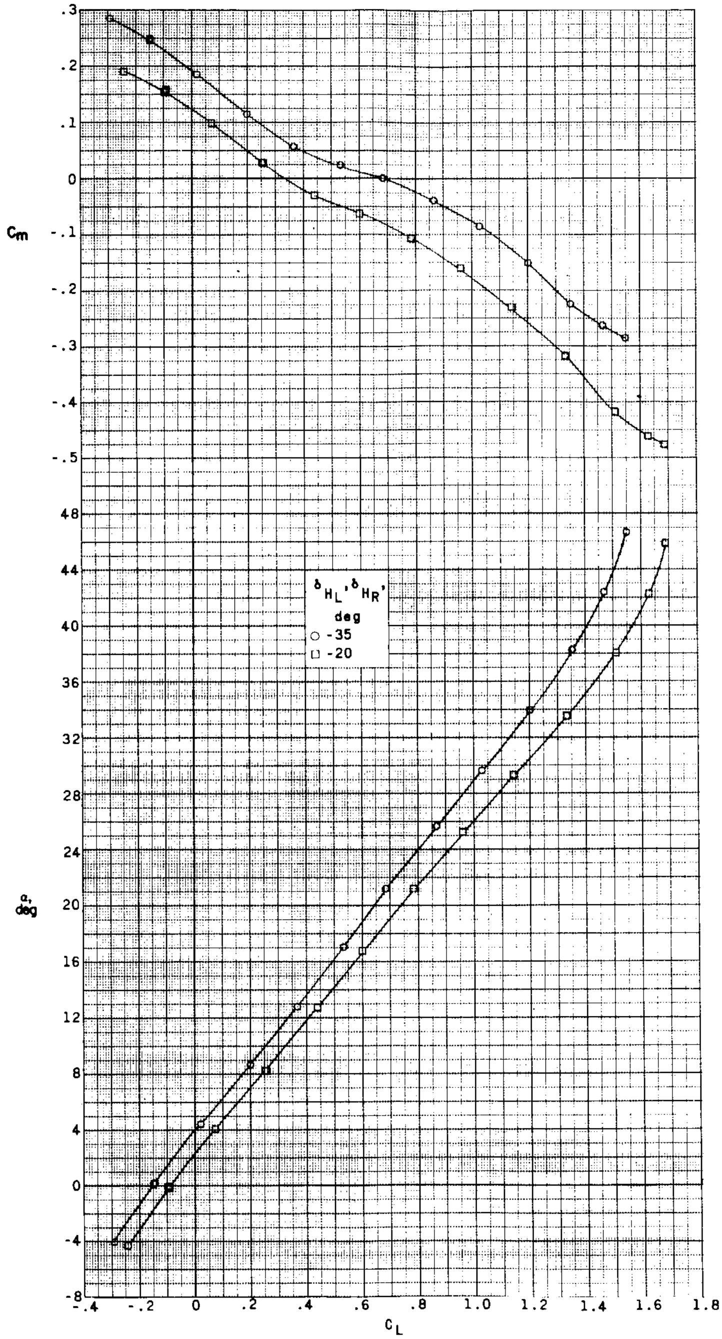

(a) M = 2.96.

Figure 8.- Effect of pitch-control deflections on aerodynamic characteristics in pitch. $\beta = 0^{\circ}$; $\delta_{V_U} = 0^{\circ}$; jettisonable portion of lower vertical stabilizer off; speed brakes retracted; WFHV.

[redacted]

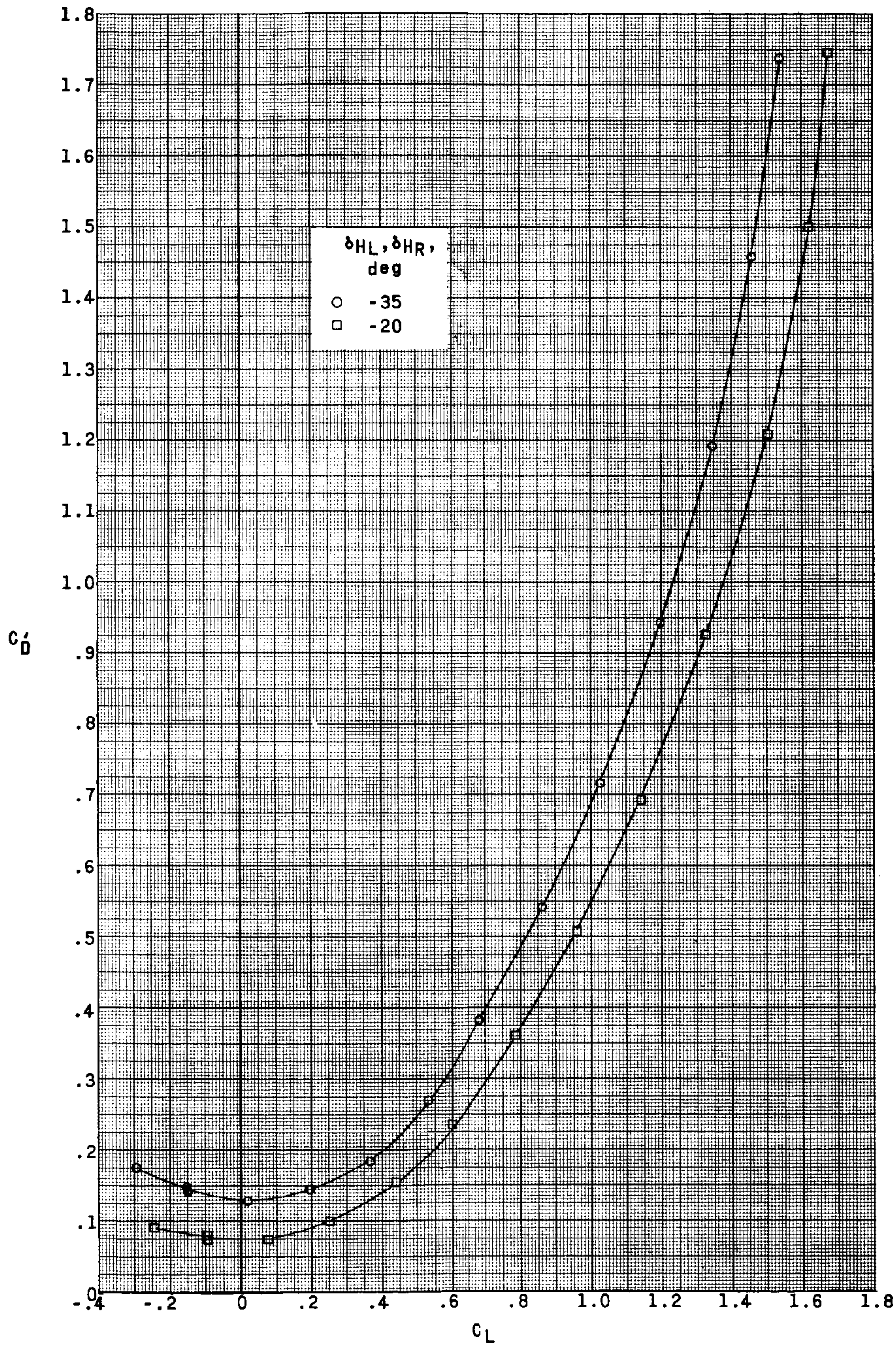

(a) Concluded.

Figure 8.- Continued.

[redacted]

[redacted]

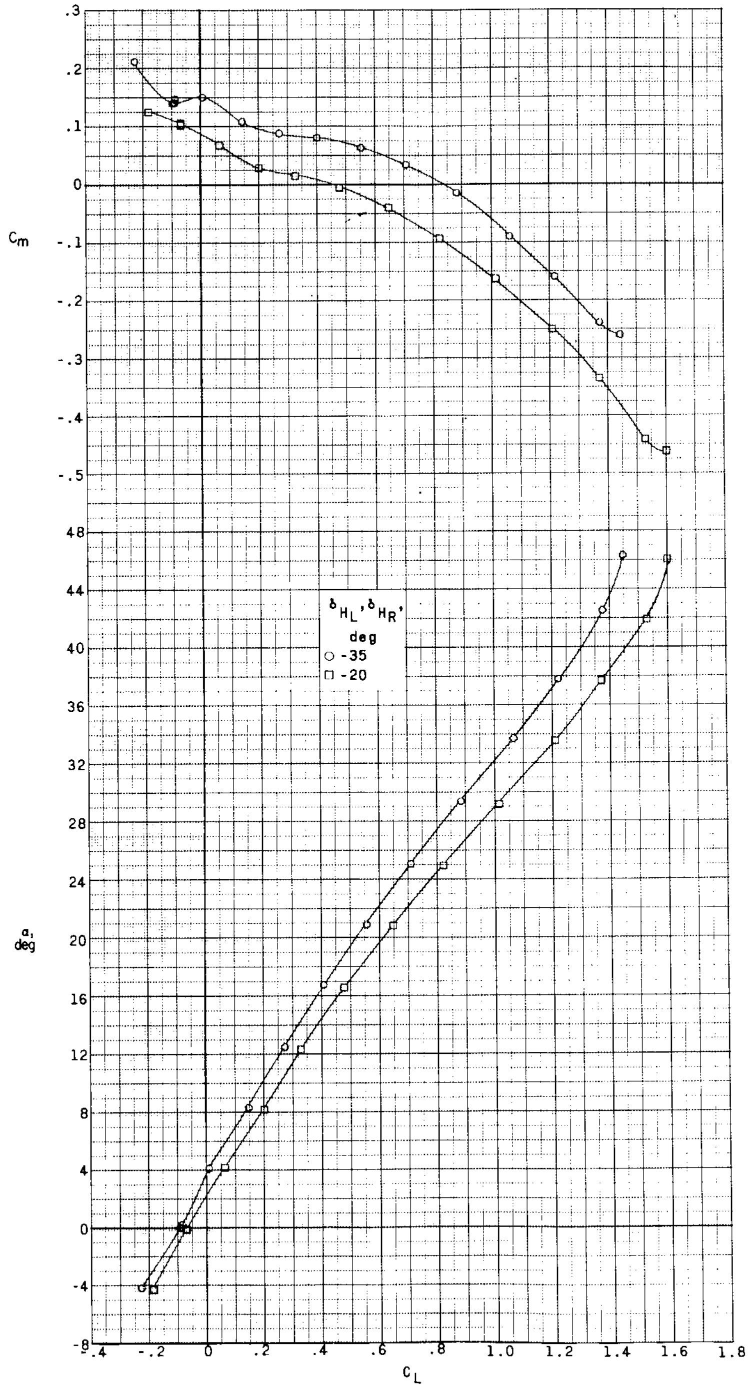

(b) M = 3.96.

Figure 8.- Continued.

[redacted]

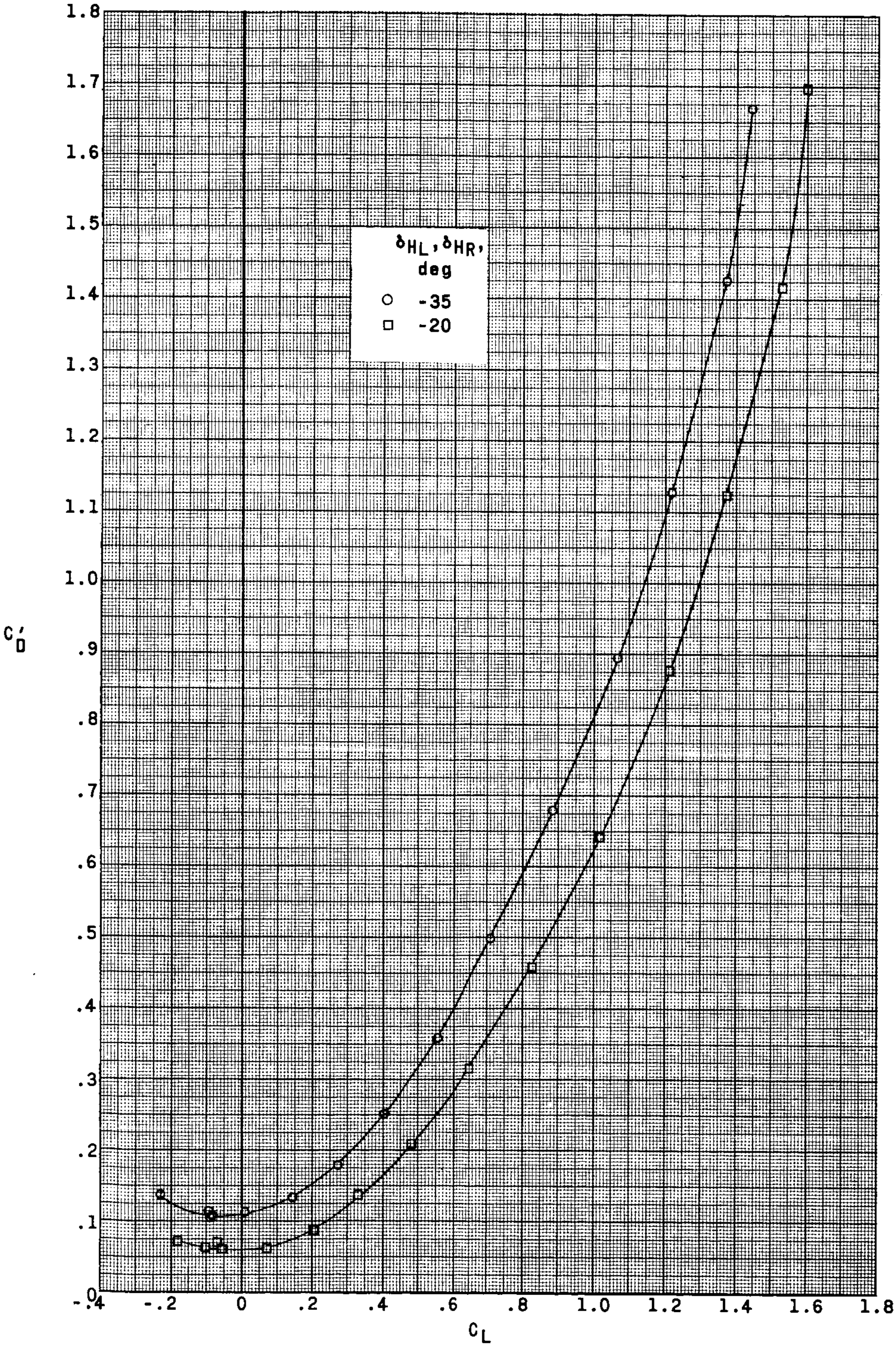

(b) Concluded.

Figure 8.- Continued.

[redacted]

[redacted]

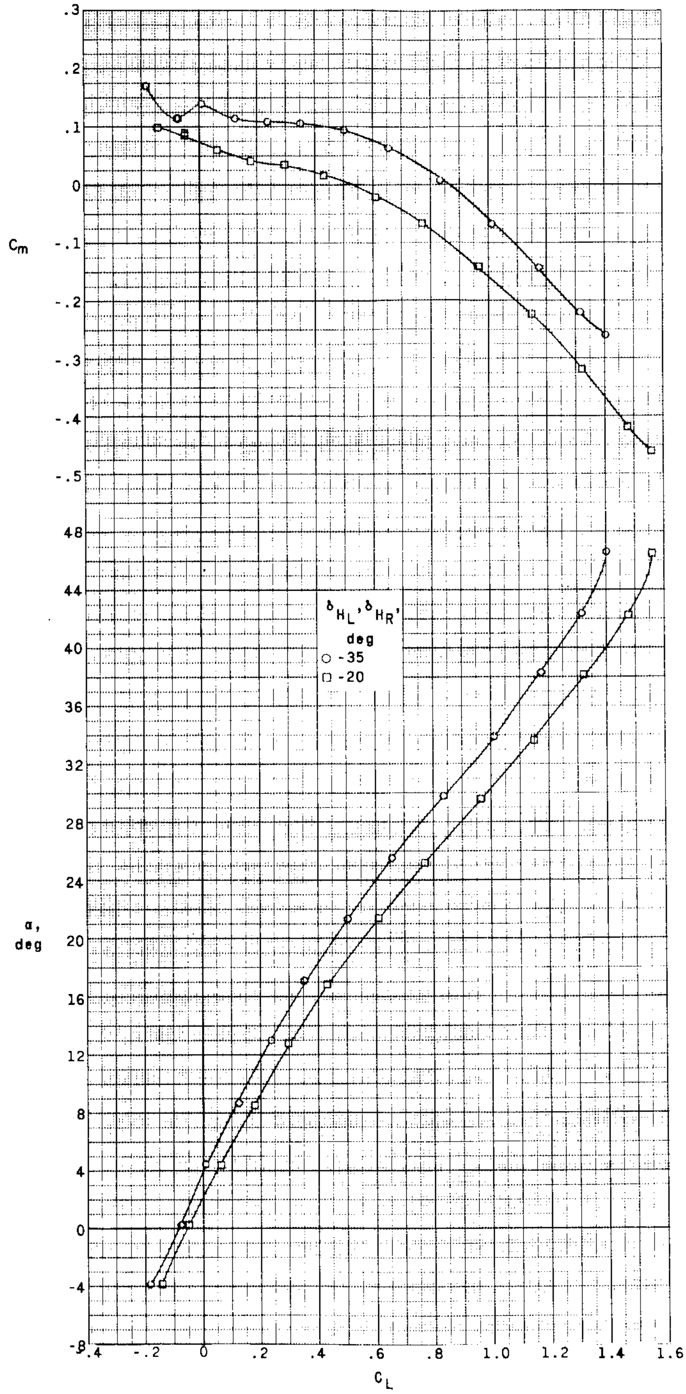

(c) M = 4.65.

Figure 8.- Continued.

[redacted]

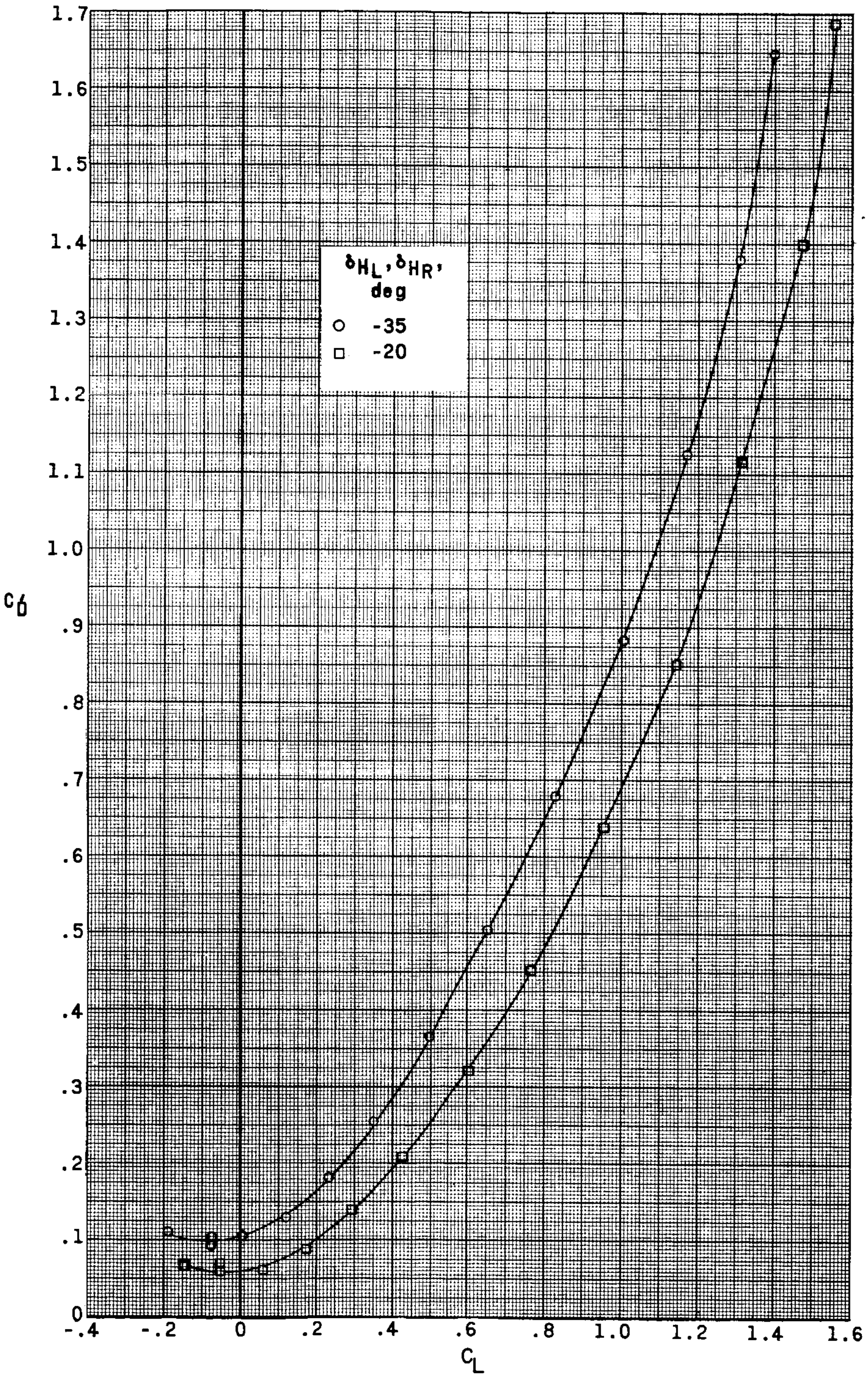

(c) Concluded.

Figure 8.- Concluded.

[redacted]

[redacted]

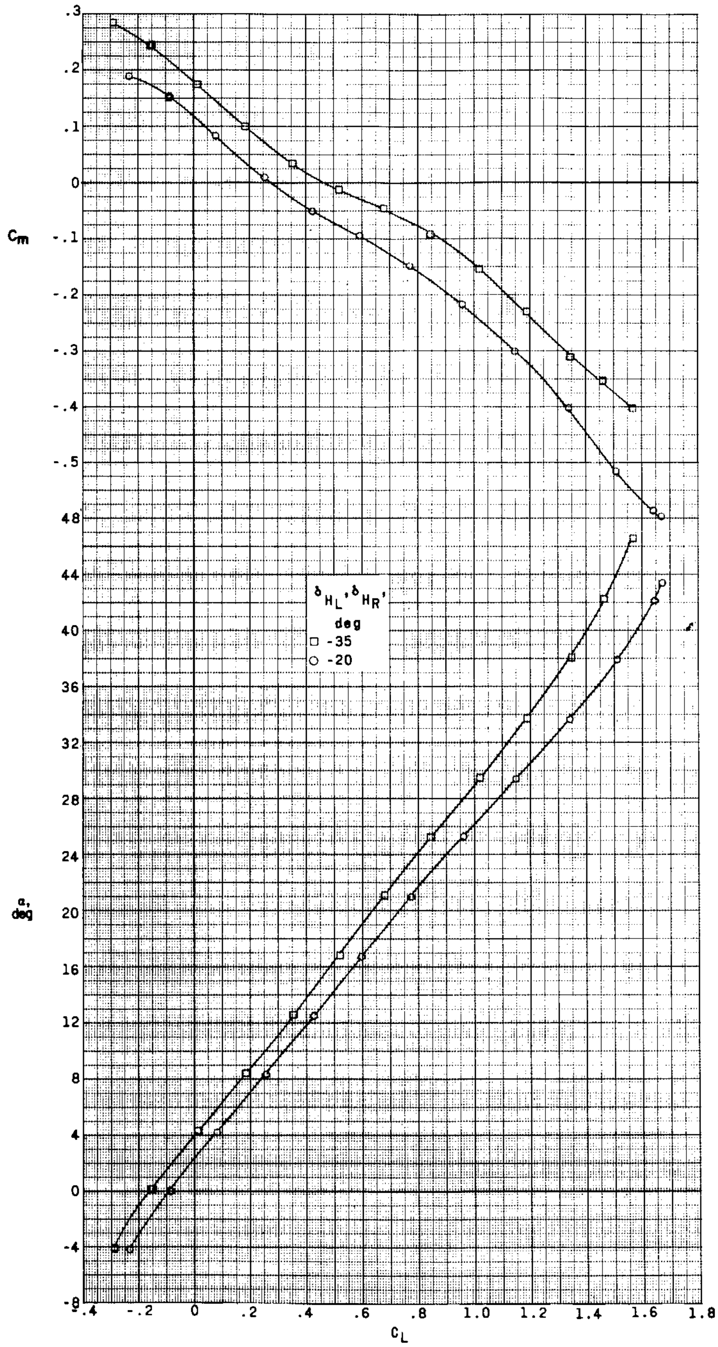

(a) M = 2.96.

Figure 9.- Effect of pitch-control deflections on aerodynamic characteristics in pitch. $\beta = 0^{\circ}$; $\delta_{V_U} = 0^{\circ}$; jettisonable portion of lower vertical stabilizer off; $\delta_{S_U} = \delta_{S_B} = 35^{\circ}$; WFHV.

[redacted]

DE[redacted]FIED

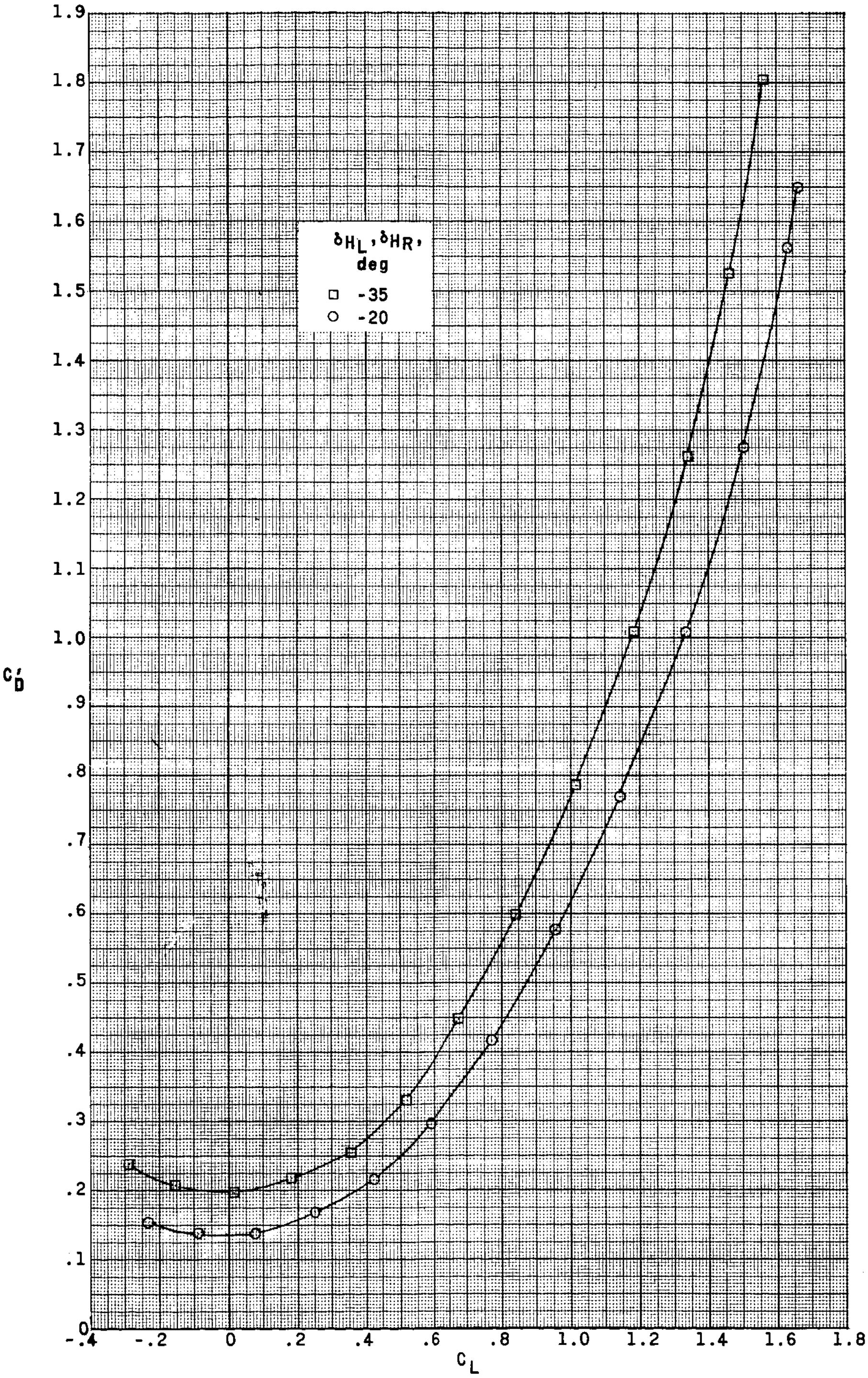

(a) Concluded.

Figure 9.- Continued.

[redacted]

[redacted]

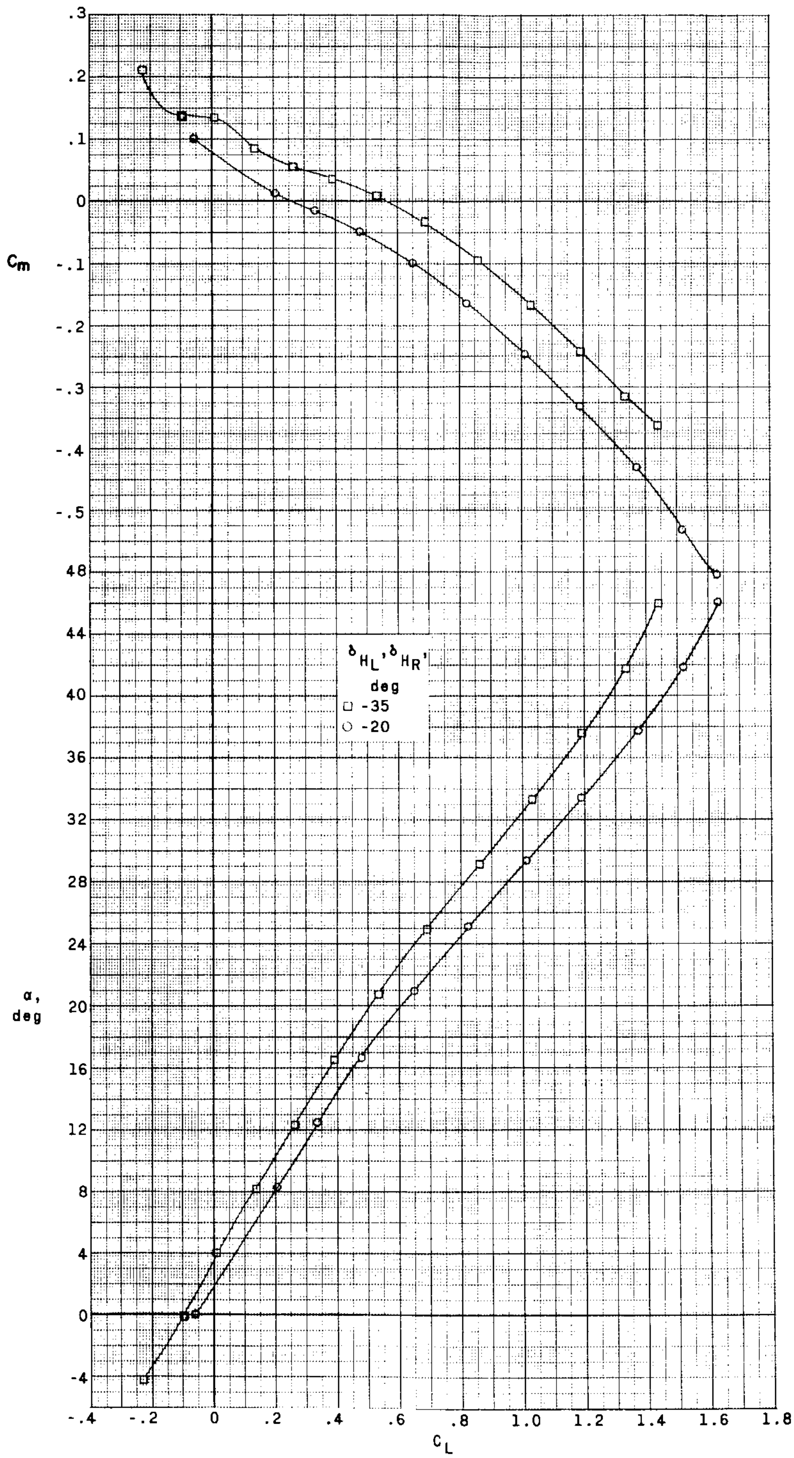

(b) M = 3.96.

Figure 9.- Continued.

[redacted]

D[redacted]FIED

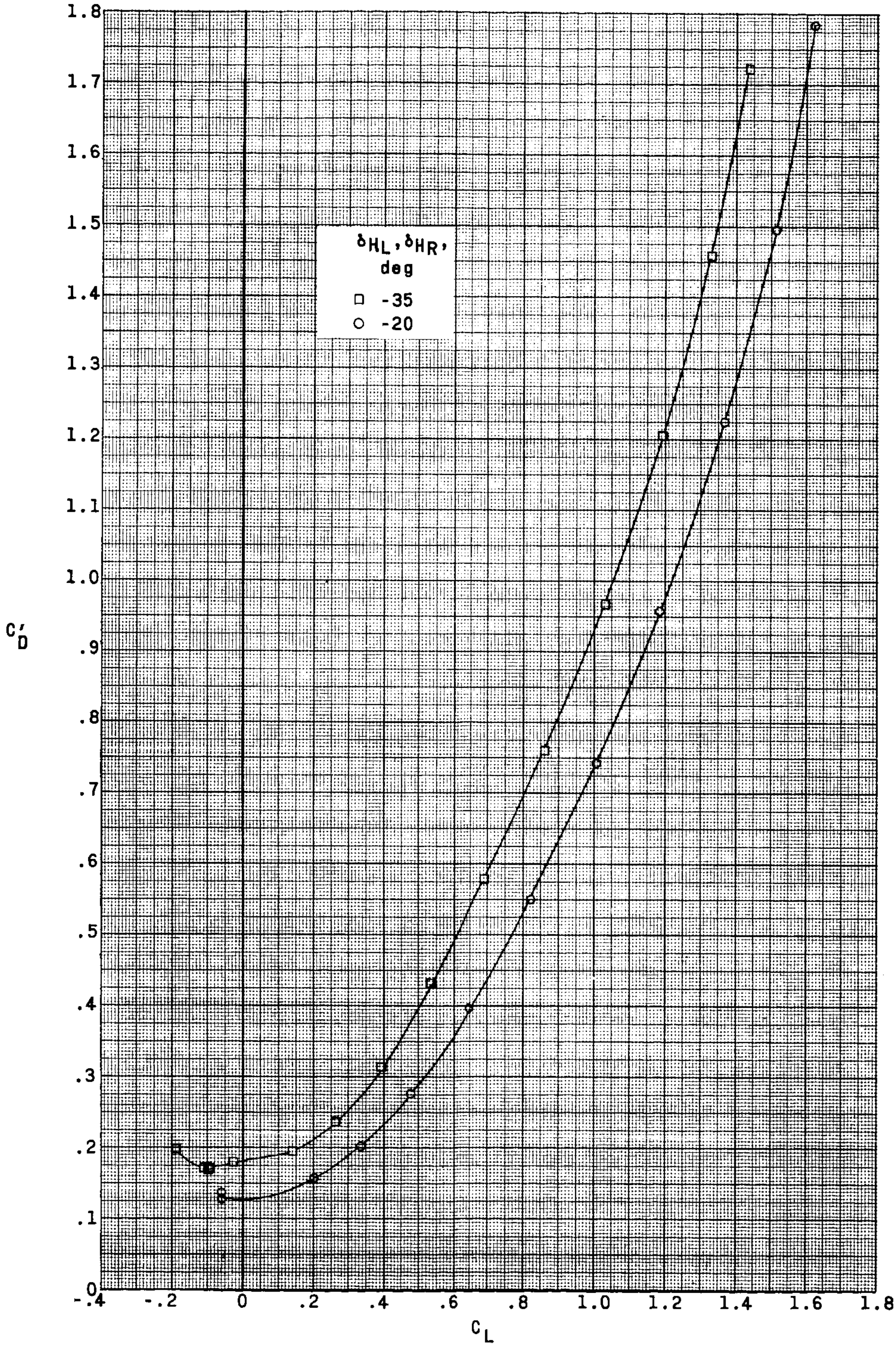

(b) Concluded.

Figure 9.- Continued.

[redacted]

[redacted]

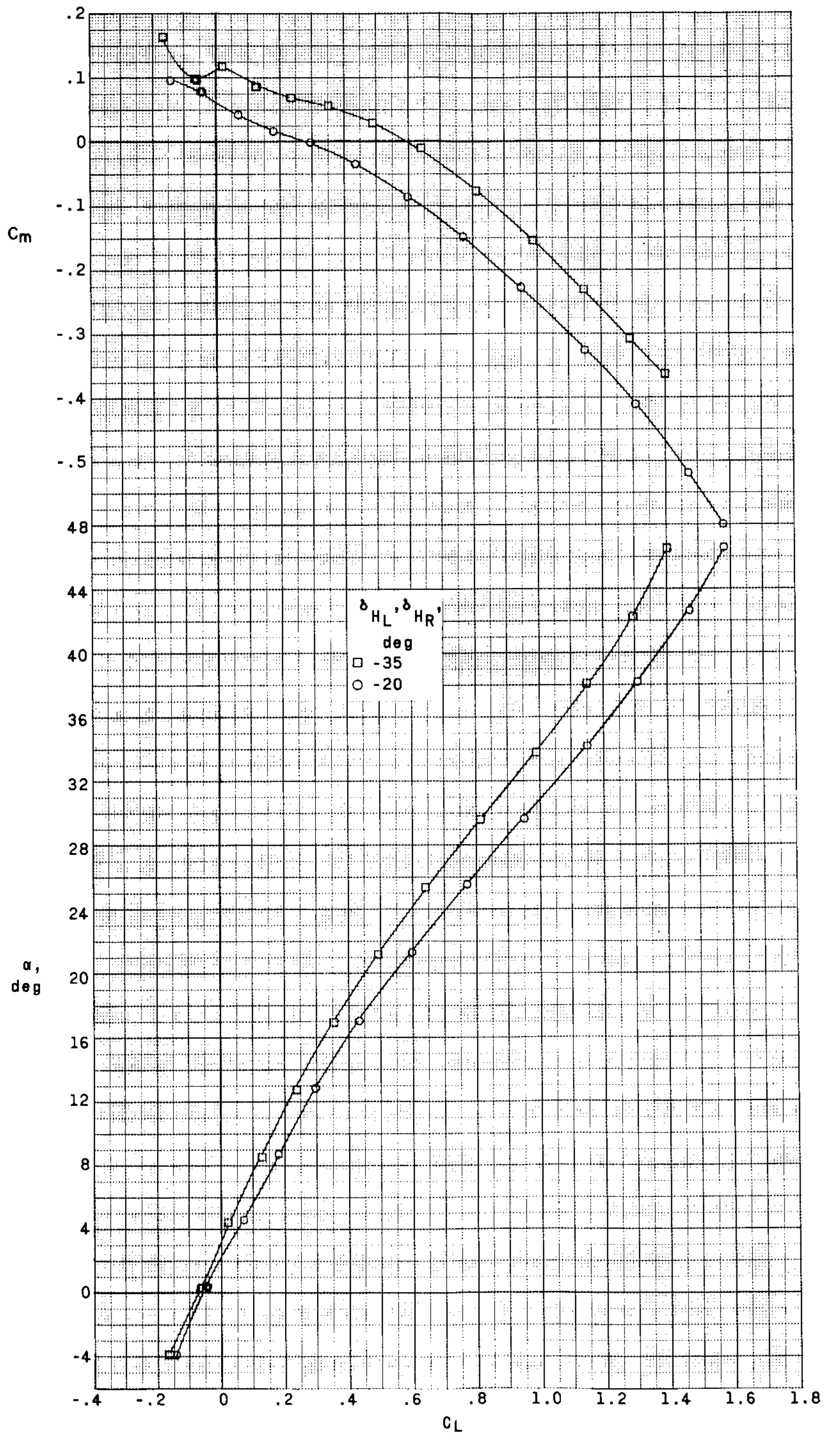

(c) M = 4.65.

Figure 9.- Continued.

[redacted]

DE [redacted] FIED

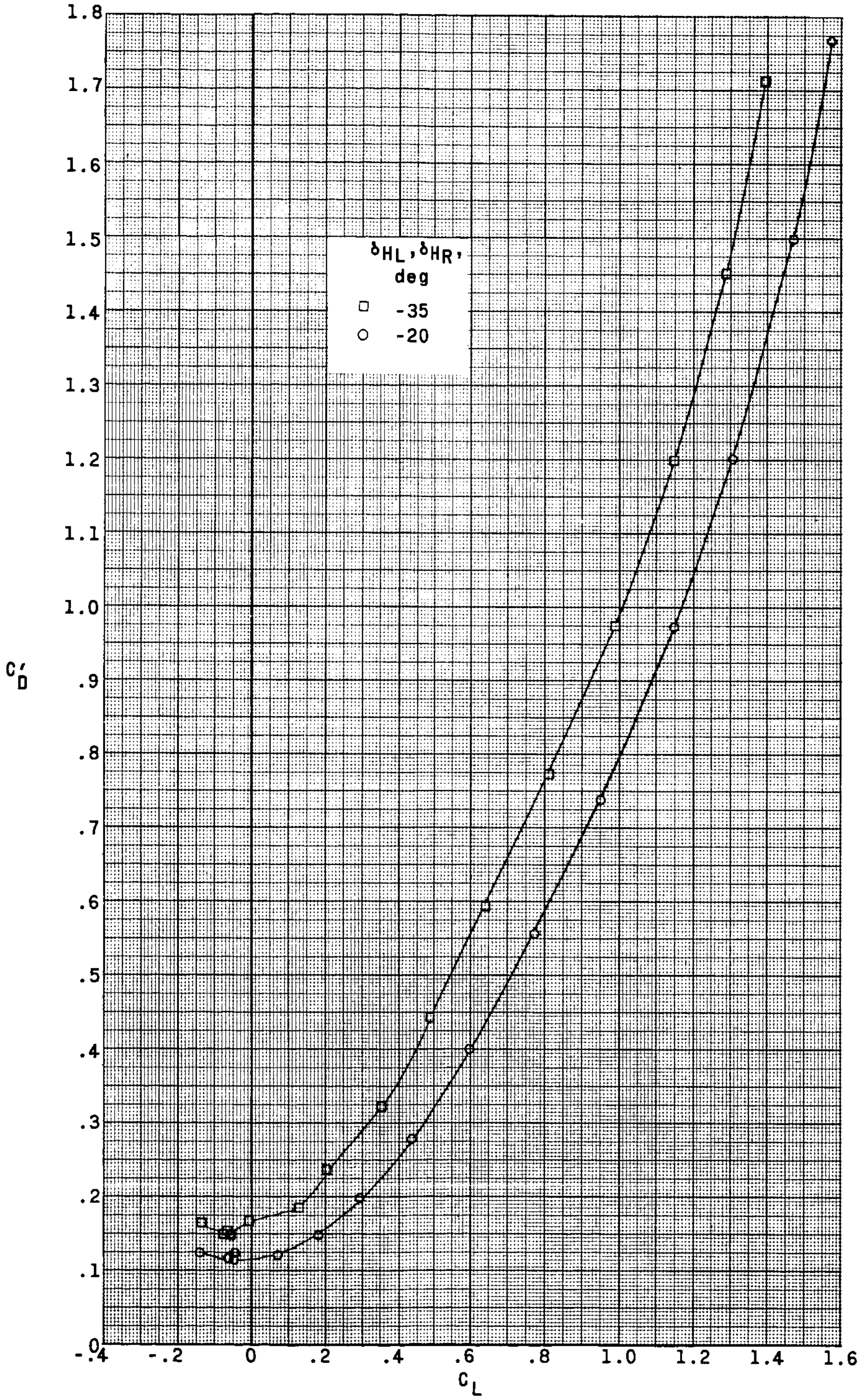

(c) Concluded.

Figure 9.- Concluded.

[redacted]

[redacted]

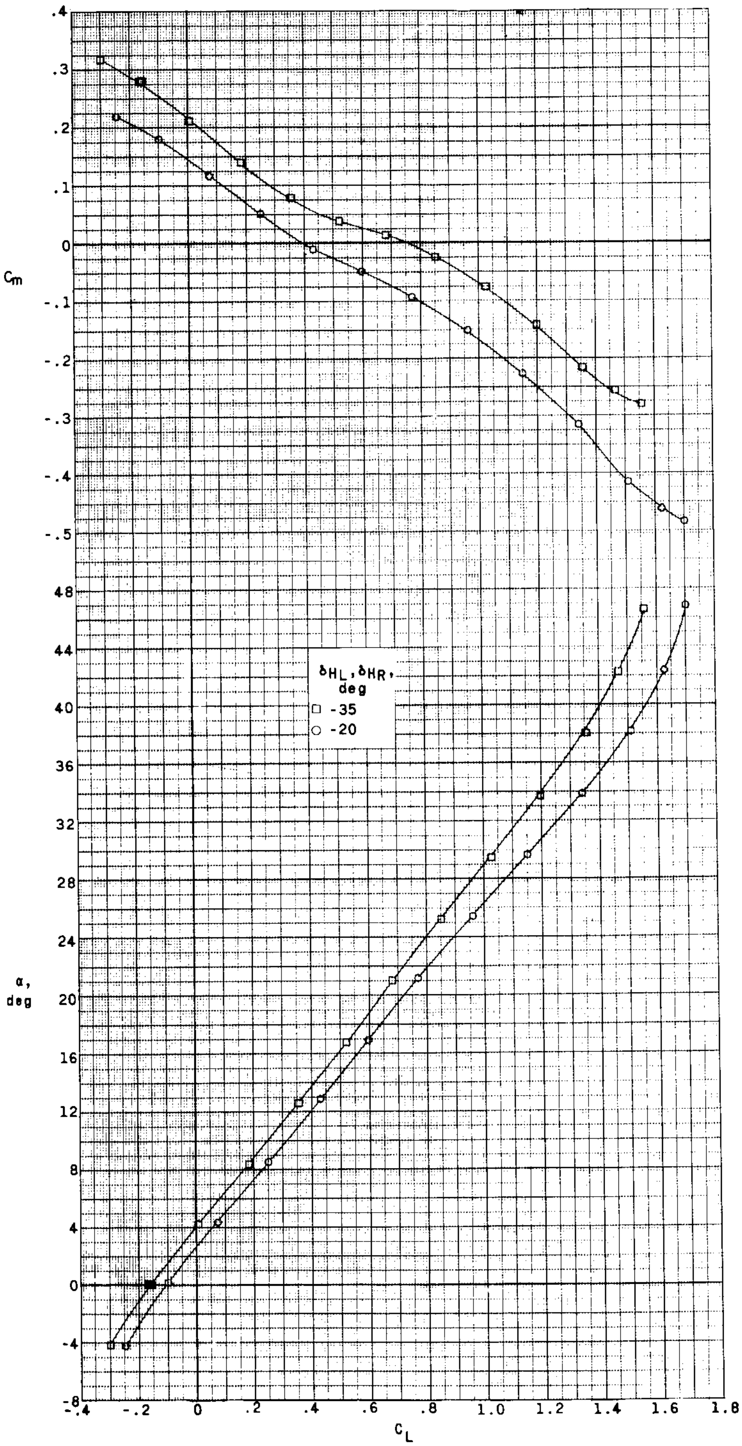

(a) M = 2.96.

Figure 10.- Effect of pitch-control deflections on aerodynamic characteristics in pitch. $\beta = 0^{\circ}$; $\delta_{V_U} = 0^{\circ}$; jettisonable portion of lower vertical stabilizer off; $\delta_{S_U} = 35^{\circ}$; $\delta_{S_B} = 0^{\circ}$; WFHV.

[redacted]

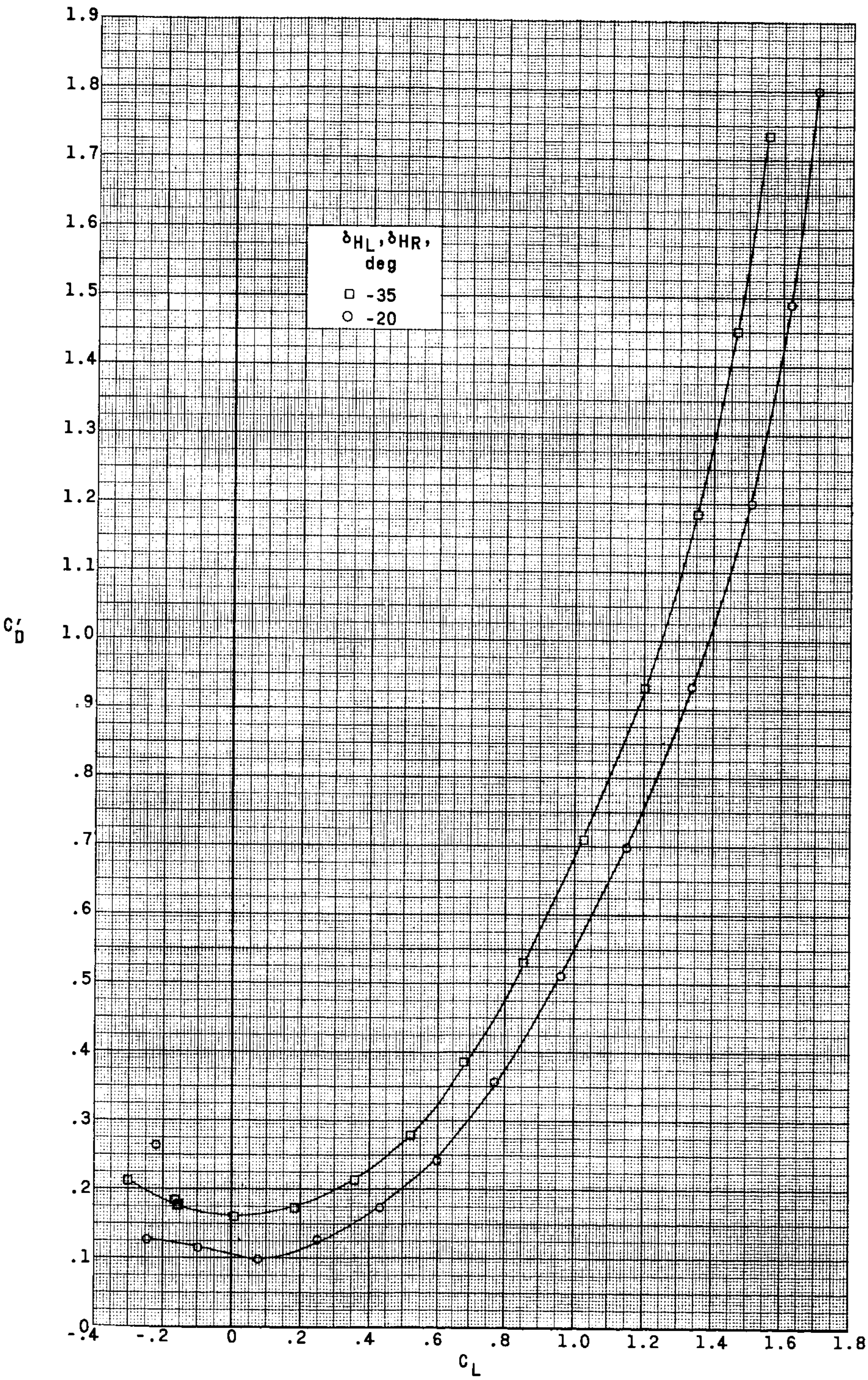

(a) Concluded.

Figure 10.- Continued.

[redacted]

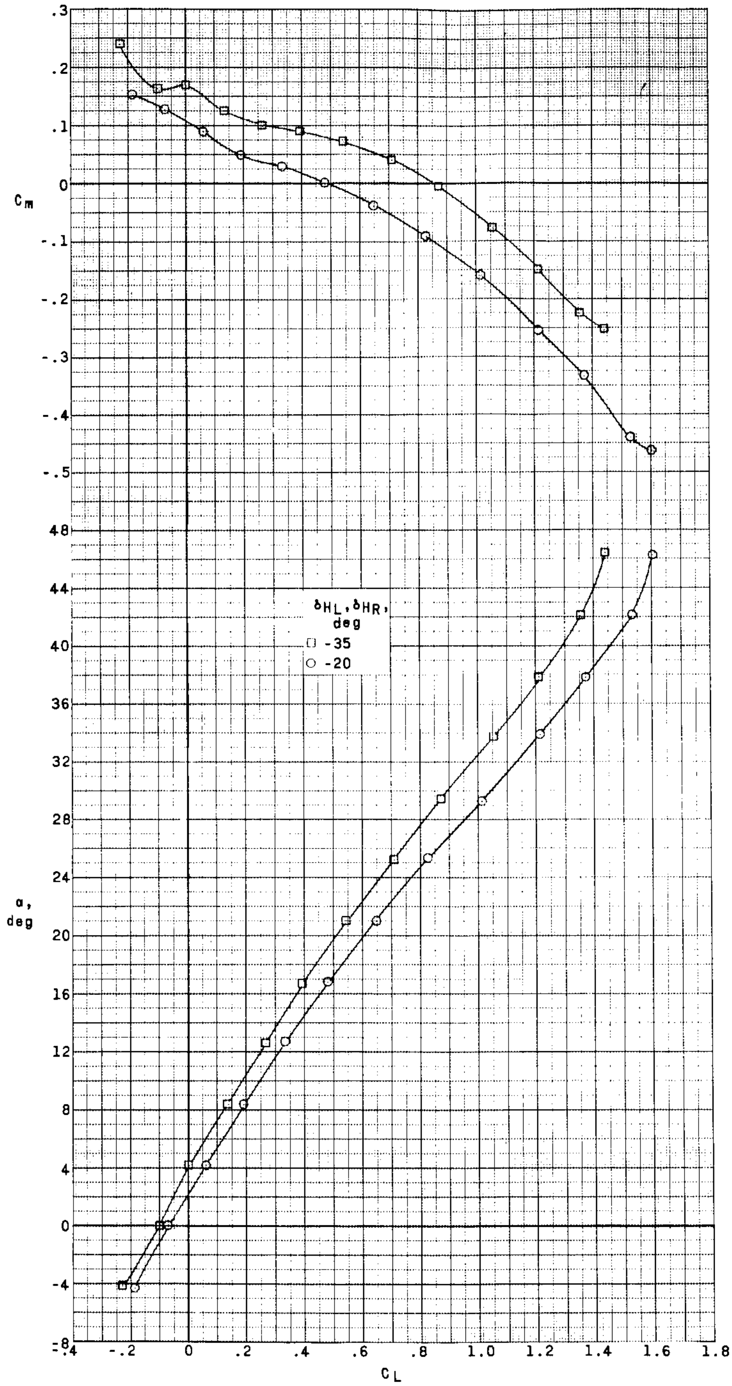

(b) M = 3.96.

Figure 10.- Continued.

D[redacted]FIED

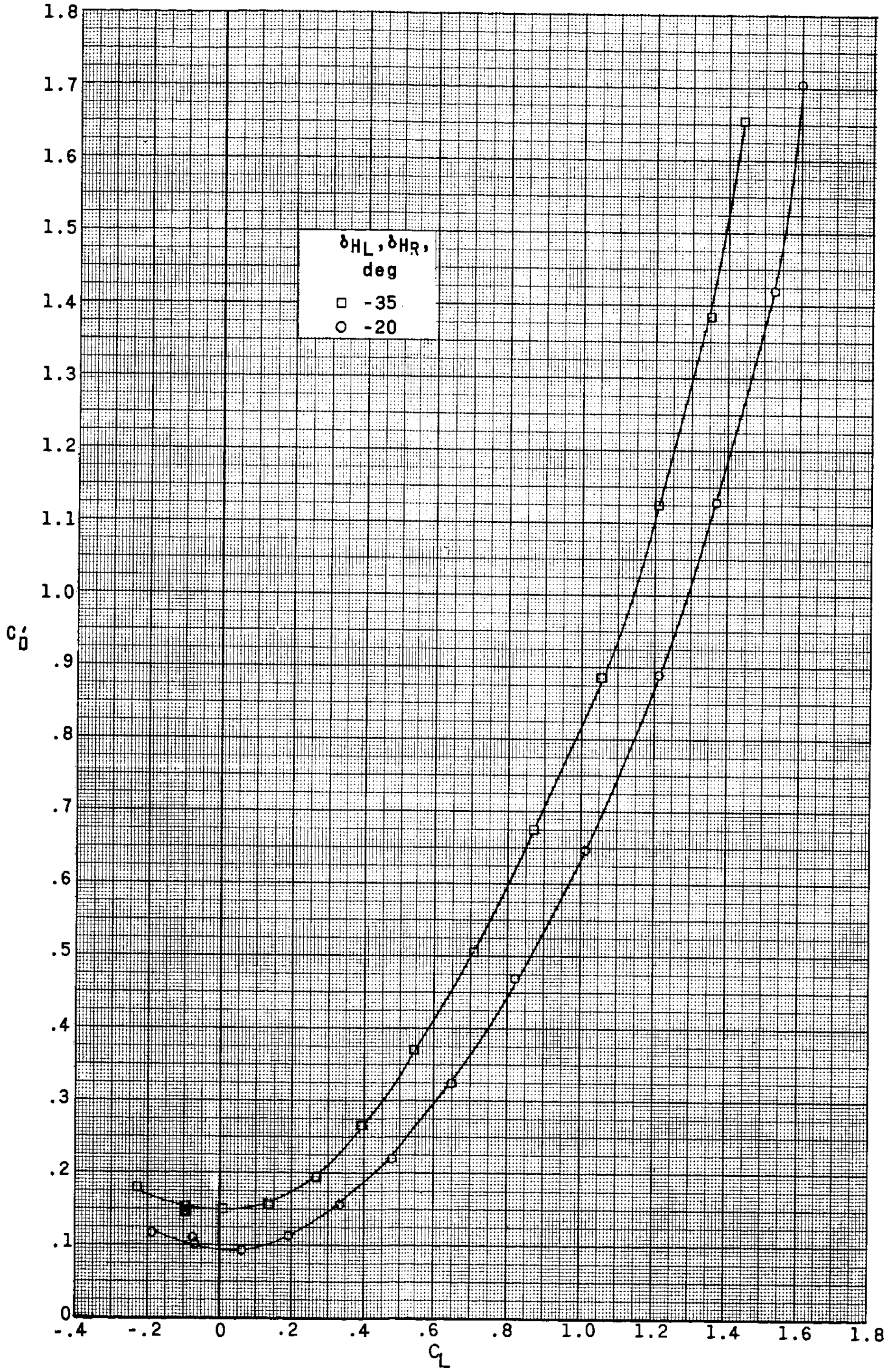

(b) Concluded.

Figure 10.- Continued.

[redacted]

[redacted]

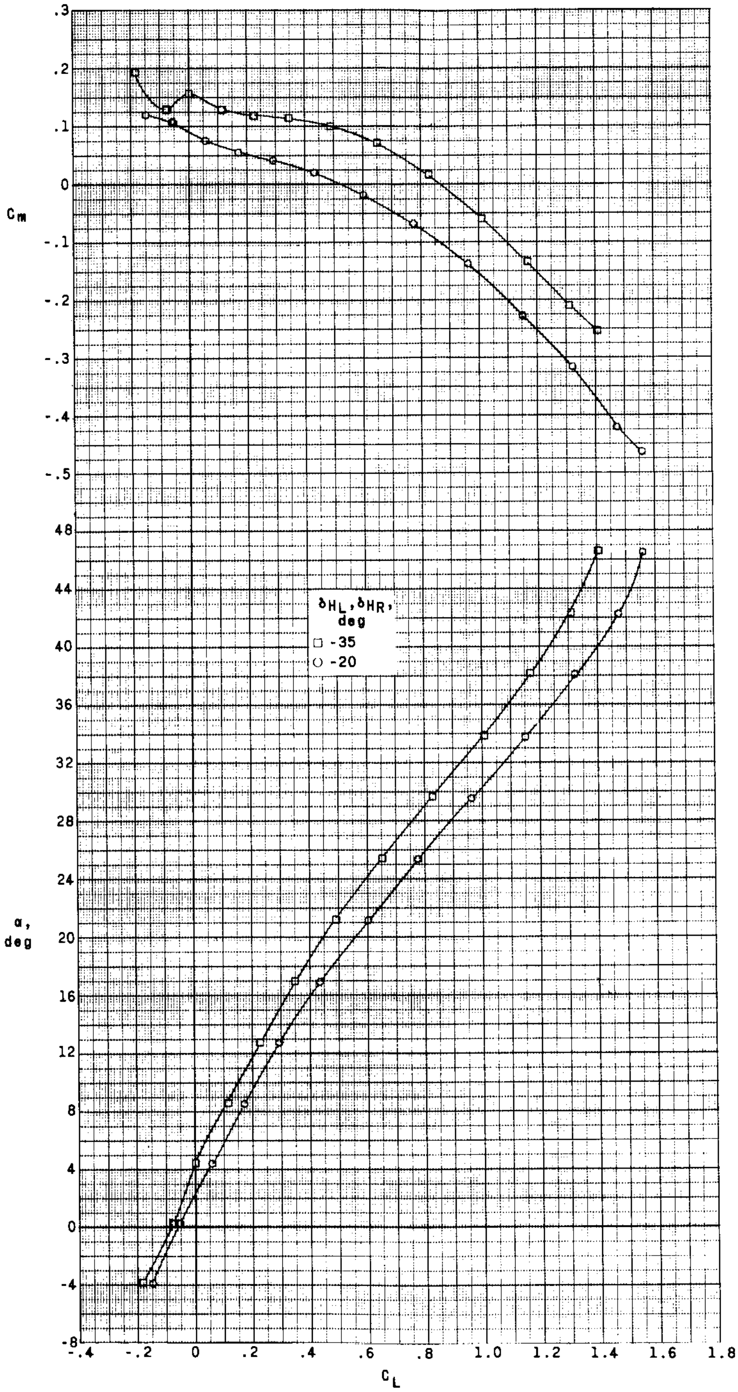

(c) M = 4.65.

Figure 10.- Continued.

[redacted]

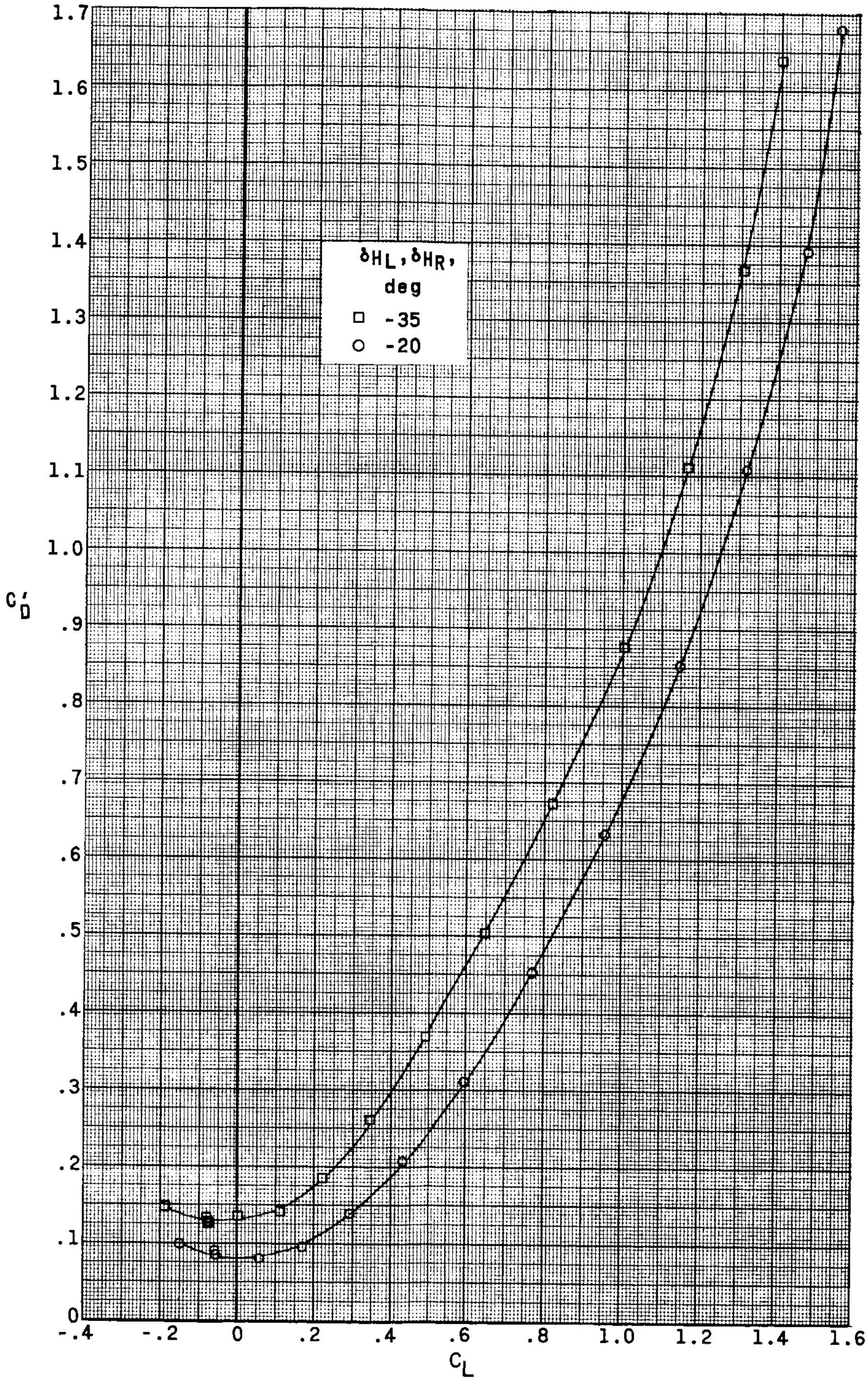

(c) Concluded.

Figure 10.- Concluded.

[redacted]

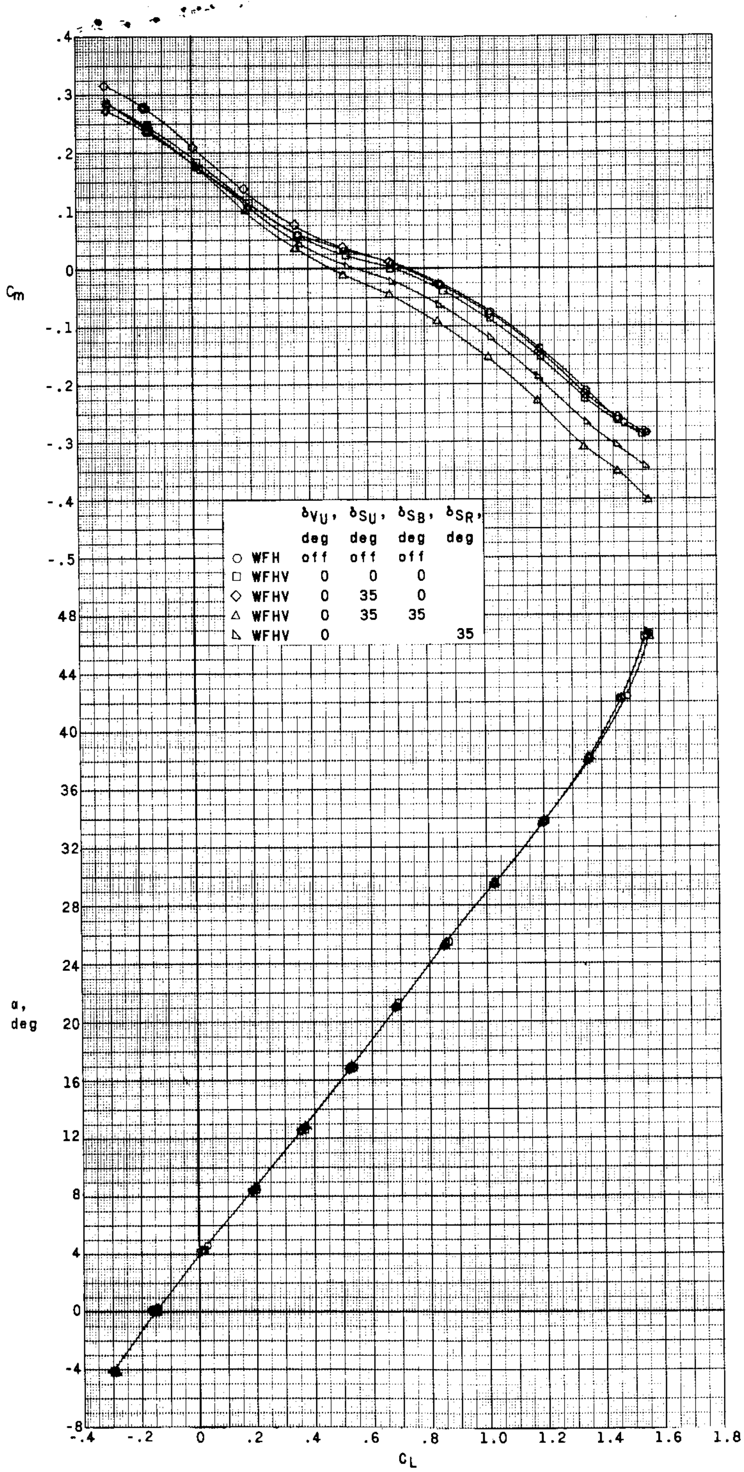

(a) M = 2.96.

Figure 11.- Effect of various configurations on aerodynamic characteristics in pitch with $\delta_{H_L} = \delta_{H_R} = -35^{\circ}$. $\beta = 0^{\circ}$; jettisonable portion of lower vertical stabilizer off.

[redacted]

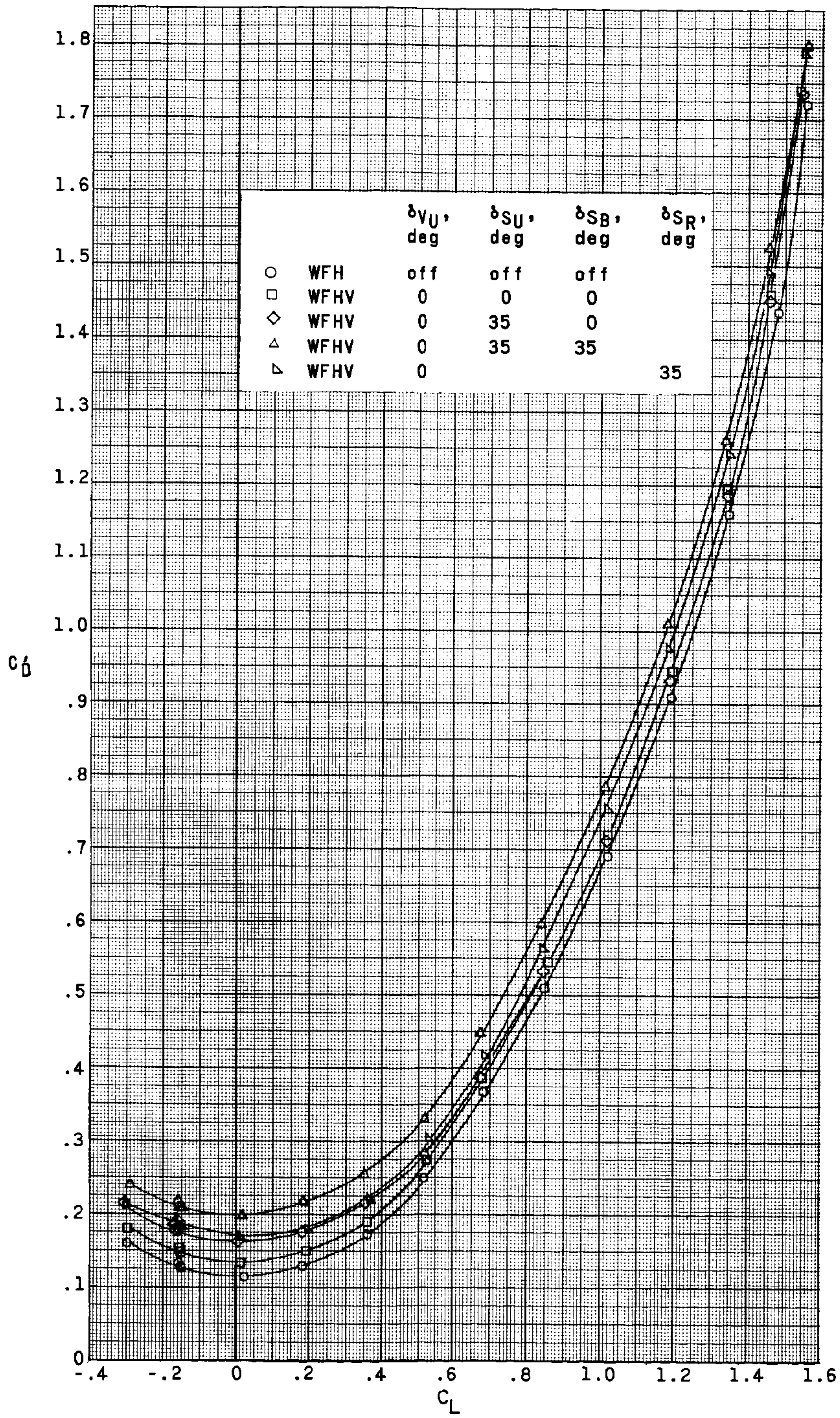

(a) Concluded.

Figure 11.- Continued.

[redacted]

[redacted]

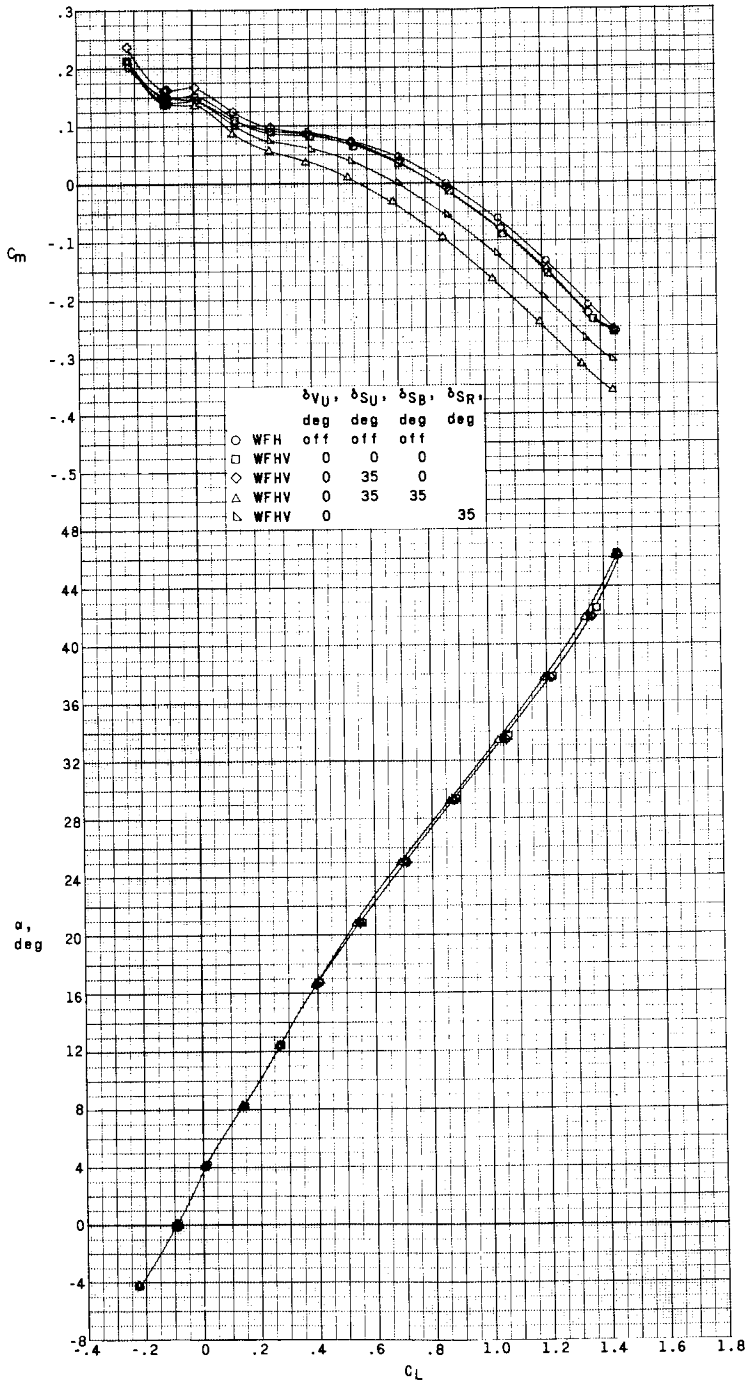

(b) M = 3.96.

Figure 11.- Continued.

[redacted]

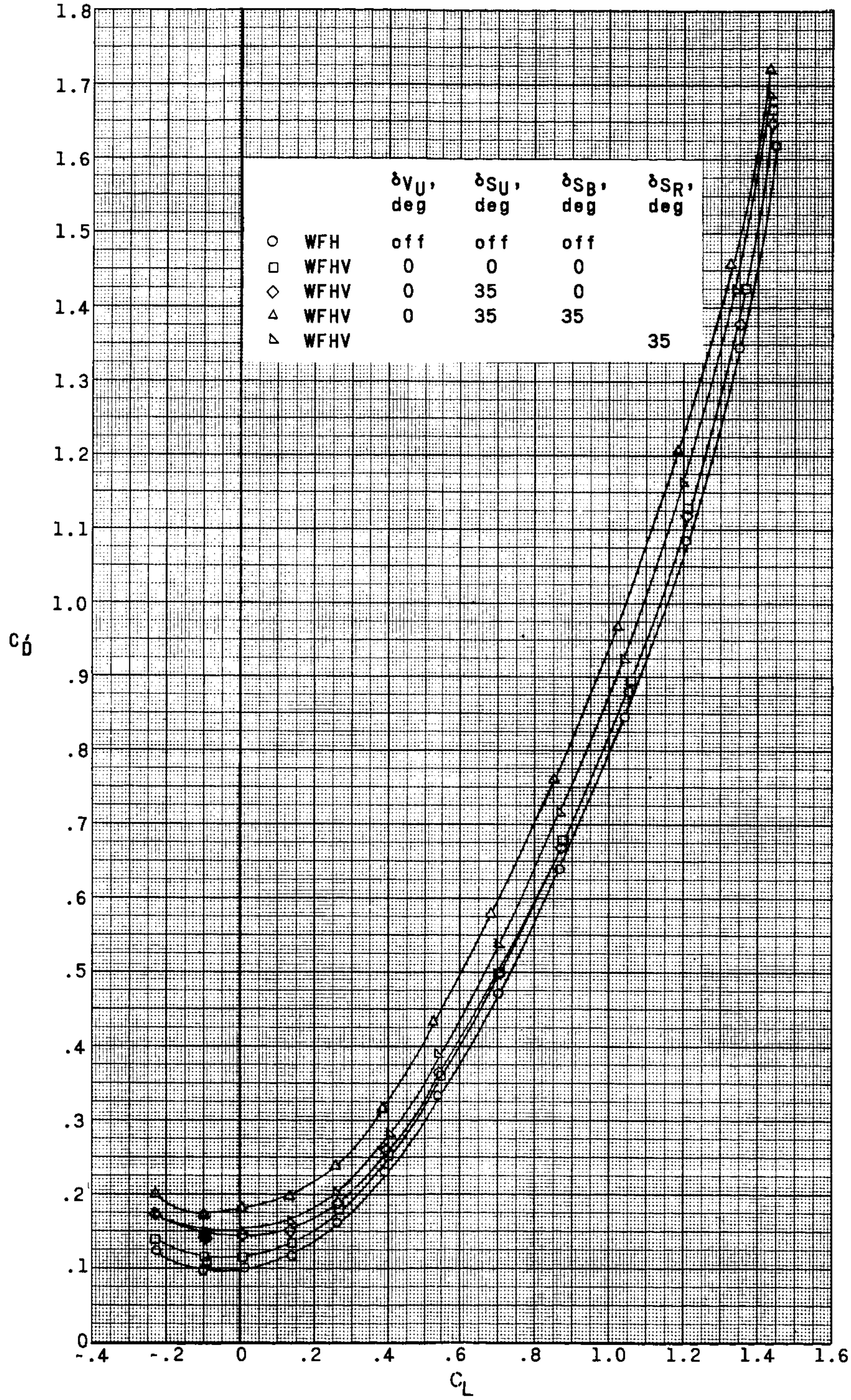

(b) Concluded.

Figure 11.- Continued.

[redacted]

[redacted]

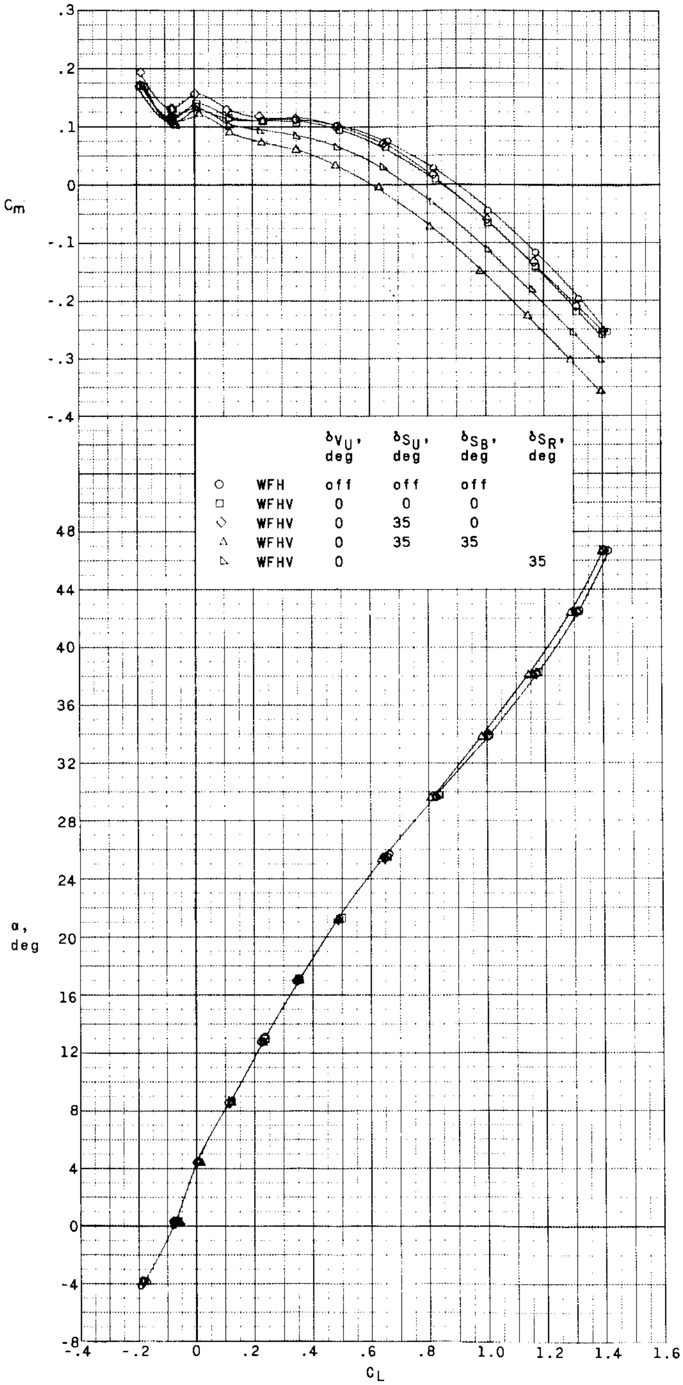

(c) M = 4.65.

Figure 11.- Continued.

[redacted]

DE[redacted]IFIED

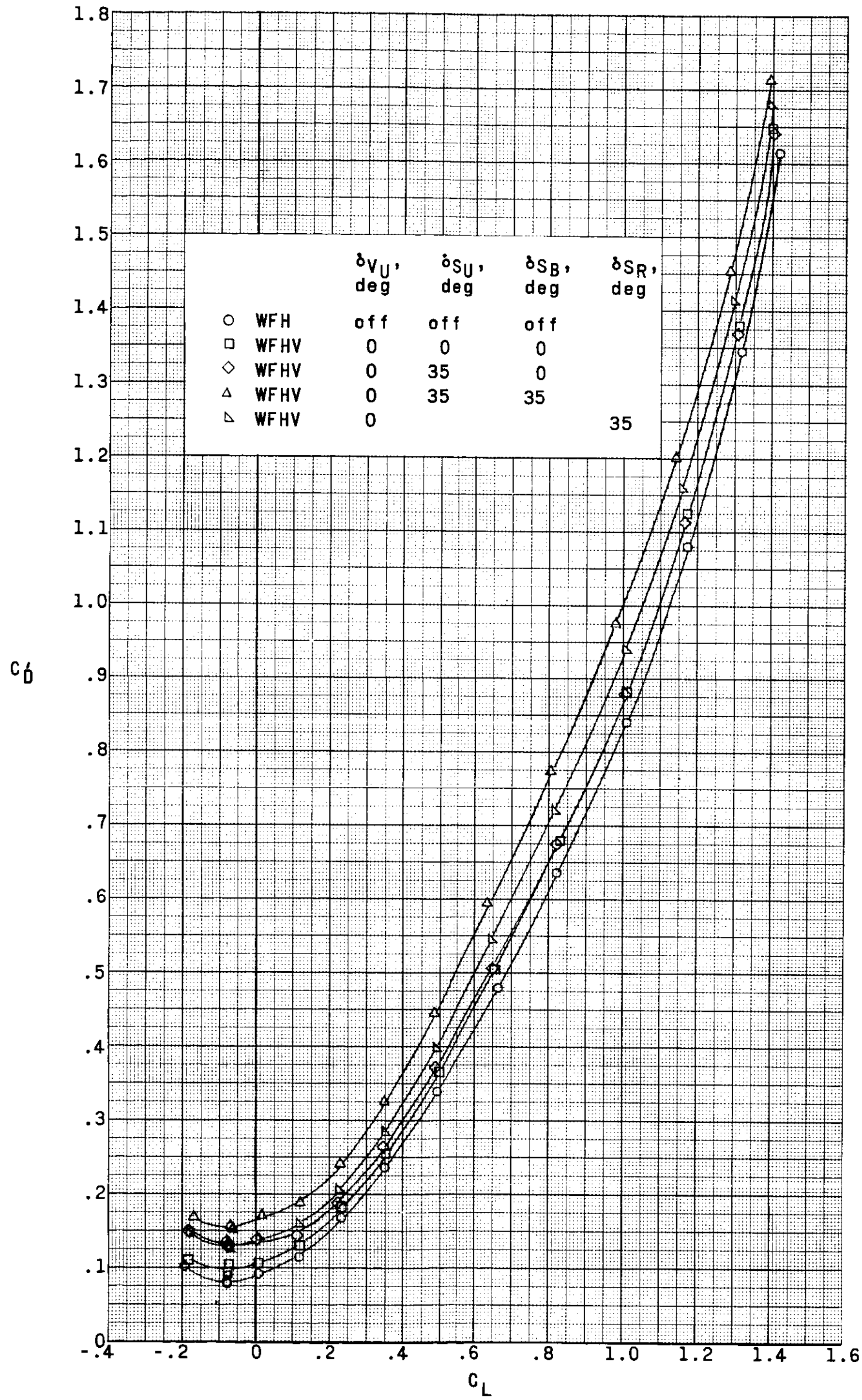

(c) Concluded.

Figure 11.- Concluded.

[redacted]

[redacted]

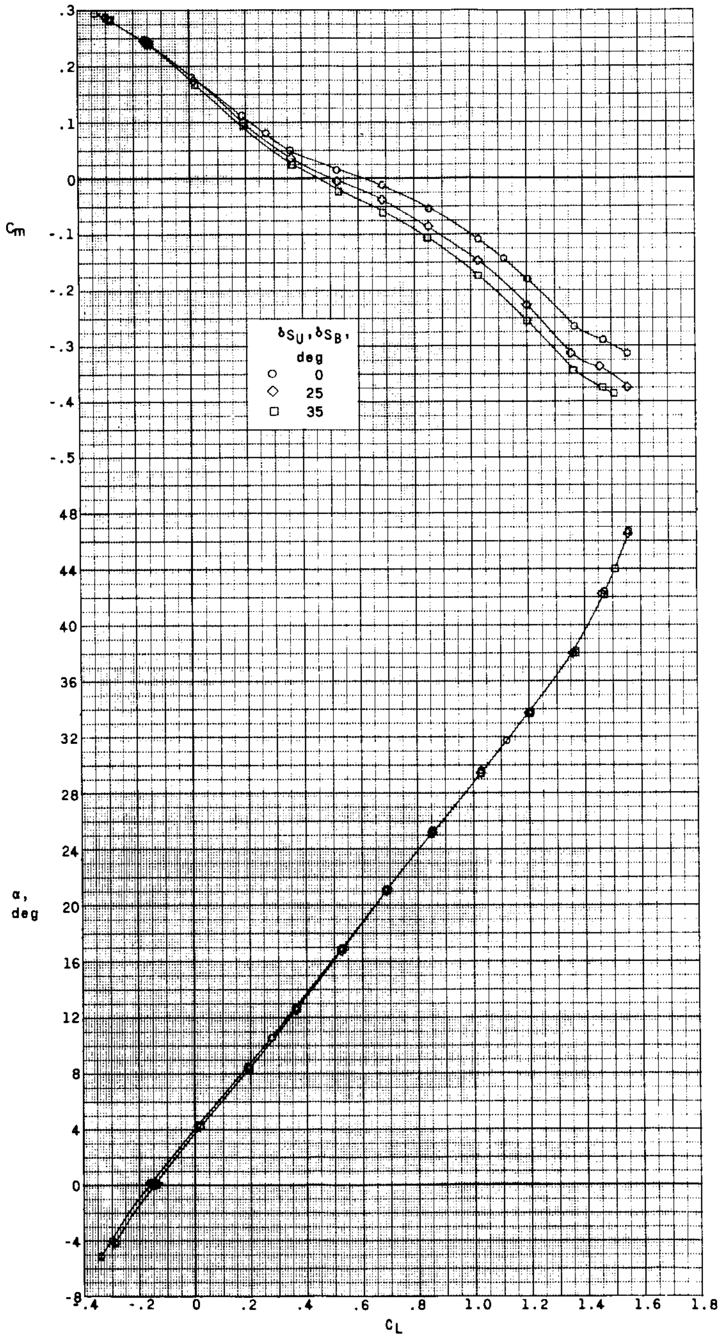

(a) M = 2.96.

Figure 12.- Effect of speed-brake deflections on aerodynamic characteristics in pitch with $\delta_{H_L} = \delta_{H_R} = -35^{\circ}$. $\beta = 0^{\circ}$; jettisonable portion of lower vertical stabilizer on; $\delta_{V_U} = \delta_{V_J} = 0^{\circ}$; WFHVJ.

[redacted]

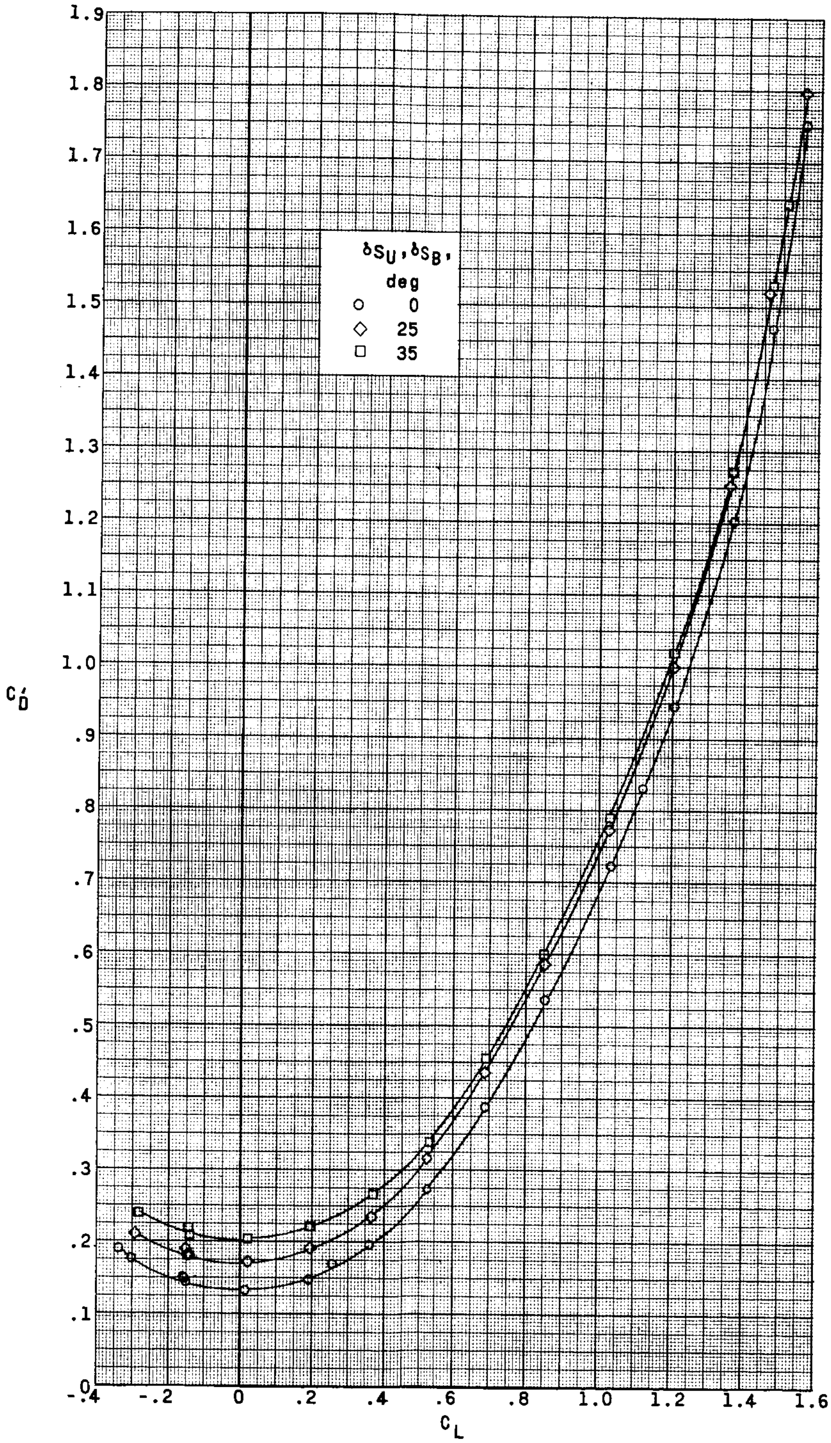

(a) Concluded.

Figure 12.- Continued.

[redacted]

[redacted]

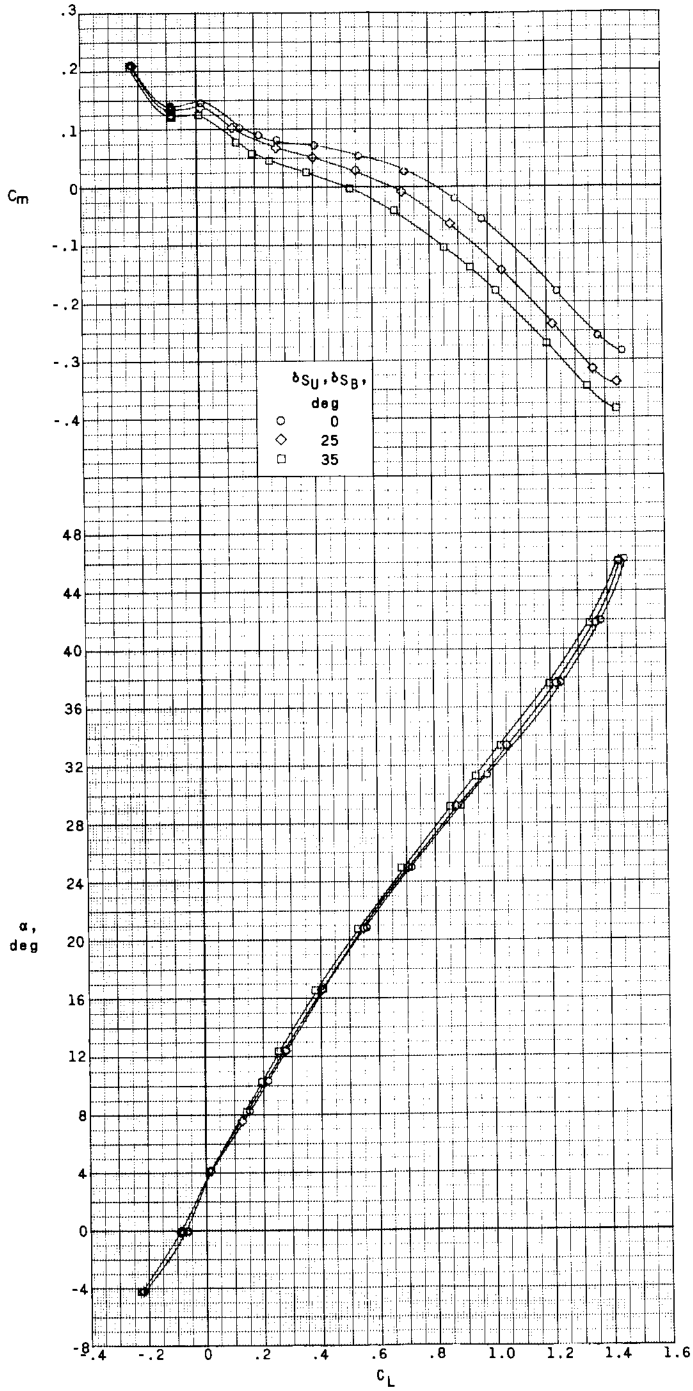

(b) M = 3.96.

Figure 12.- Continued.

[redacted]

[redacted]

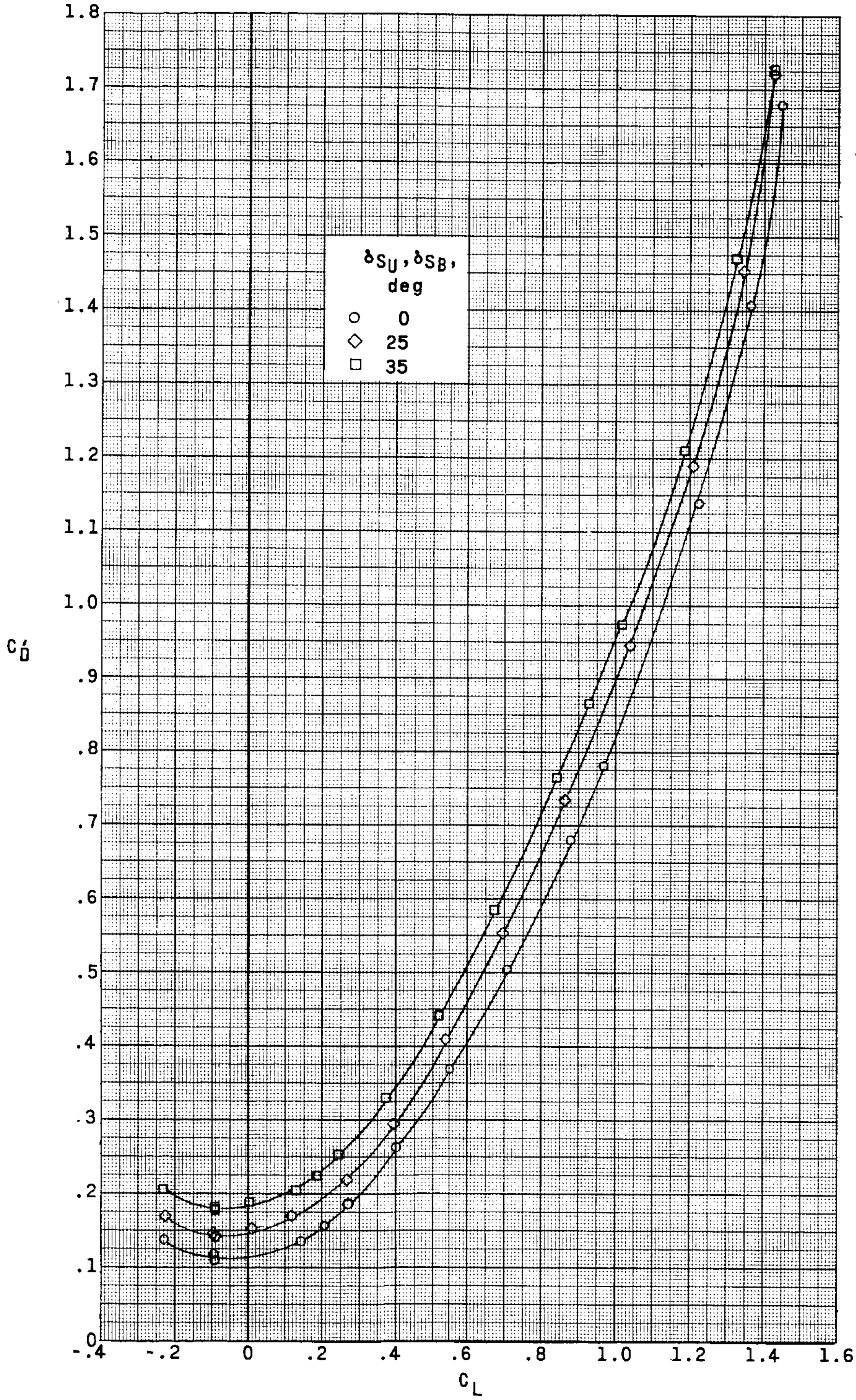

(b) Concluded.

Figure 12.- Continued.

[redacted]

[redacted]

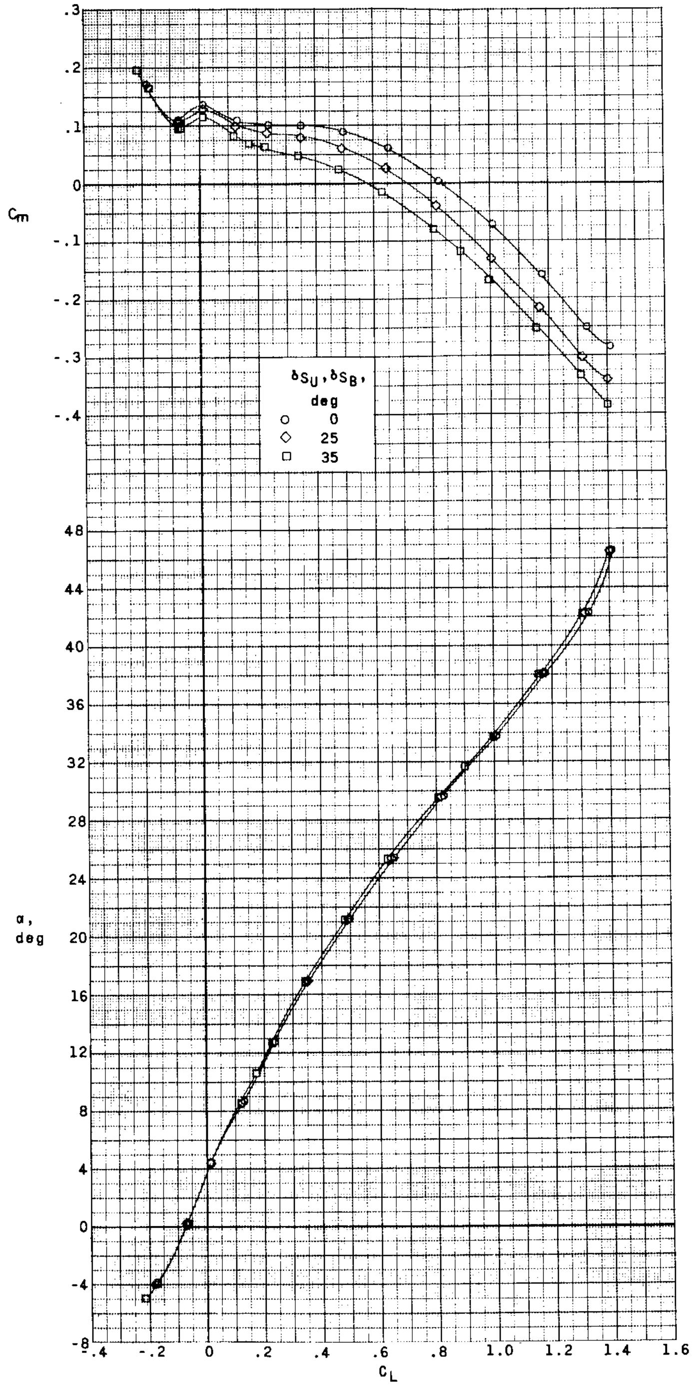

(c) M = 4.65.

Figure 12.- Continued.

[redacted]

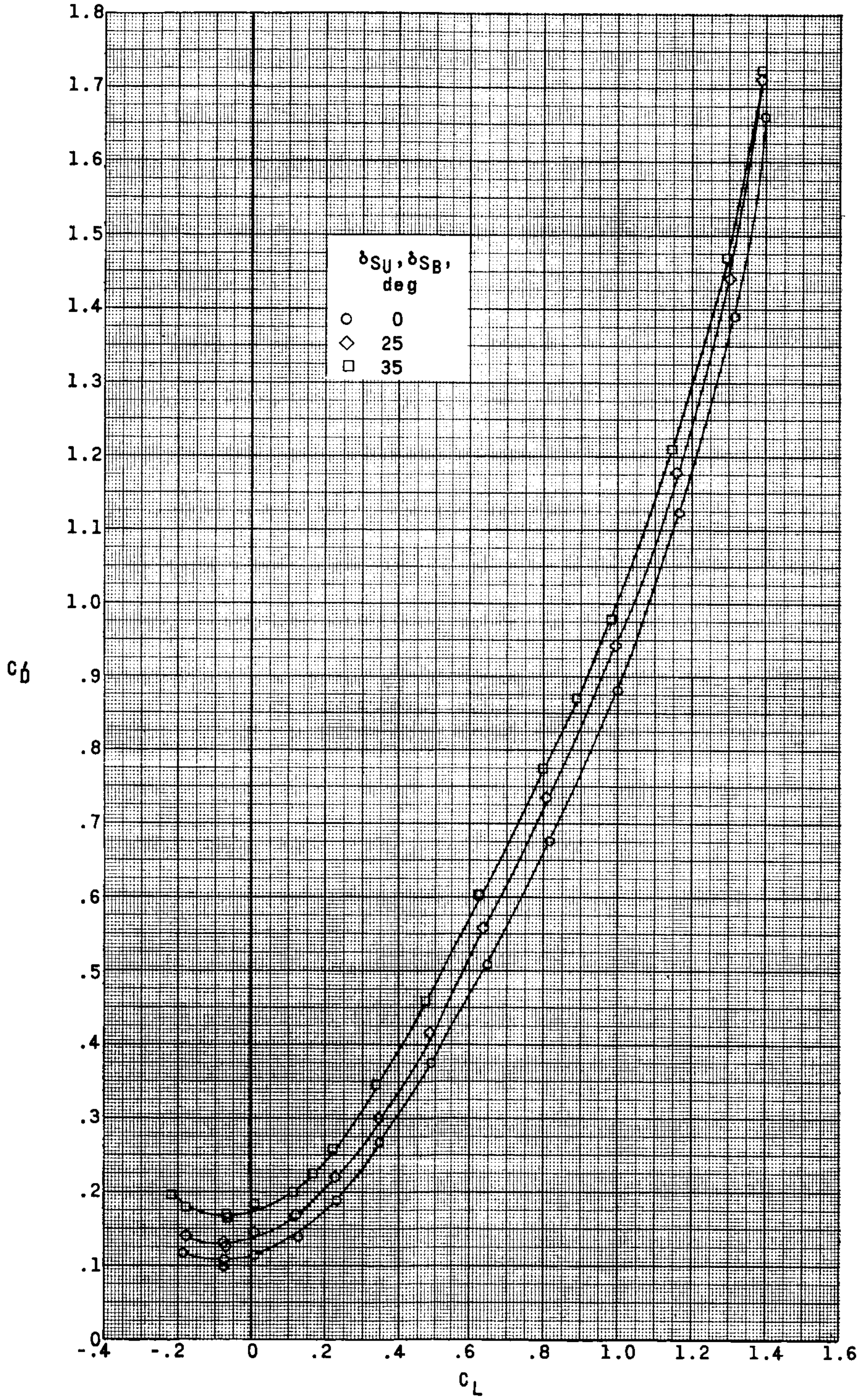

(c) Concluded.

Figure 12.- Concluded.

[redacted]

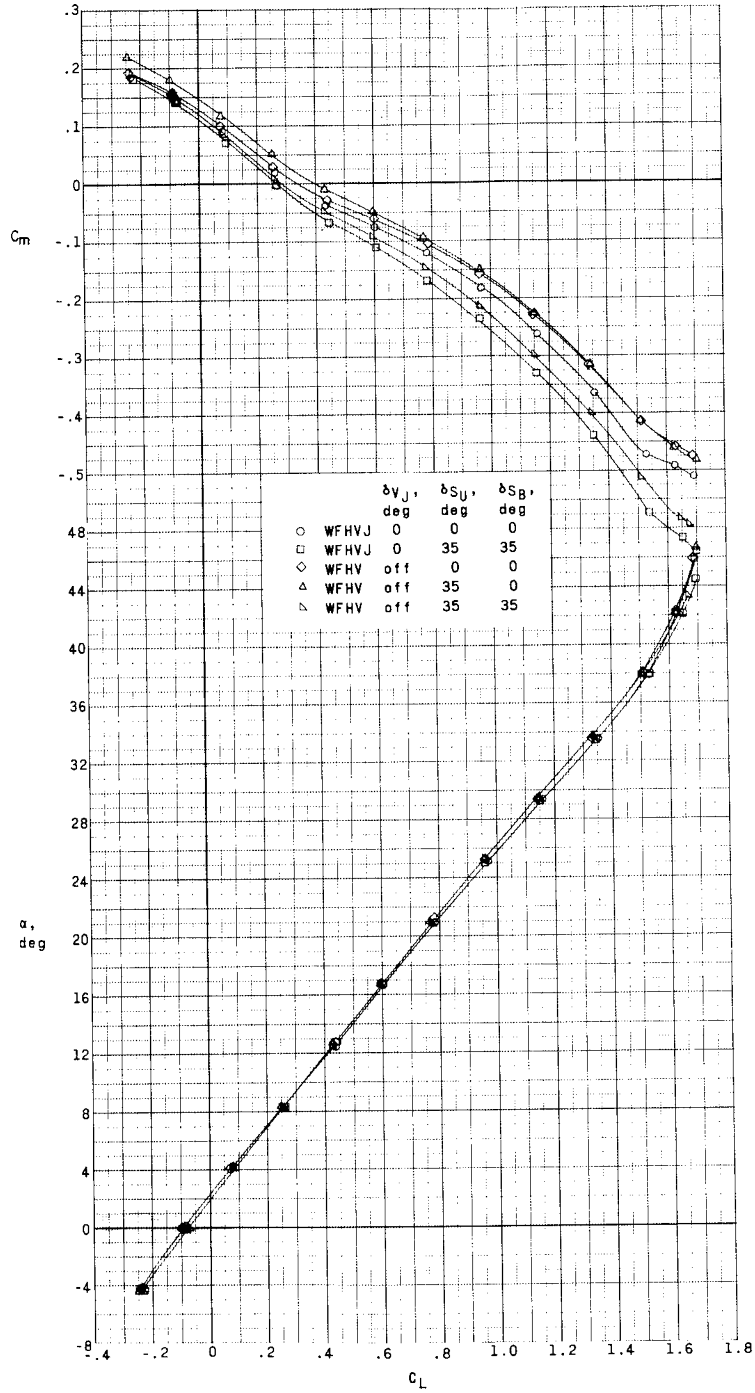

(a) M = 2.96.

Figure 13.- Effect of speed-brake deflections on aerodynamic characteristics in pitch with $\delta_{H_L} = \delta_{H_R} = -20^{\circ}$. $\beta = 0^{\circ}$; $\delta_{V_U} = 0^{\circ}$.

[redacted]

[redacted]

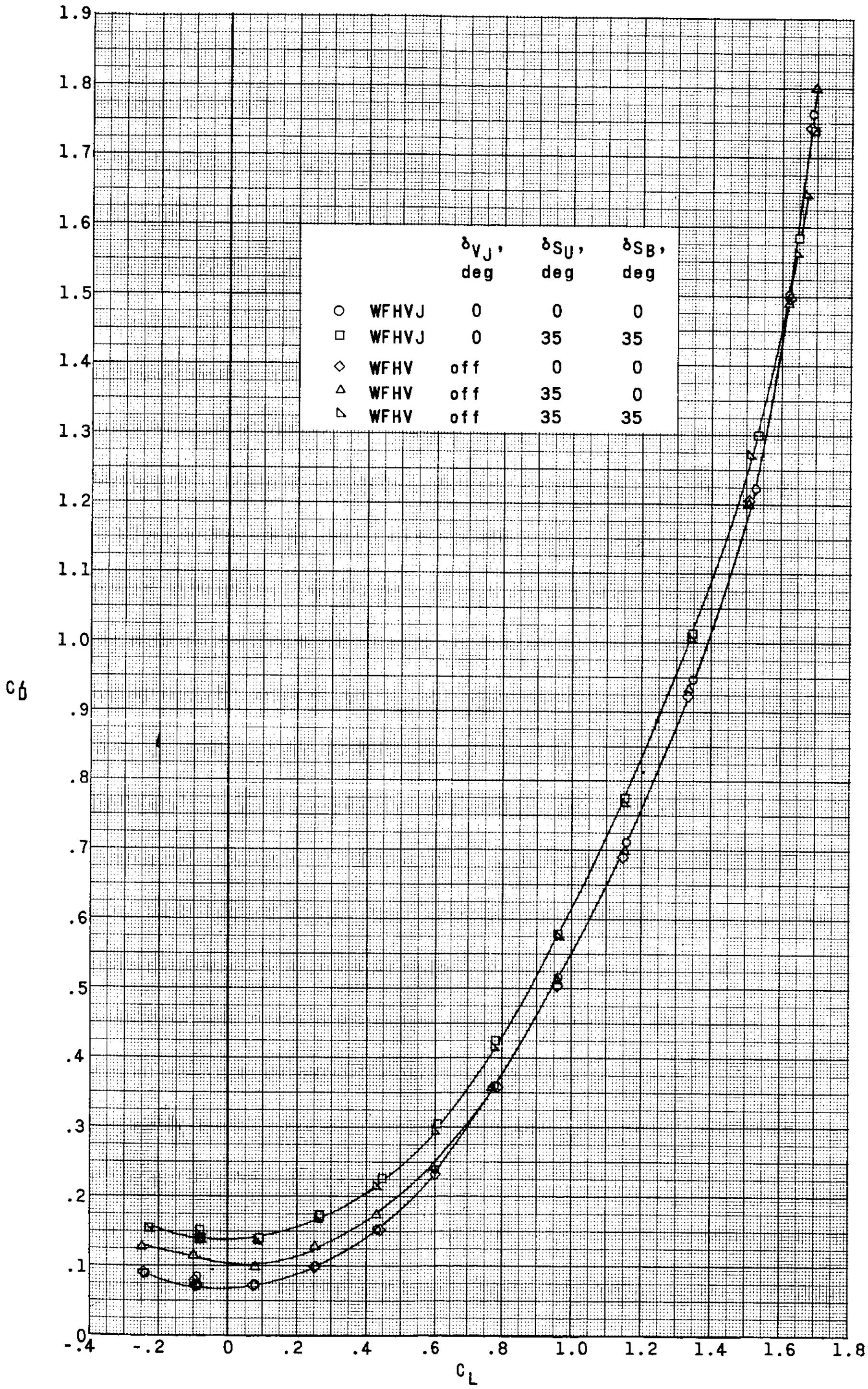

(a) Concluded.

Figure 13.- Continued.

[redacted]

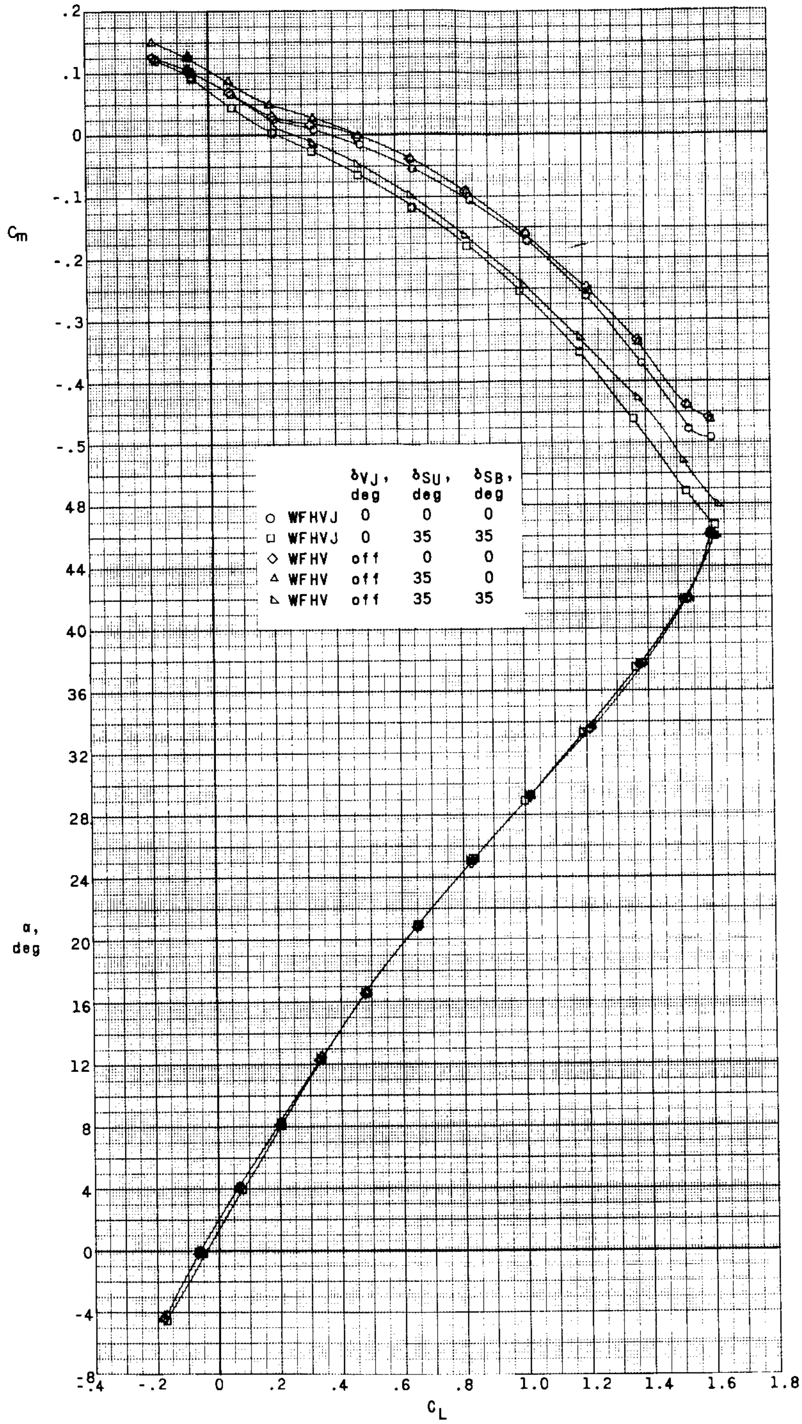

(b) M = 3.96.

Figure 13.- Continued.

[redacted]

[redacted]

UNCLASSIFIED

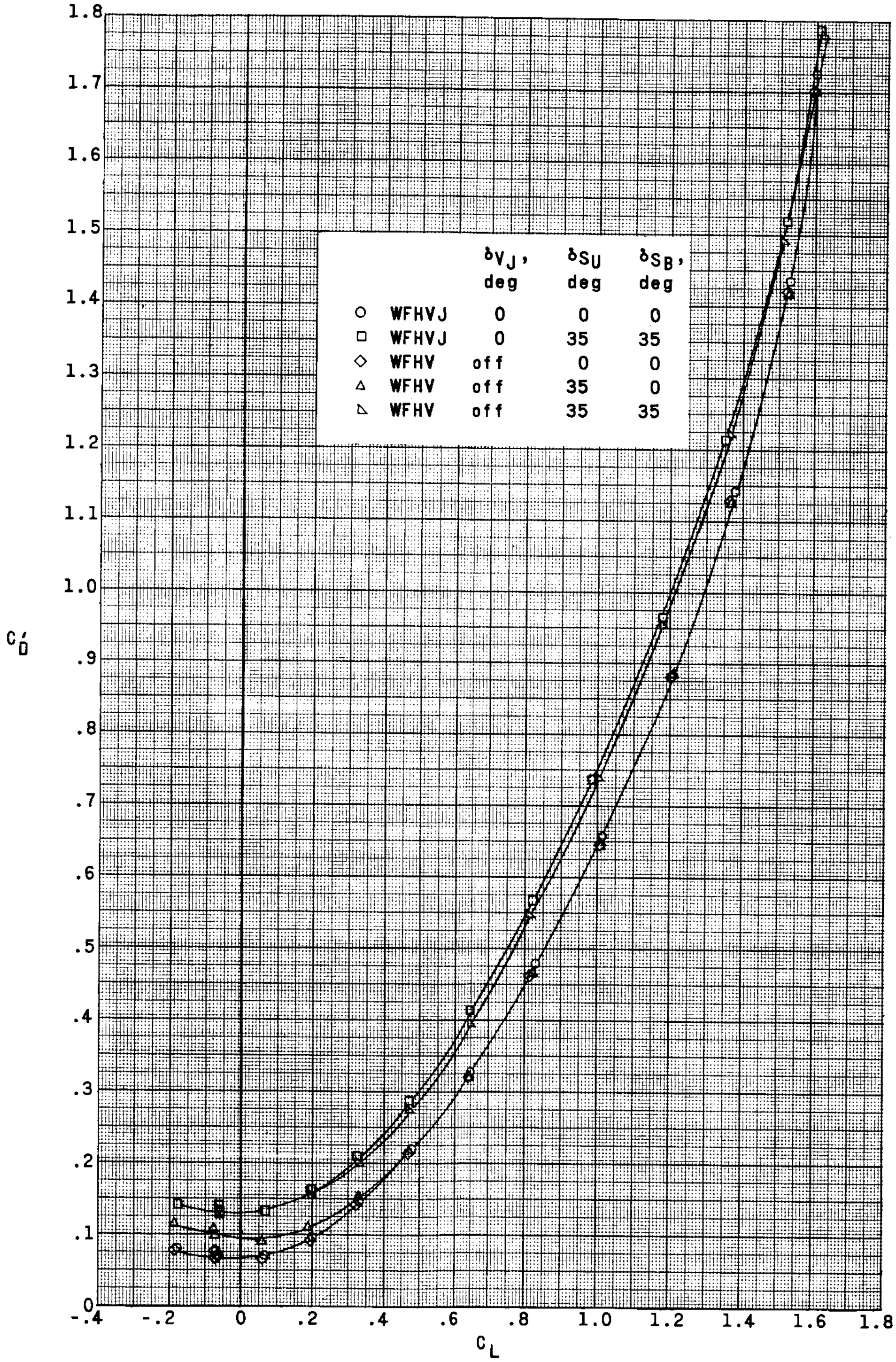

(b) Concluded.

Figure 13.- Continued.

[redacted]

[redacted]

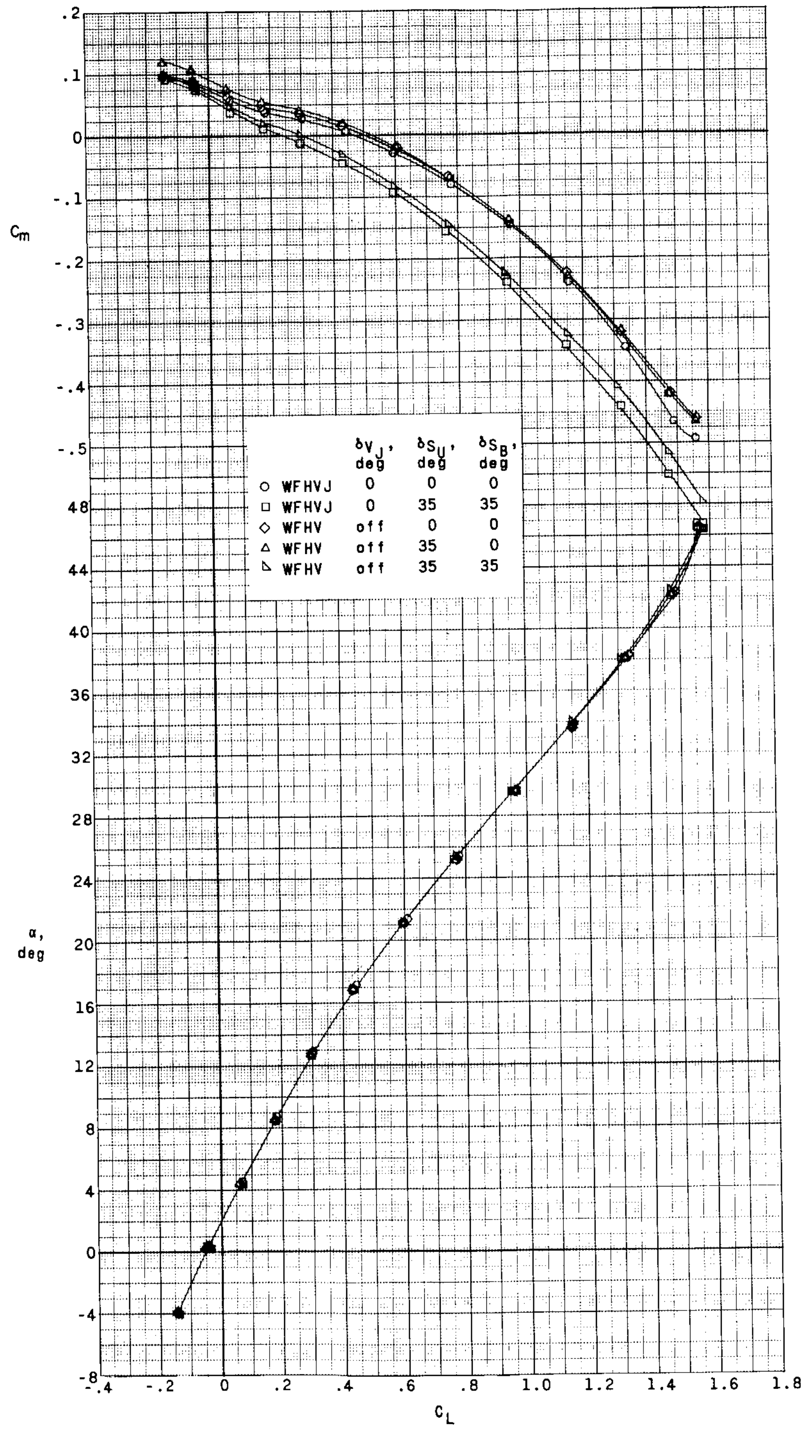

(c) M = 4.65.

Figure 13.- Continued.

[redacted]

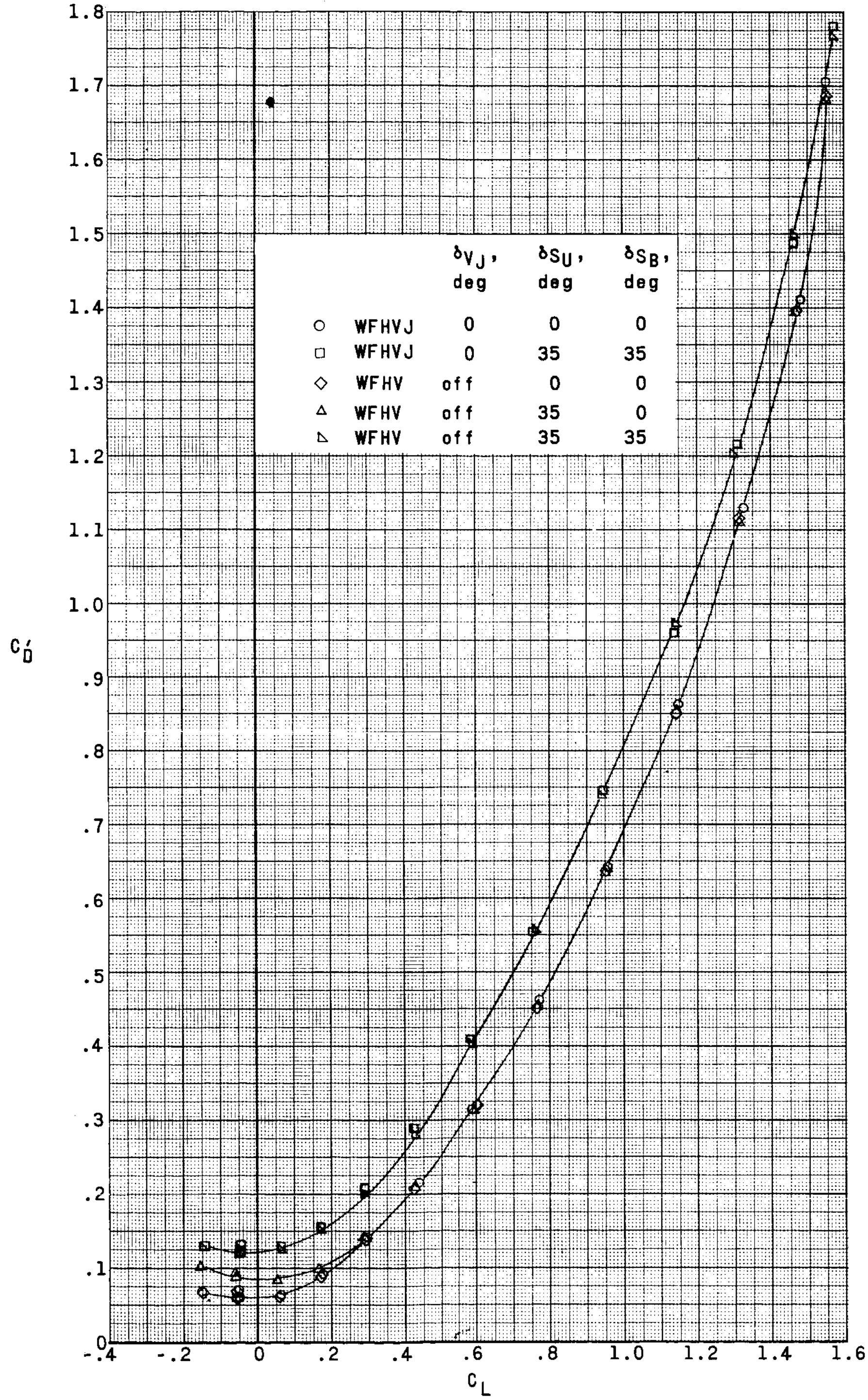

(c) Concluded.

Figure 13.- Concluded.

[redacted]

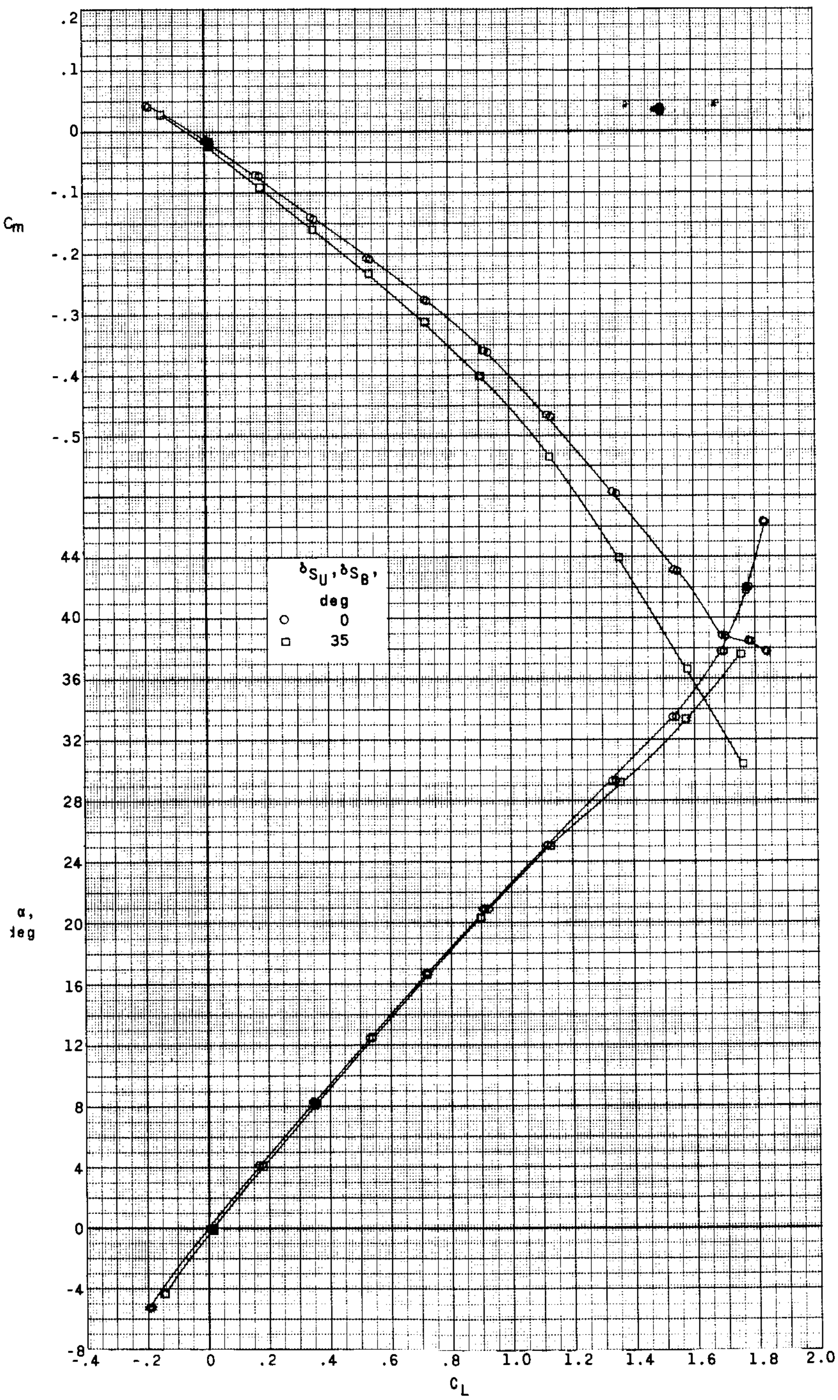

(a) M = 2.96.

Figure 14.- Effect of speed-brake deflections on aerodynamic characteristics in pitch with $\delta_{H_L} = \delta_{H_R} = 0^{\circ}$. $\beta = 0^{\circ}$; $\delta_{V_U} = \delta_{V_J} = 0^{\circ}$; WFHVJ.

[redacted]

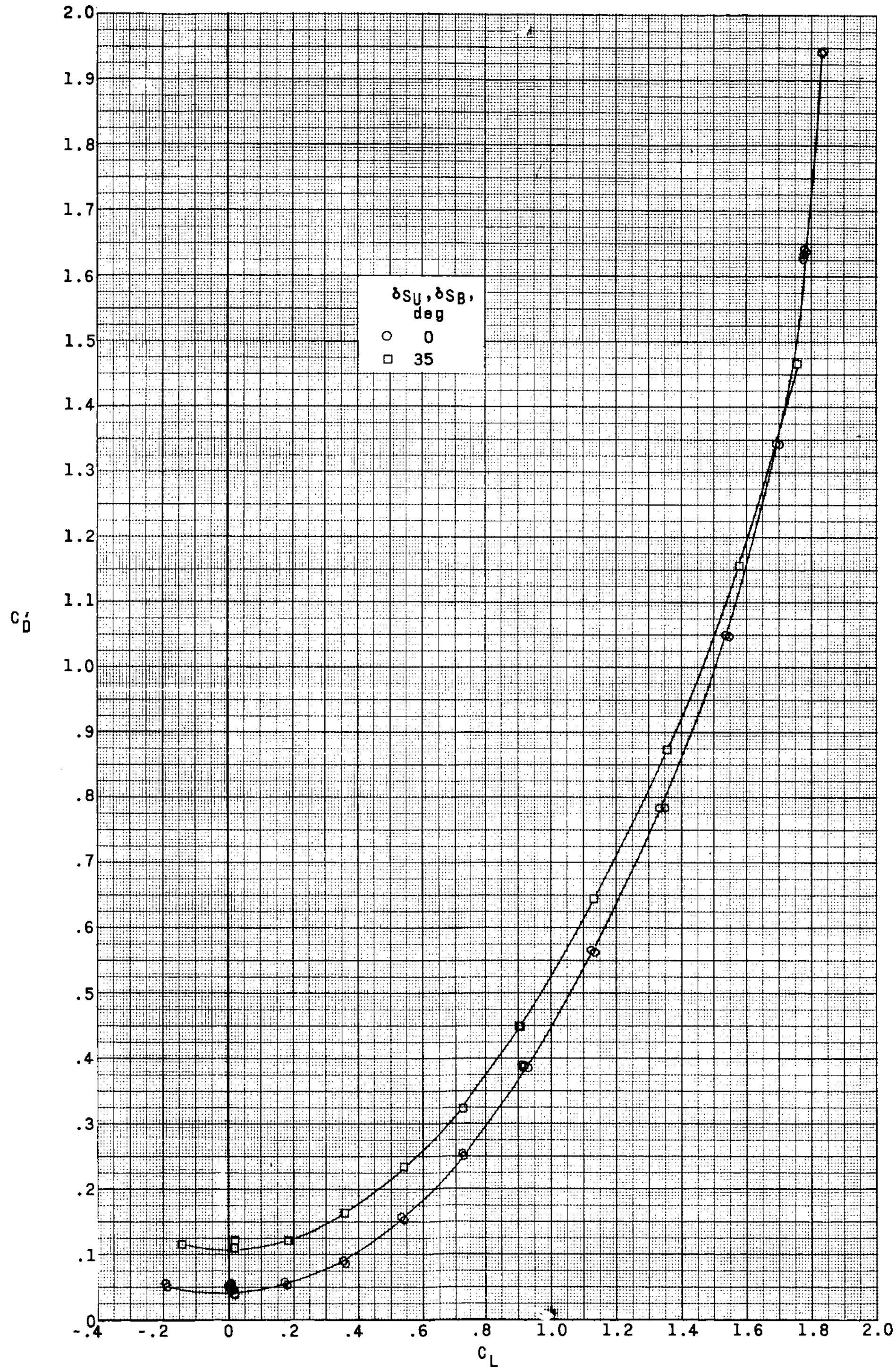

(a) Concluded.

Figure 14.- Continued.

[redacted]

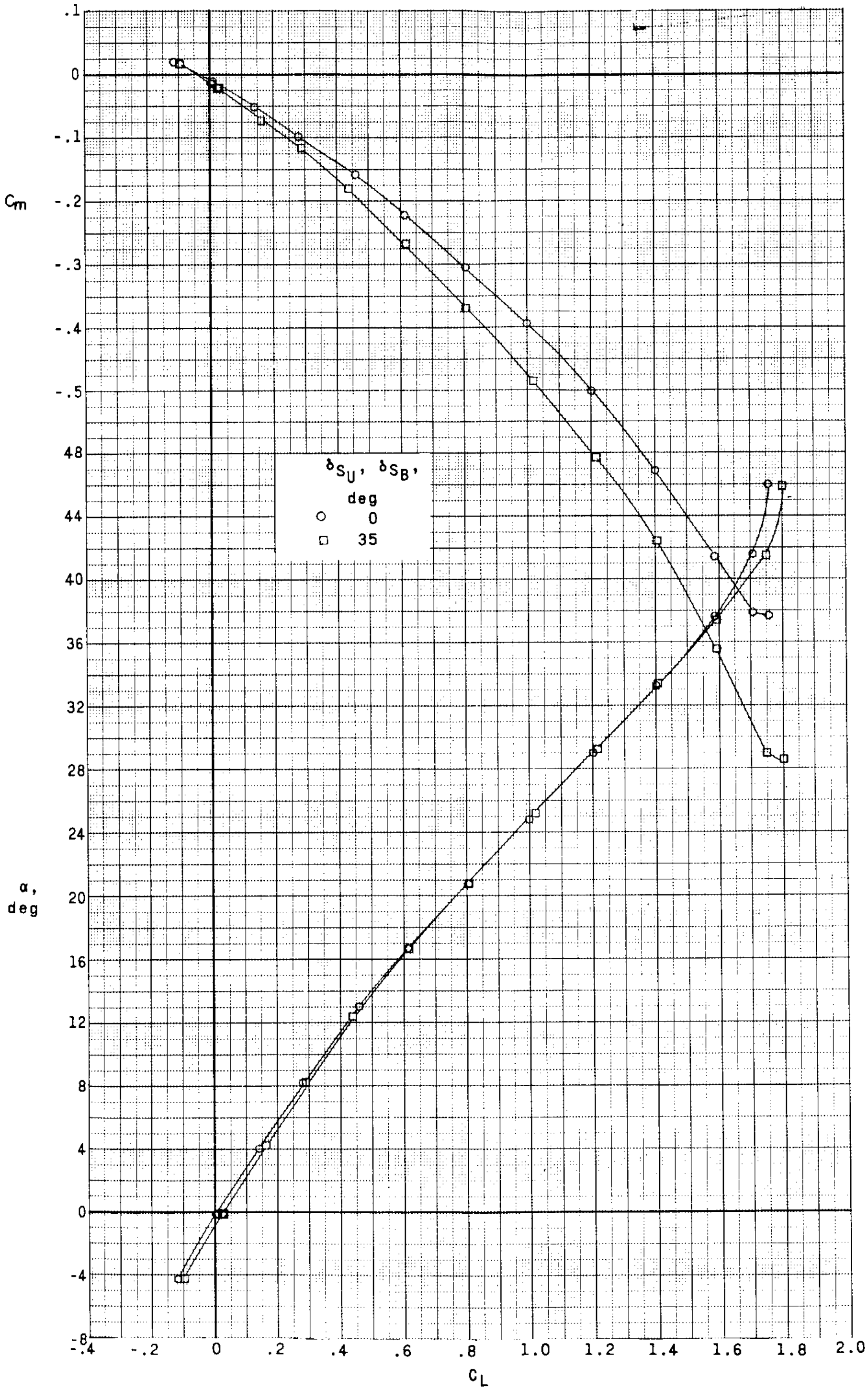

(b) M = 3.96.

Figure 14.- Continued.

[redacted]

[redacted]

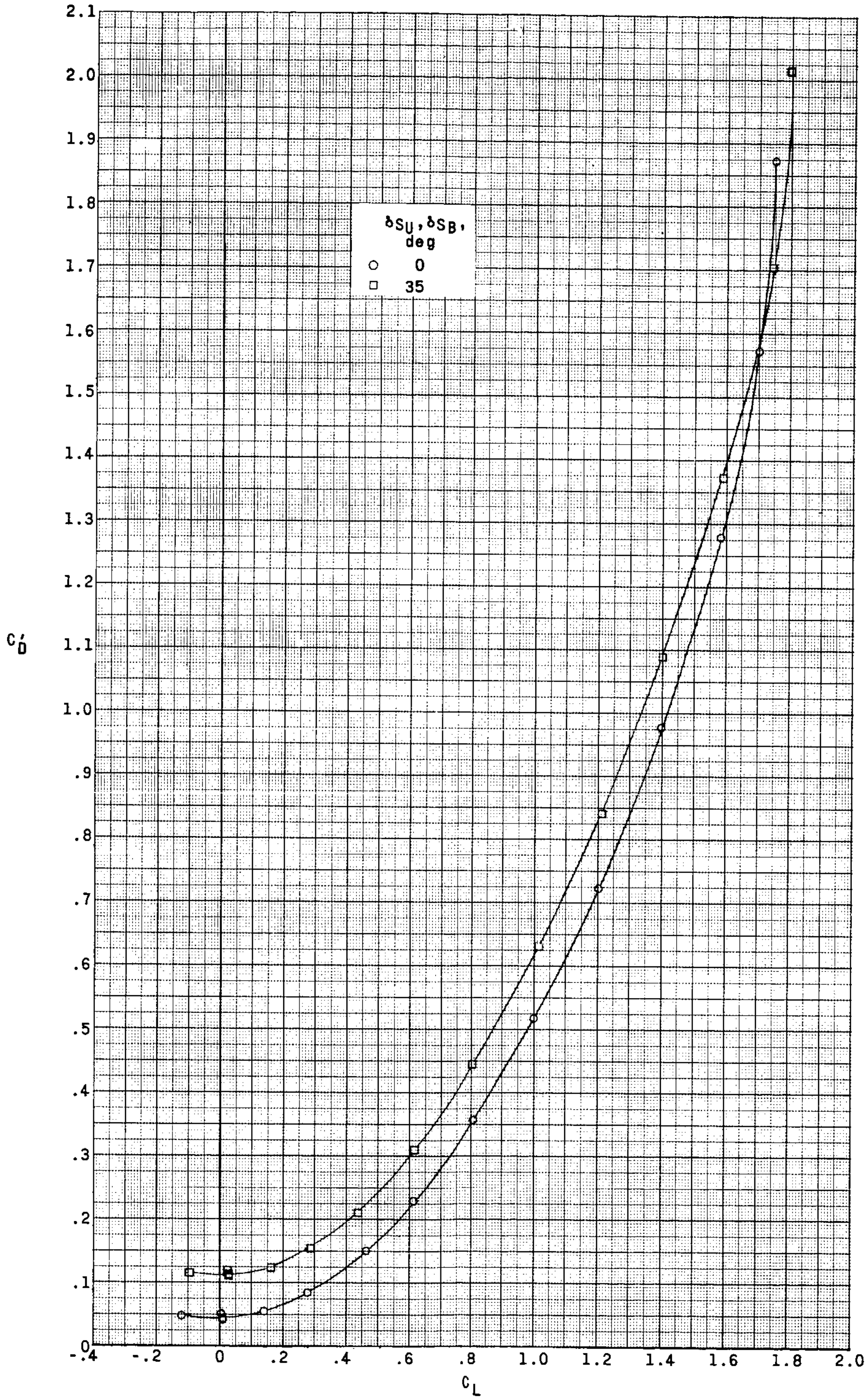

(b) Concluded.

Figure 14.- Continued.

[redacted]

[redacted]

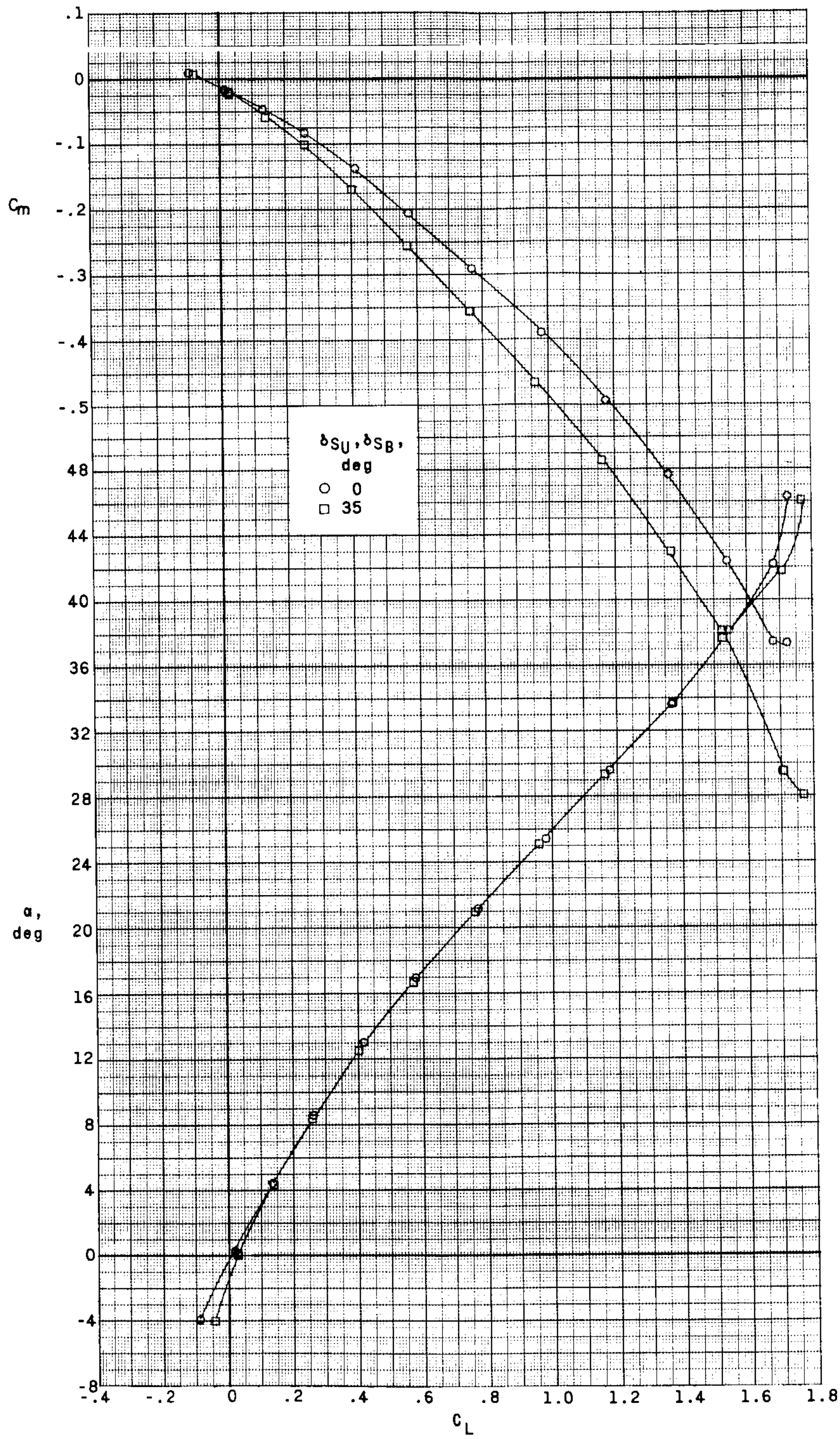

(c) M = 4.65.

Figure 14.- Continued.

[redacted]

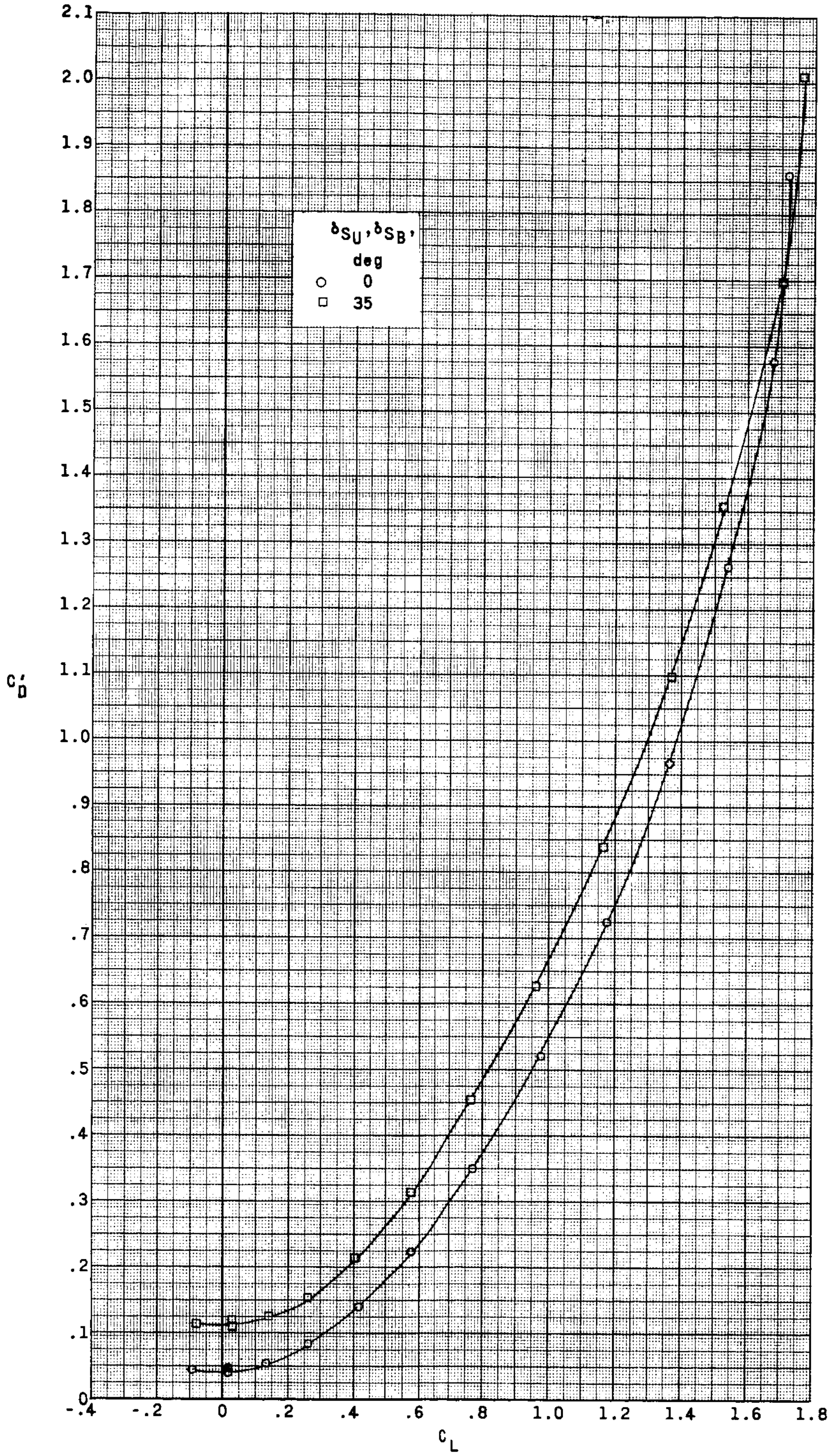

(c) Concluded.

Figure 14.- Concluded.

[redacted]

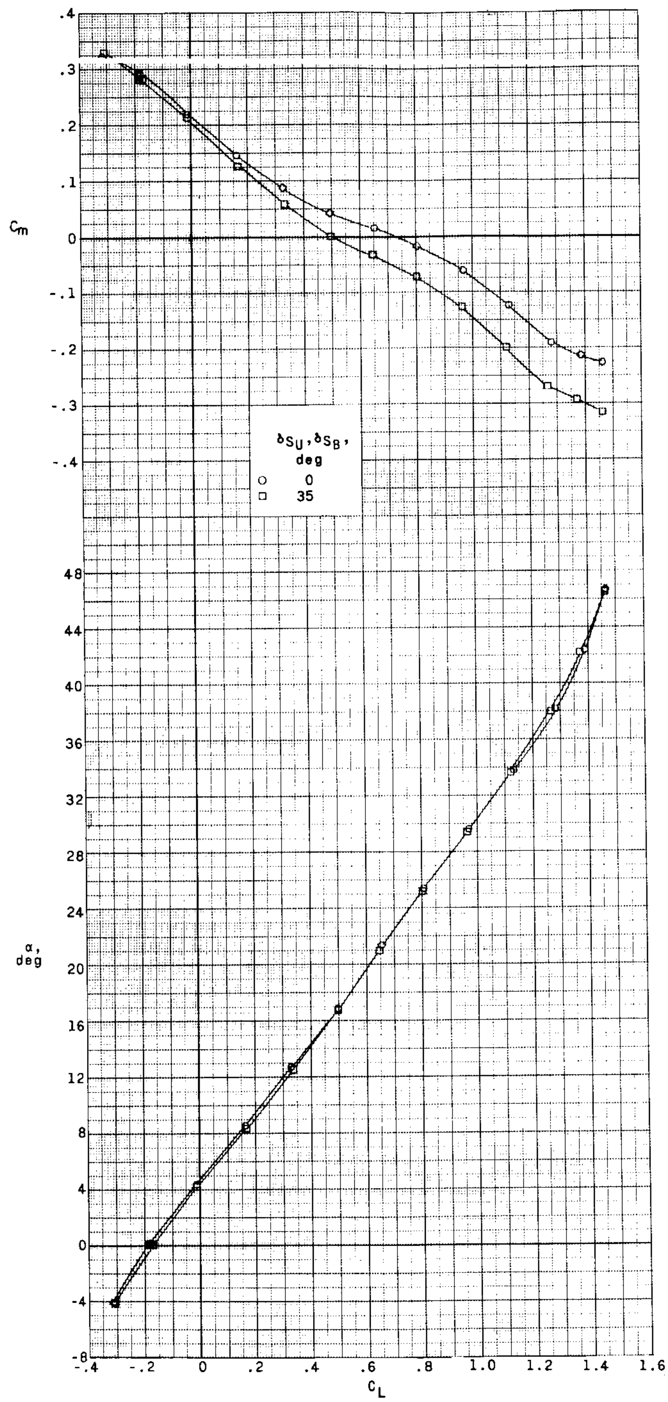

(a) M = 2.96.

Figure 15.- Effect of speed-brake deflections on aerodynamic characteristics in pitch with $\delta_{H_L} = \delta_{H_R} = -45^{\circ}$. $\beta = 0^{\circ}$; $\delta_{V_U} = \delta_{V_J} = 0^{\circ}$; WFHVJ.

[redacted]

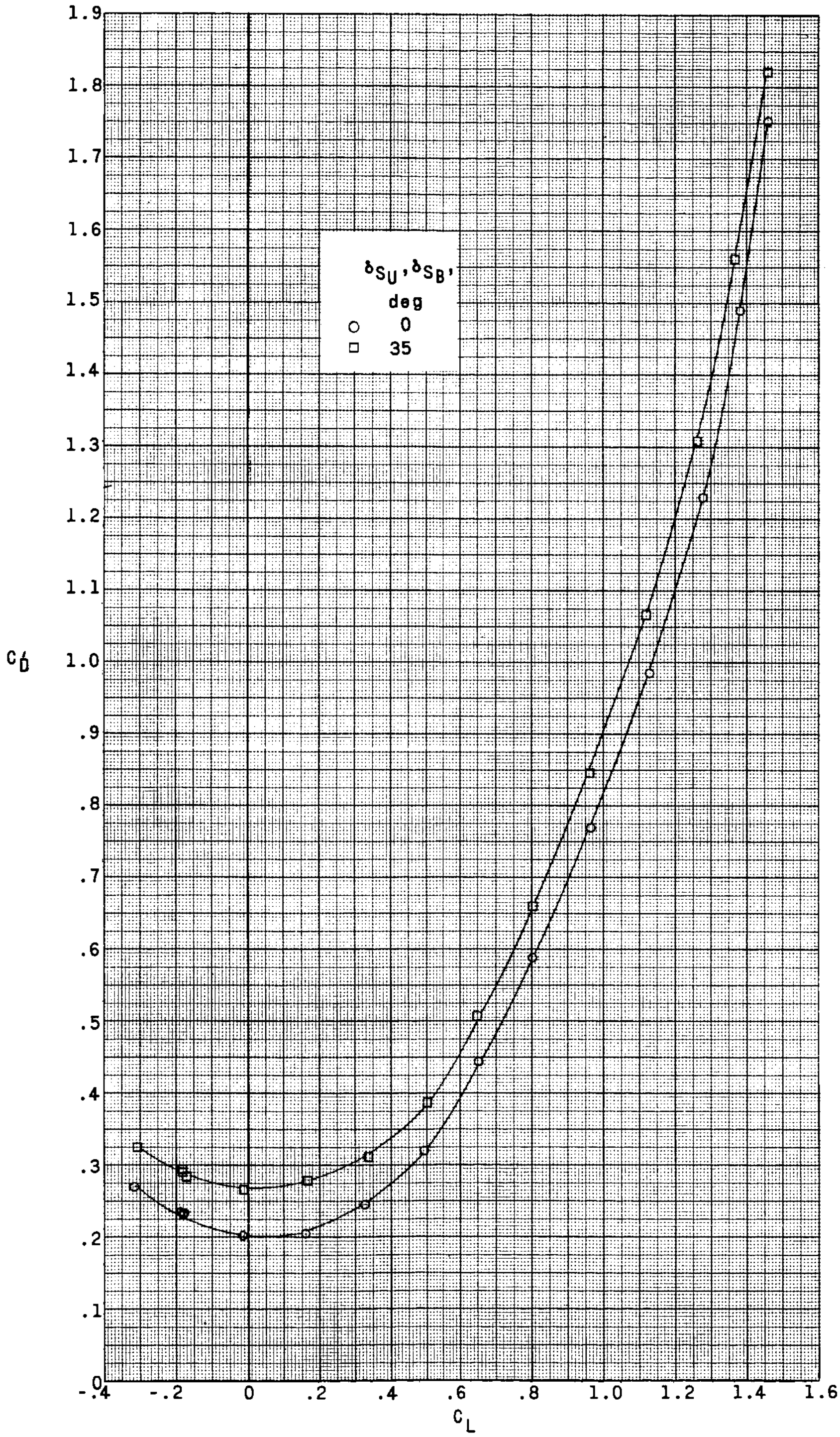

(a) Concluded.

Figure 15.- Continued.

[redacted]

[redacted]

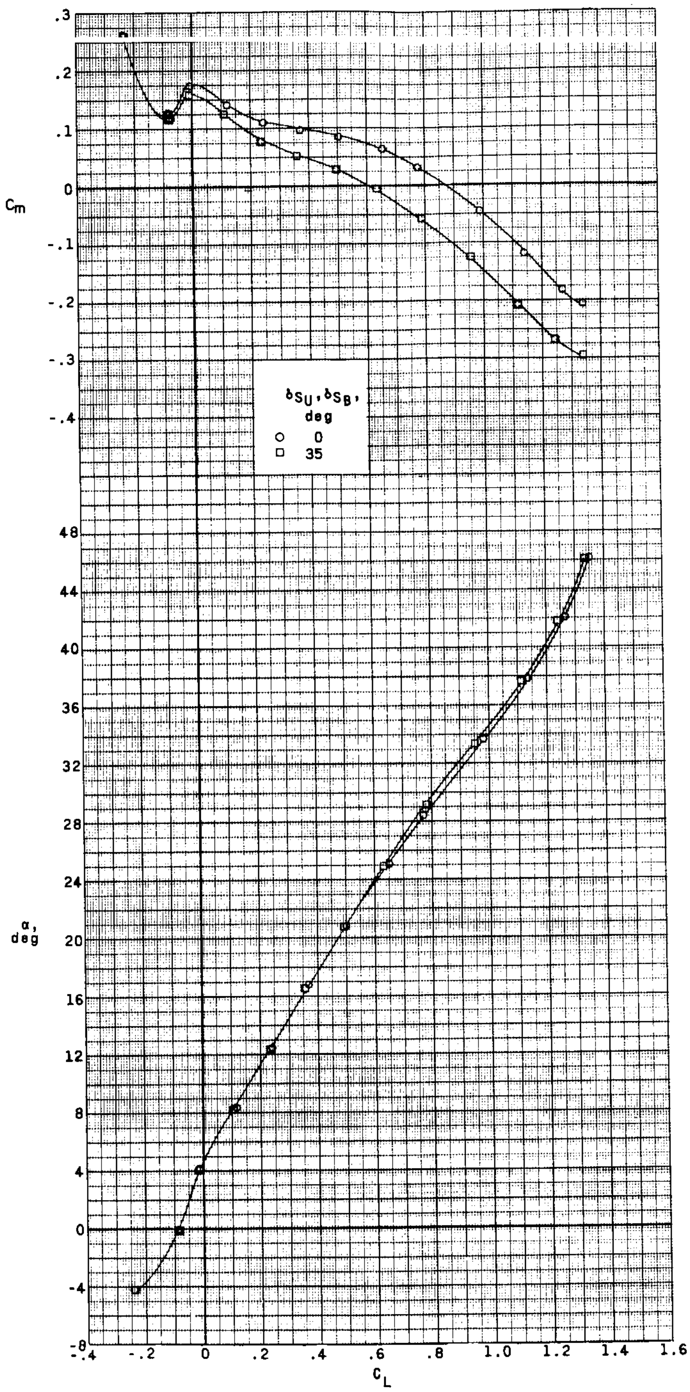

(b) M = 3.96.

Figure 15.- Continued.

[redacted]

[redacted]

UNCLASSIFIED

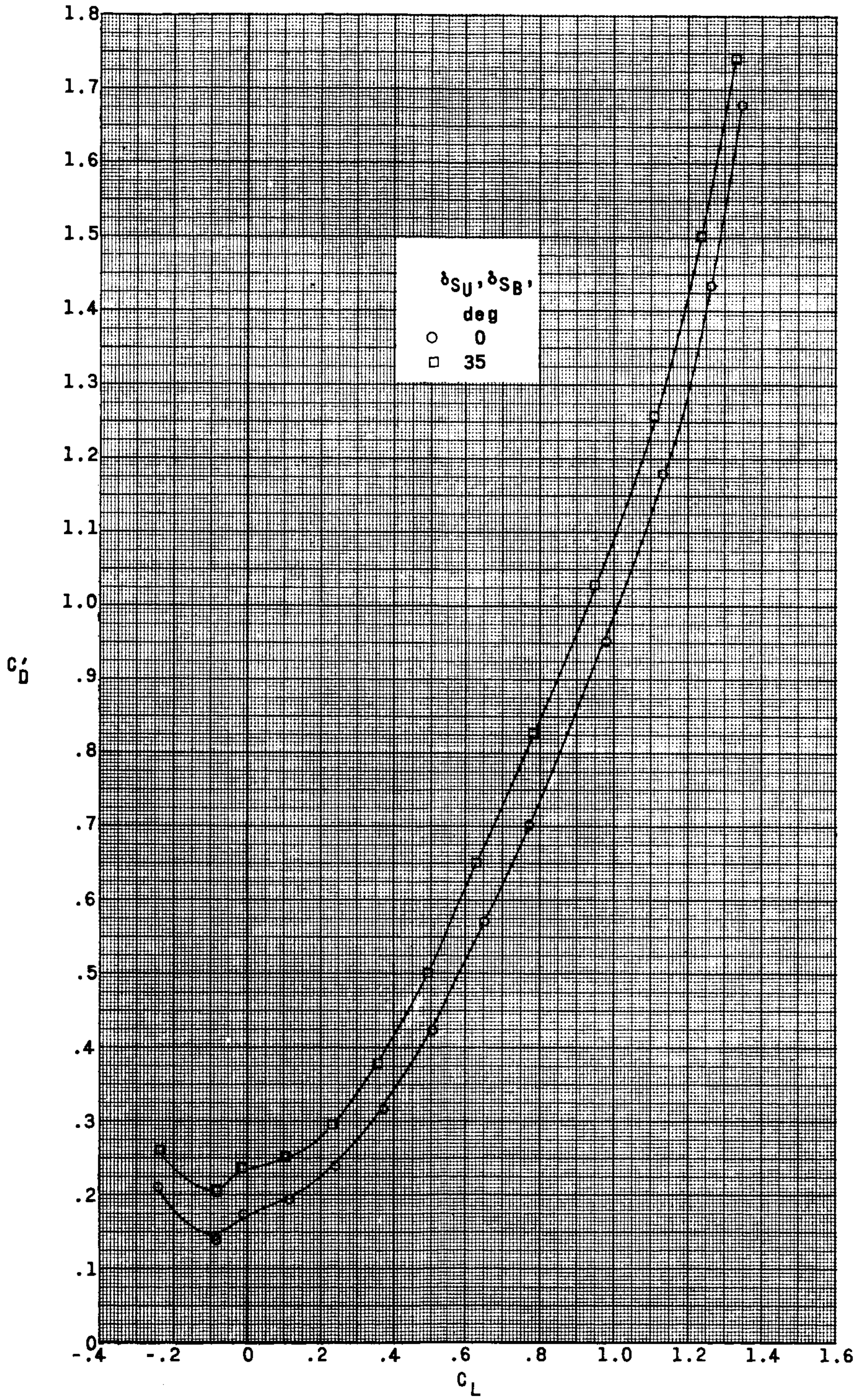

(b) Concluded.

Figure 15.- Continued.

[redacted]

[redacted]

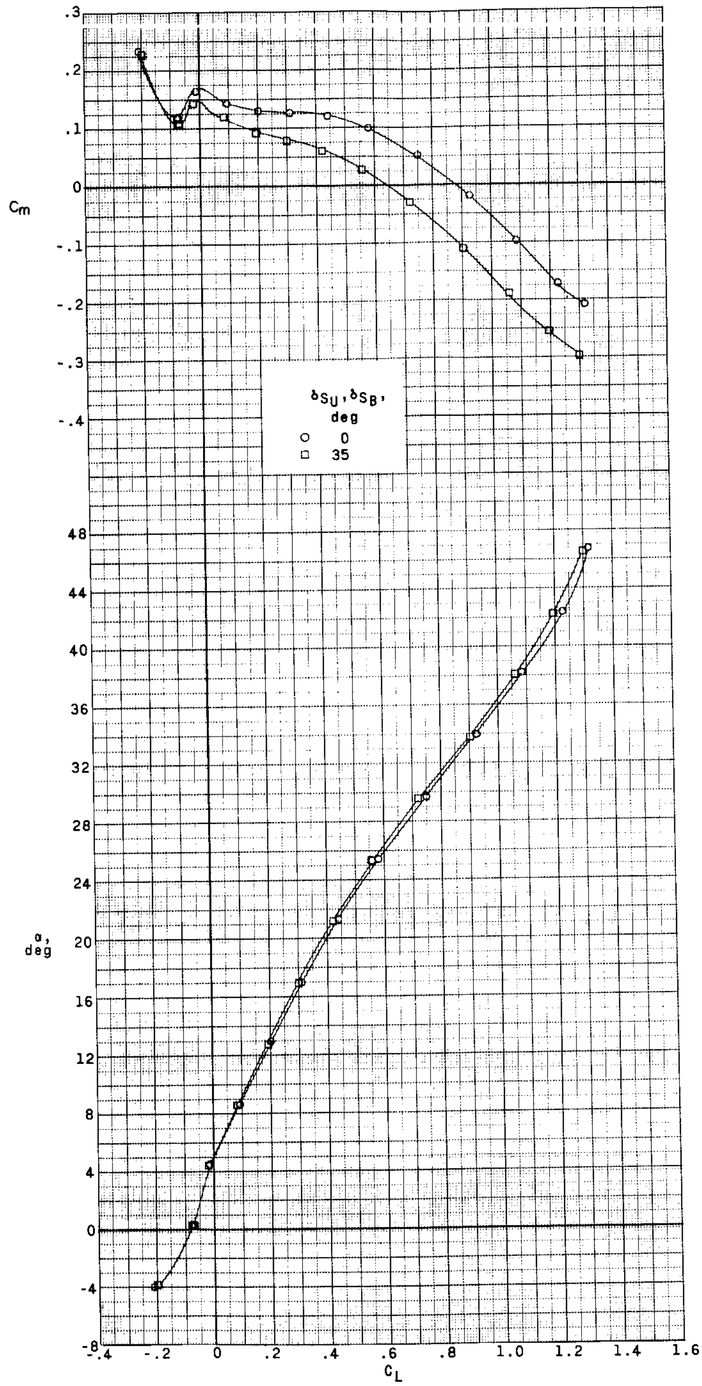

(c) M = 4.65.

Figure 15.- Continued.

[redacted]

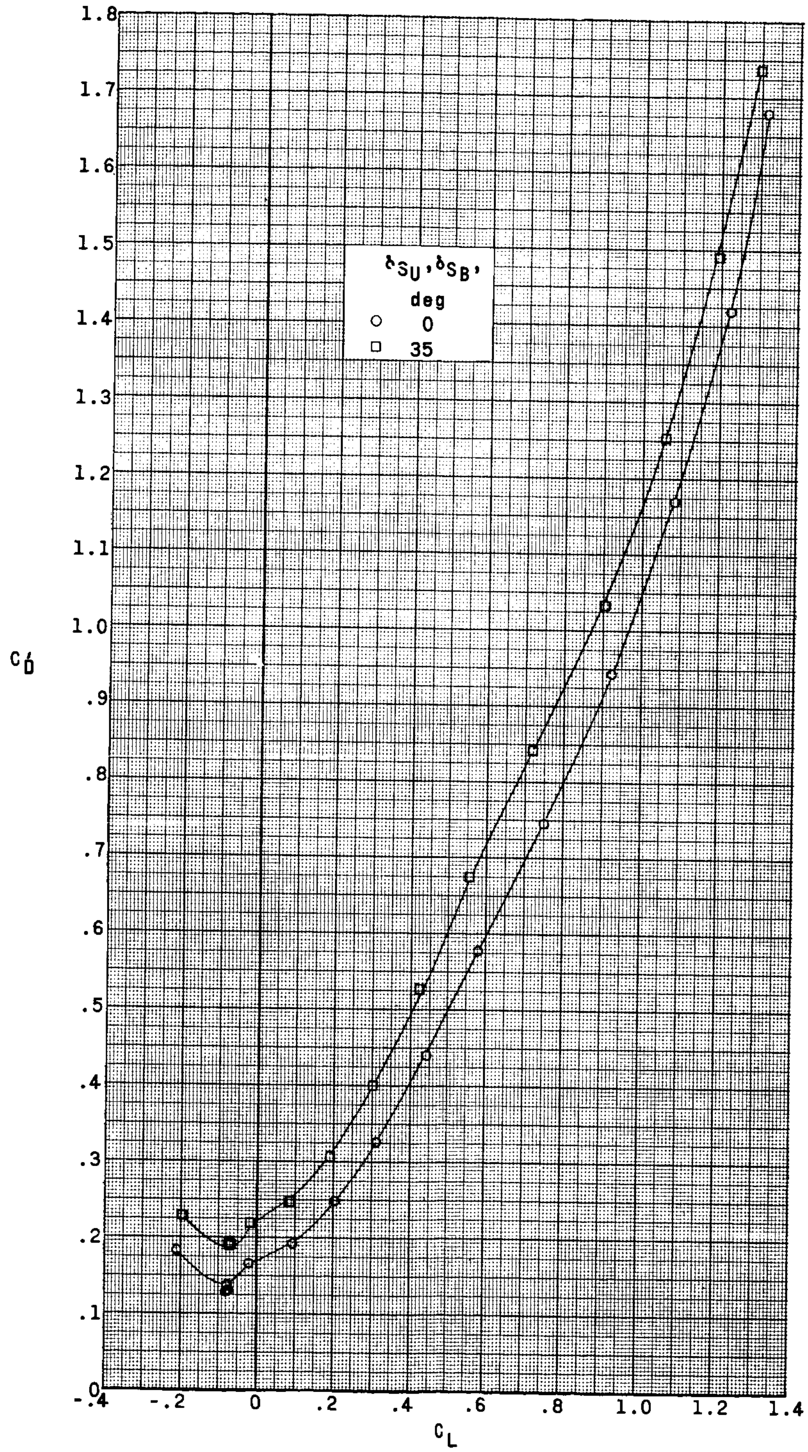

(c) Concluded.

Figure 15.- Concluded.

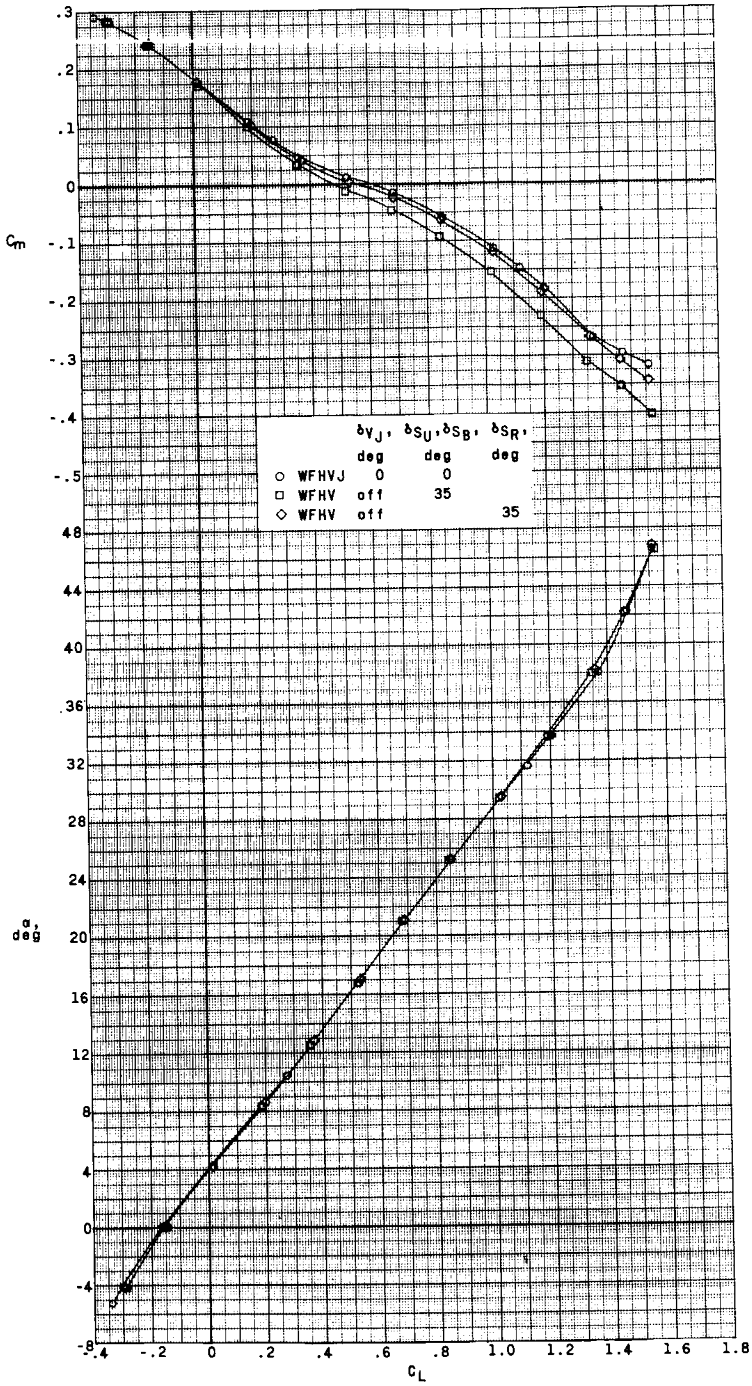

(a) M = 2.96.

Figure 16.- Effect of using unsymmetrical speed-brake deflections as directional controls on aerodynamic characteristics in pitch. $\beta = 0^{\circ}$; $\delta_{H_L} = \delta_{H_R} = -35^{\circ}$; $\delta_{V_U} = 0^{\circ}$.

[redacted]

[redacted]

DECLASSIFIED

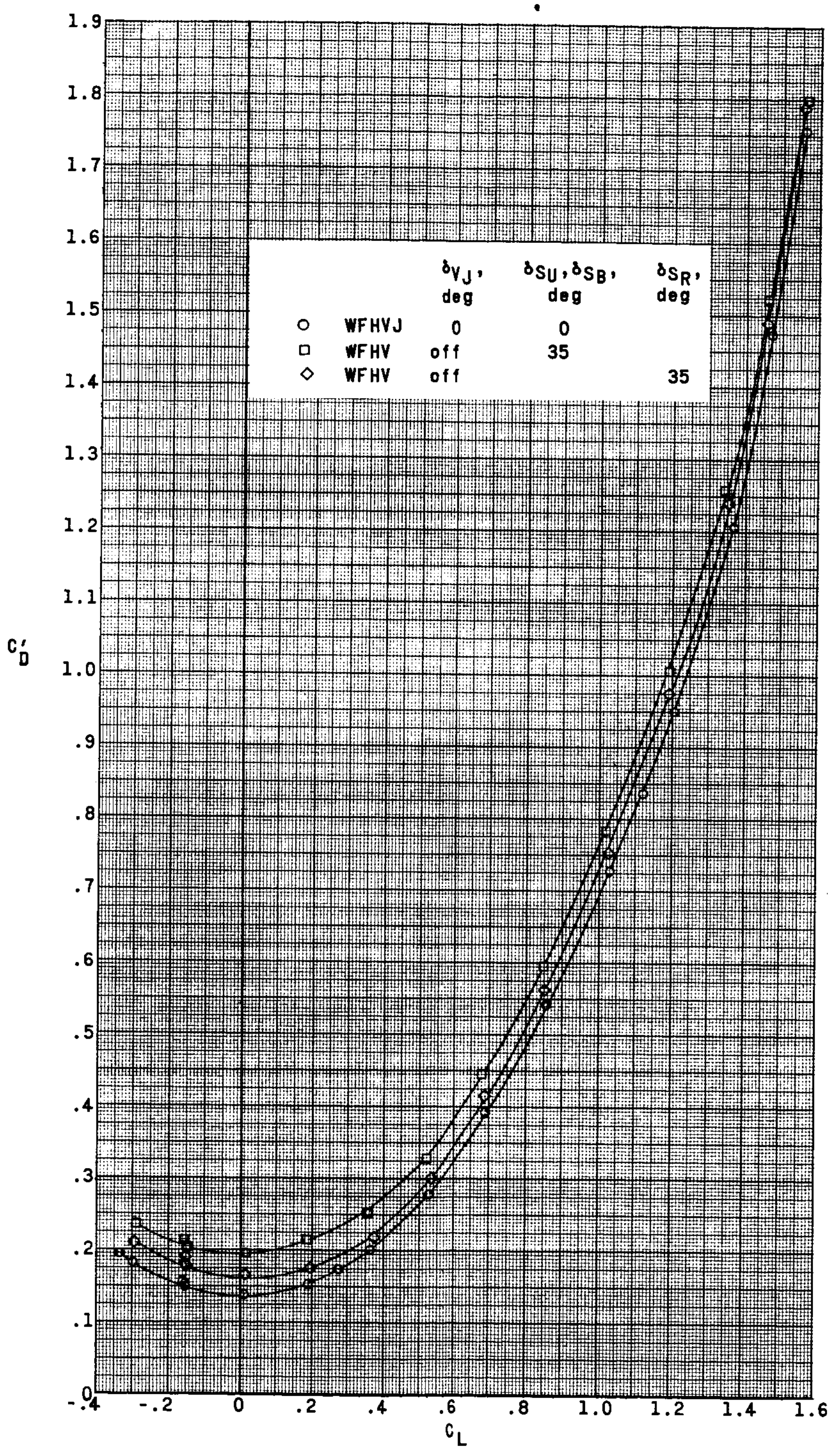

(a) Concluded.

Figure 16.- Continued.

[redacted]

[redacted]

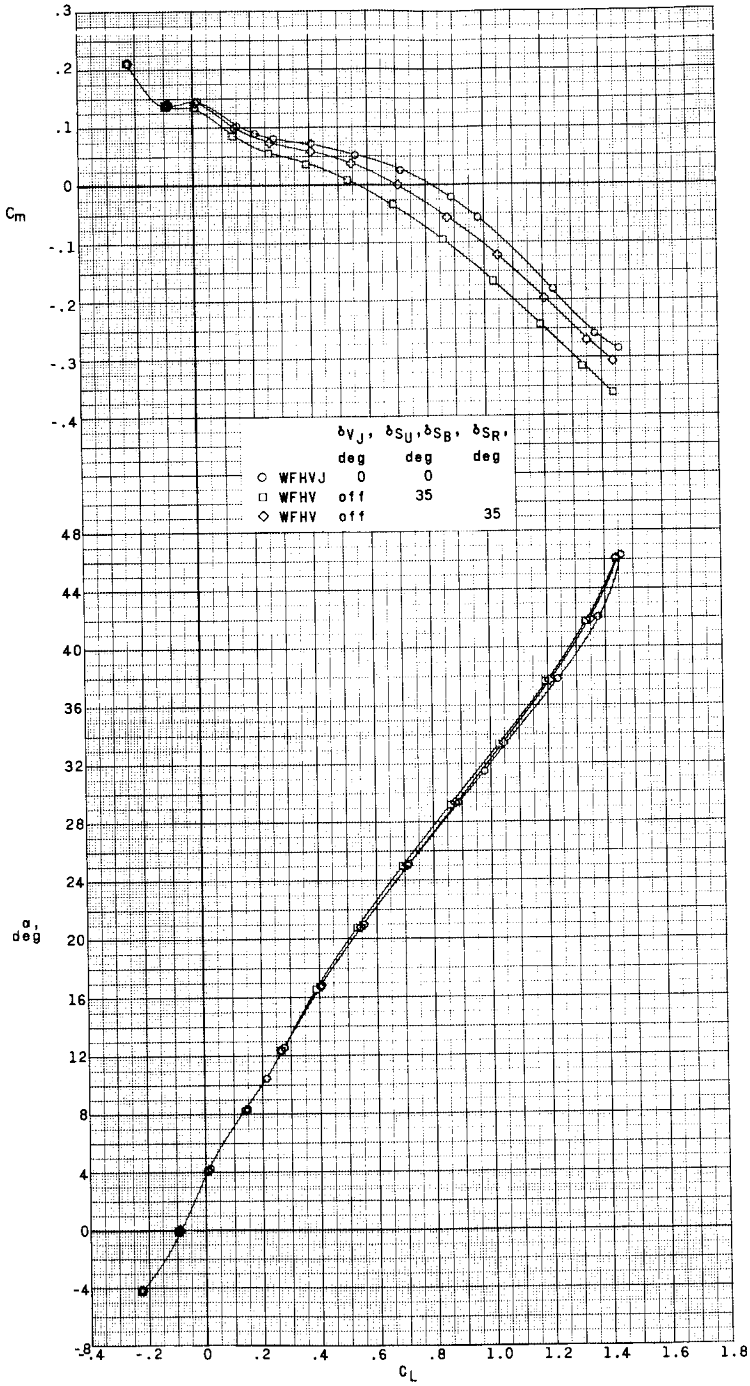

(b) M = 3.96.

Figure 16.- Continued.

[redacted]

[redacted]SSIFIED

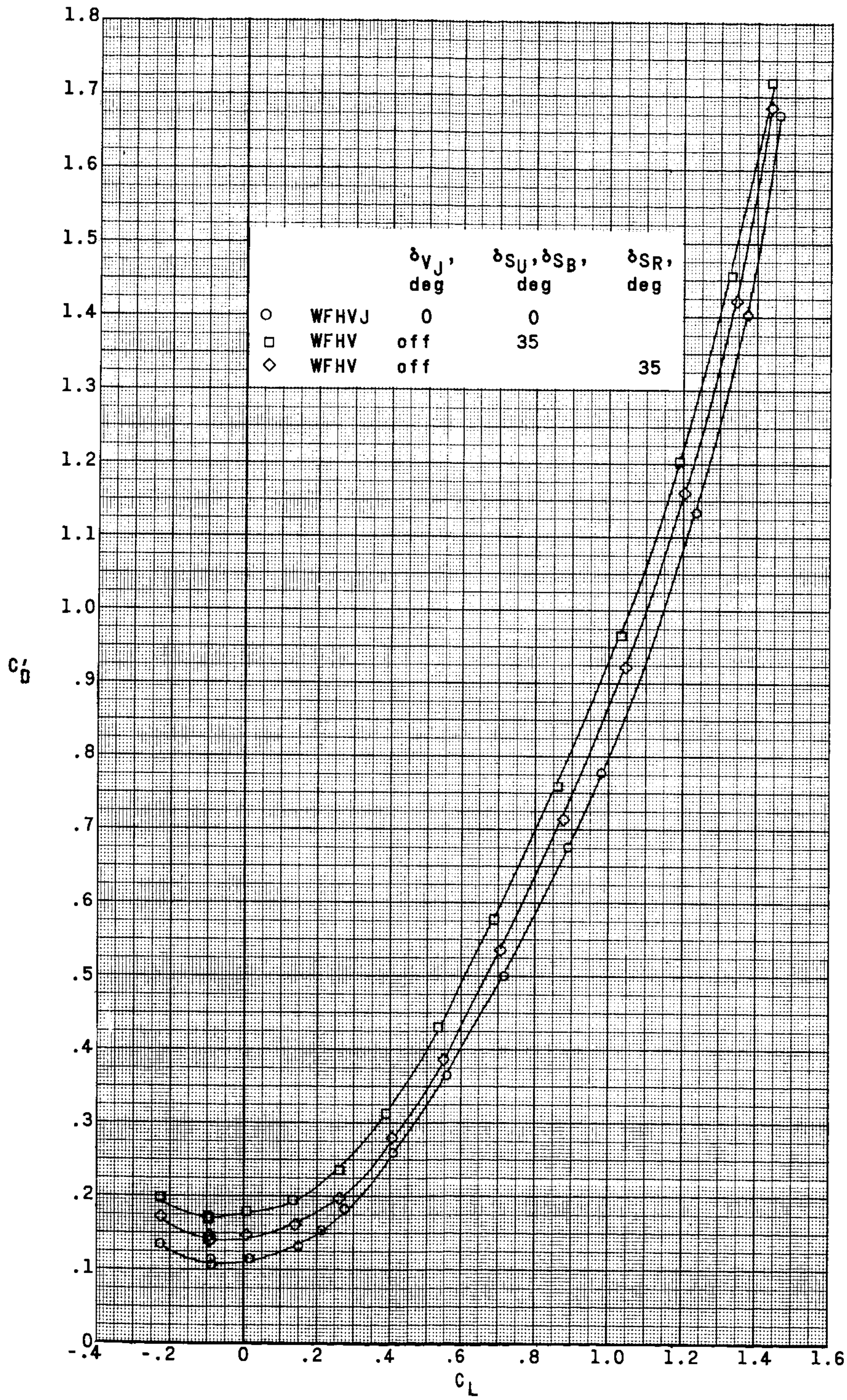

(b) Concluded.

Figure 16.- Continued.

[redacted]

[redacted]

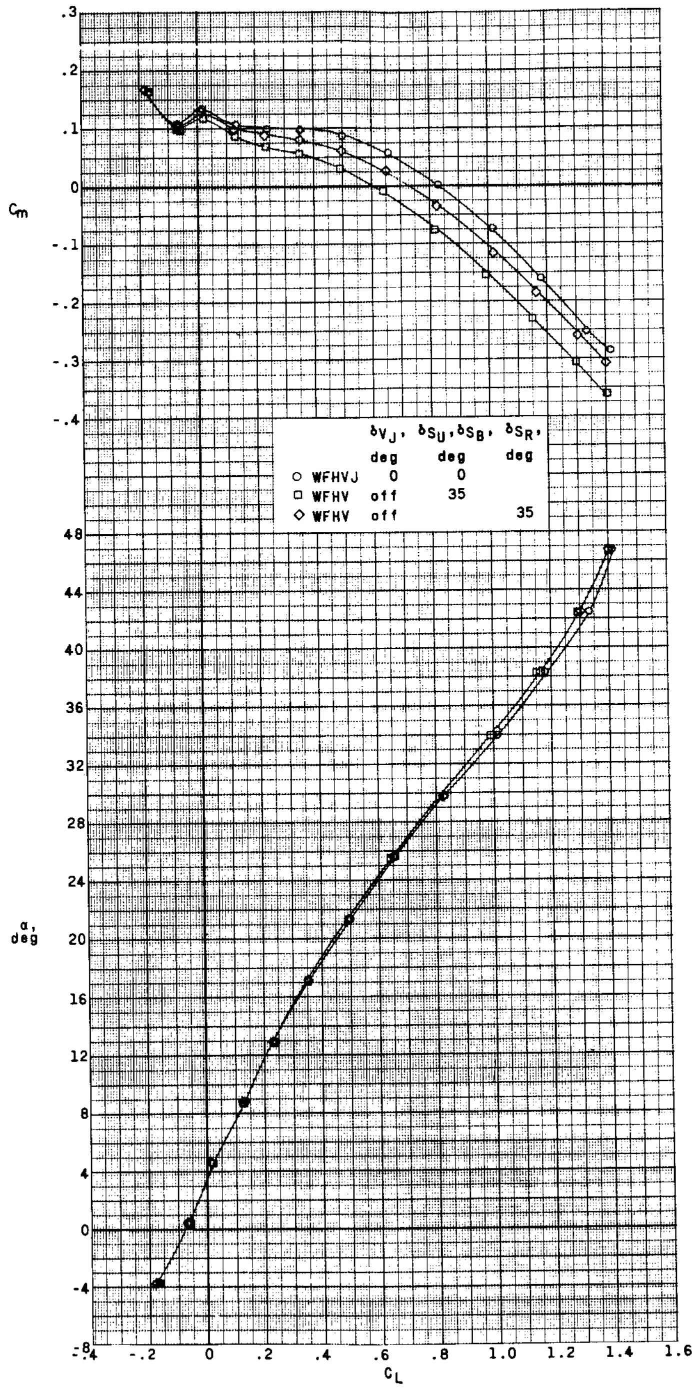

(c) M = 4.65.

Figure 16.- Continued.

[redacted]

[redacted]

DECLASSIFIED

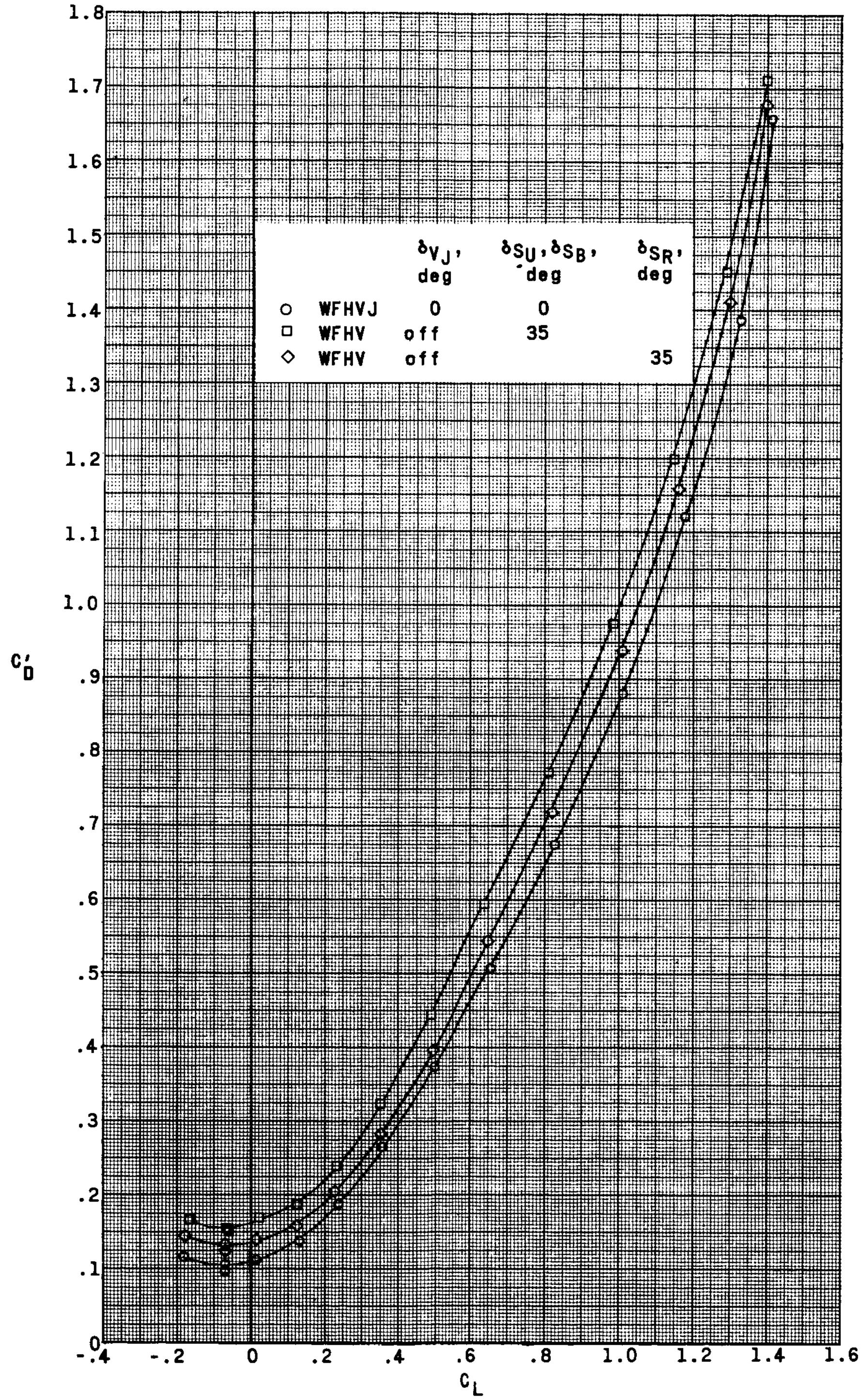

(c) Concluded.

Figure 16.- Concluded.

[redacted]

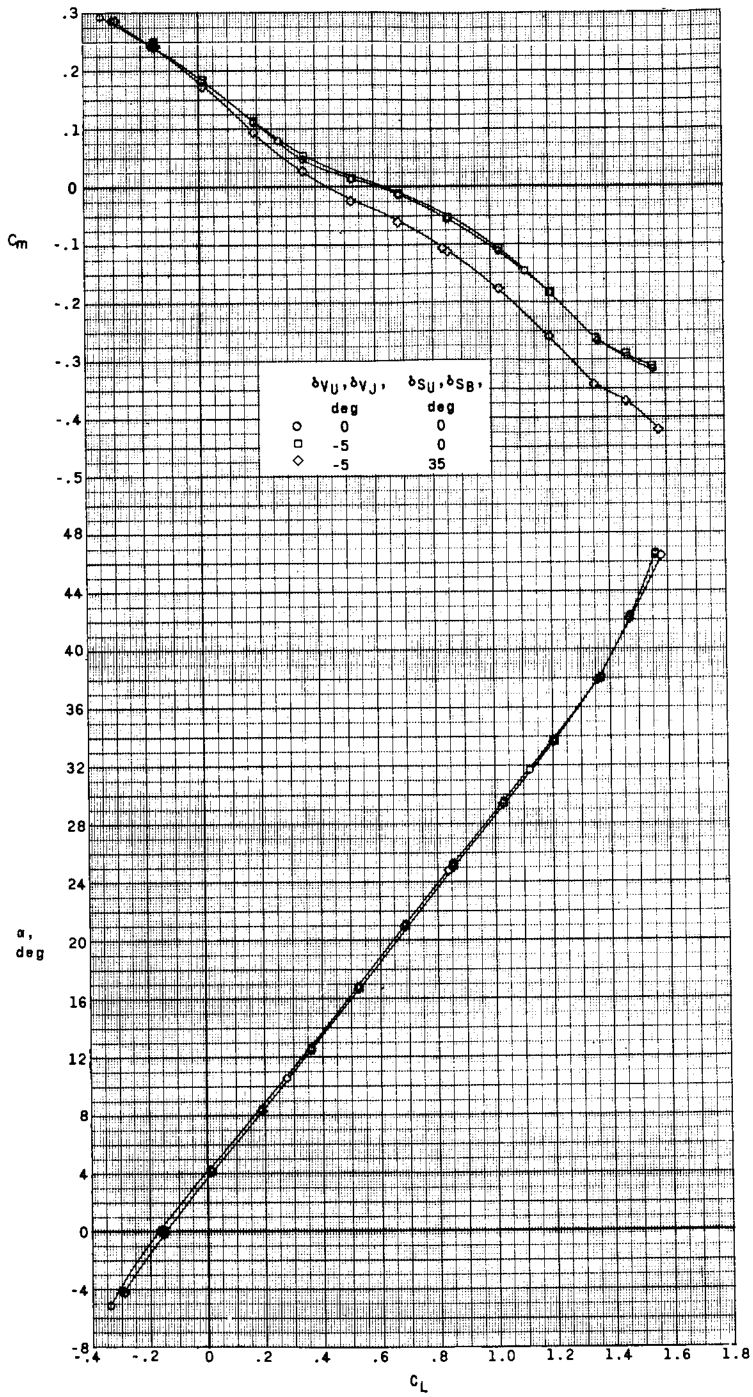

(a) M = 2.96.

Figure 17.- Effect of directional-control deflections on aerodynamic characteristics in pitch with $\delta_{H_L} = \delta_{H_R} = -35^{\circ}$. $\beta = 0^{\circ}$; WFHVJ.

[redacted]

[redacted]

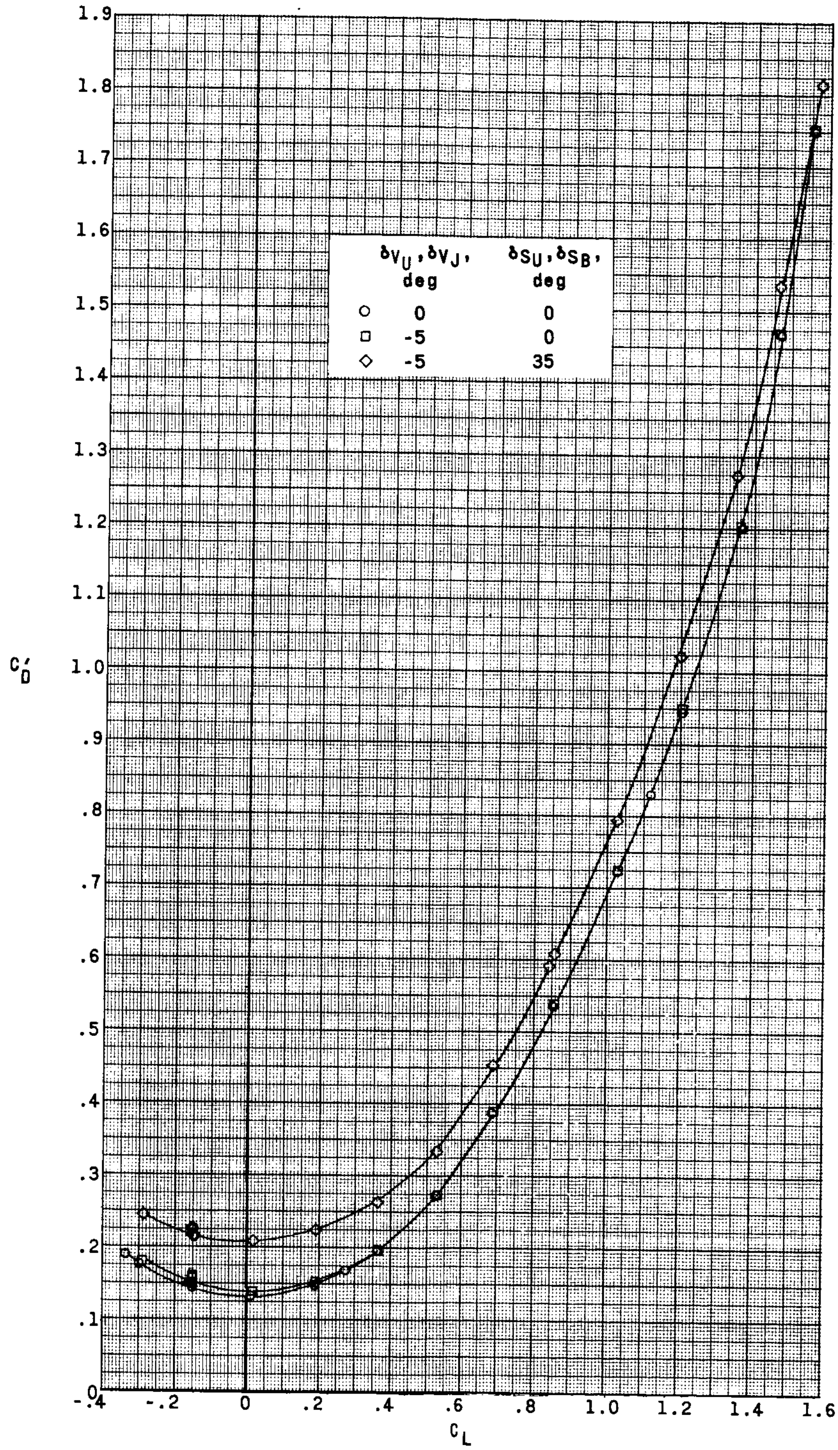

(a) Concluded.

Figure 17.- Continued.

[redacted]

[redacted]

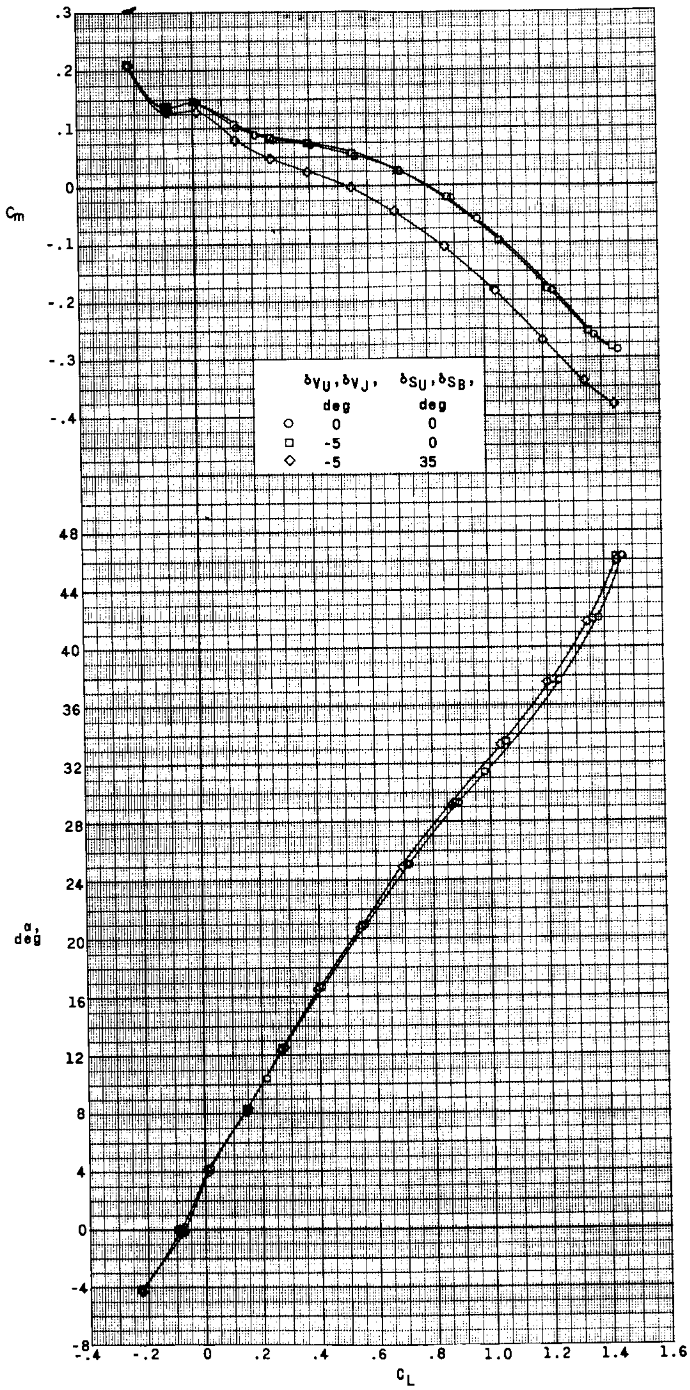

(b) M = 3.96.

Figure 17.- Continued.

[redacted]

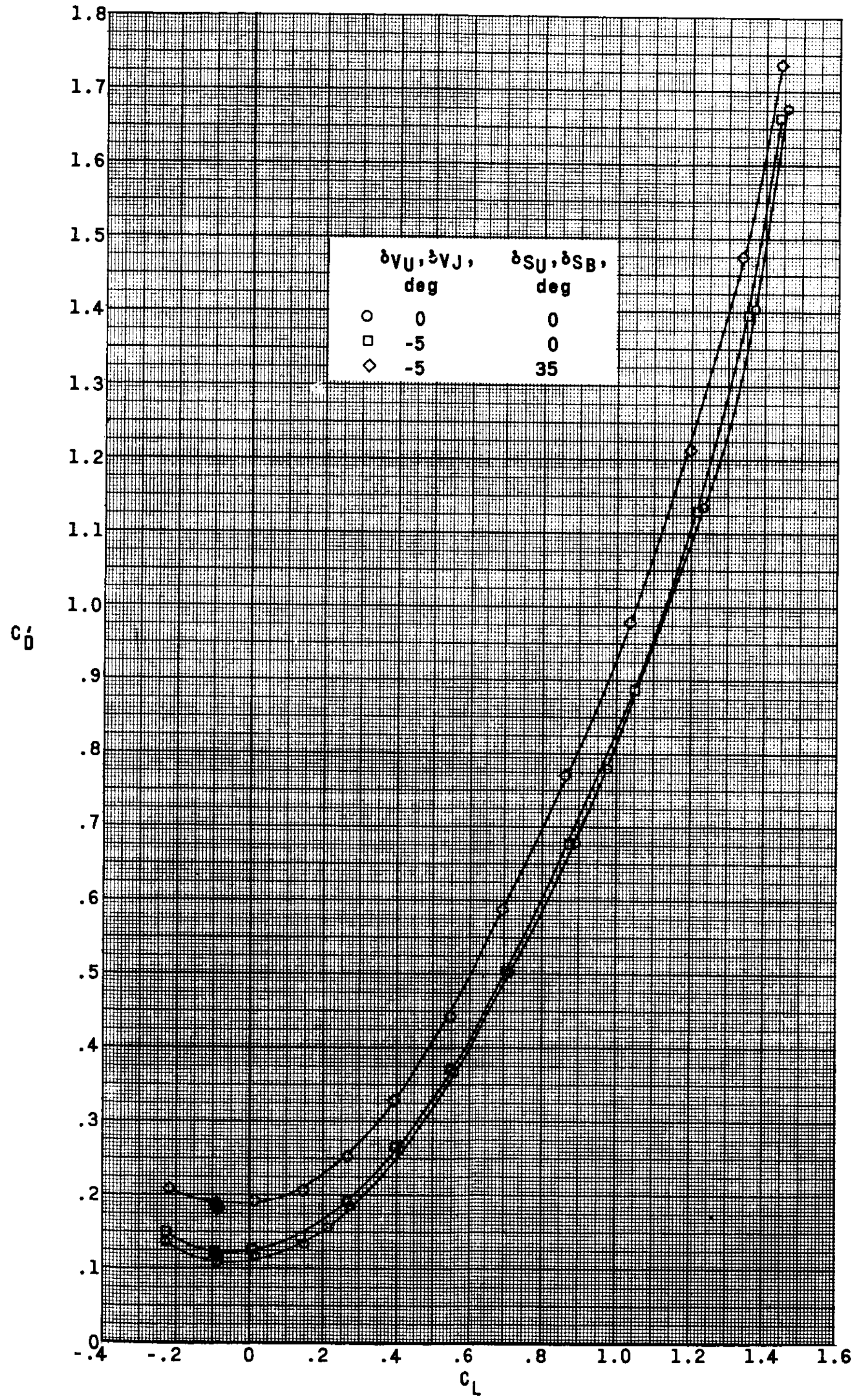

(b) Concluded.

Figure 17.- Continued.

[redacted]

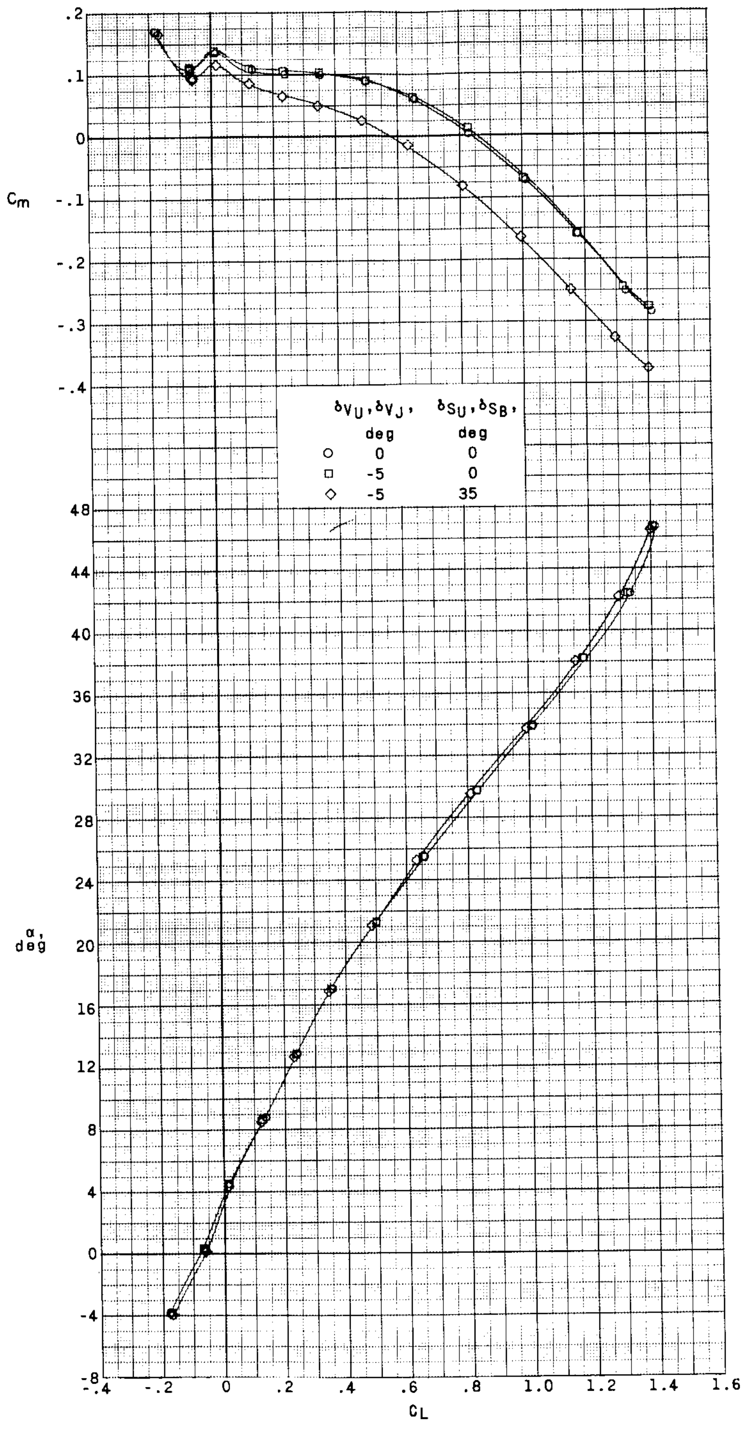

(c) M = 4.65.

Figure 17.- Continued.

[redacted]

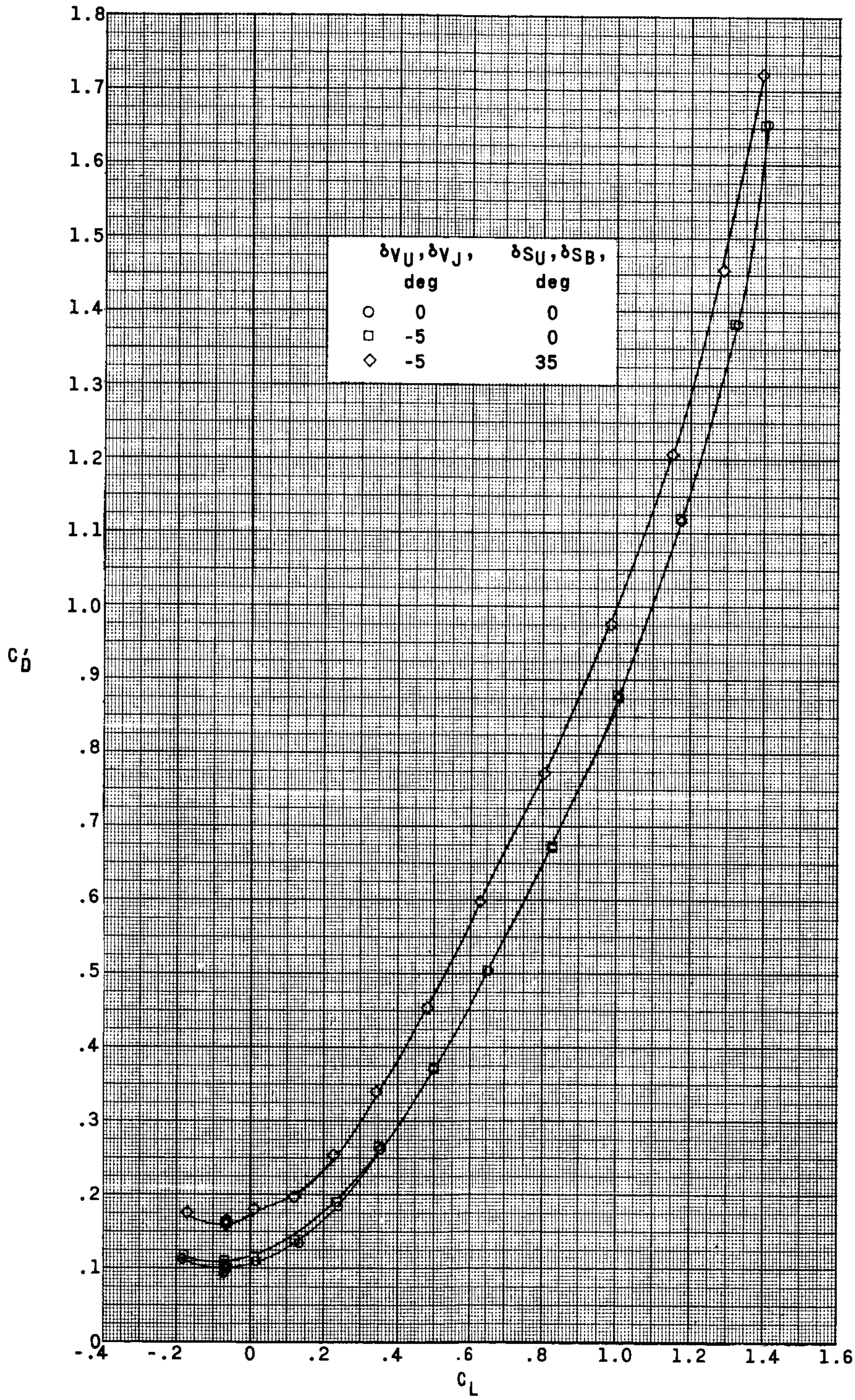

(c) Concluded.

Figure 17.- Concluded.

[redacted]

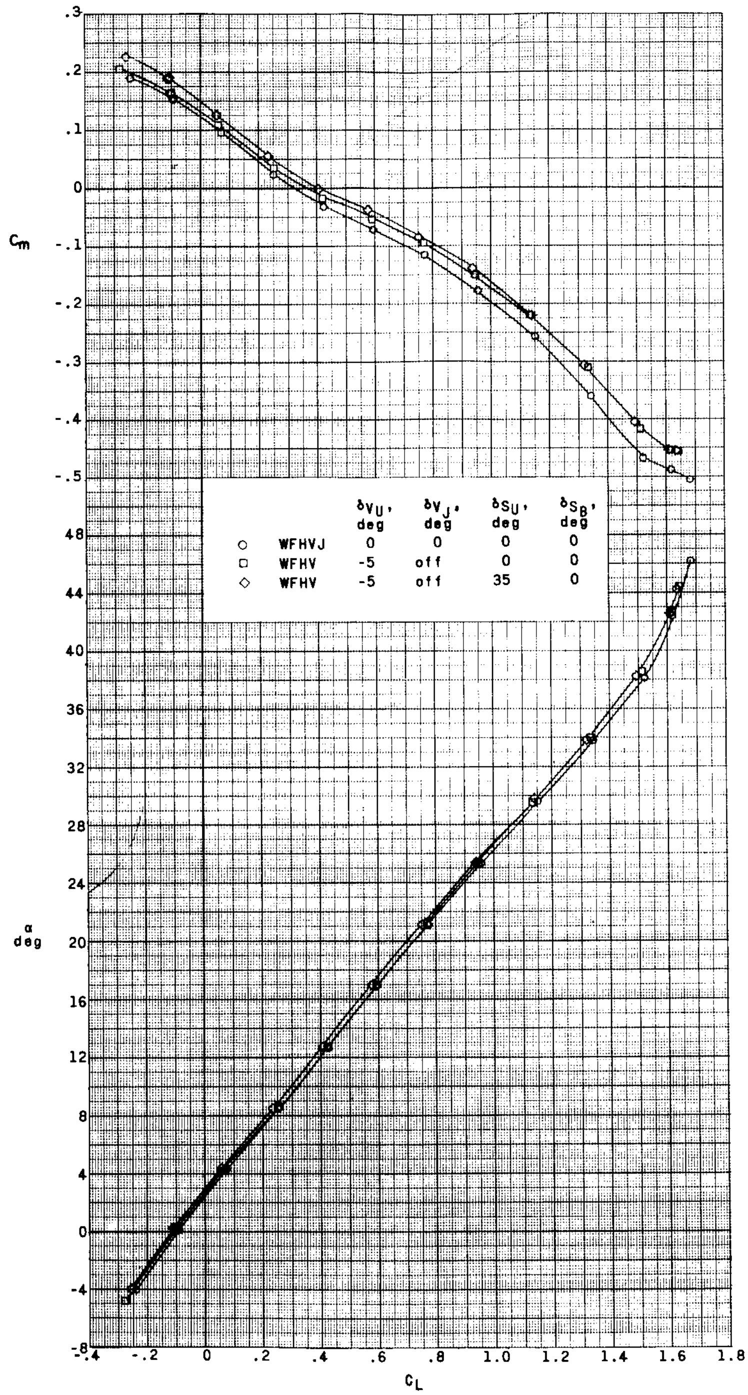

(a) M = 2.96.

Figure 18.- Effect of directional-control deflections on aerodynamic characteristics in pitch with $\delta_{H_L} = \delta_{H_R} = -20^{\circ}$. $\beta = 0^{\circ}$.

[redacted]

[redacted]

DECLASSIFIED

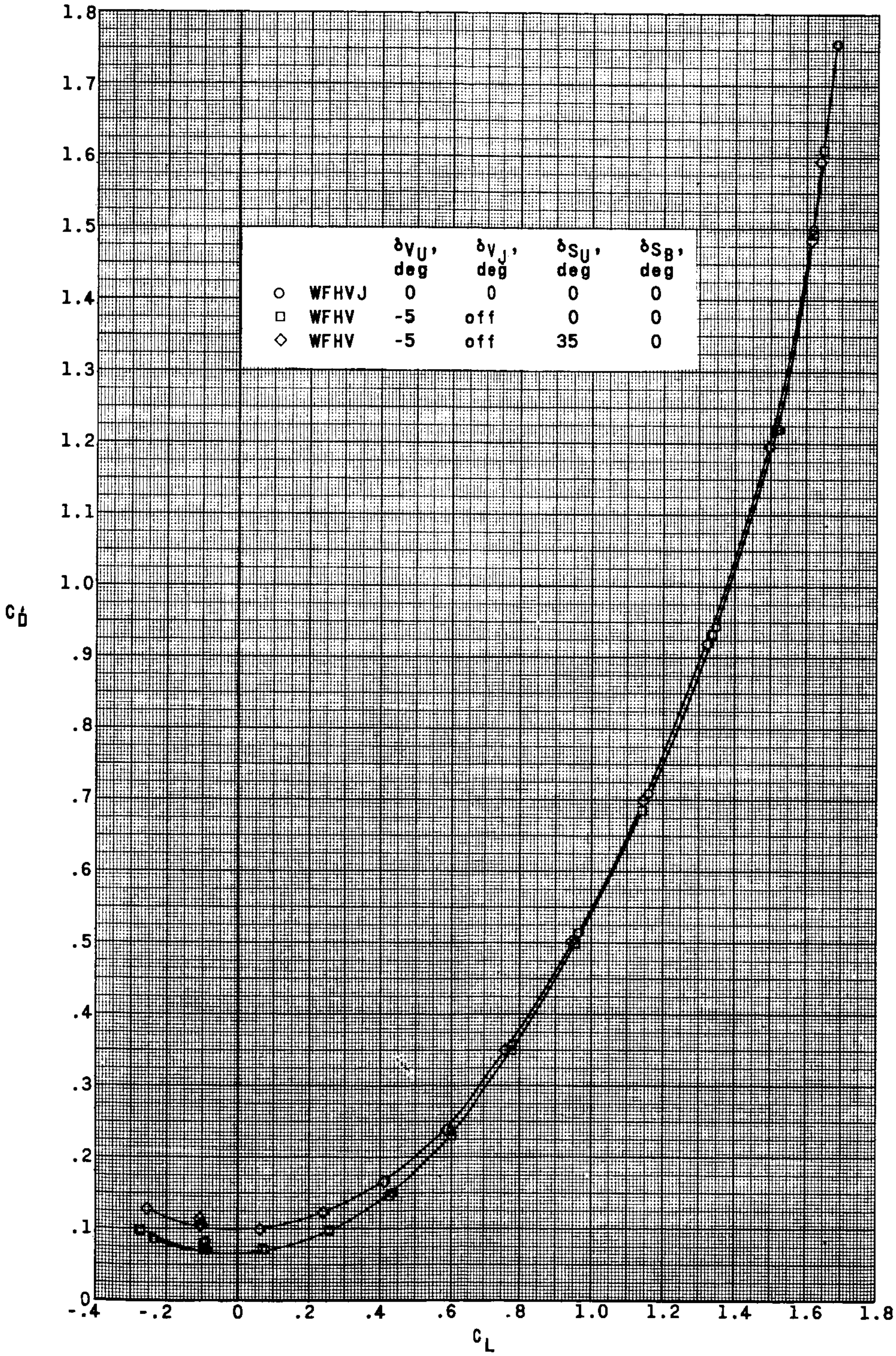

(a) Concluded.

Figure 18.- Continued.

[redacted]

[redacted]

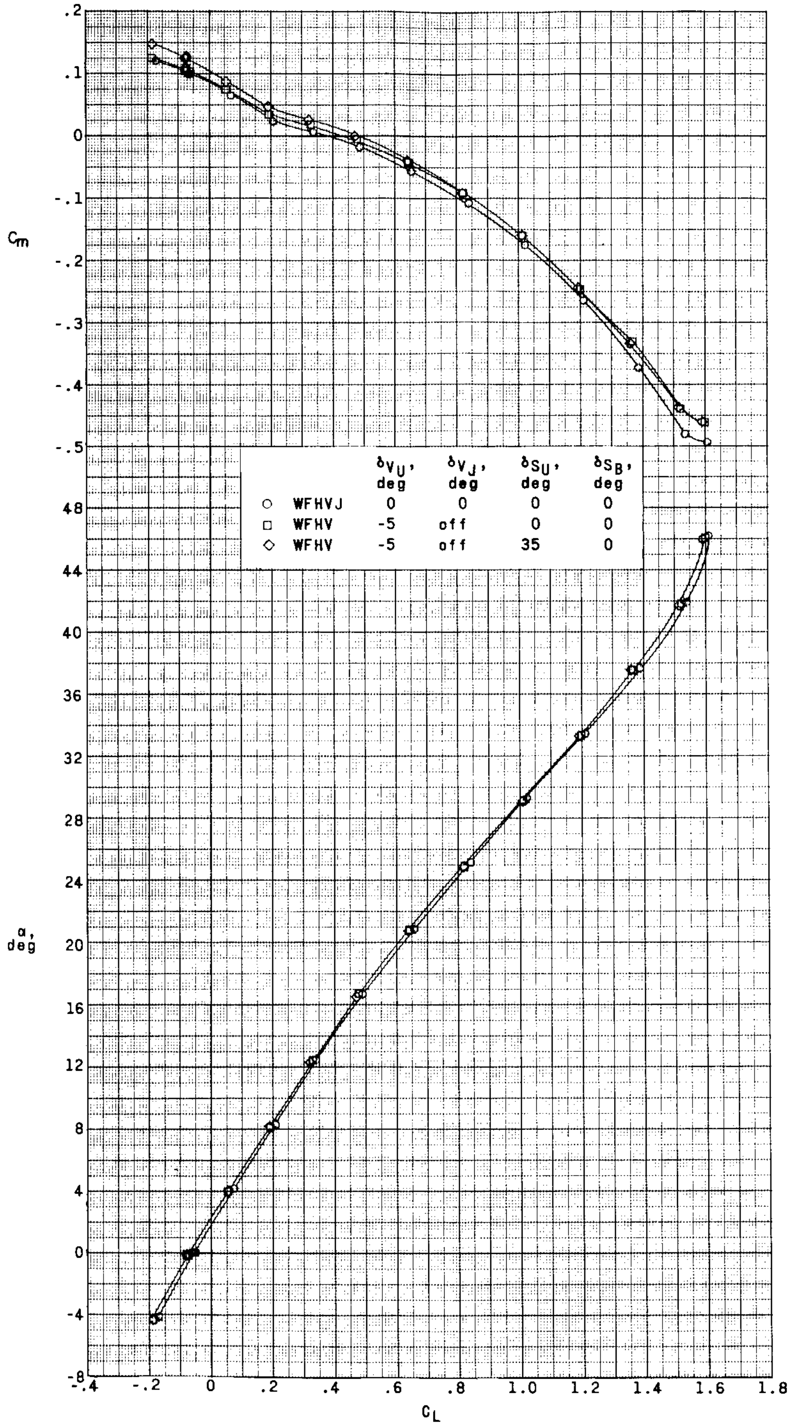

(b) M = 3.96.

Figure 18.- Continued.

[redacted]

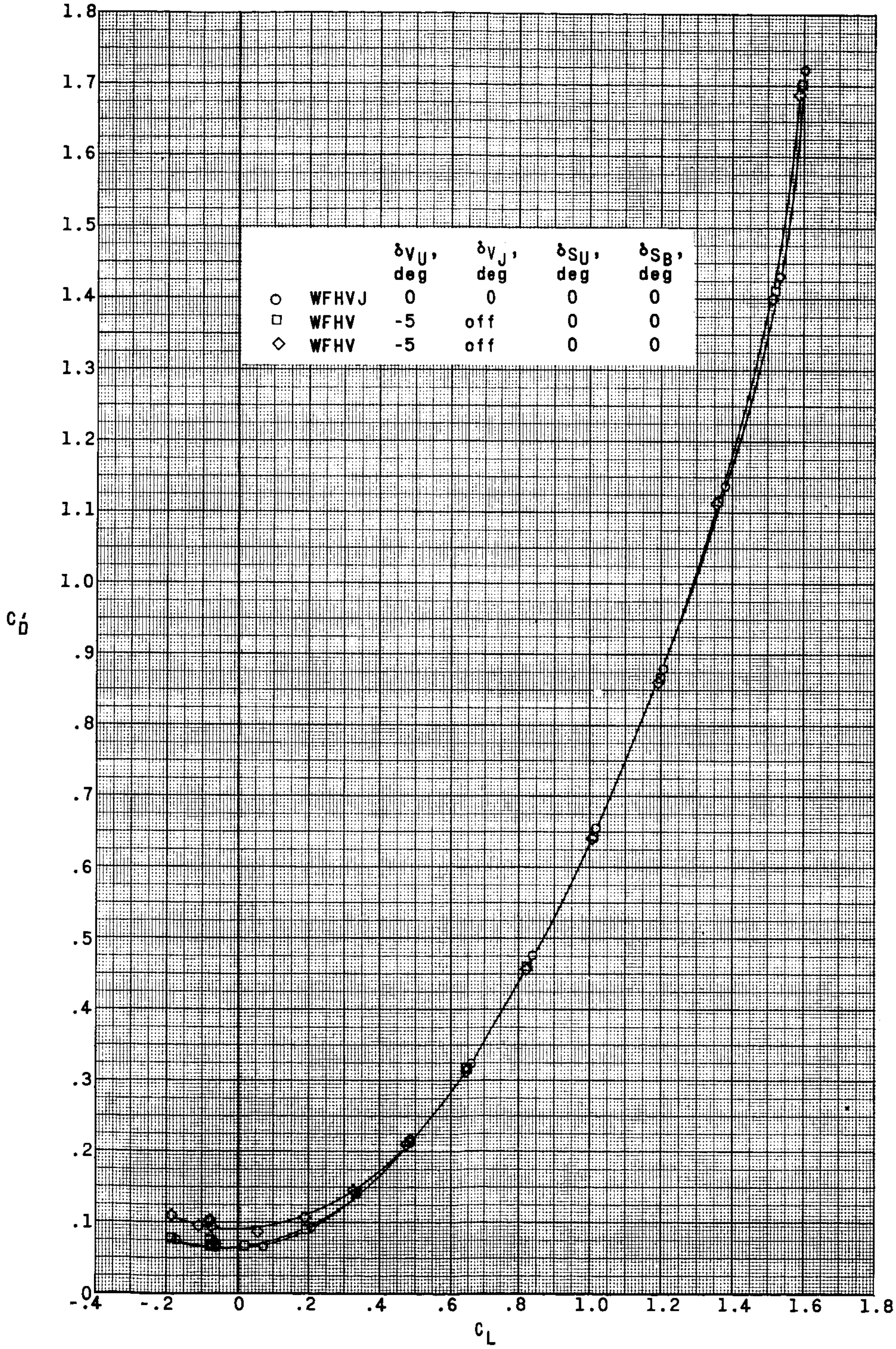

(b) Concluded.

Figure 18.- Continued.

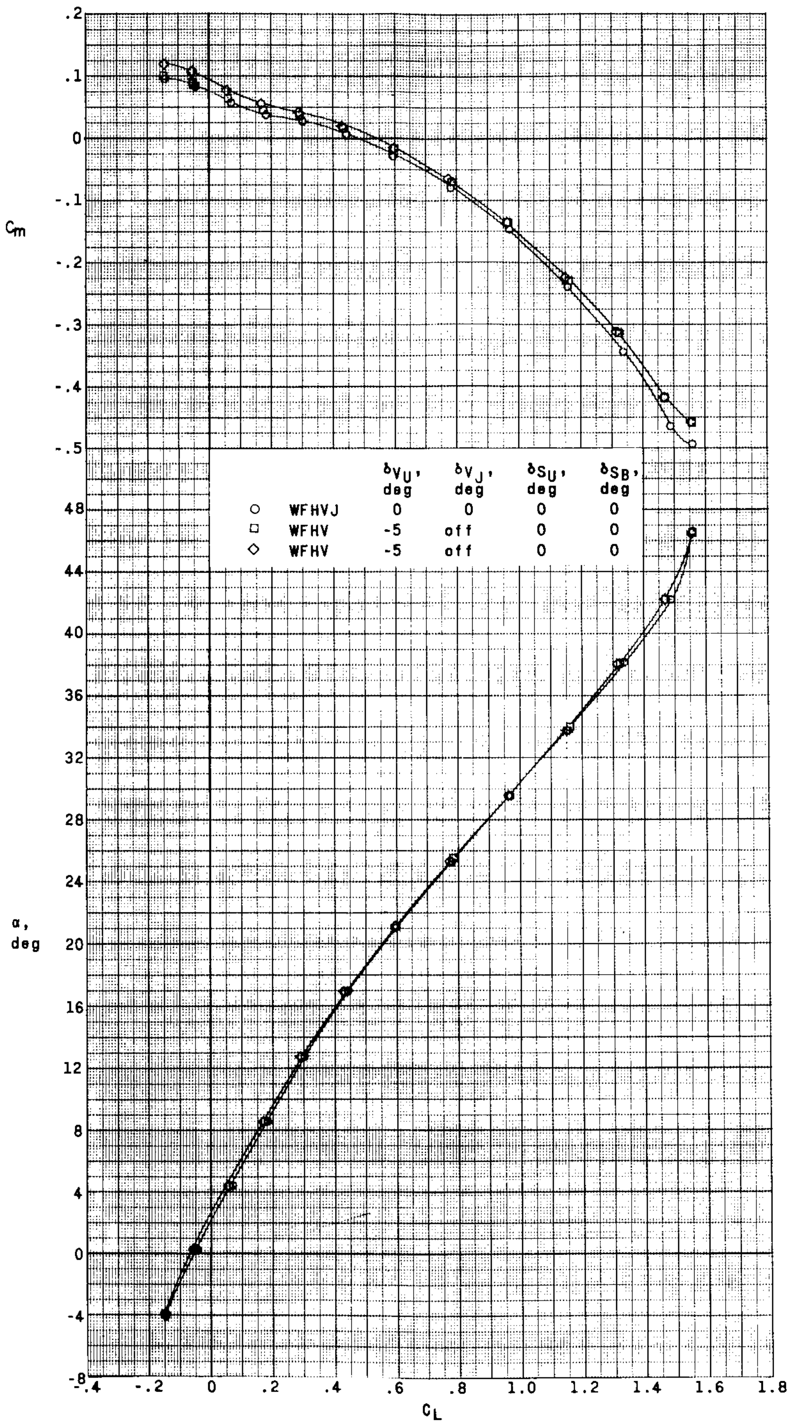

(c) M = 4.65.

Figure 18.- Continued.

[redacted]

[redacted]

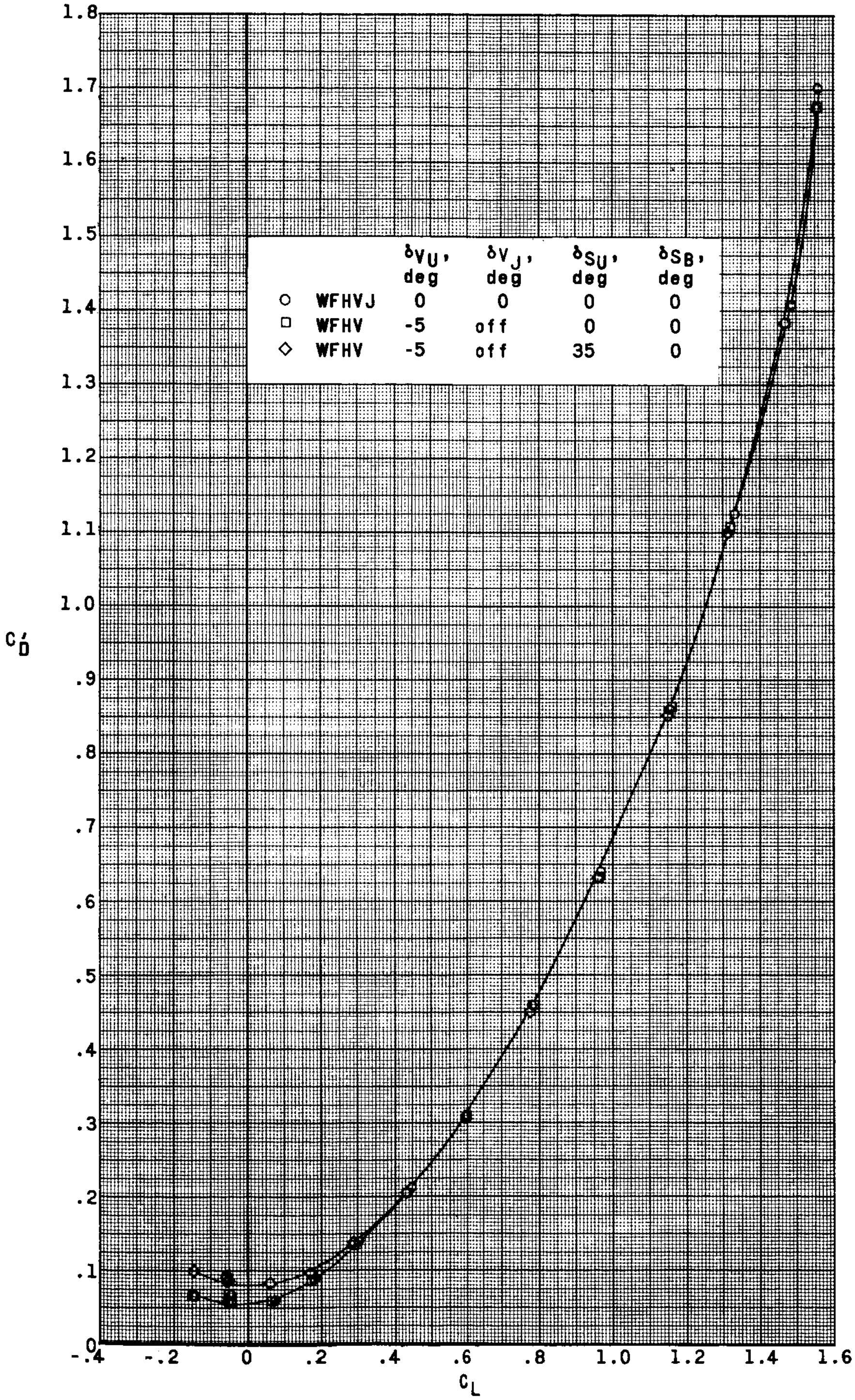

(c) Concluded.

Figure 18.- Concluded.

[redacted]

[redacted]

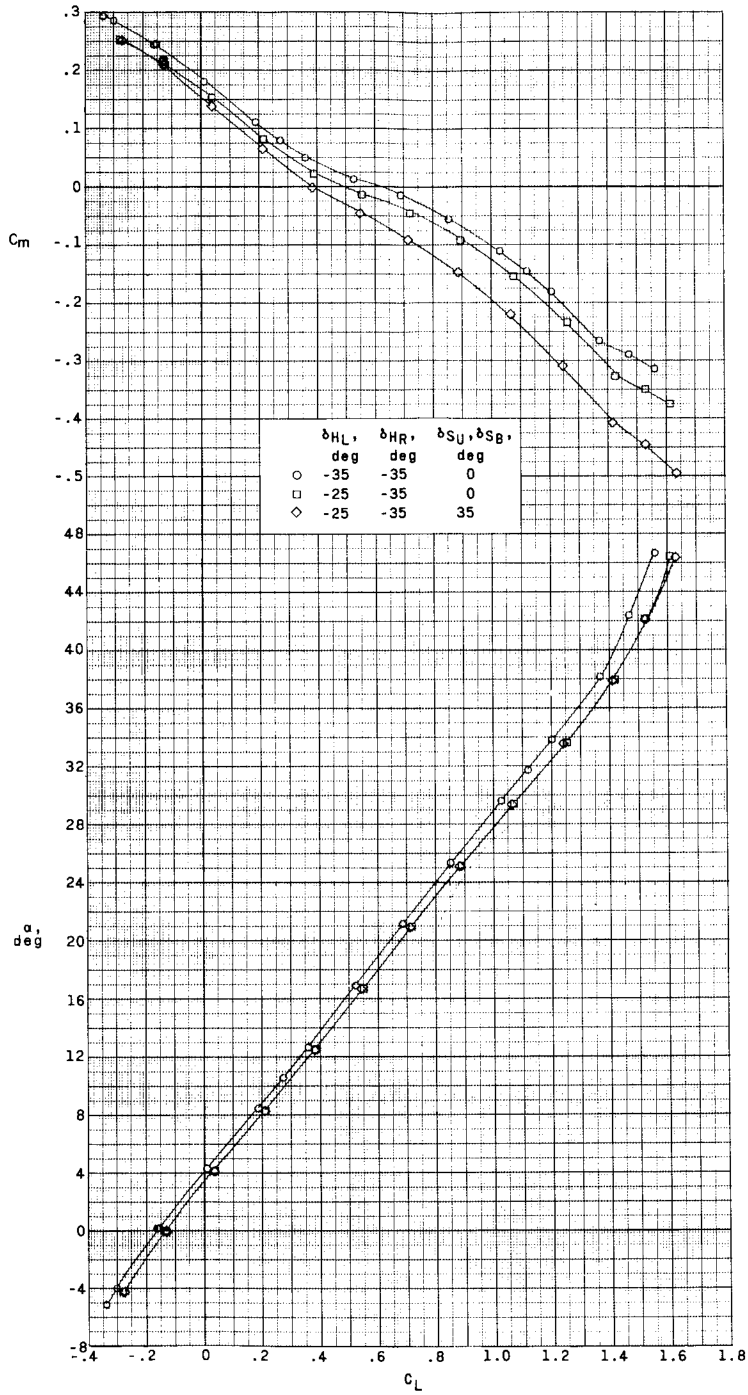

(a) M = 2.96.

Figure 19.- Effect of lateral-control deflections on aerodynamic characteristics in pitch of the complete model. $\beta = 0^{\circ}$; $\delta_{V_U} = \delta_{V_J} = 0^{\circ}$; WFHVJ.

[redacted]

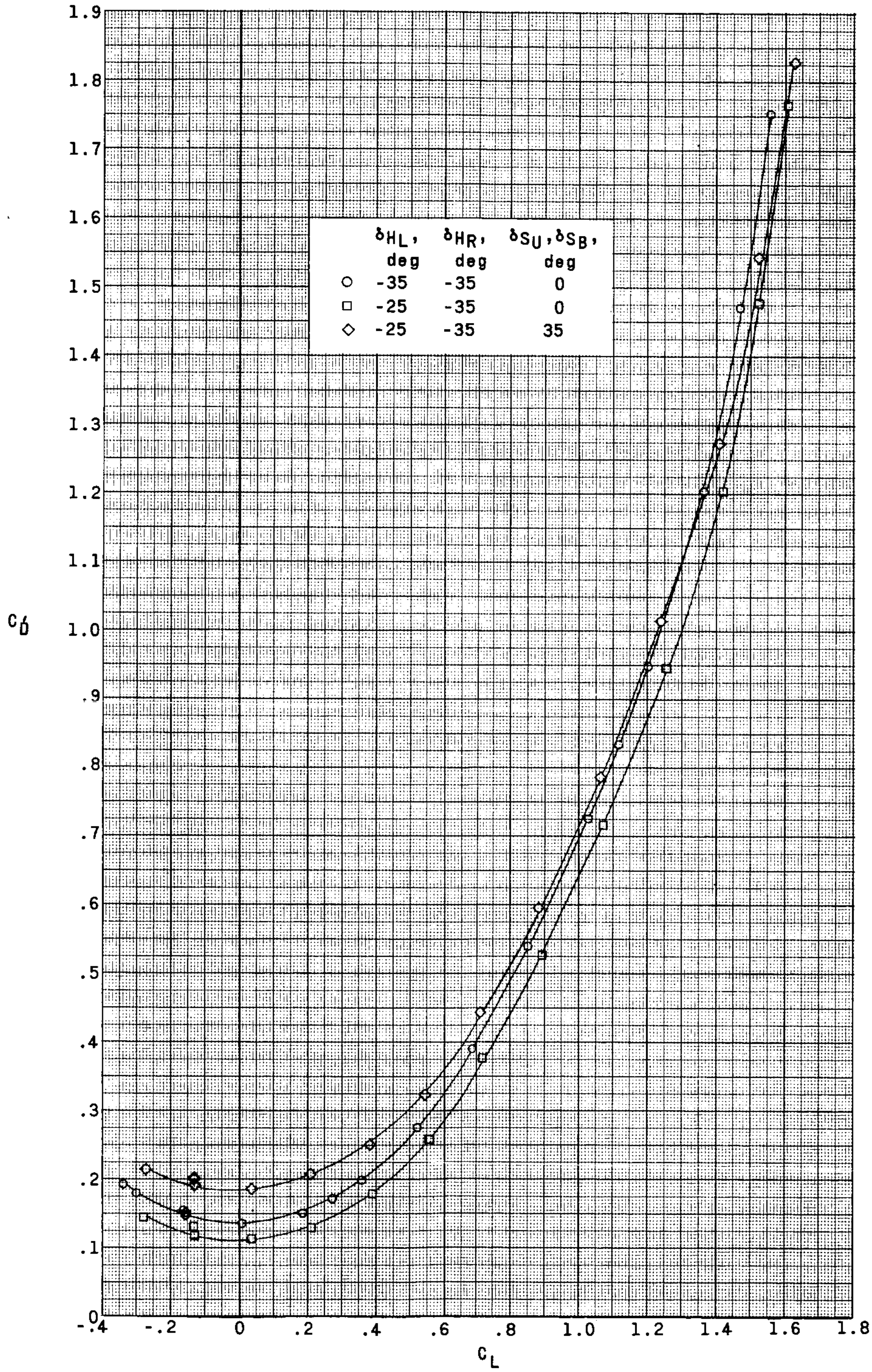

(a) Concluded.

Figure 19.- Continued.

[redacted]

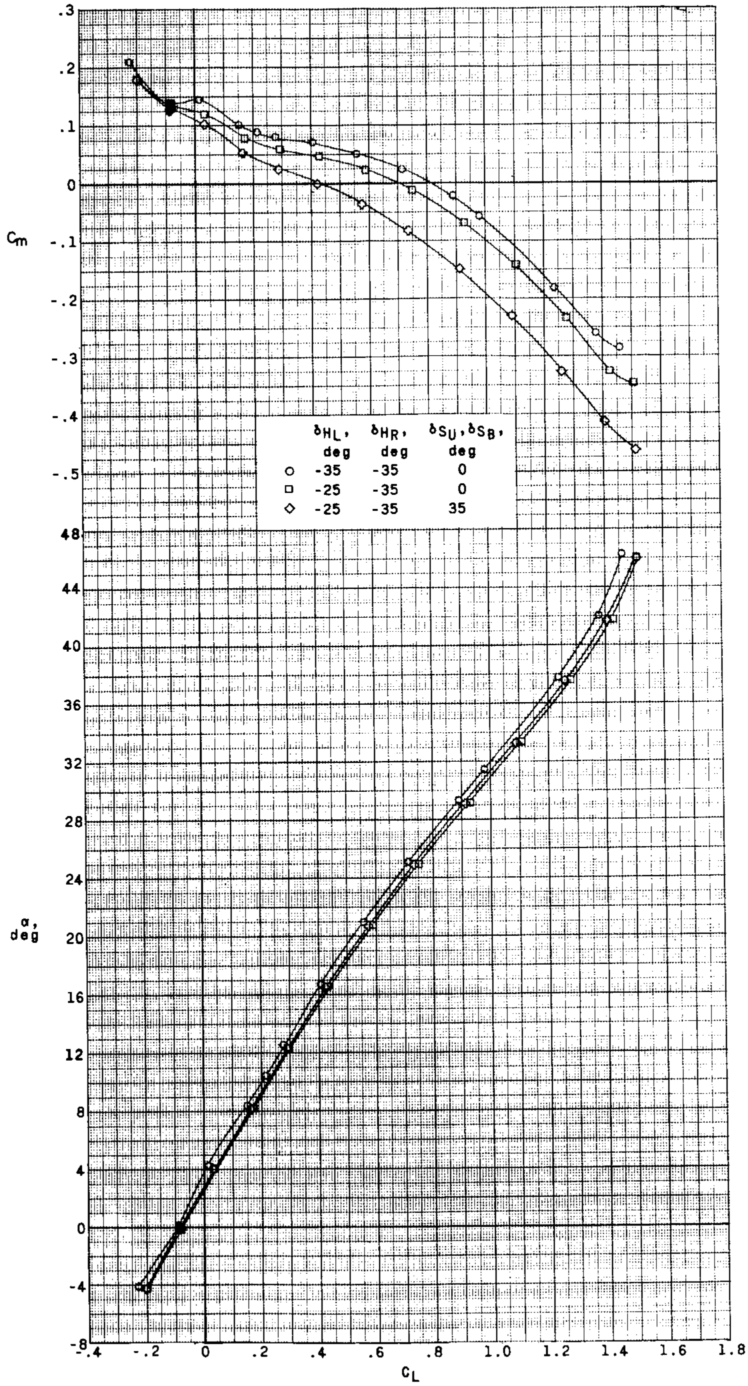

(b) M = 3.96.

Figure 19.- Continued.

[redacted]

[redacted]

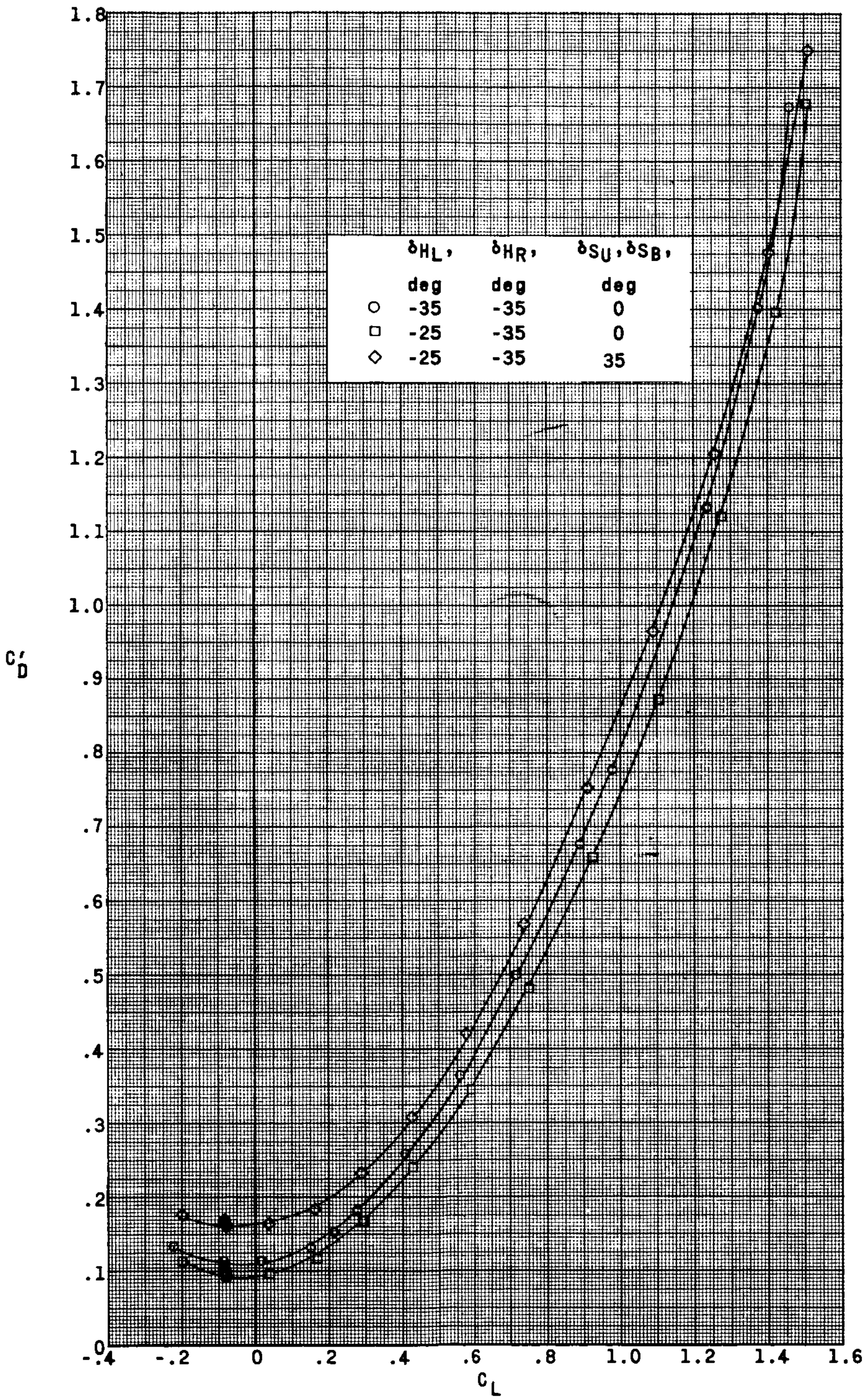

(b) Concluded.

Figure 19.- Continued.

[redacted]

[redacted]

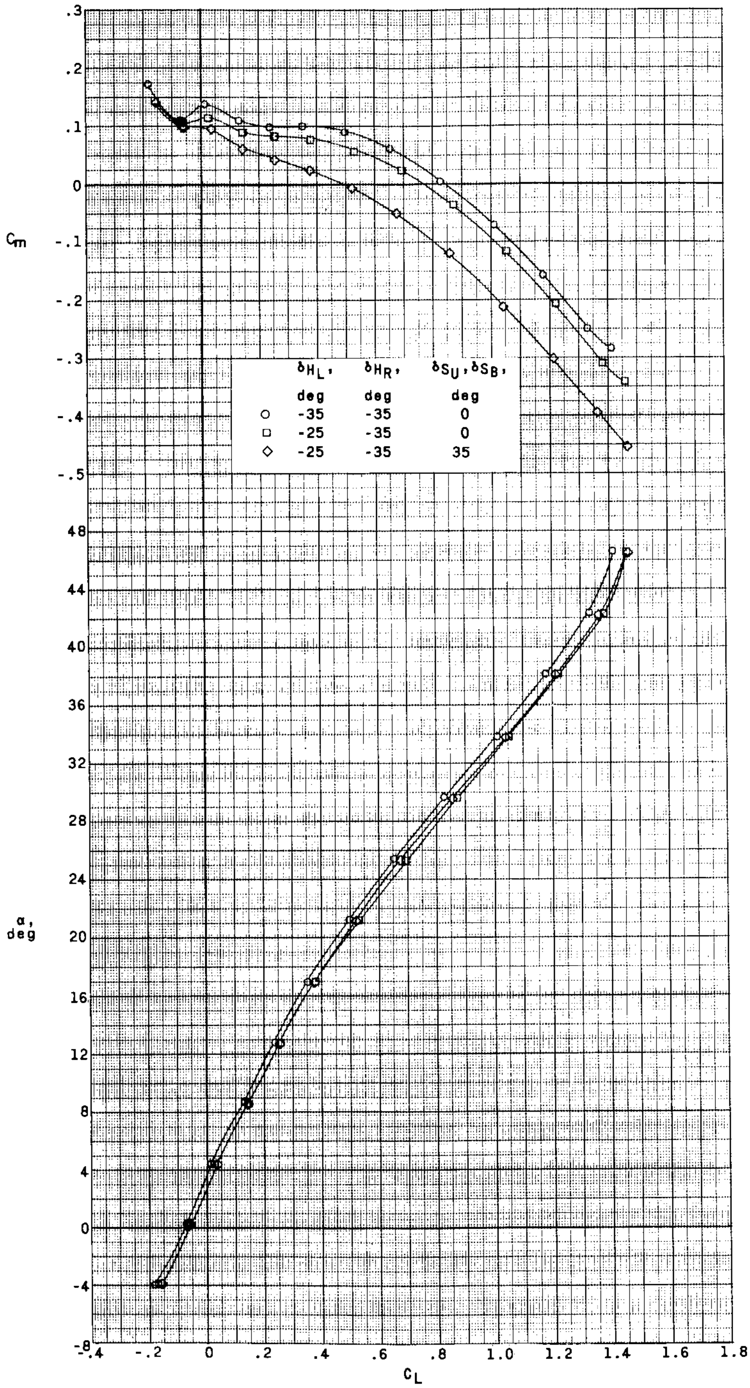

(c) M = 4.65.

Figure 19.- Continued.

[redacted]

[redacted]

DECLASSIFIED

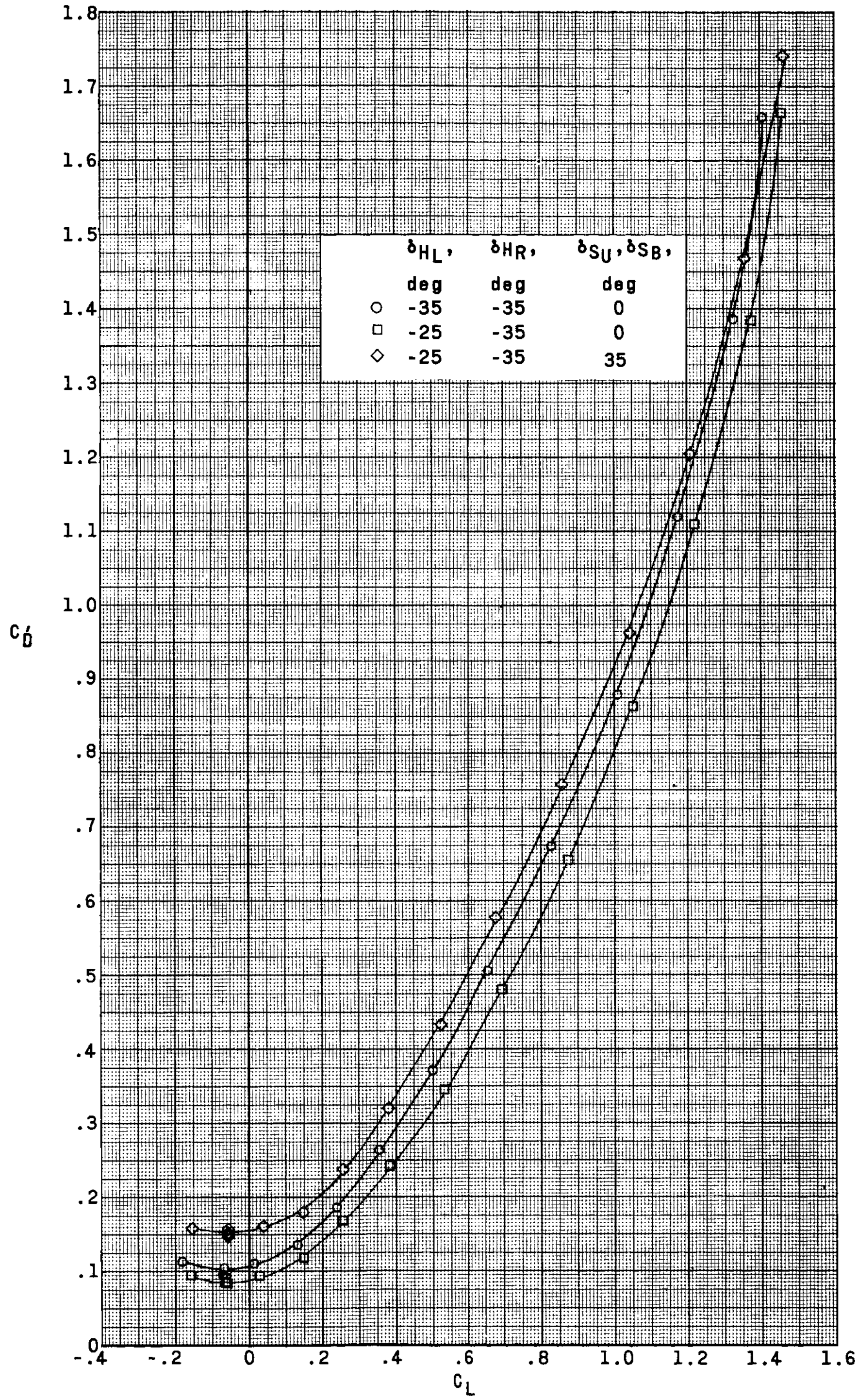

(c) Concluded.

Figure 19.- Concluded.

[redacted]

[redacted]

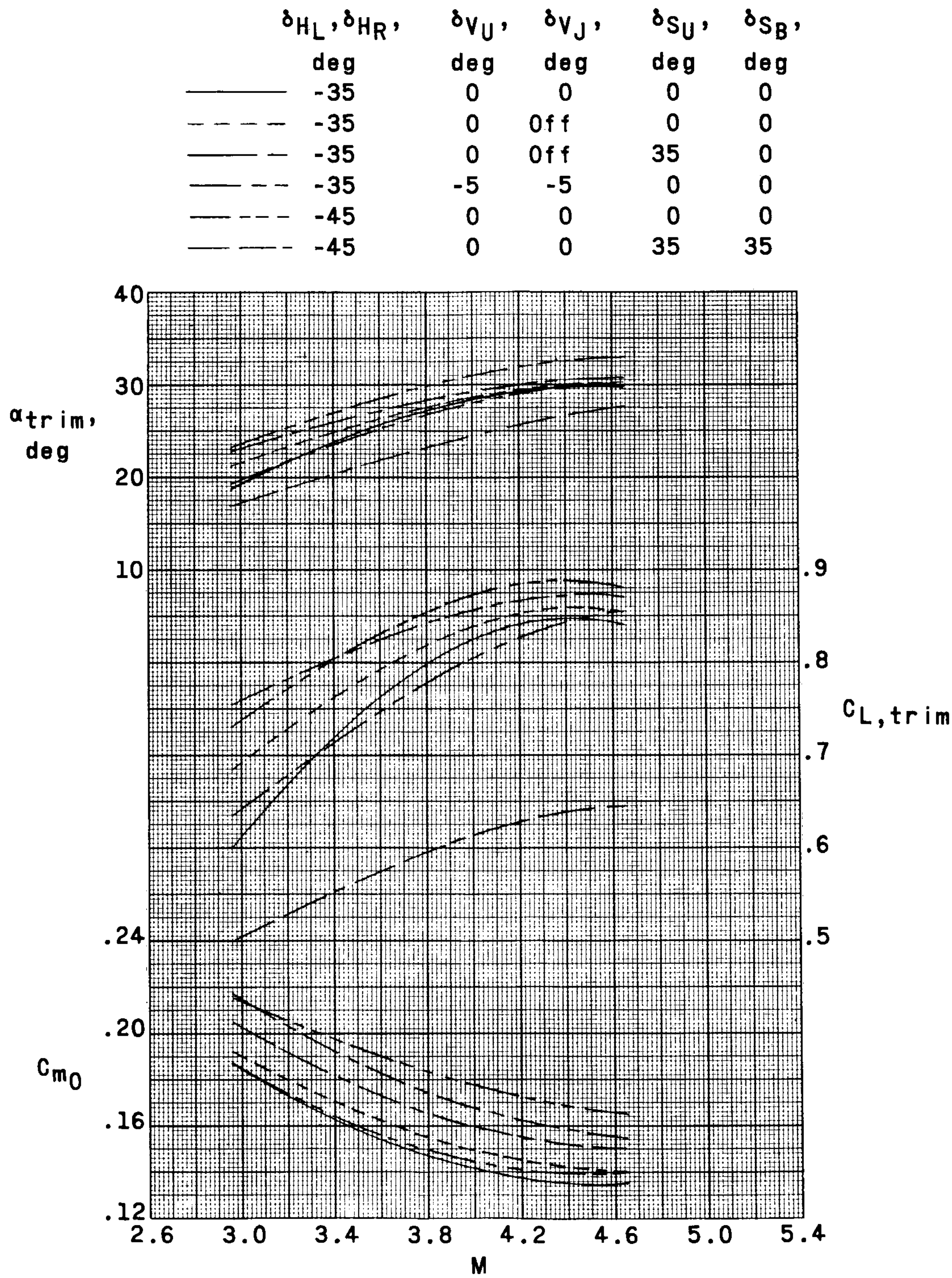

Figure 20.- Variation of maximum trimmed conditions and zero-lift pitching-moment coefficient of various configurations with Mach number.

[redacted]

[redacted]

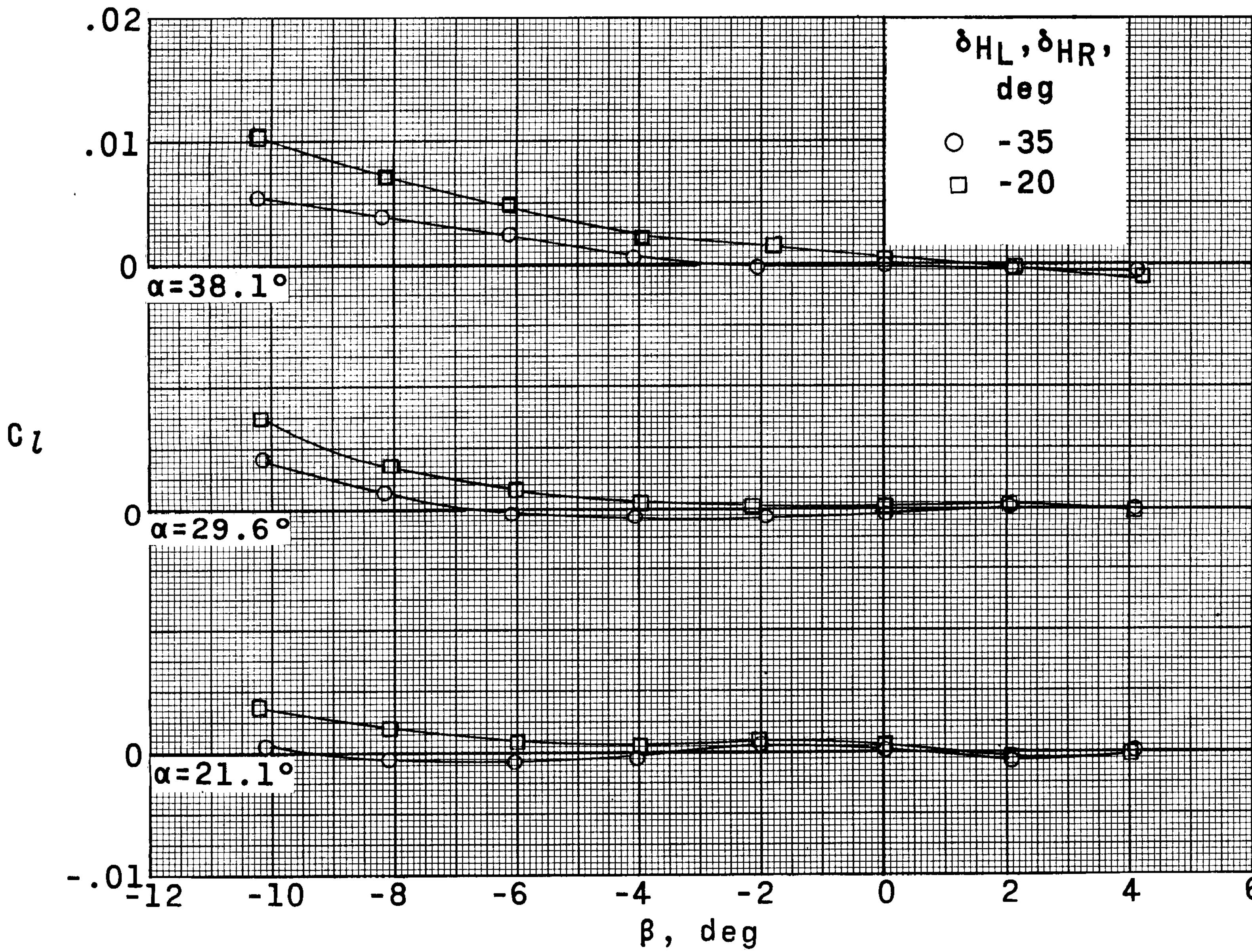

(a) M = 2.96.

Figure 21.- Effect of pitch-control deflections on aerodynamic characteristics in yaw at various angles of attack. $\delta_{V_U} = \delta_{V_J} = 0^{\circ}$; speed brakes retracted; WFHVJ.

[redacted]

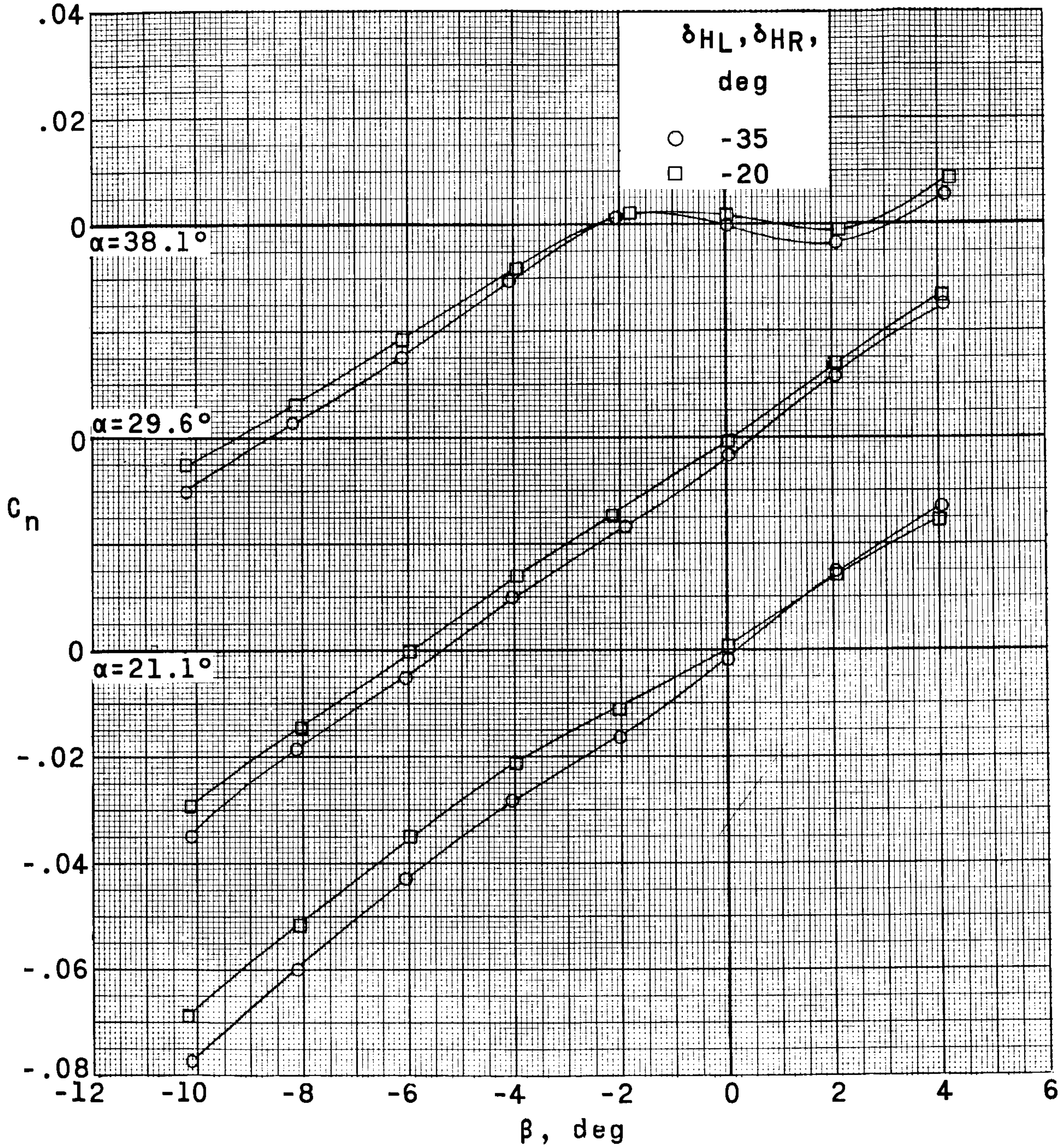

(a) Continued.

Figure 21.- Continued.

[redacted]

[redacted]

DECLASSIFIED

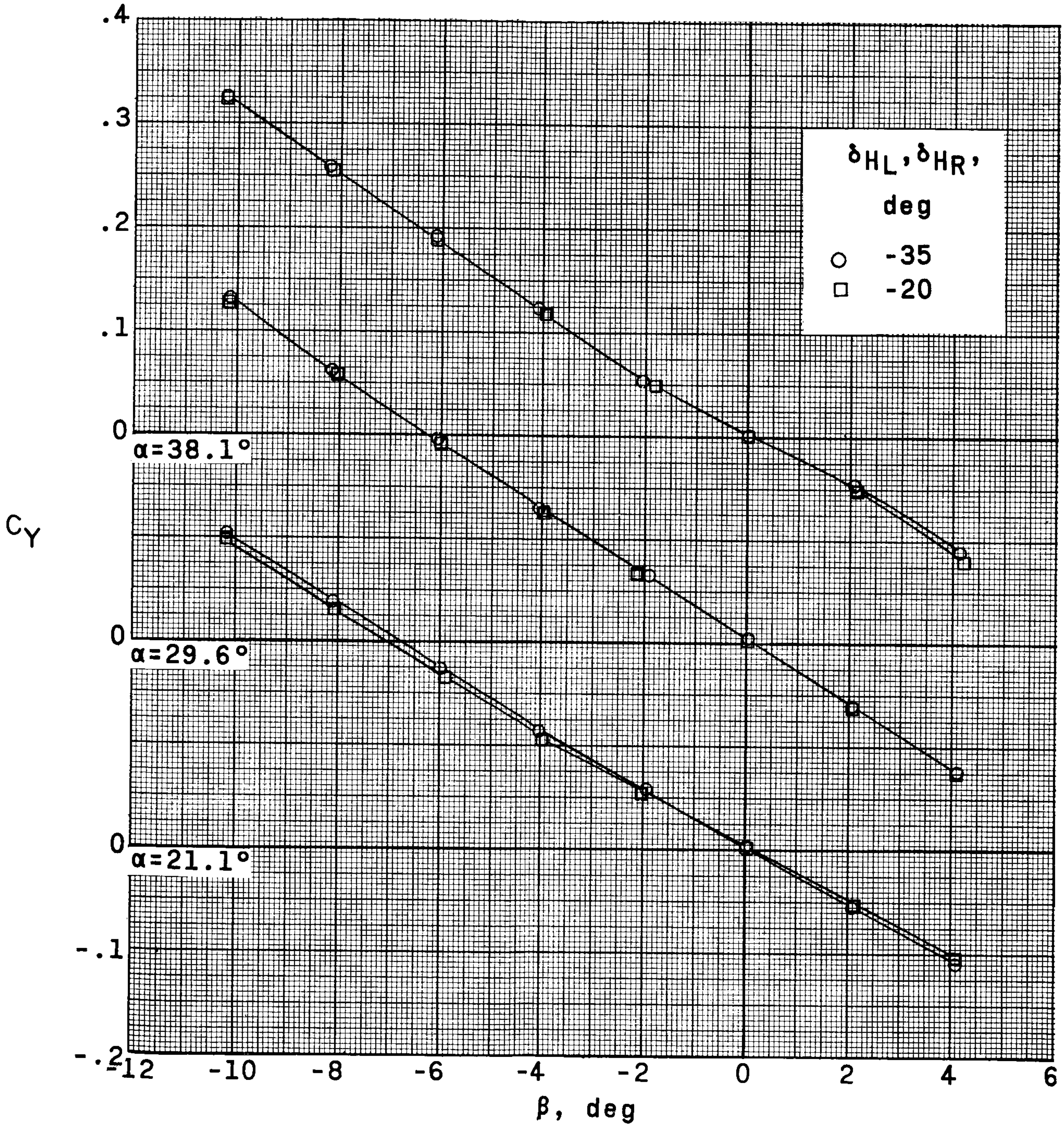

(a) Concluded.

Figure 21.- Continued.

[redacted]

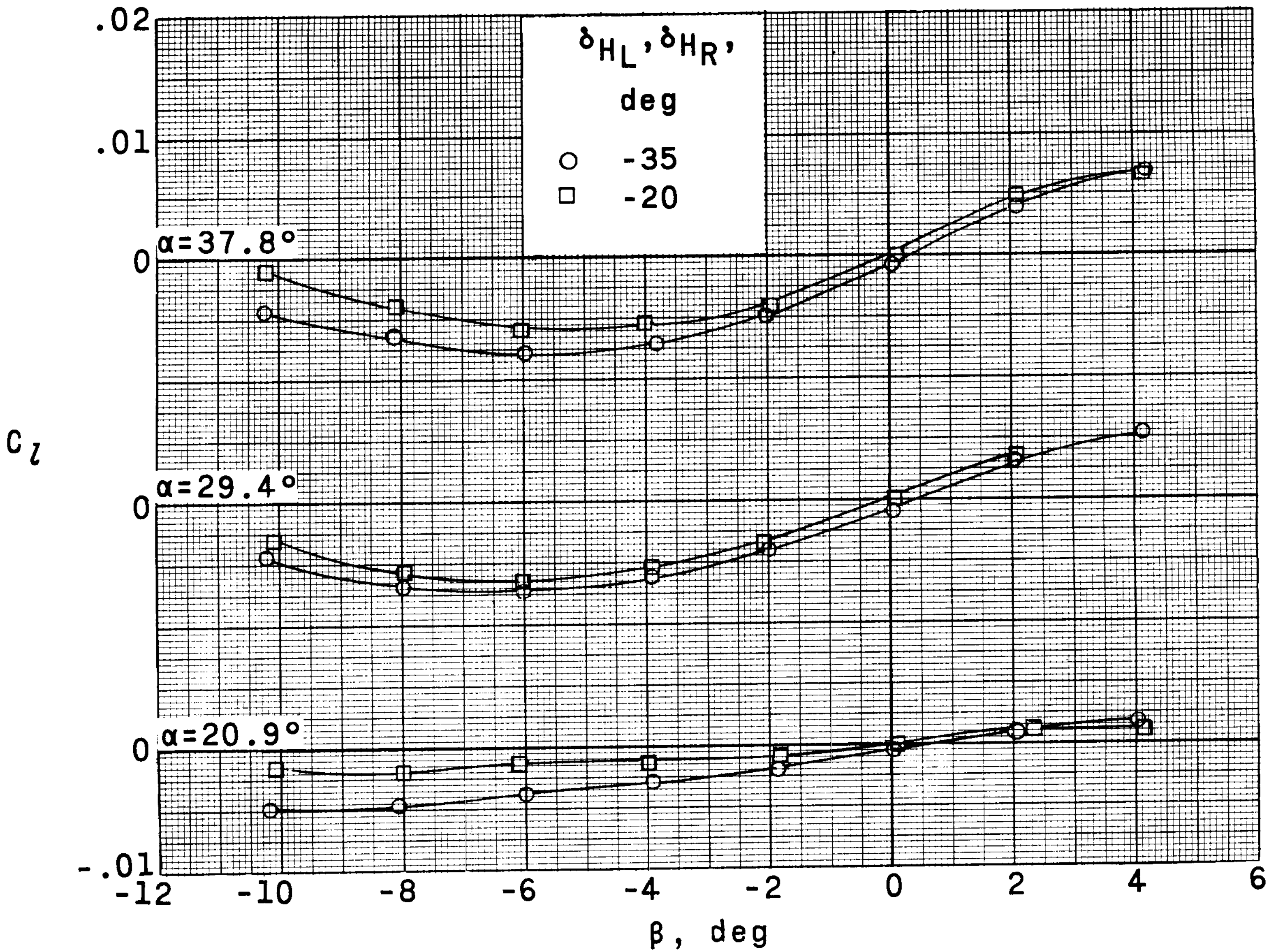

(b) M = 3.96.

Figure 21.- Continued.

[redacted]

DECLASSIFIED

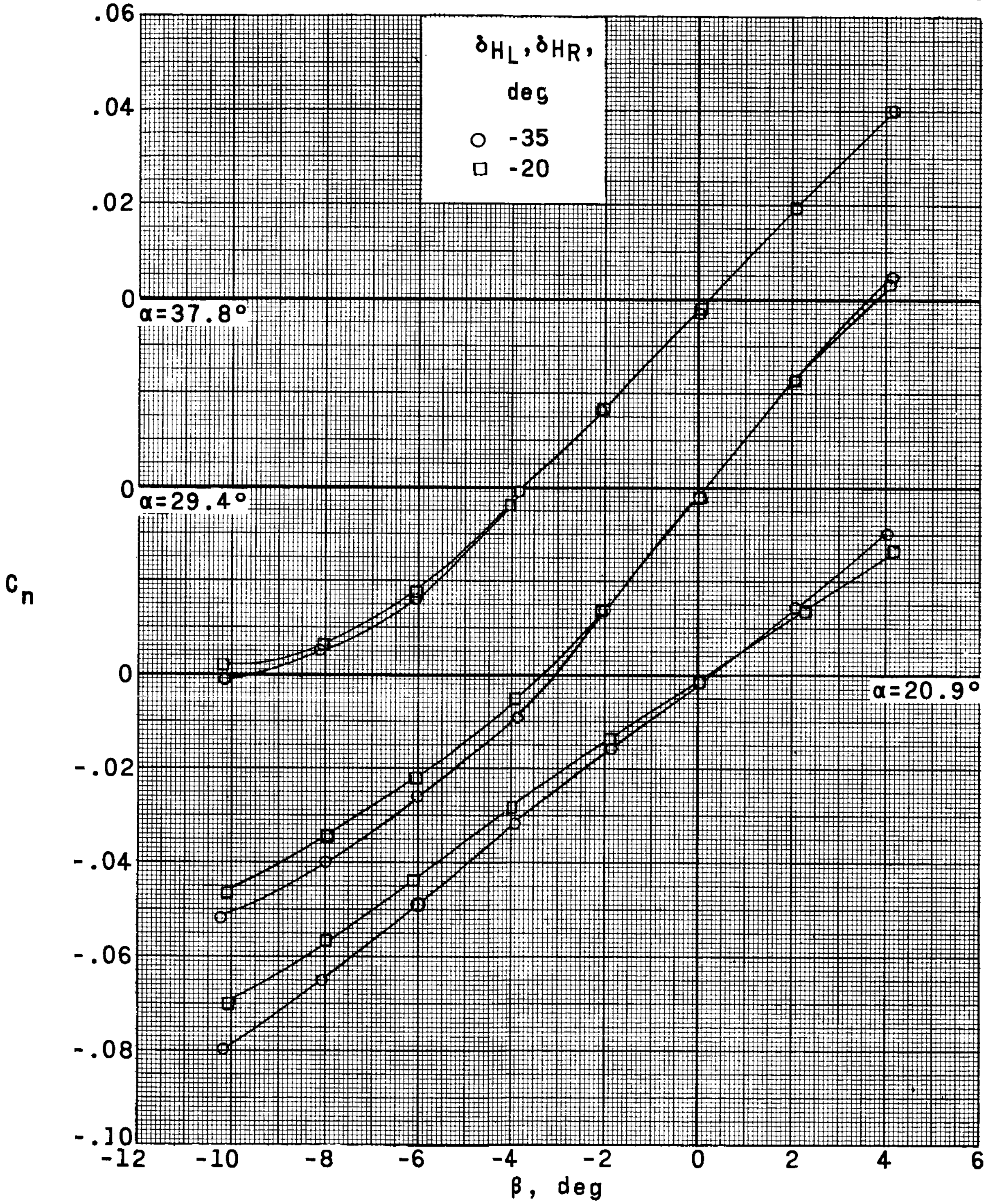

(b) Continued.

Figure 21.- Continued.

[redacted]

[redacted]

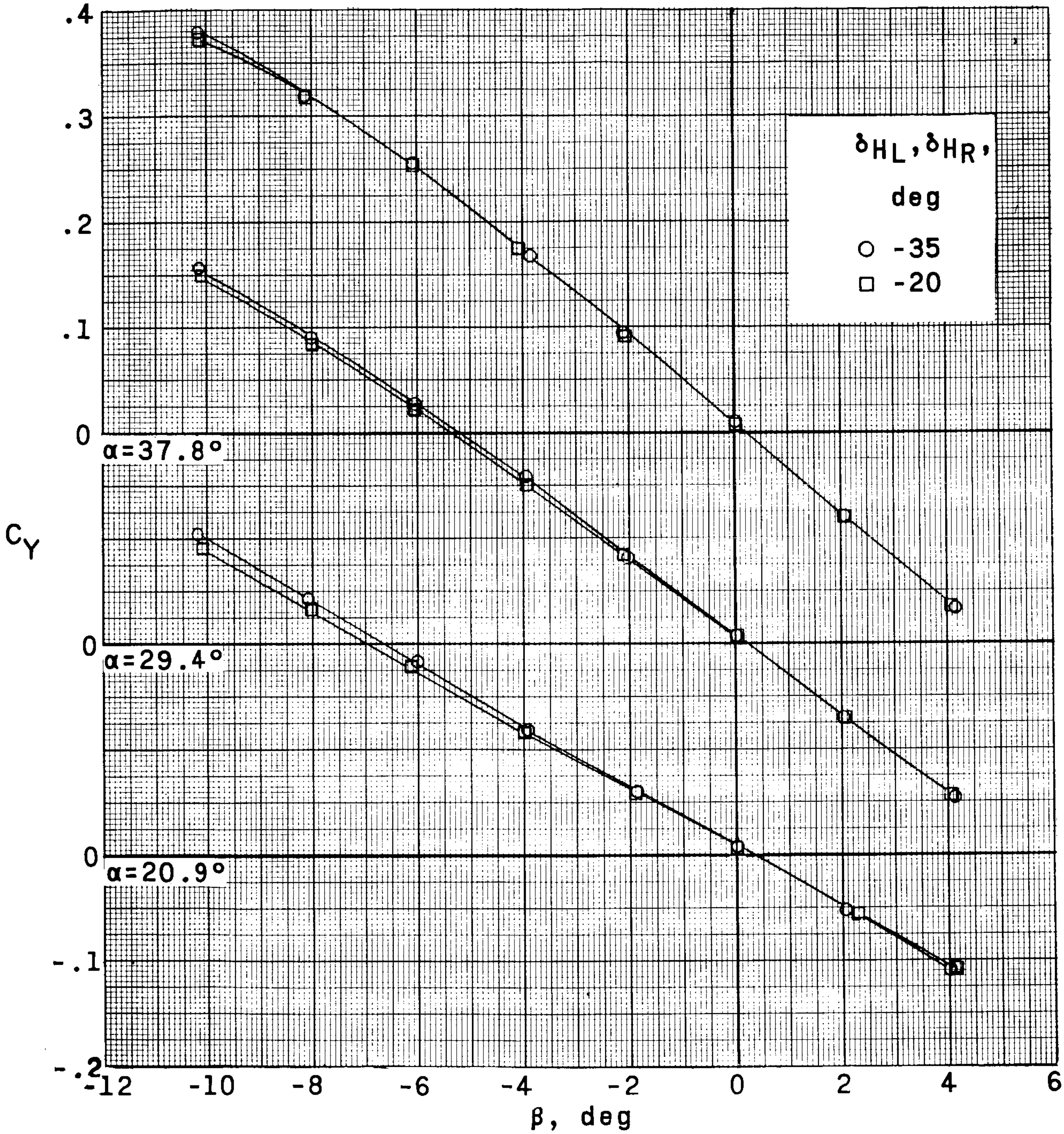

(b) Concluded.

Figure 21.- Continued.

[redacted]

[redacted]

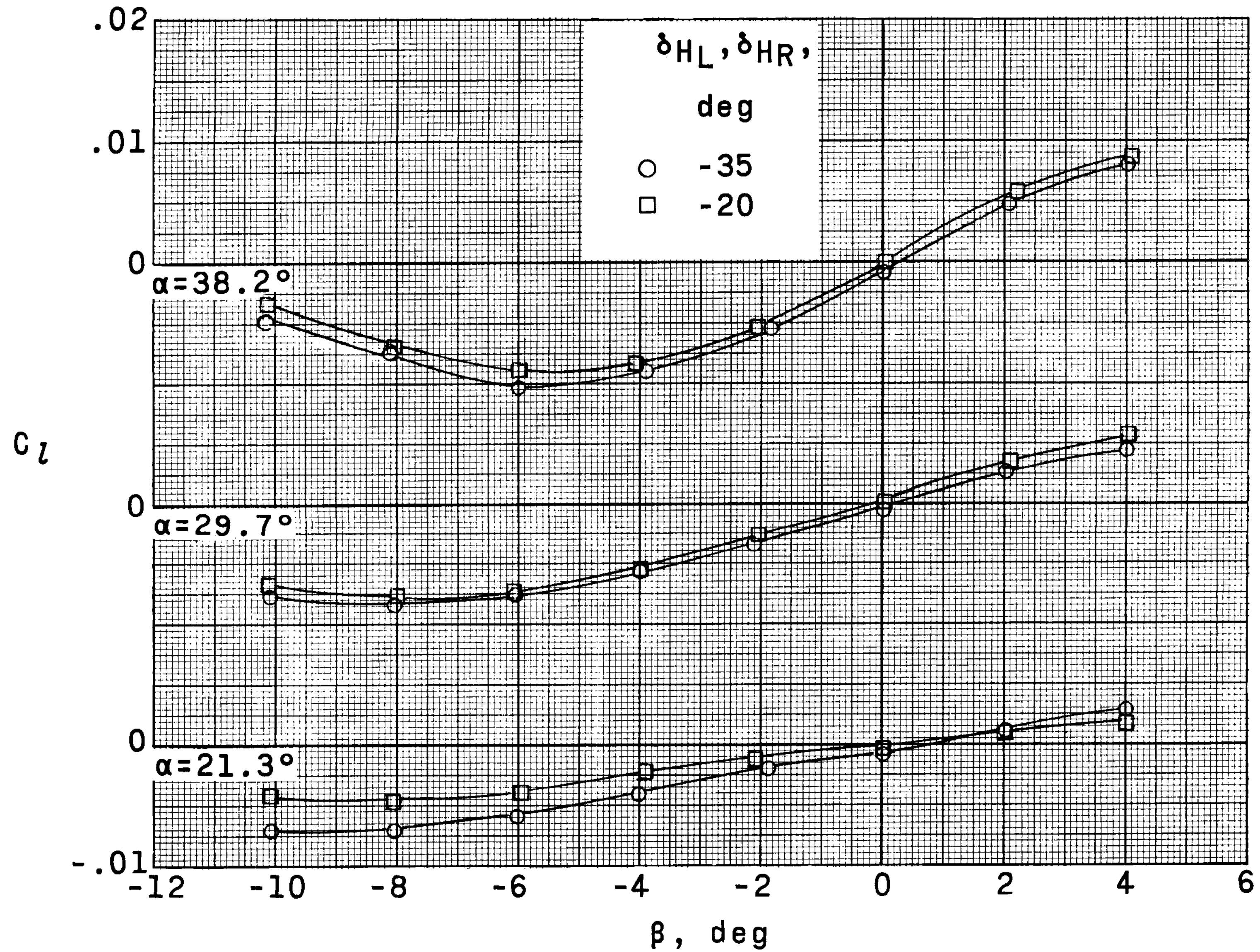

(c) M = 4.65.

Figure 21.- Continued.

[redacted]

[redacted]

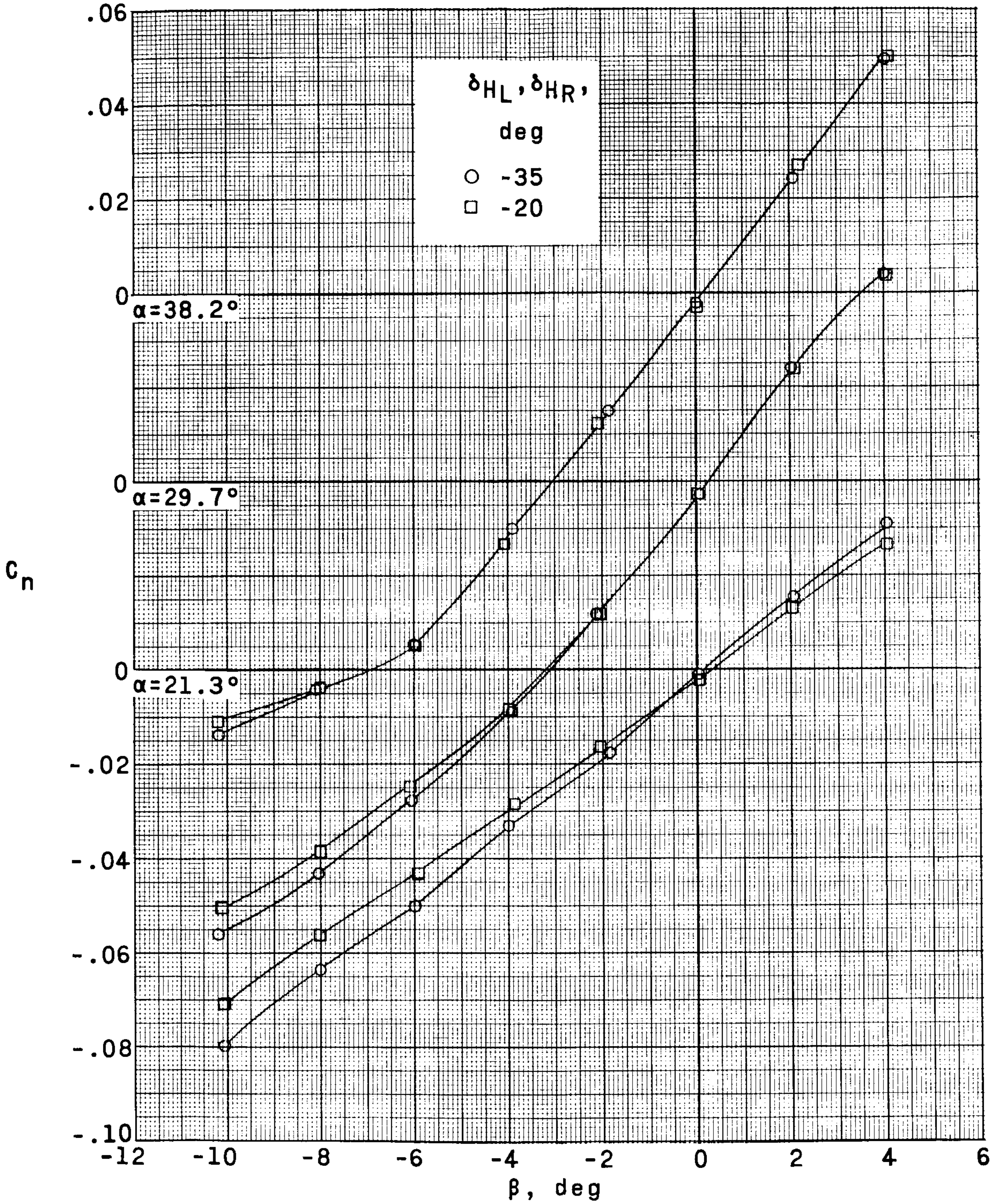

(c) Continued.

Figure 21.- Continued.

[redacted]

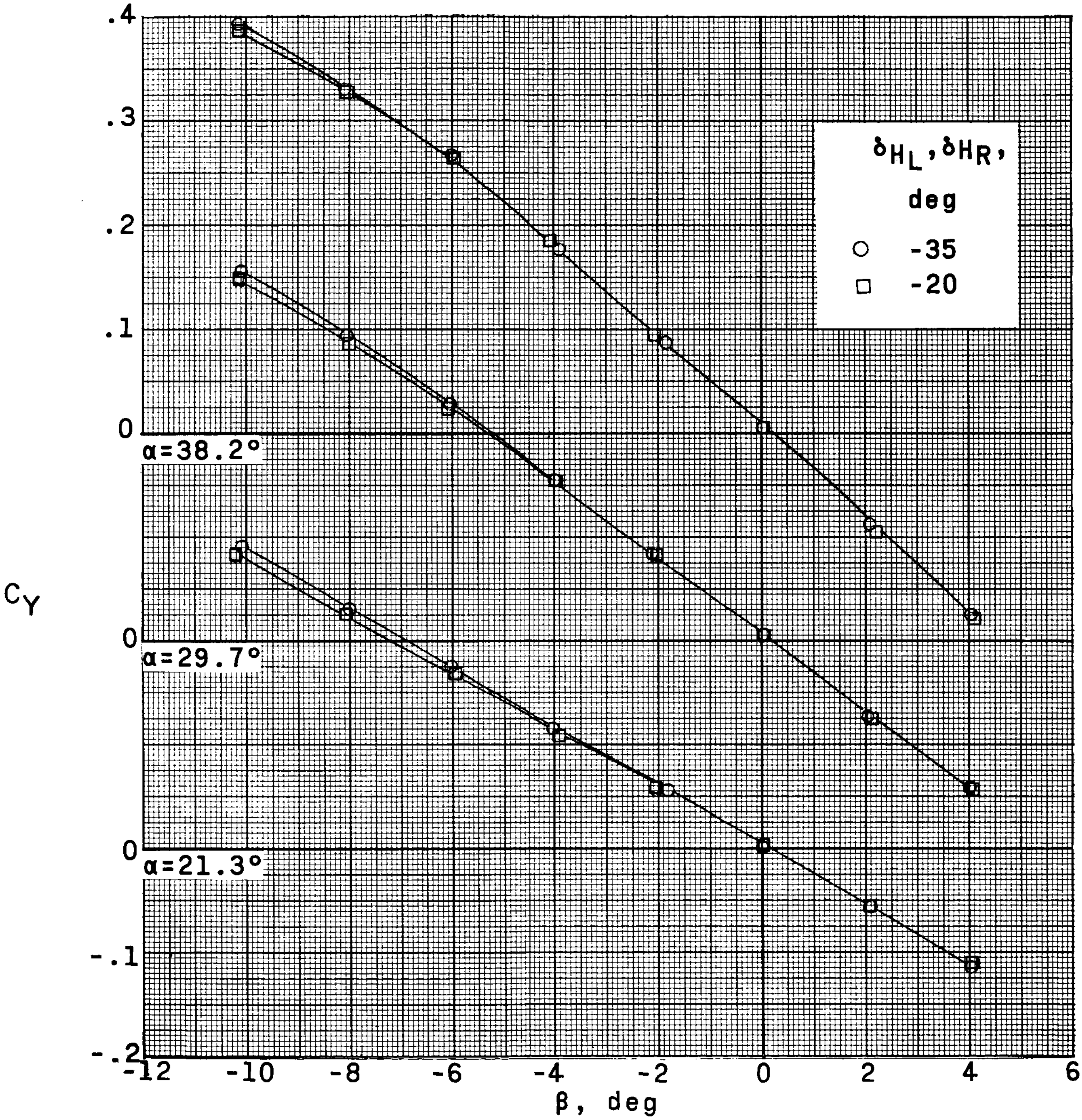

(c) Concluded.

Figure 21.- Concluded.

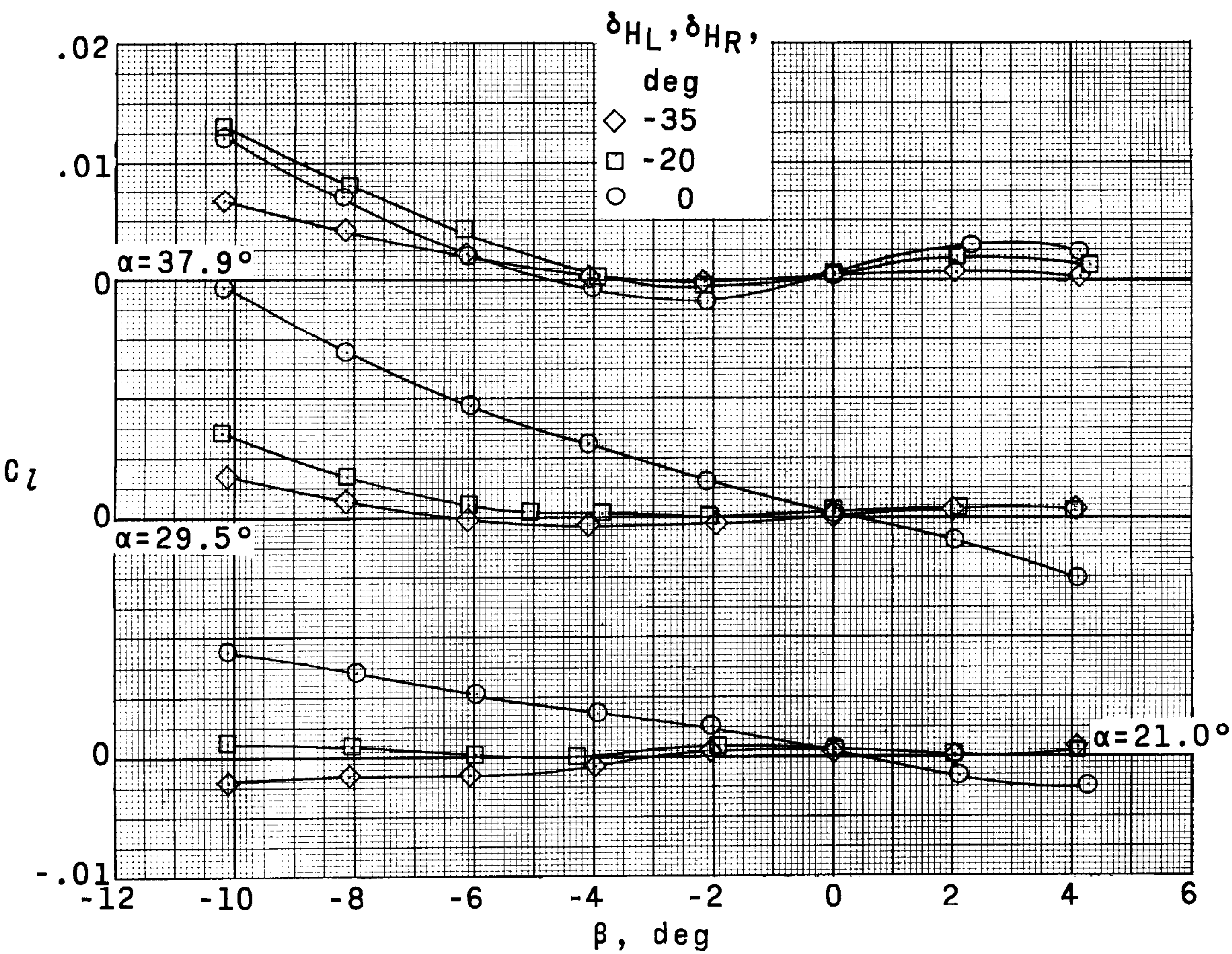

(a) M = 2.96.

Figure 22.- Effect of pitch-control deflections on aerodynamic characteristics in yaw at various angles of attack. $\delta_{V_U} = \delta_{V_J} = 0^{\circ}$; $\delta_{S_U} = \delta_{S_B} = 35^{\circ}$; WFHVJ.

[redacted]

[redacted]

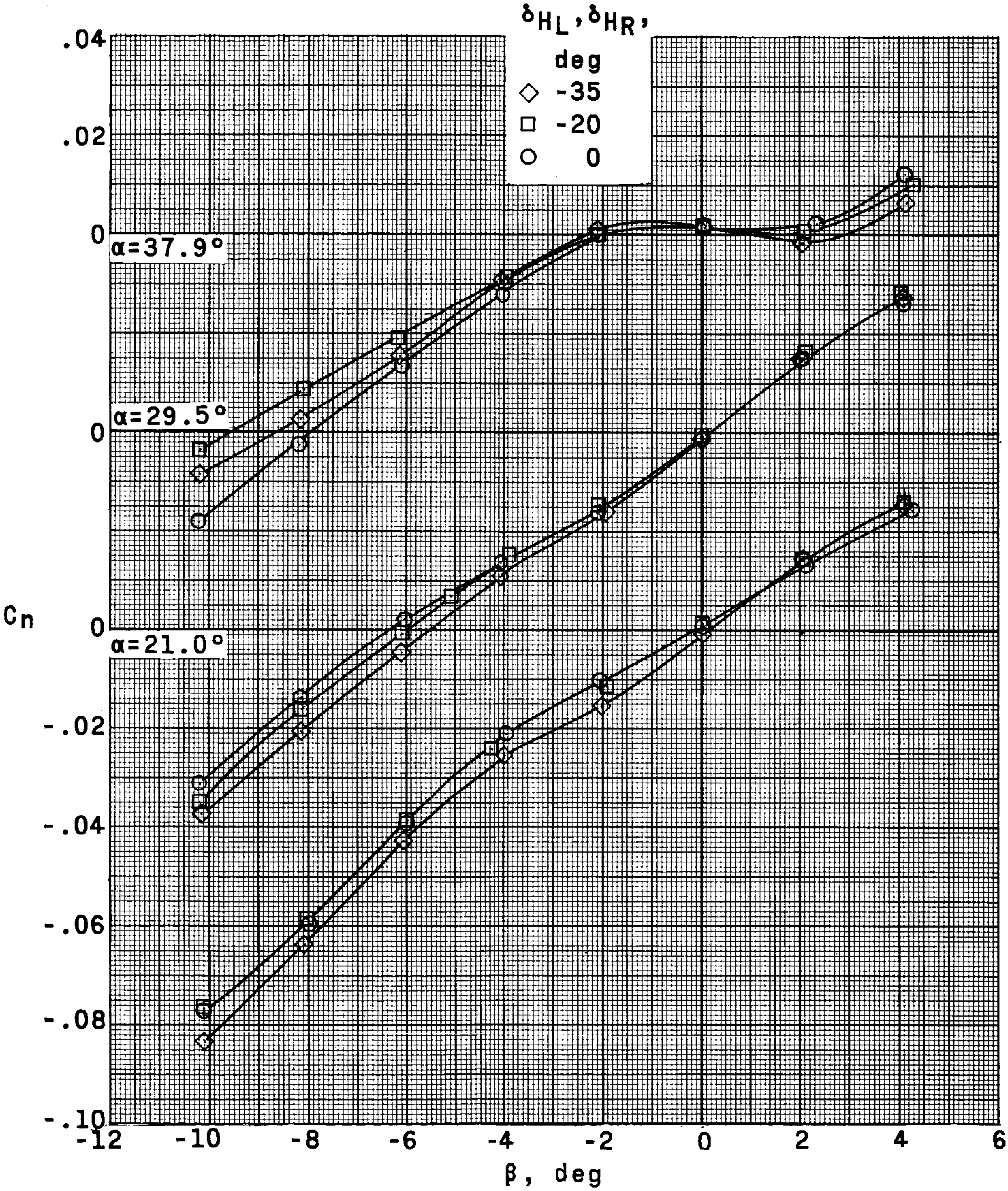

(a) Continued.

Figure 22.- Continued.

[redacted]

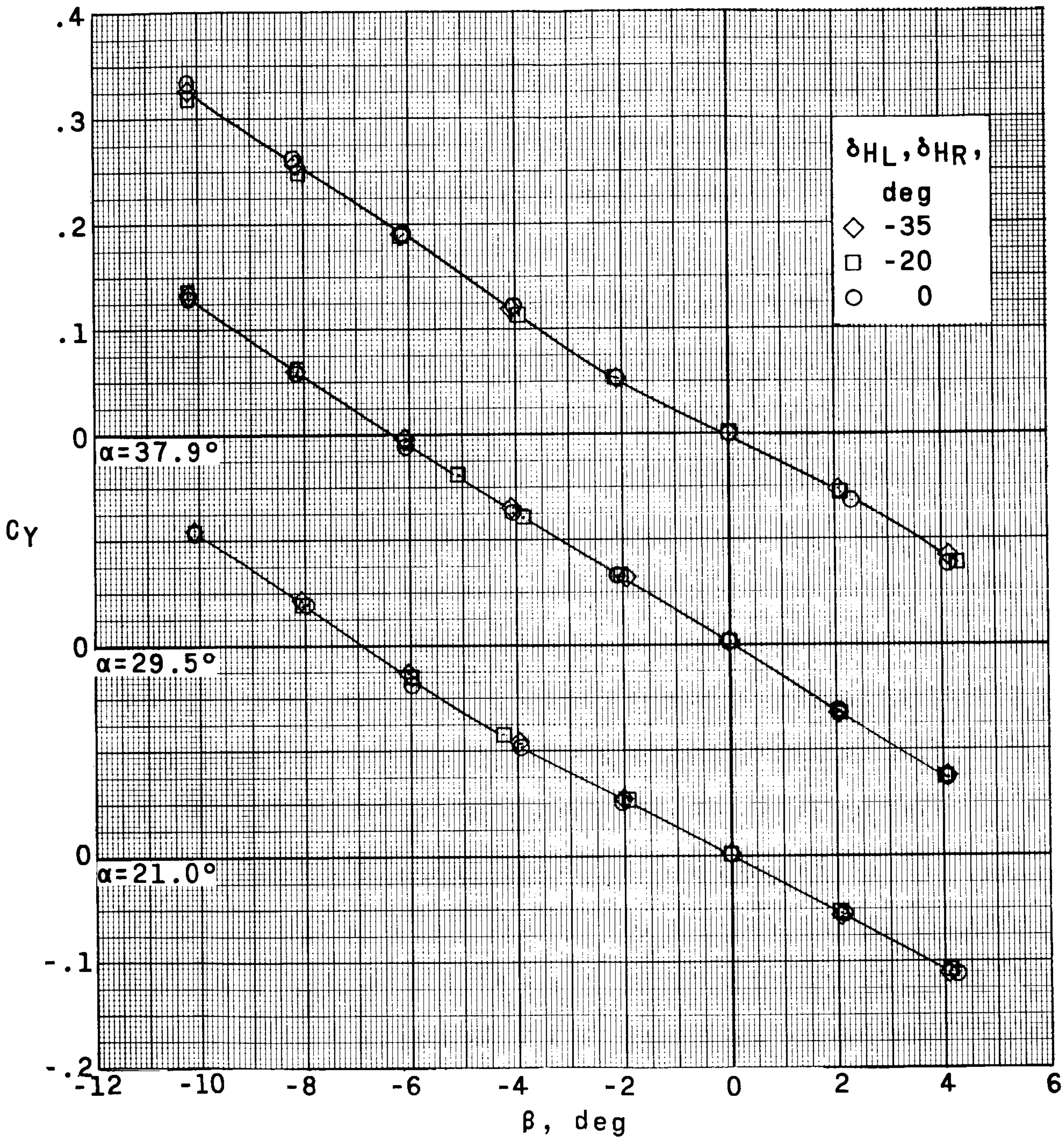

(a) Concluded.

Figure 22.- Continued.

[redacted]

[redacted]

DECLASSIFIED

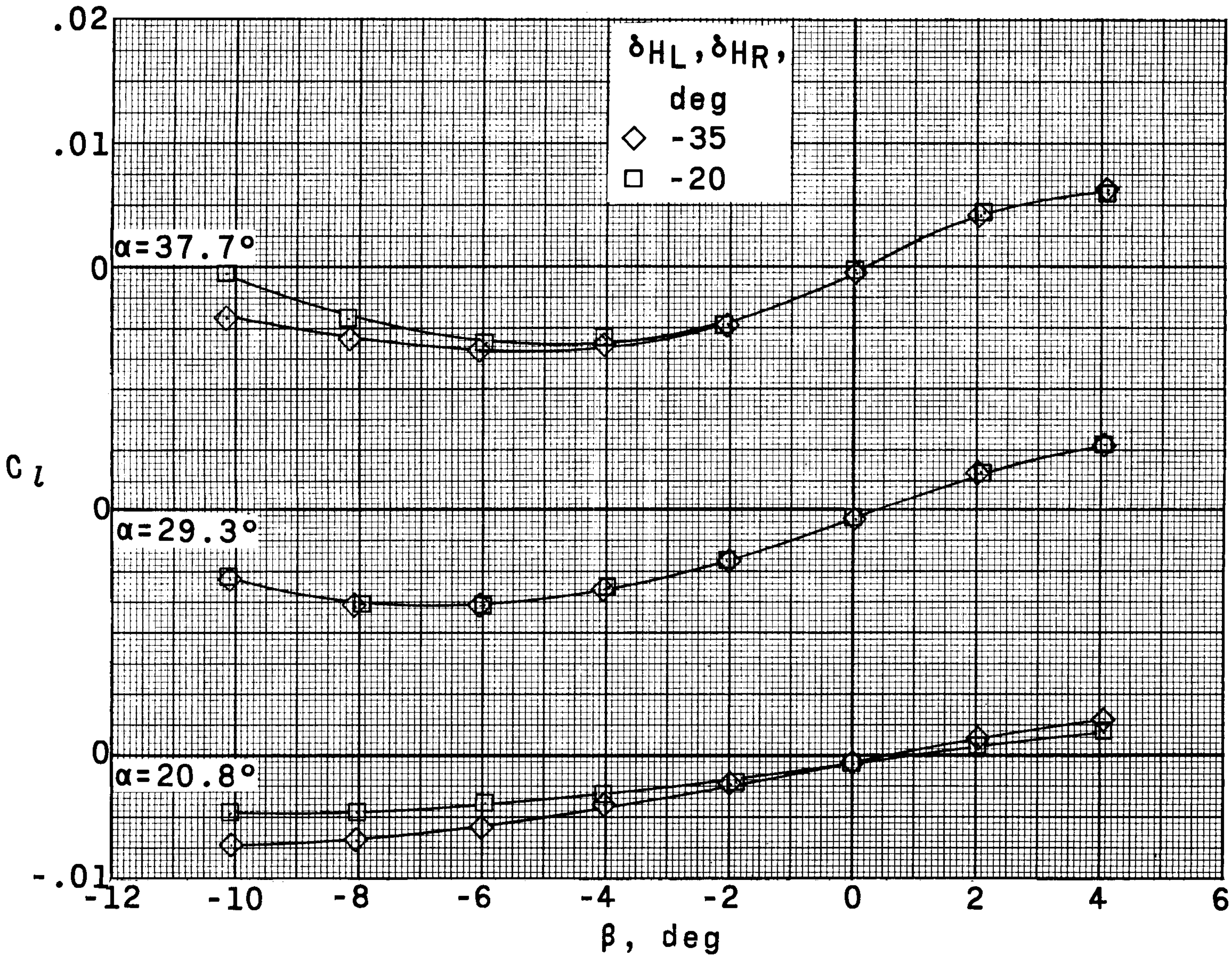

(b) M = 3.96.

Figure 22.- Continued.

[redacted]

[redacted]

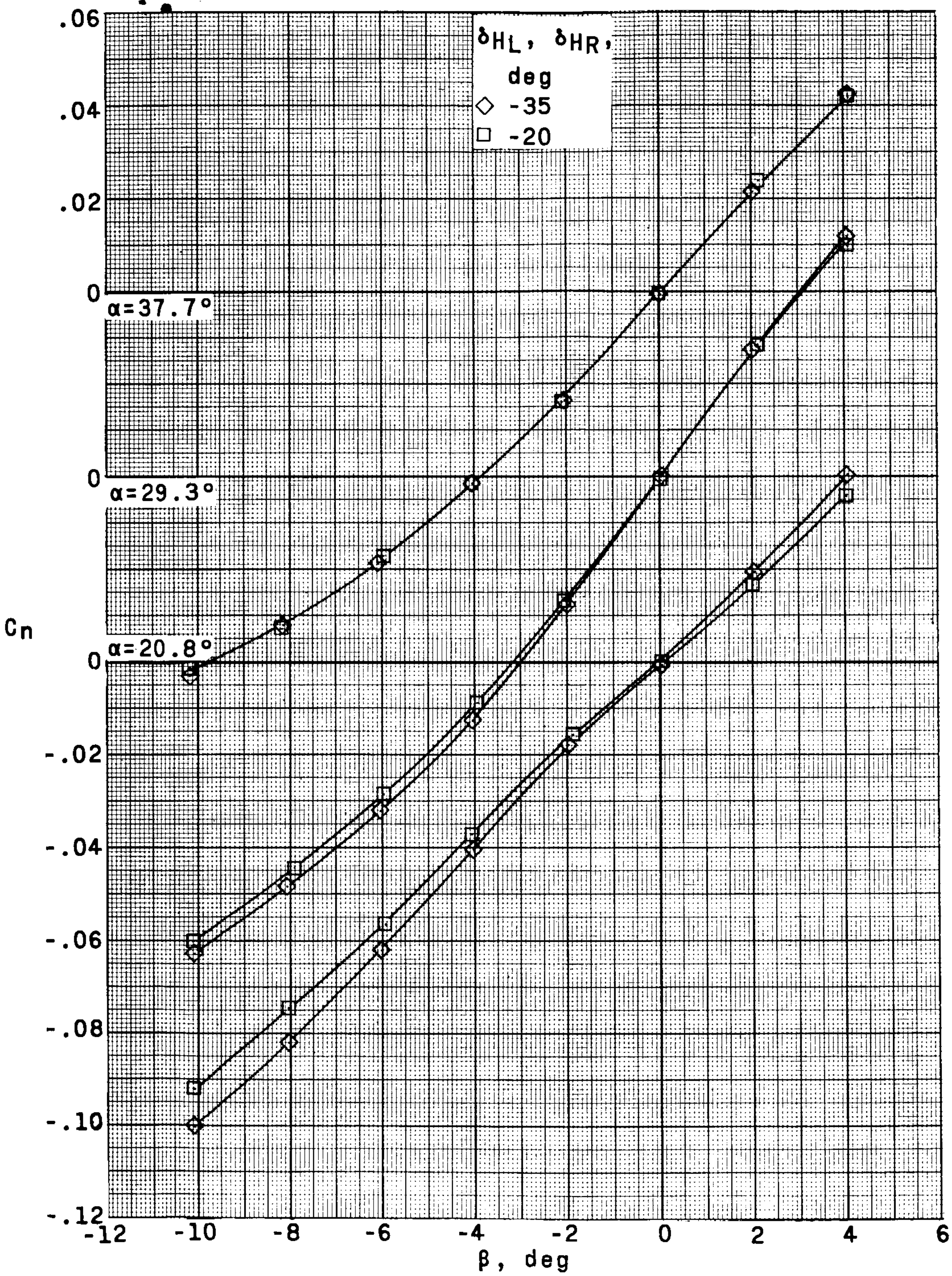

(b) Continued.

Figure 22.- Continued.

[redacted]

[redacted]LASSIFIED

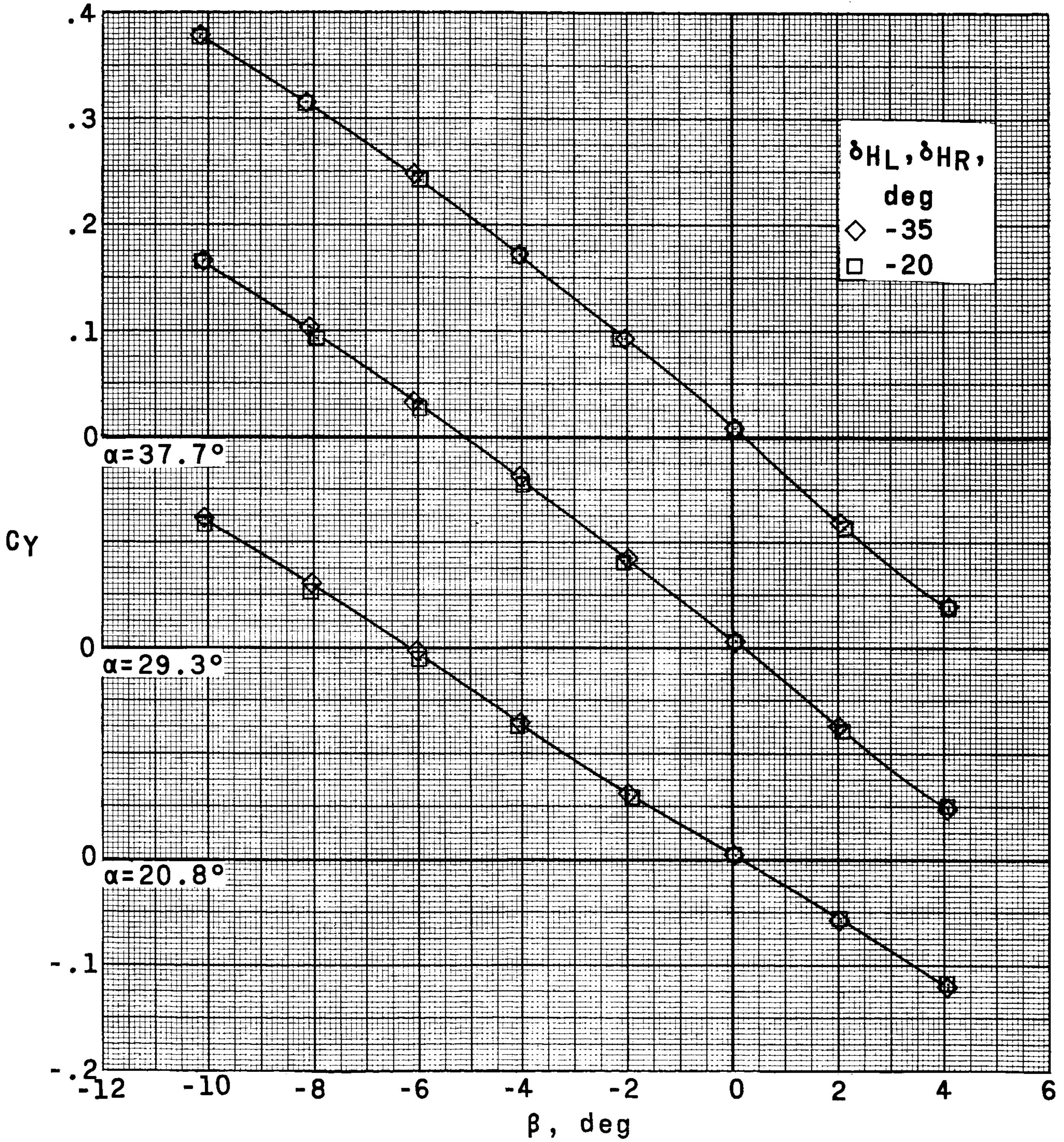

(b) Concluded.

Figure 22.- Continued.

[redacted]

[redacted]

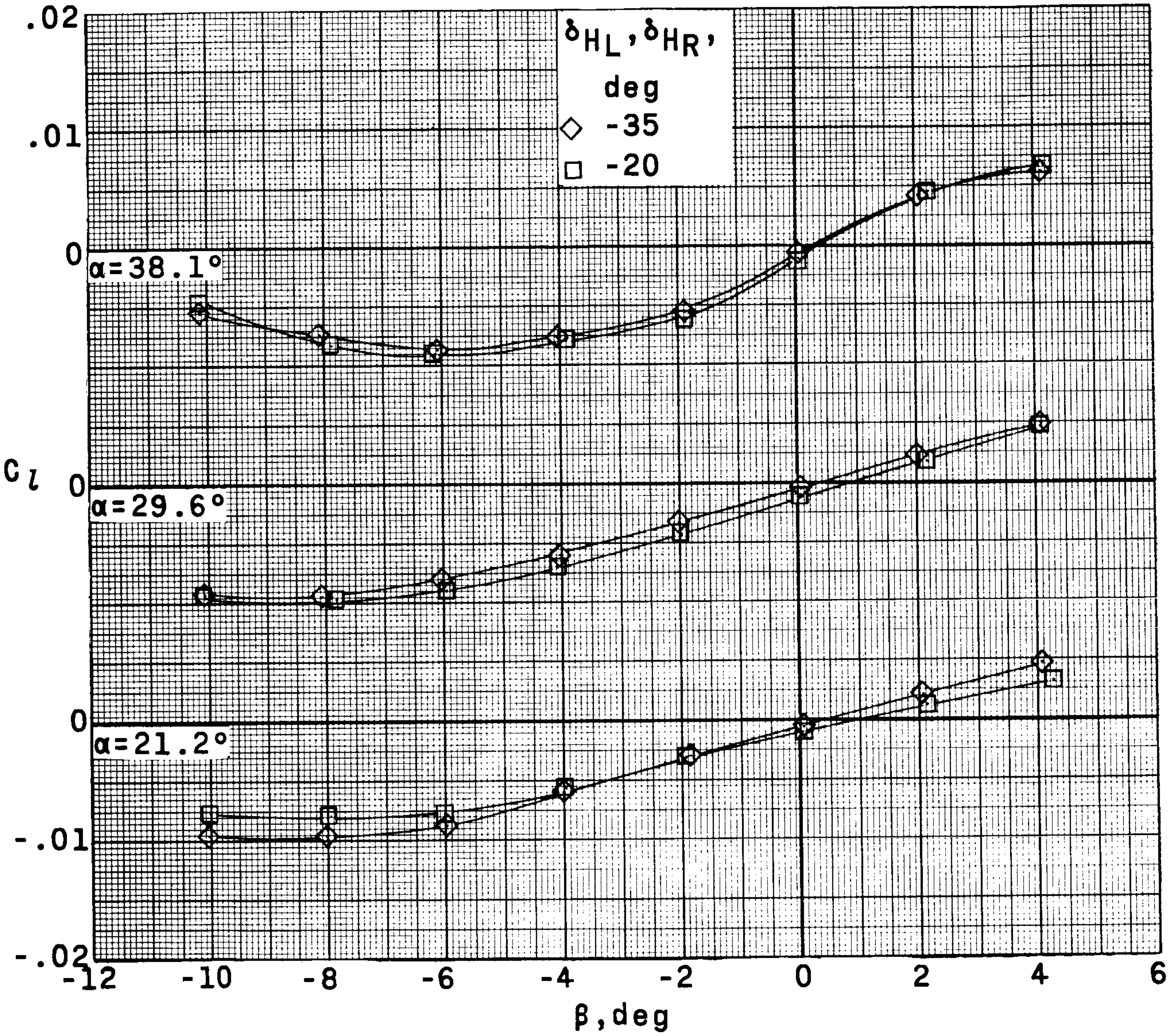

(c) M = 4.65.

Figure 22.- Continued.

[redacted]

[redacted]

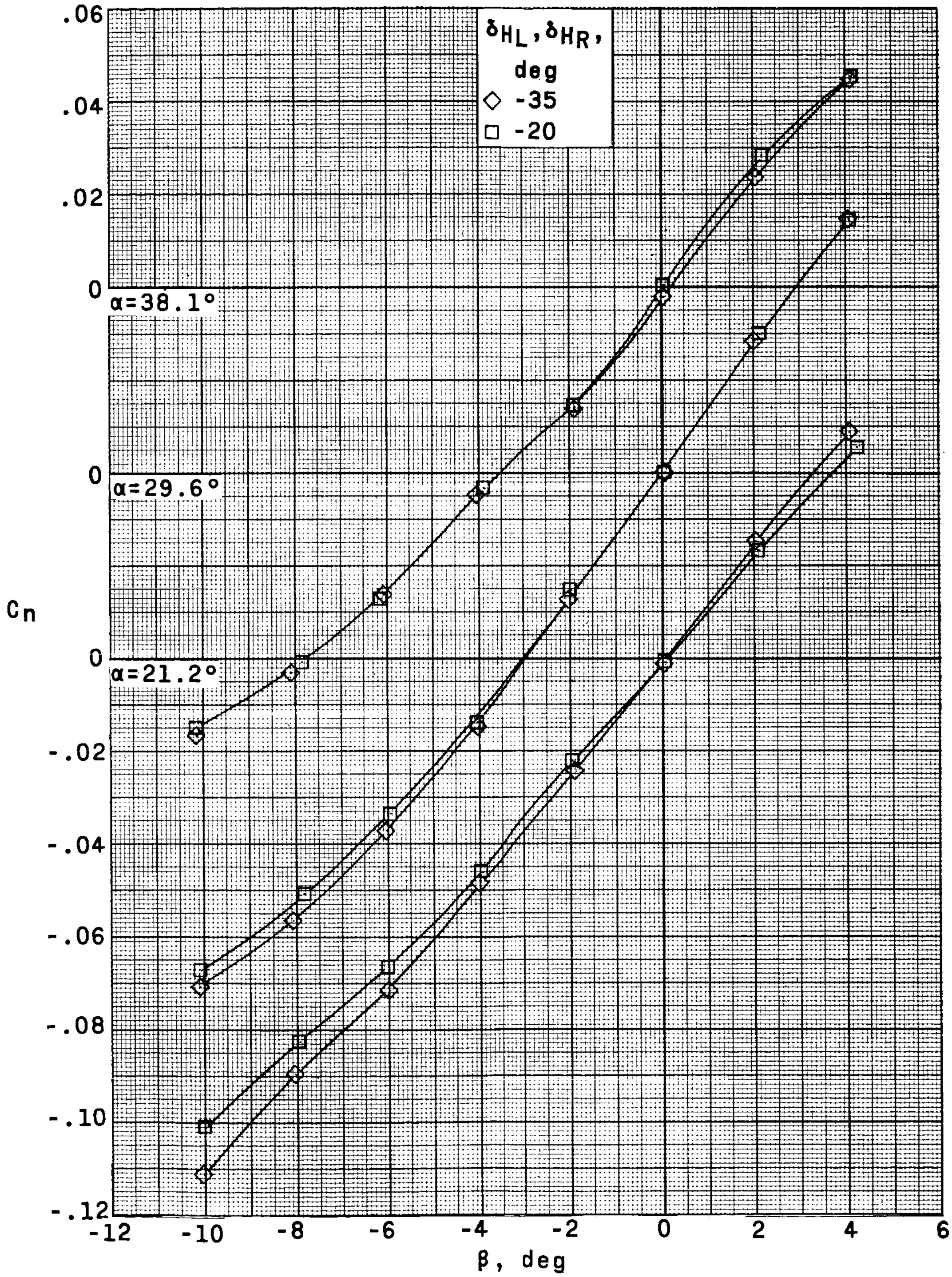

(c) Continued.

Figure 22.- Continued.

[redacted]

[redacted]

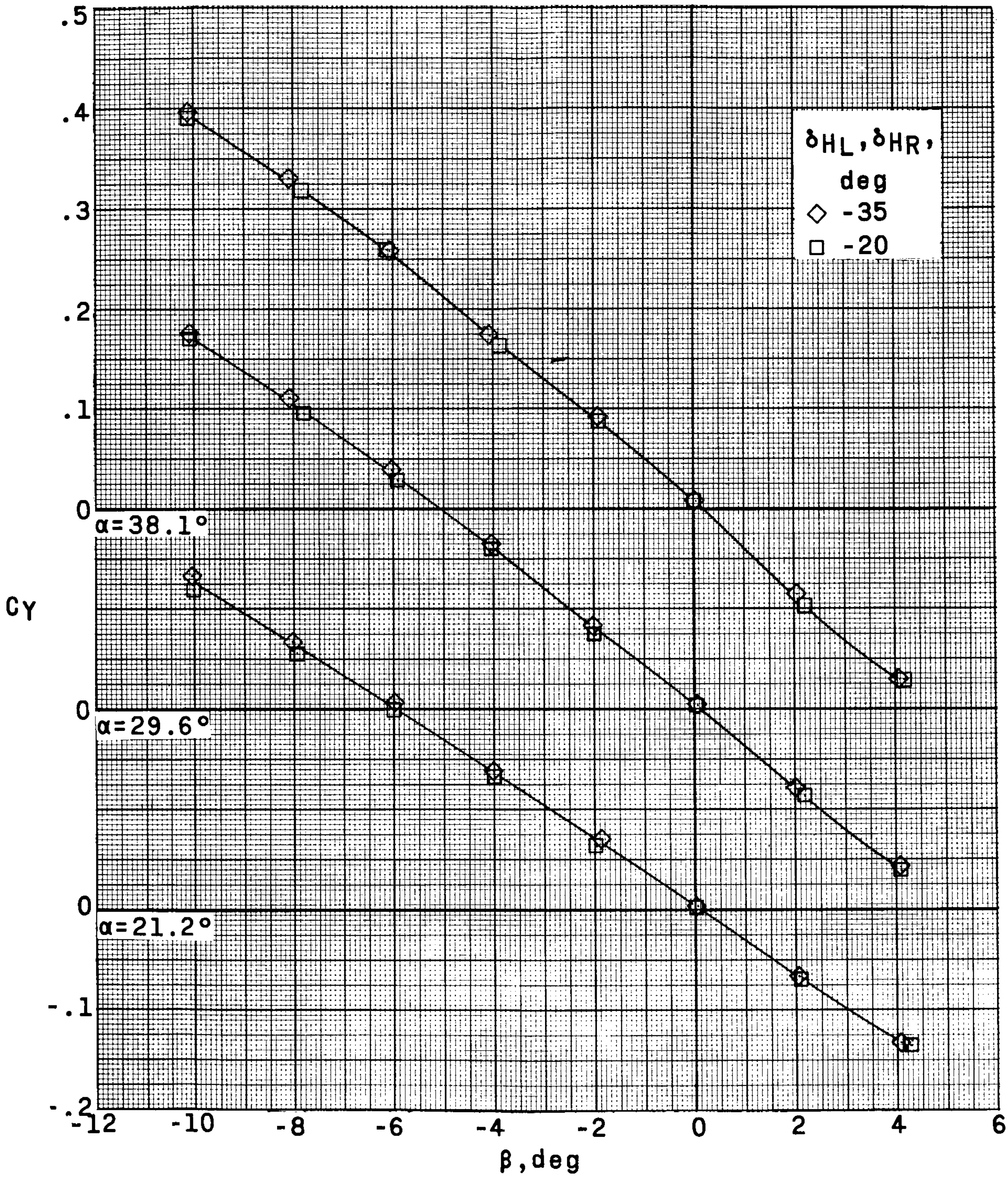

(c) Concluded.

Figure 22.- Concluded.

[redacted]

[redacted]

DECLASSIFIED

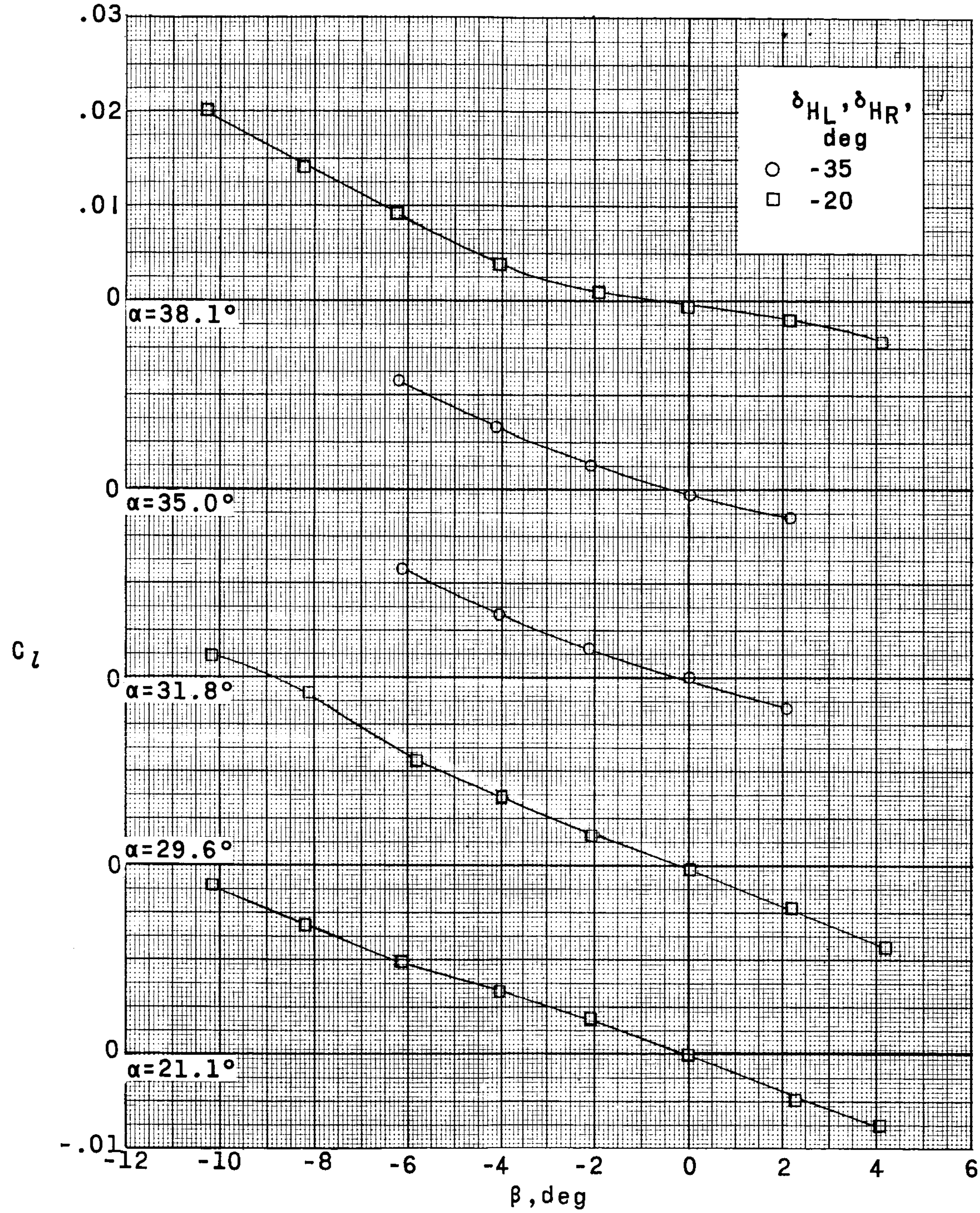

(a) M = 2.96.

Figure 23.- Aerodynamic characteristics in yaw at various angles of attack. $\delta_{V_U} = 0^{\circ}$; jettisonable portion of lower vertical stabilizer off; speed brakes retracted; WFHV.

[redacted]

[redacted]

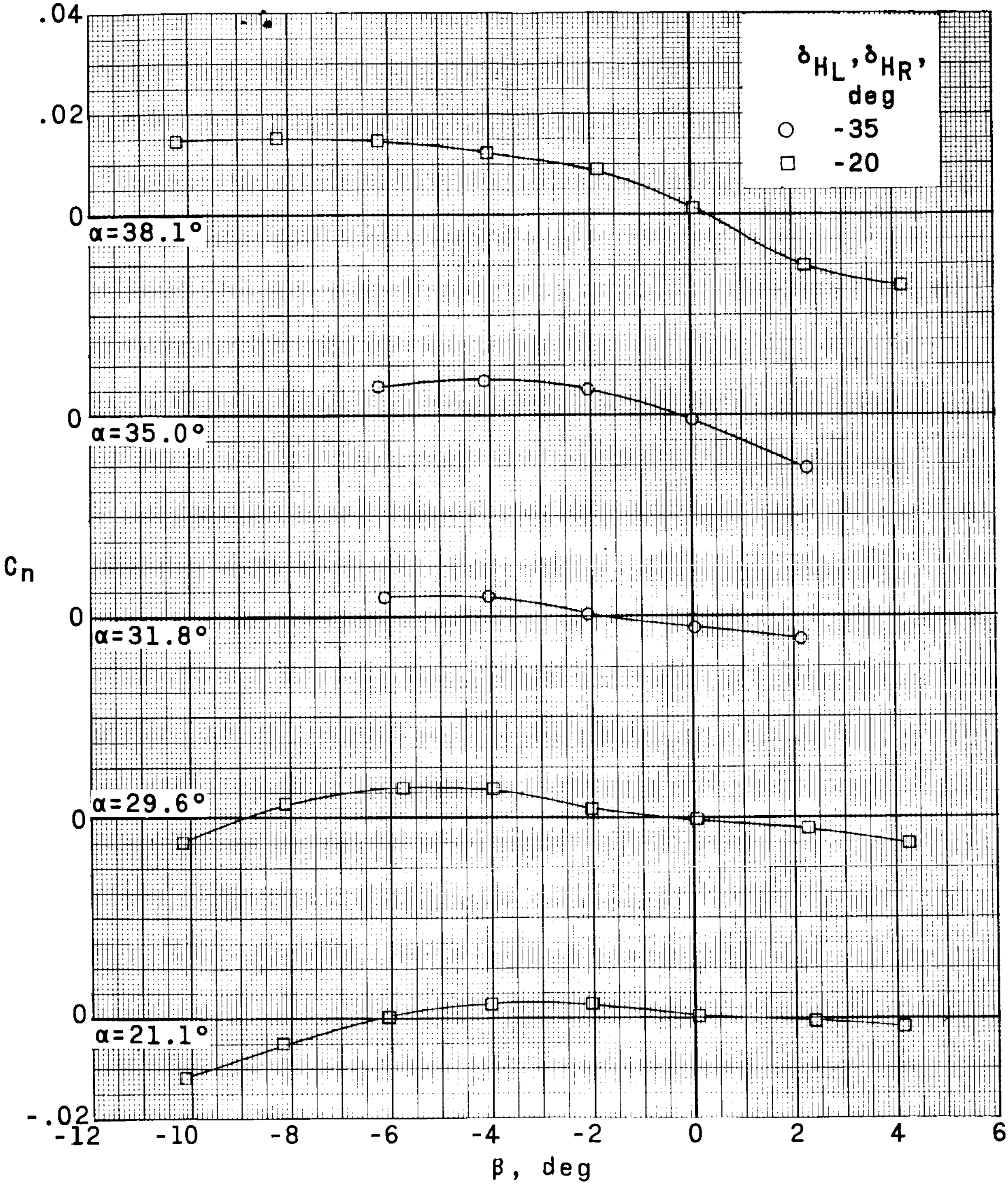

(a) Continued.

Figure 23.- Continued.

[redacted]

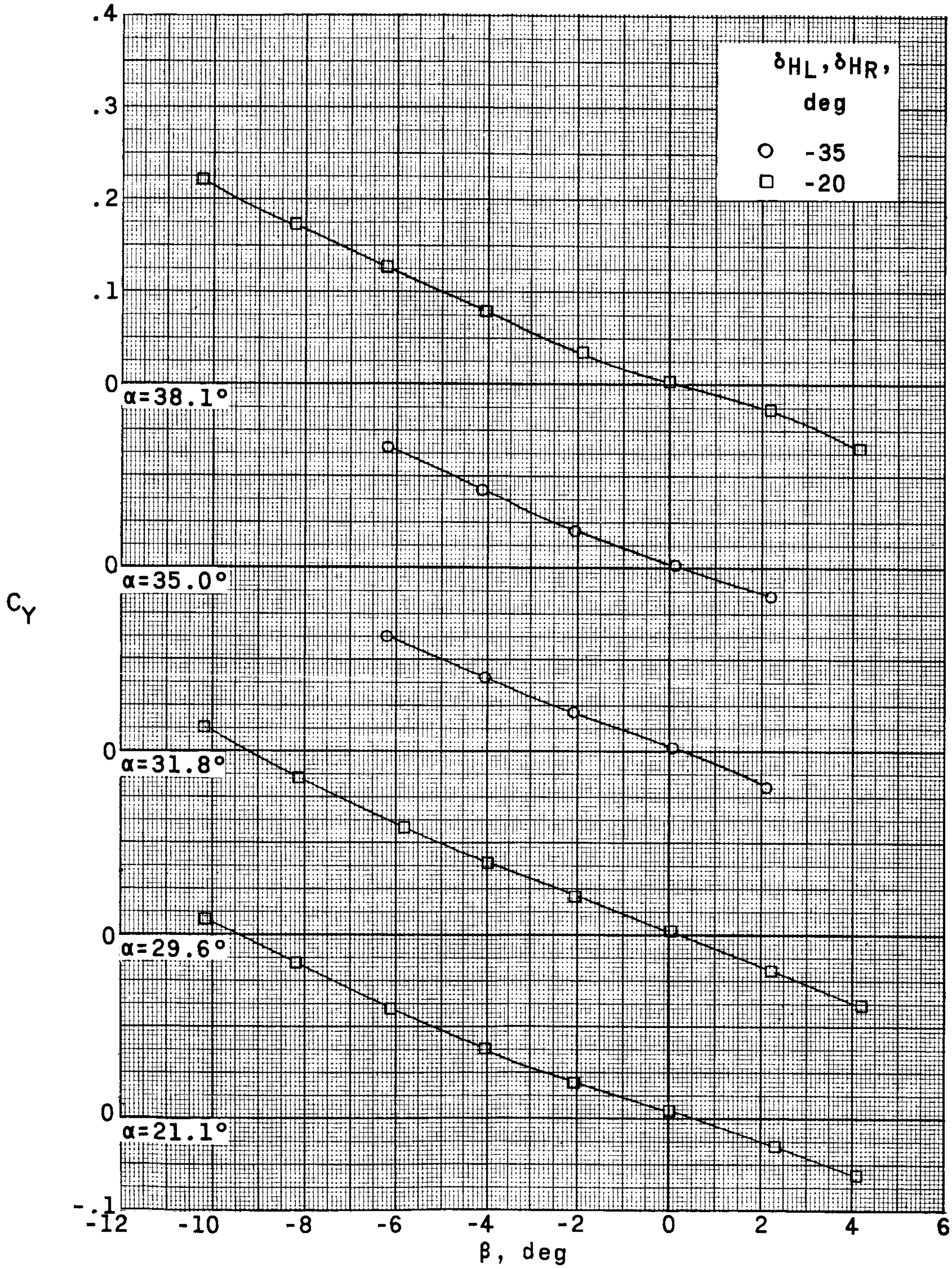

(a) Concluded.

Figure 23.- Continued.

[redacted]

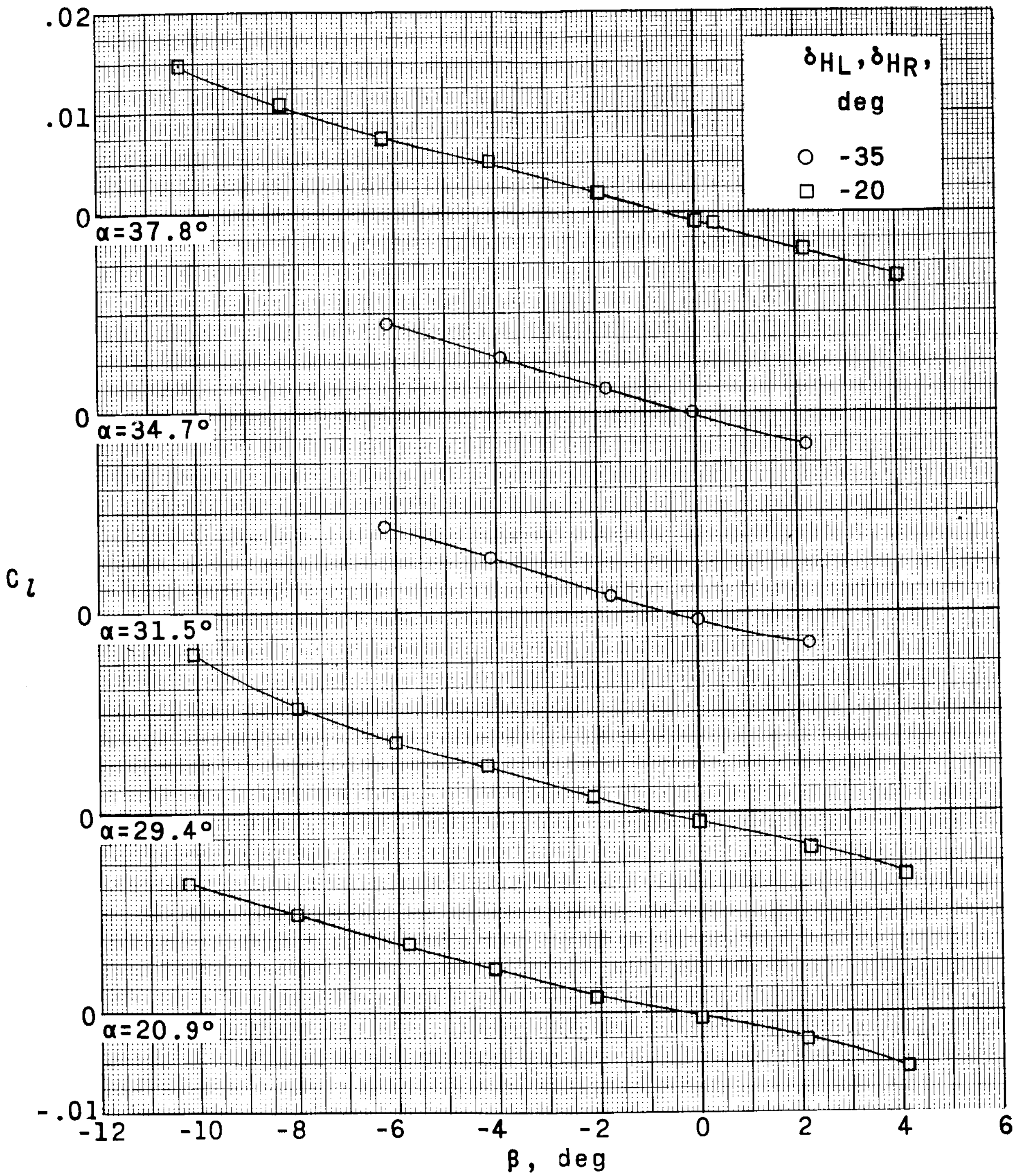

(b) M = 3.96.

Figure 23.- Continued.

[redacted]

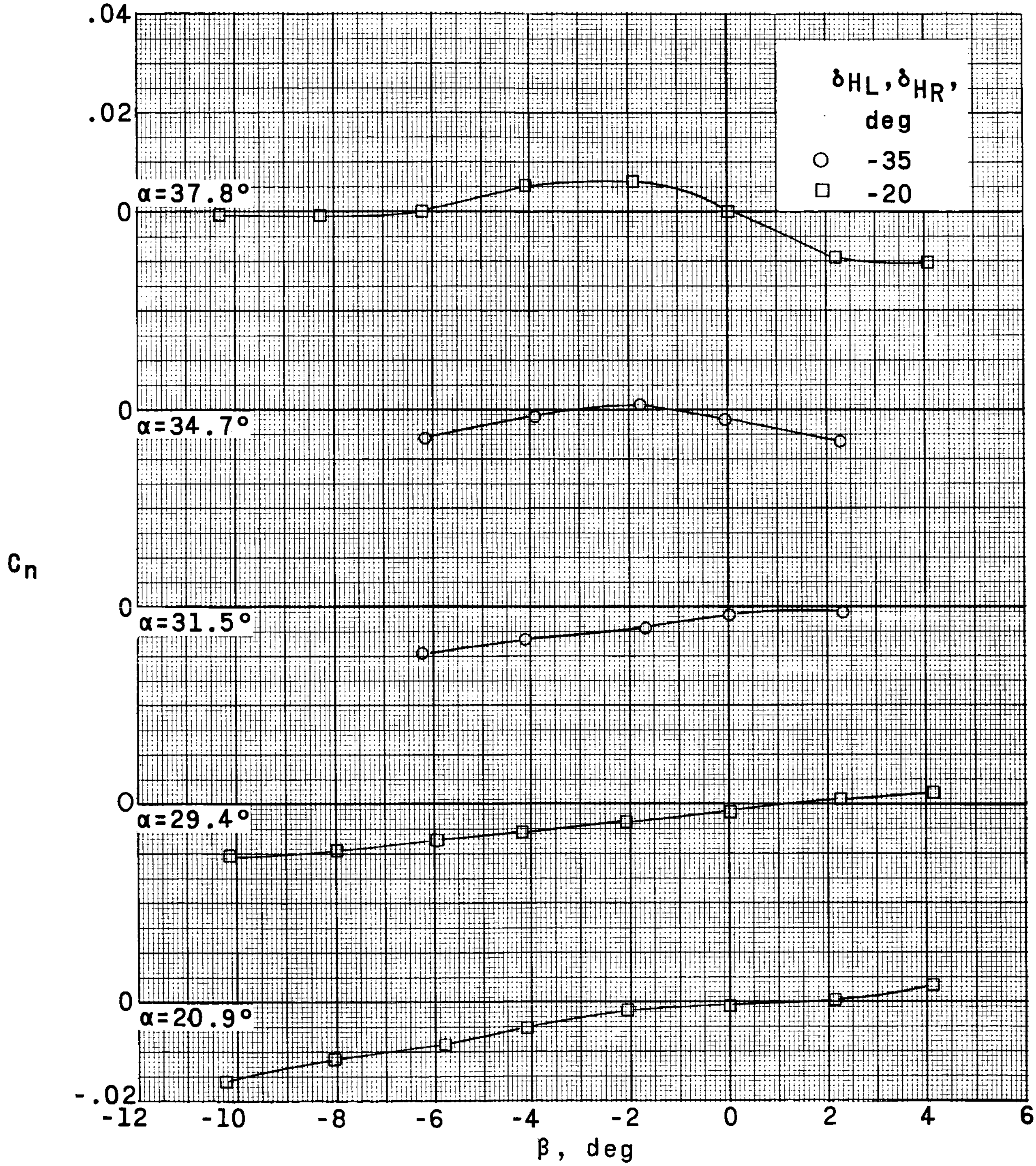

(b) Continued.

Figure 23.- Continued.

[redacted]

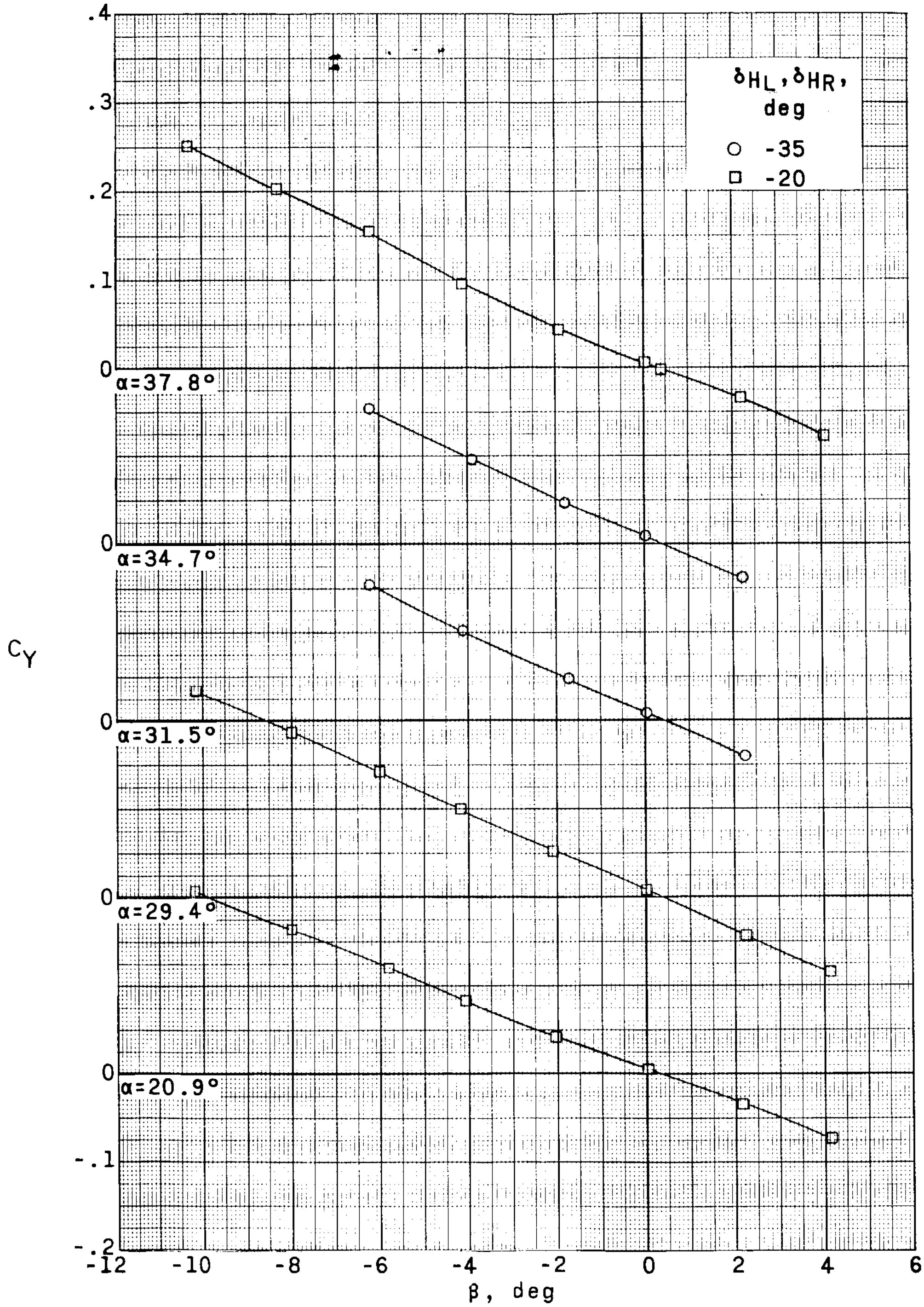

(b) Concluded.

Figure 23.- Continued.

[redacted]

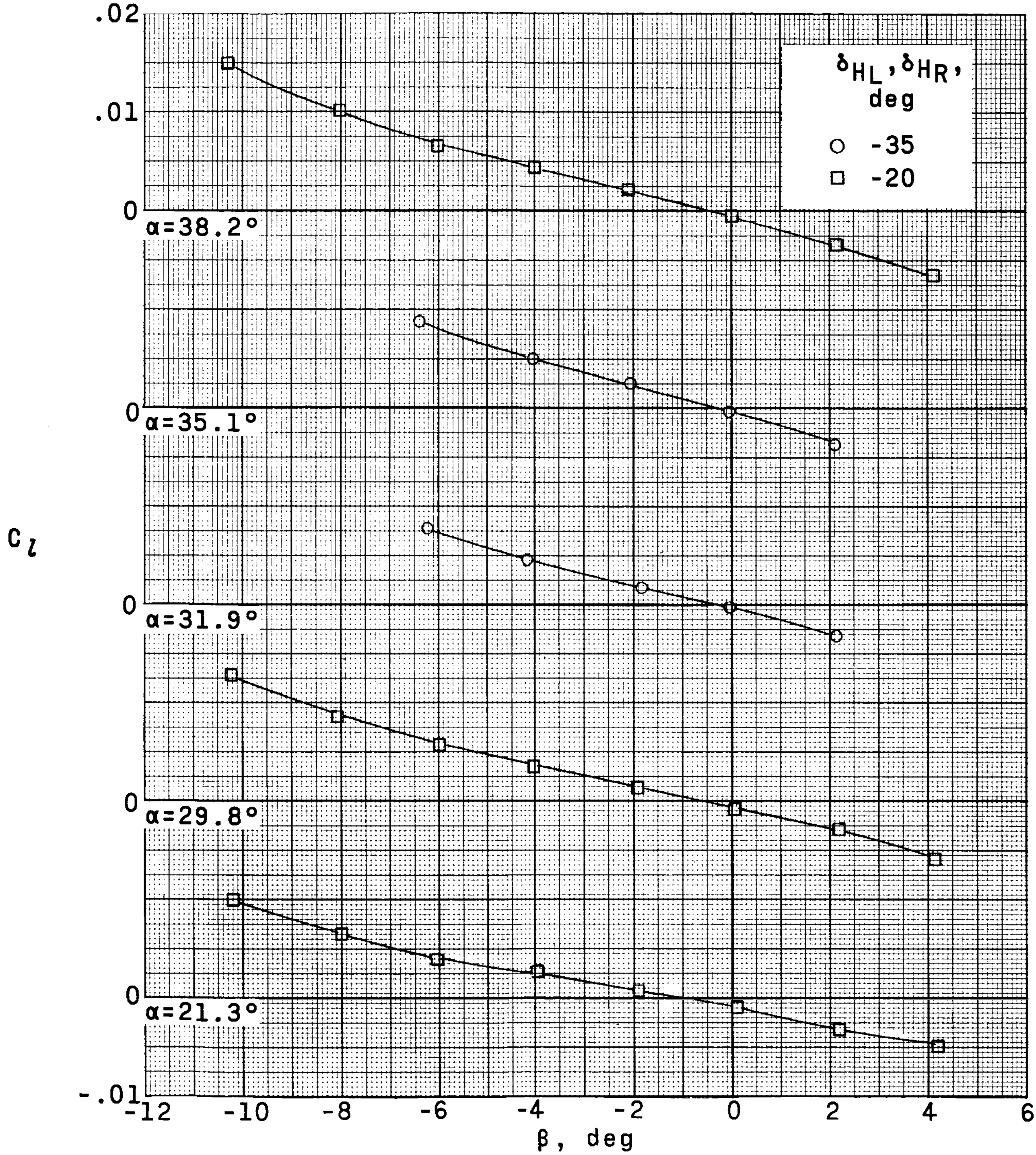

(c) M = 4.65.

Figure 23.- Continued.

[redacted]

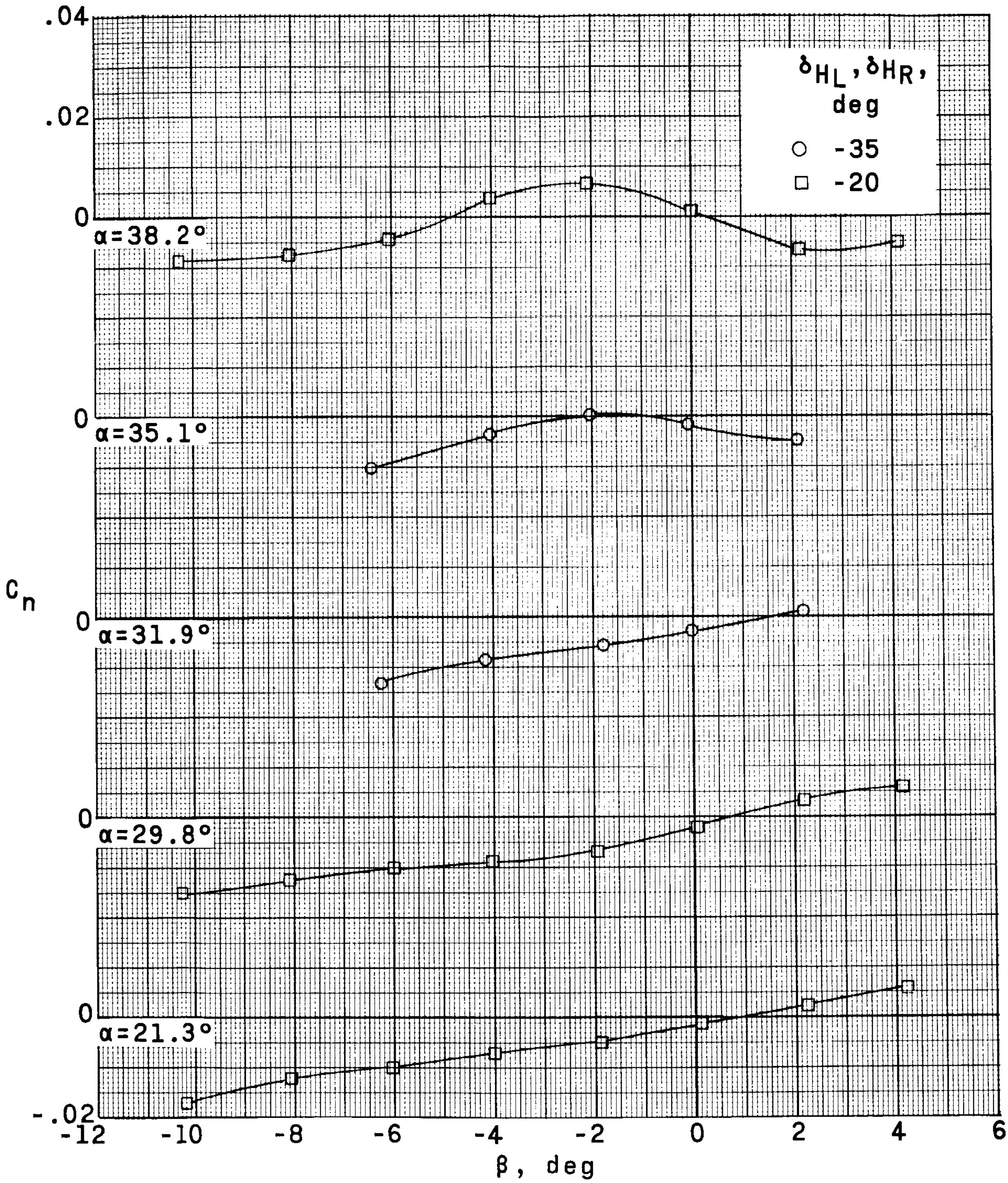

(c) Continued.

Figure 23.- Continued.

[redacted]

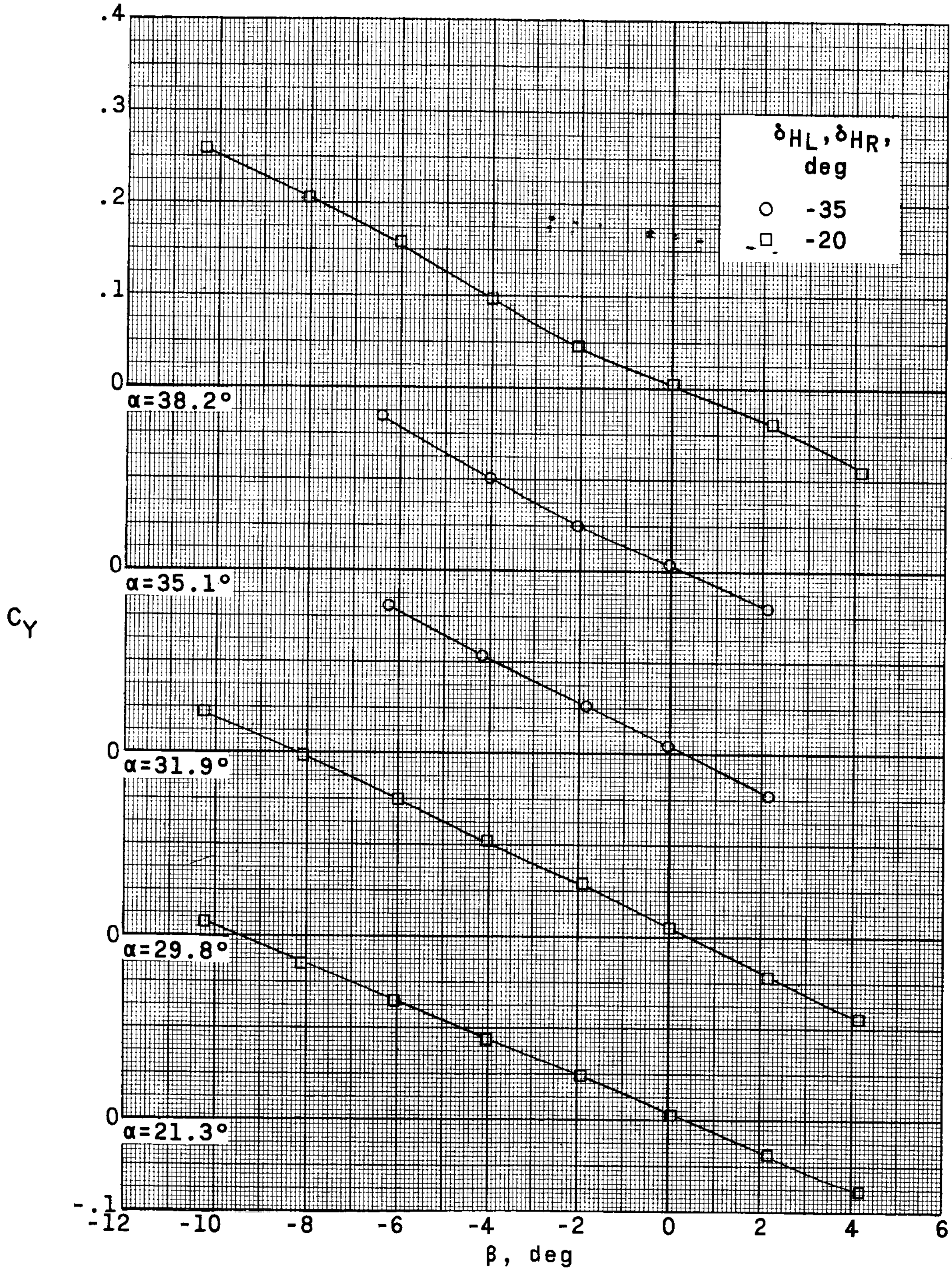

(c) Concluded.

Figure 23.- Concluded.

[redacted]

[redacted]

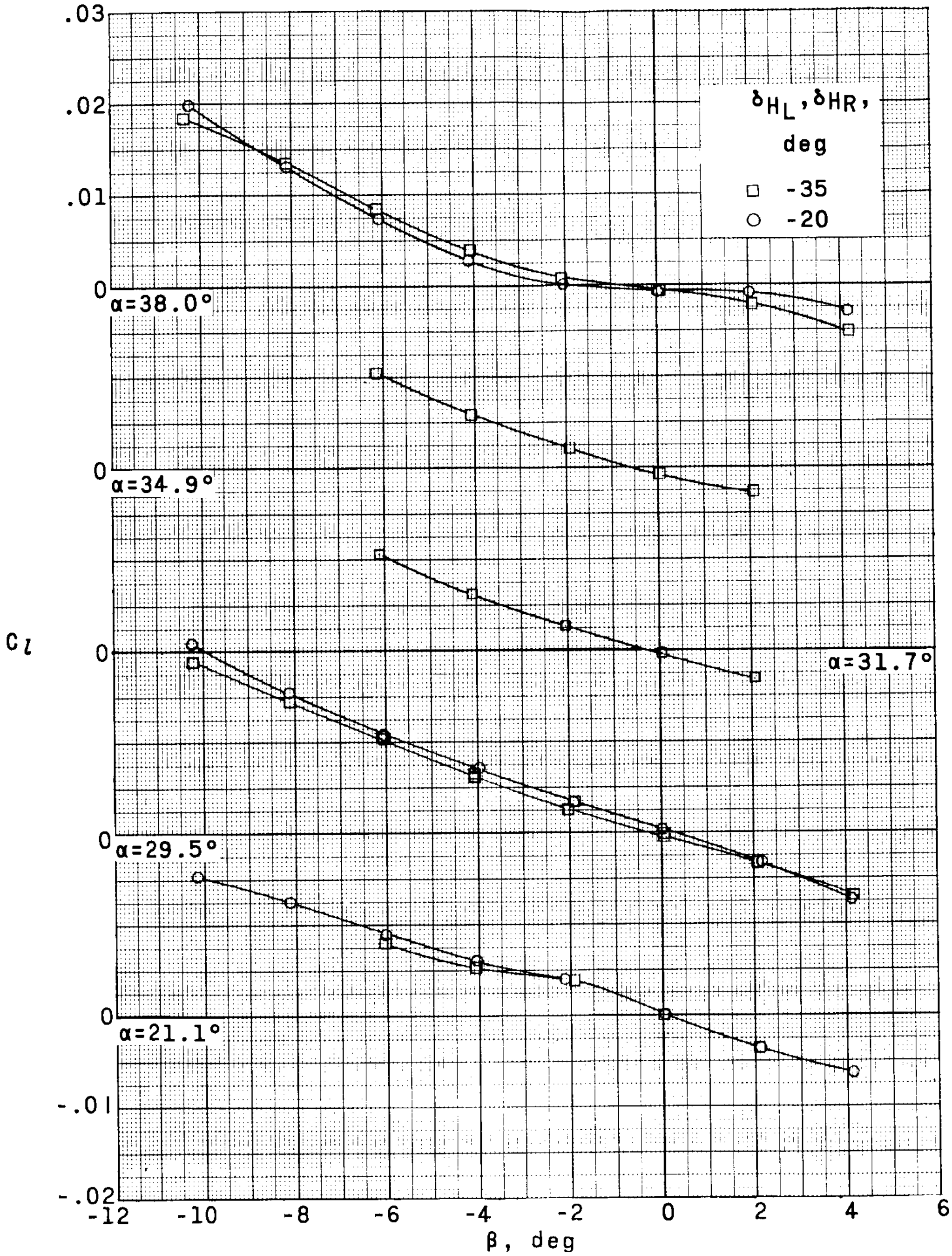

(a) M = 2.96.

Figure 24.- Effect of pitch-control deflections on aerodynamic characteristics in yaw at various angles of attack. $\delta_{V_U} = 0^{\circ}$; jettisonable portion of lower vertical stabilizer off; $\delta_{S_U} = \delta_{S_B} = 35^{\circ}$; WFHV.

[redacted]

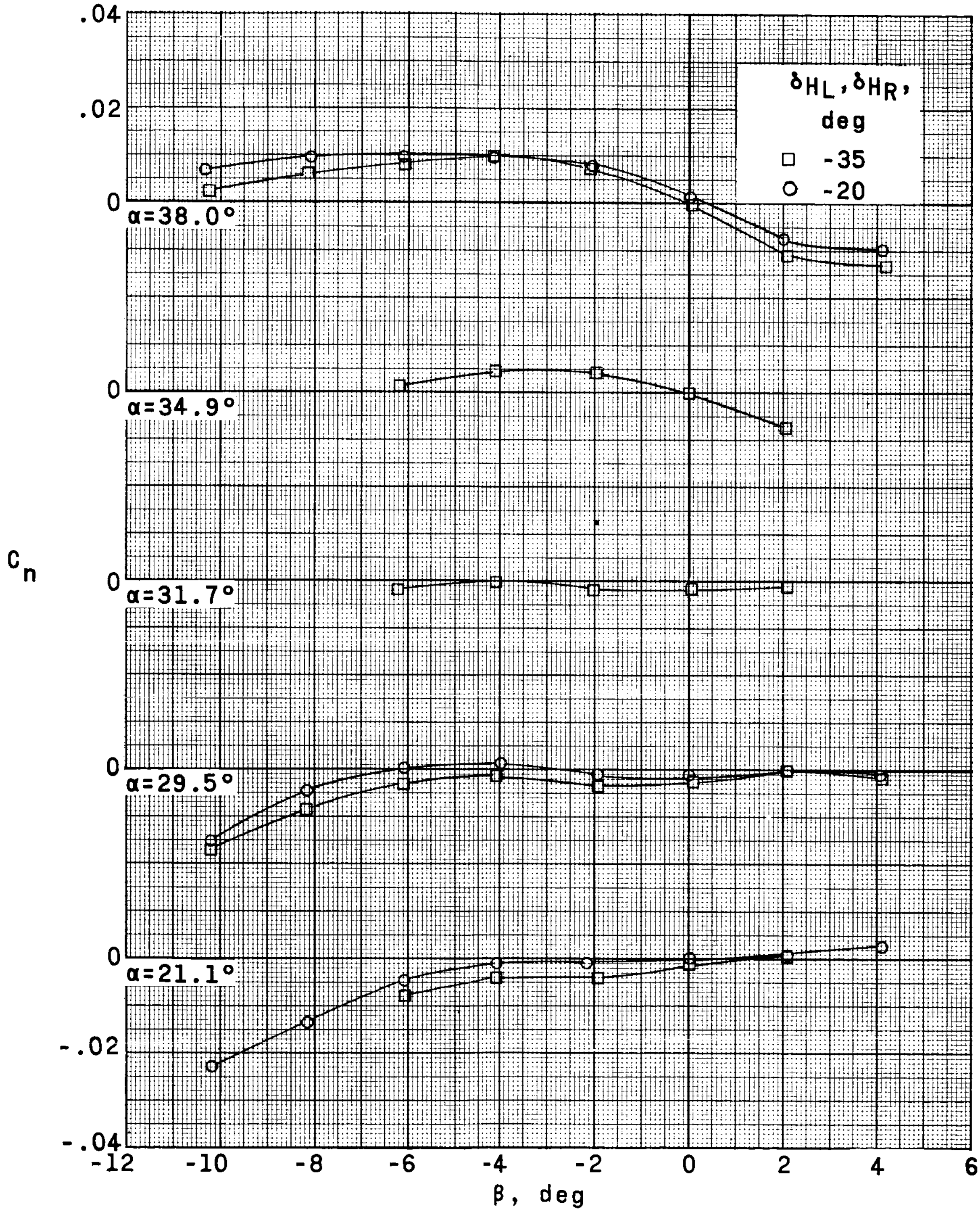

(a) Continued.

Figure 24.- Continued.

[redacted]

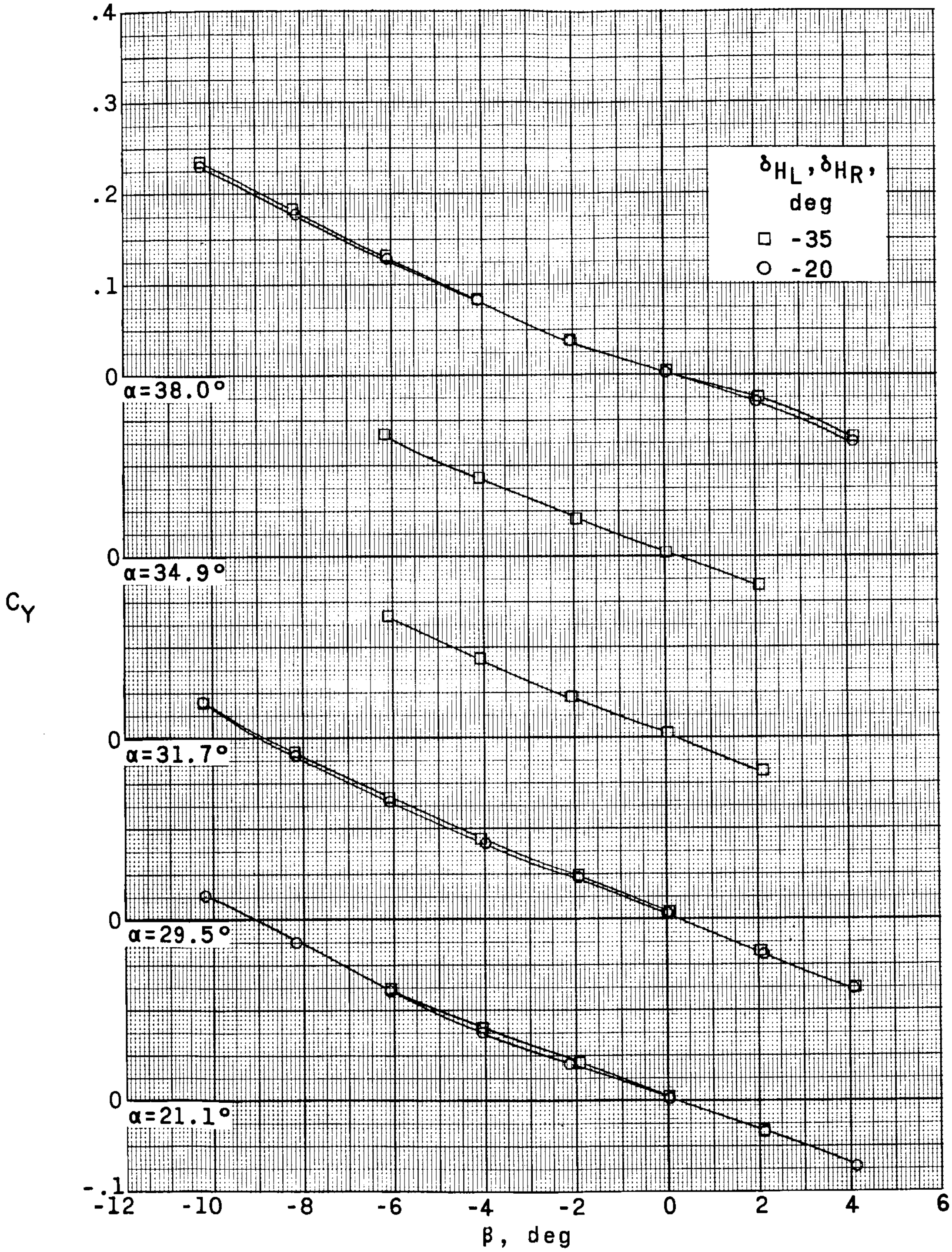

(a) Concluded.

Figure 24.- Continued.

[redacted]

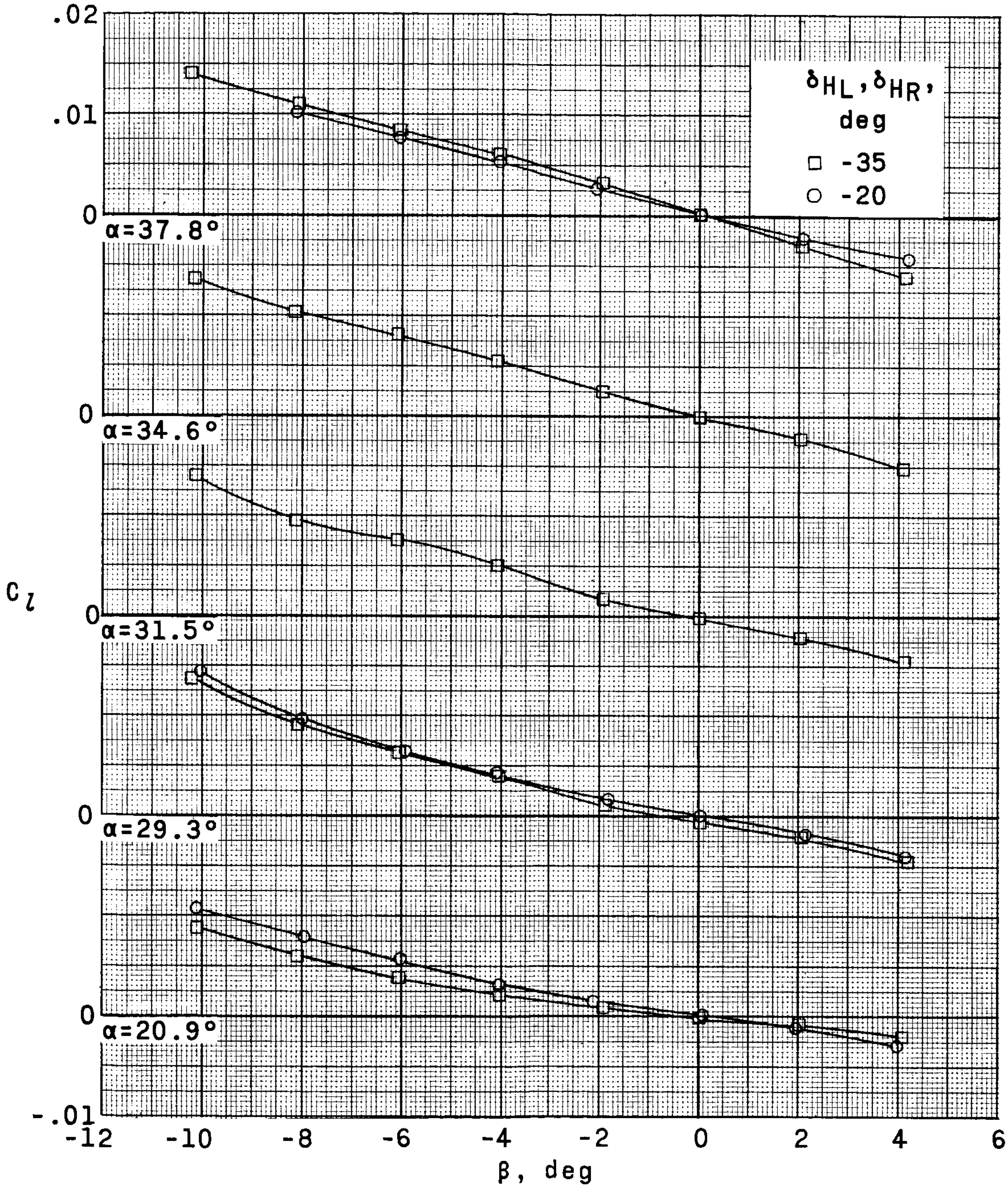

(b) M = 3.96.

Figure 24.- Continued.

[redacted]

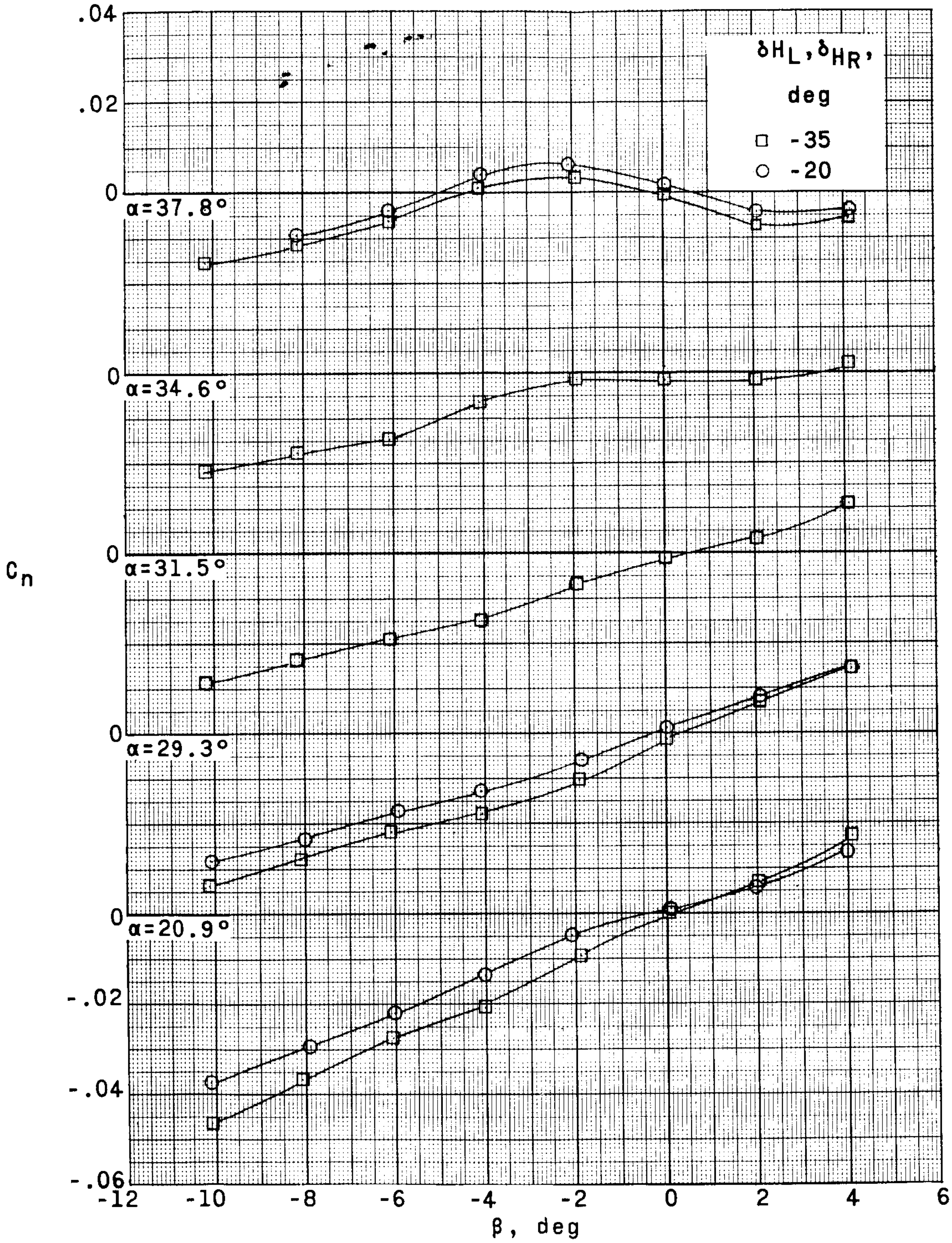

(b) Continued.

Figure 24.- Continued.

[redacted]

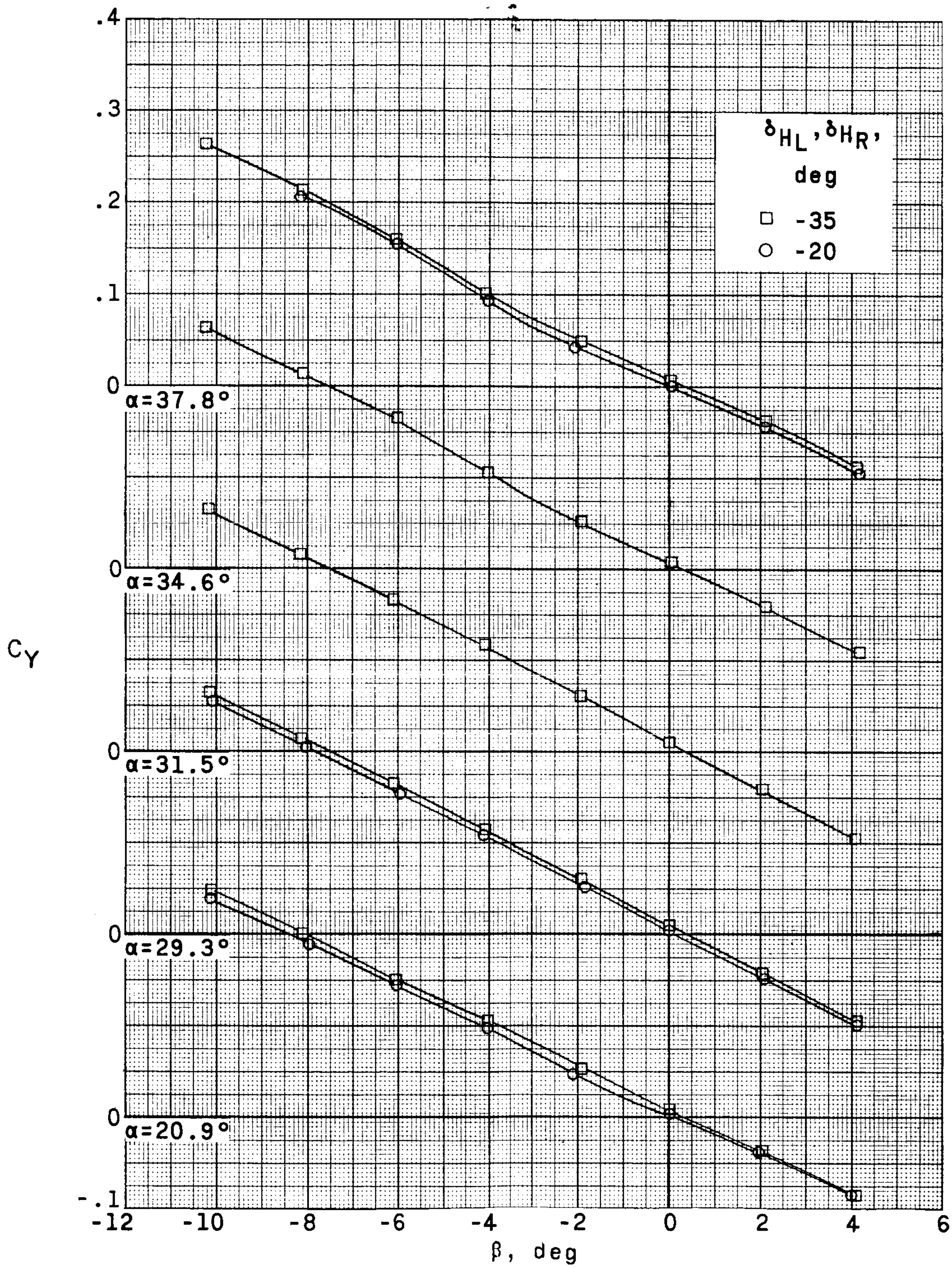

(b) Concluded.

Figure 24.- Continued.

[redacted]

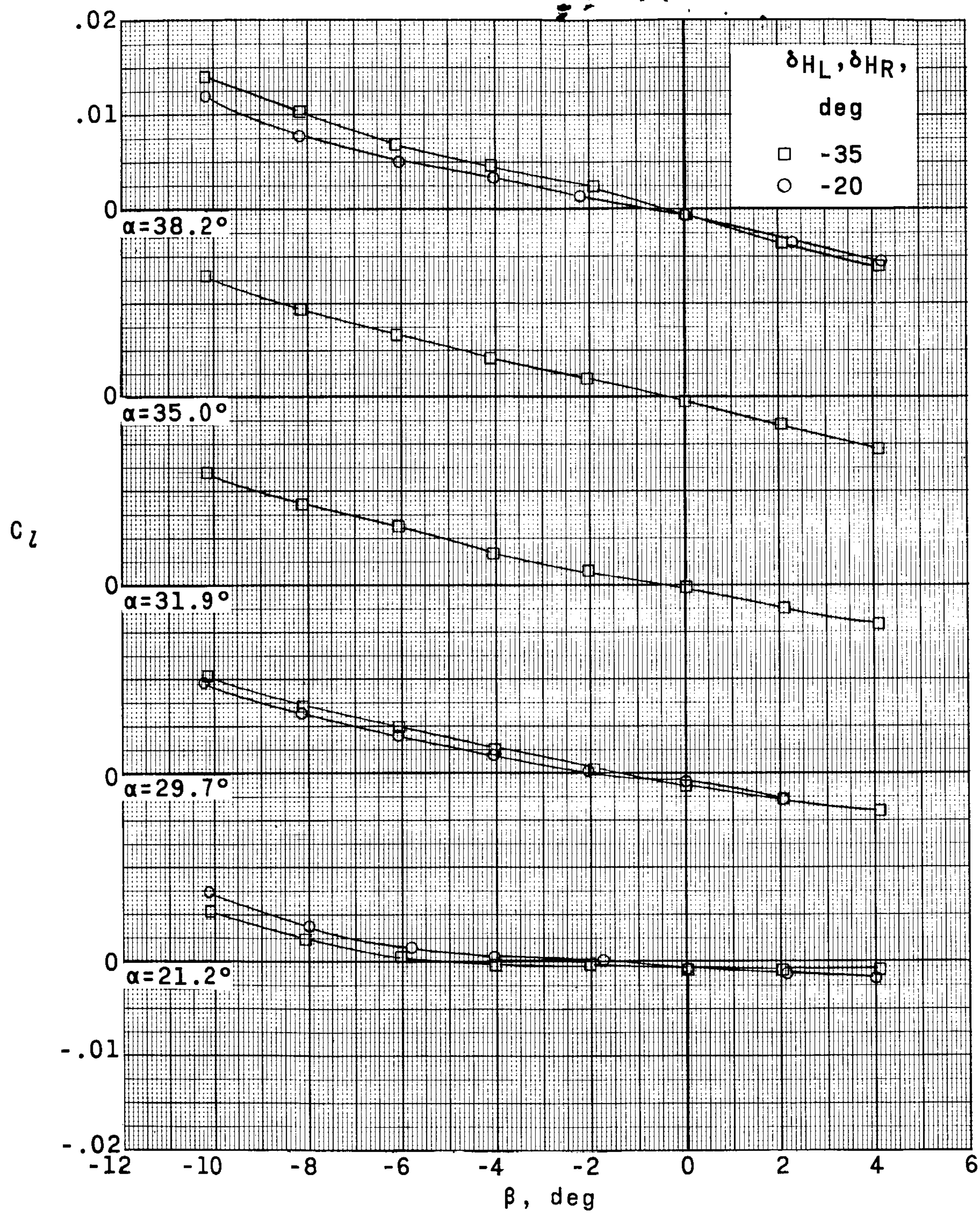

(c) M = 4.65.

Figure 24.- Continued.

[redacted]

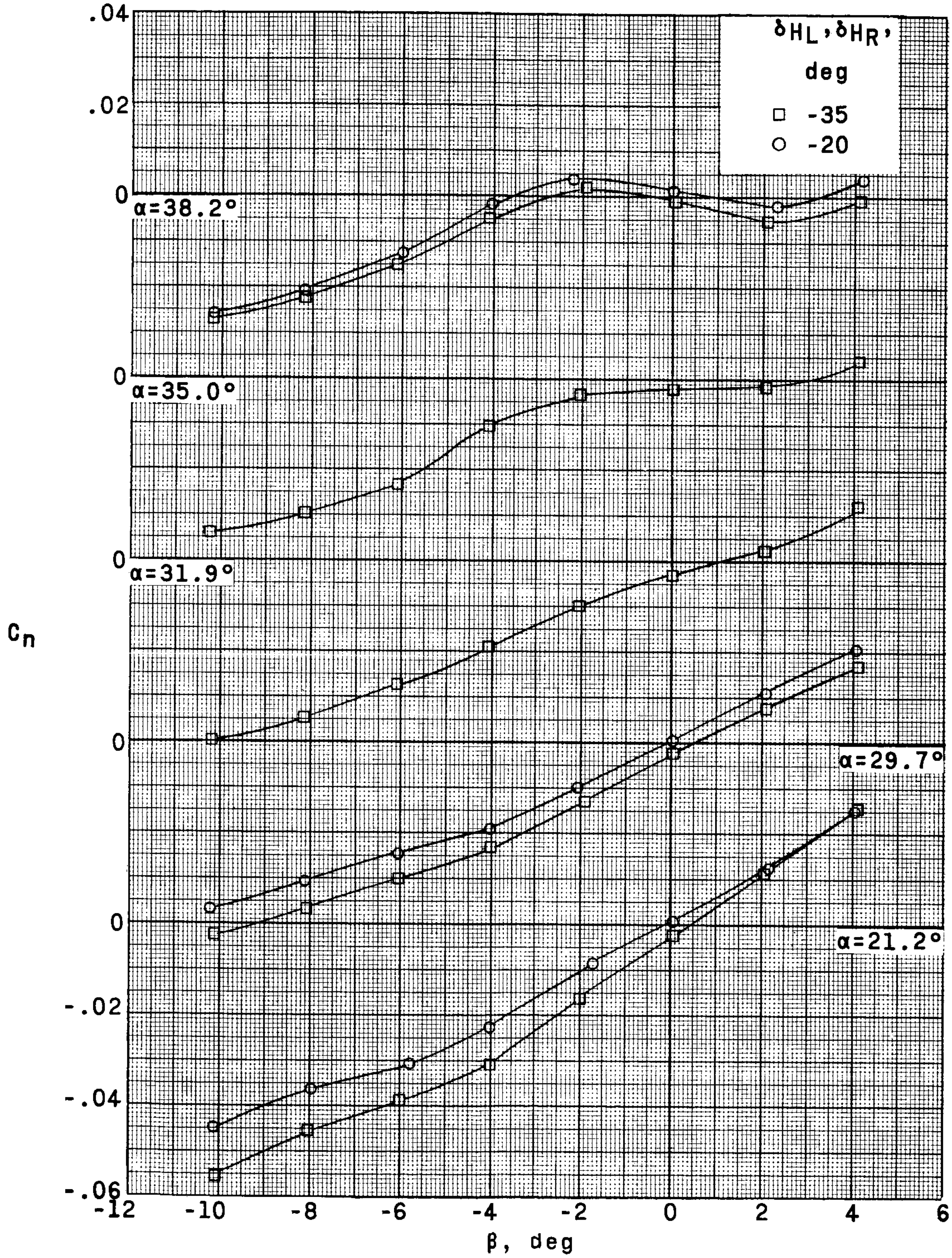

(c) Continued.

Figure 24.- Continued.

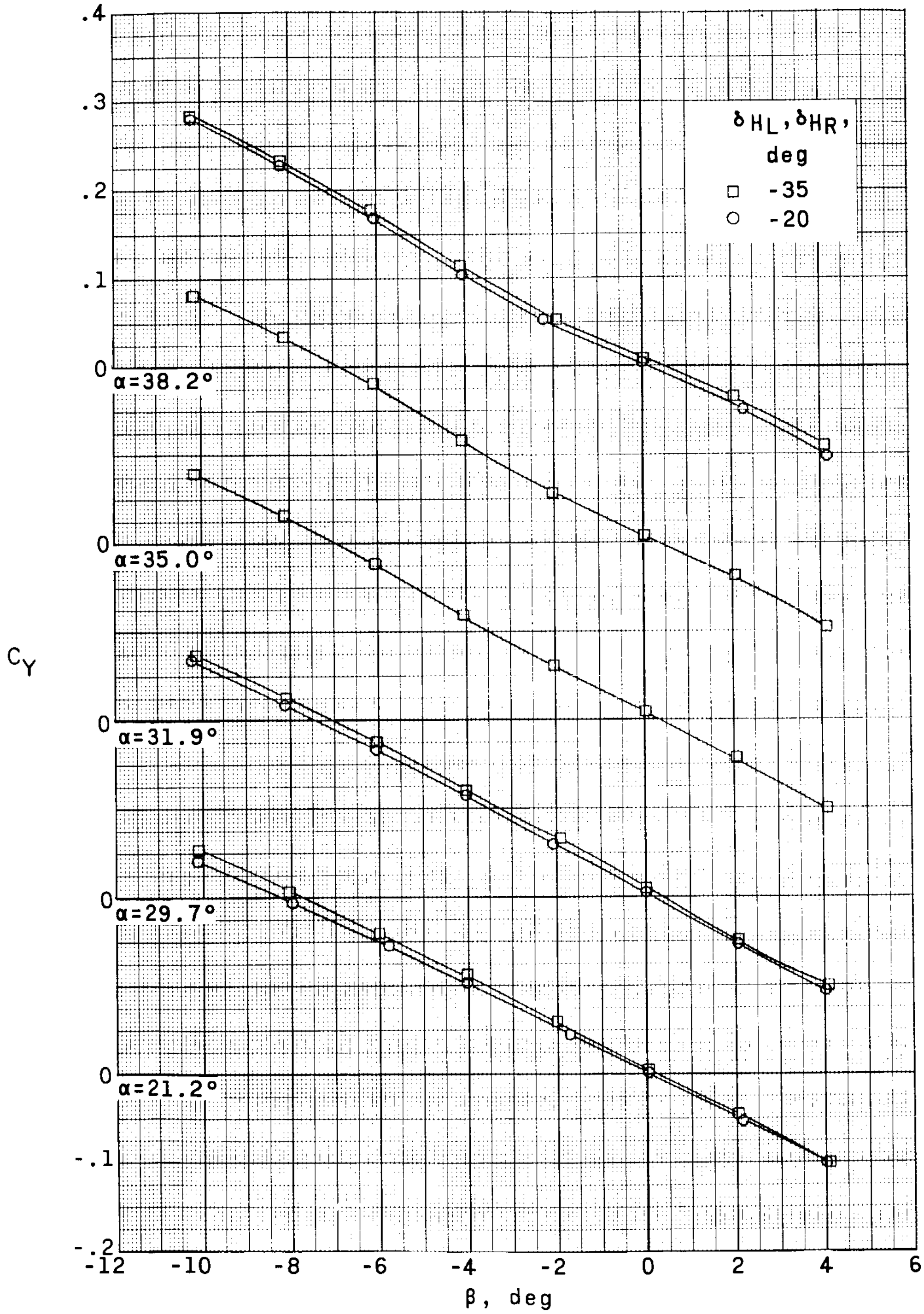

(c) Concluded.

Figure 24.- Concluded.

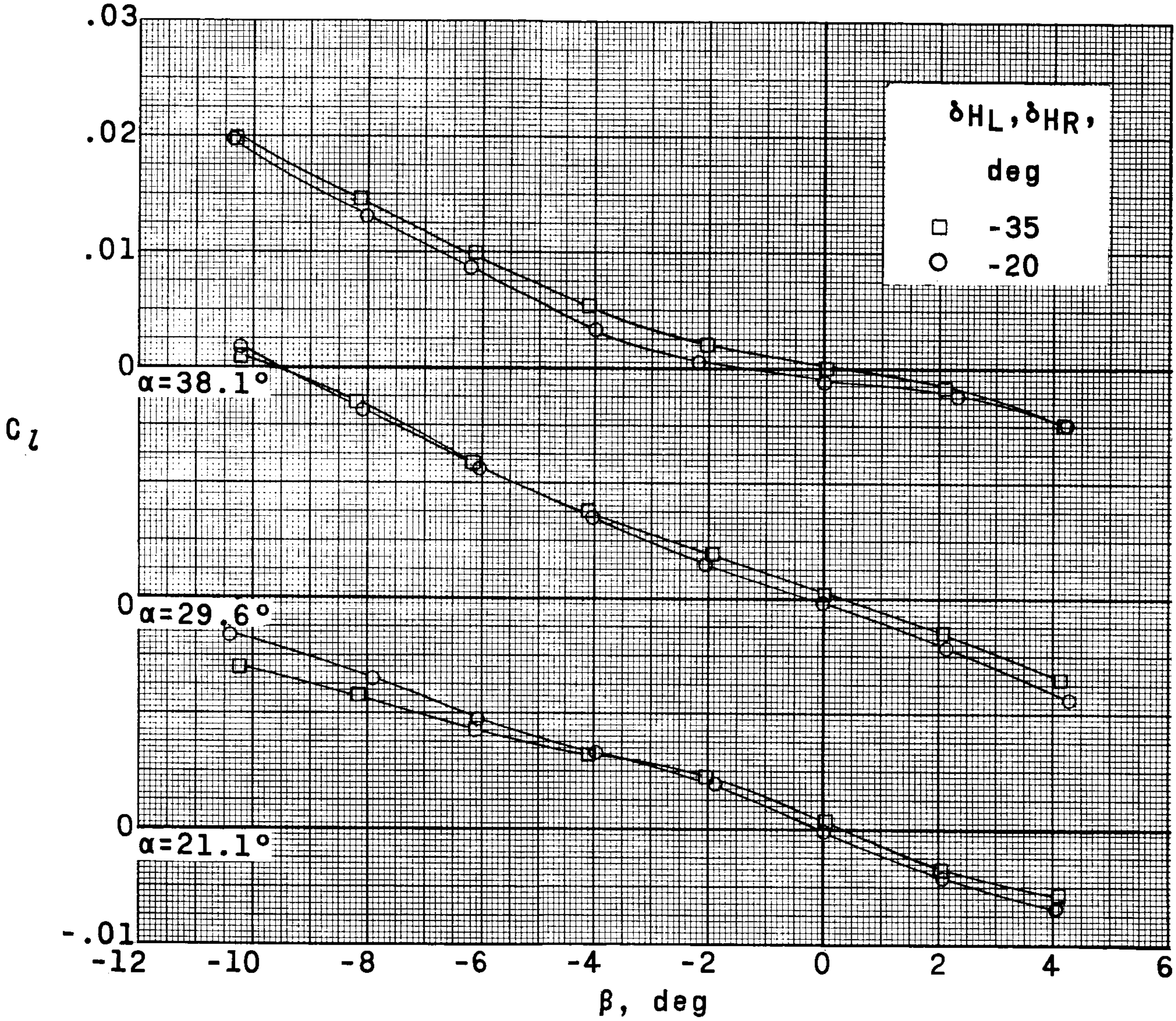

(a) M = 2.96.

Figure 25.- Effect of pitch-control deflections on aerodynamic characteristics in yaw at various angles of attack. $\delta_{V_U} = 0^{\circ}$; jettisonable portion of lower vertical stabilizer off; $\delta_{S_U} = 35^{\circ}$; $\delta_{S_B} = 0^{\circ}$; WFHV.

[redacted]

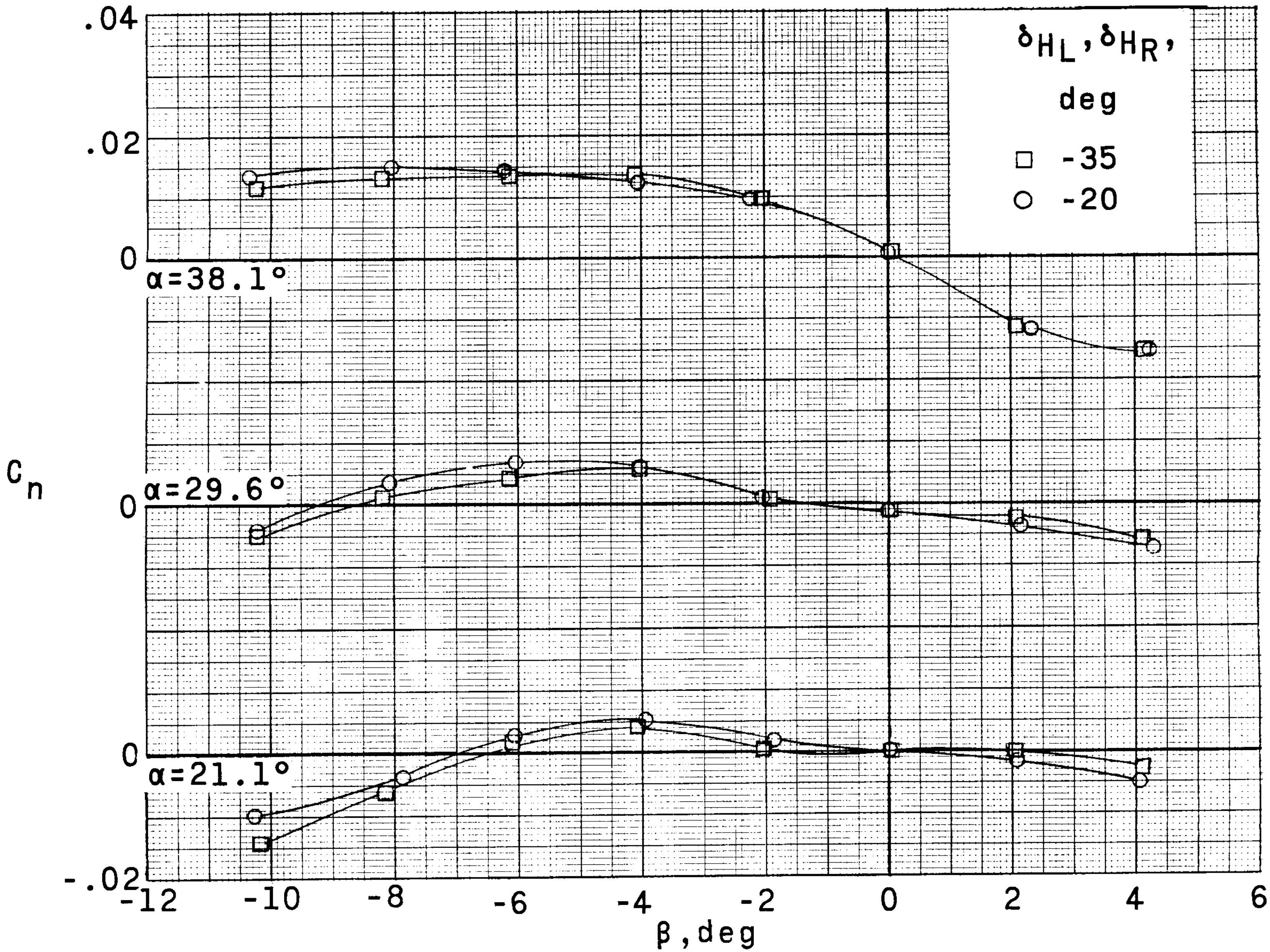

(a) Continued.

Figure 25.- Continued.

[redacted]

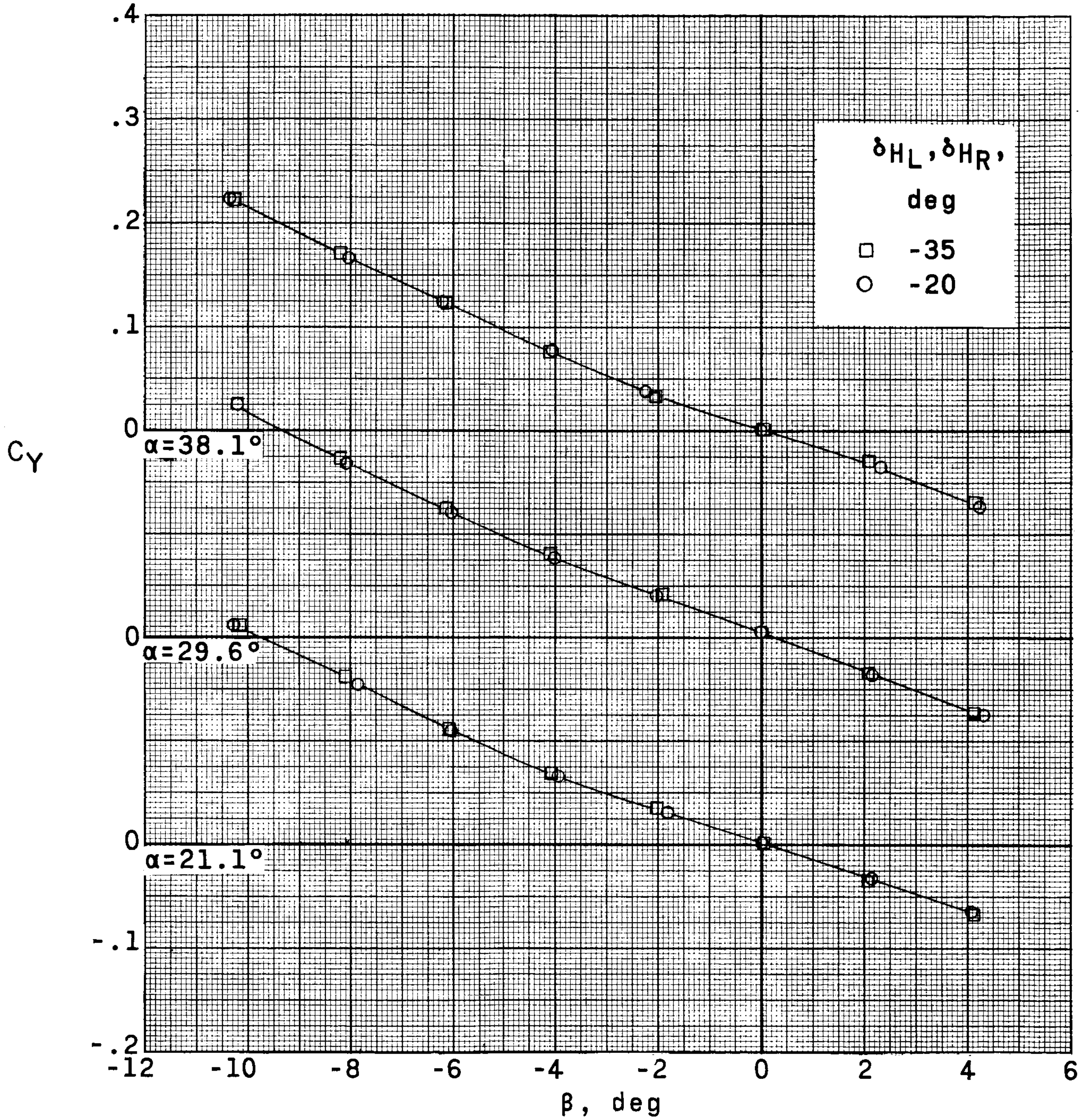

(a) Concluded.

Figure 25.- Continued.

[redacted]

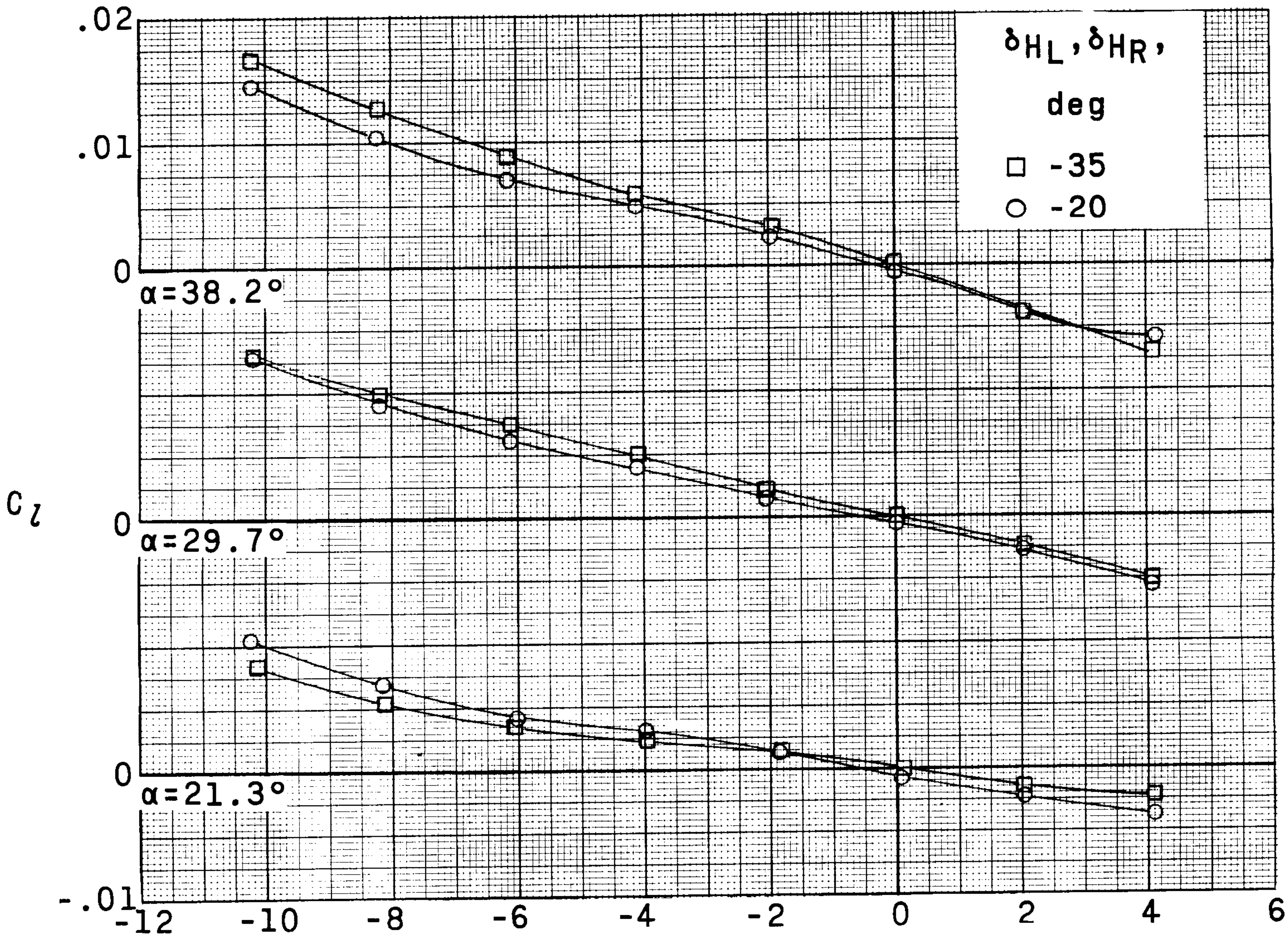

(b) M = 4.65.

Figure 25.- Continued.

[redacted]SIFIED

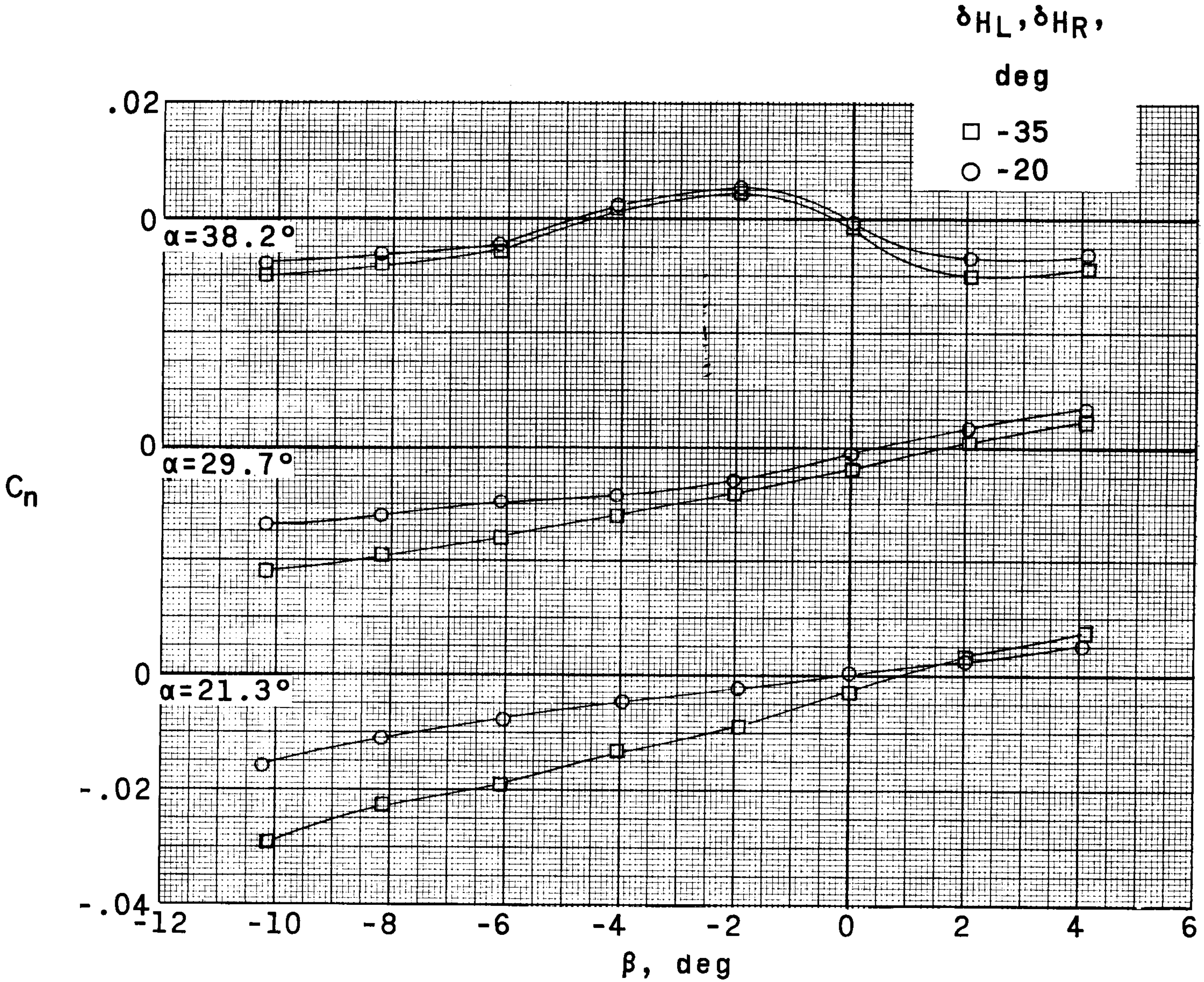

(b) Continued.

Figure 25.- Continued.

[redacted]

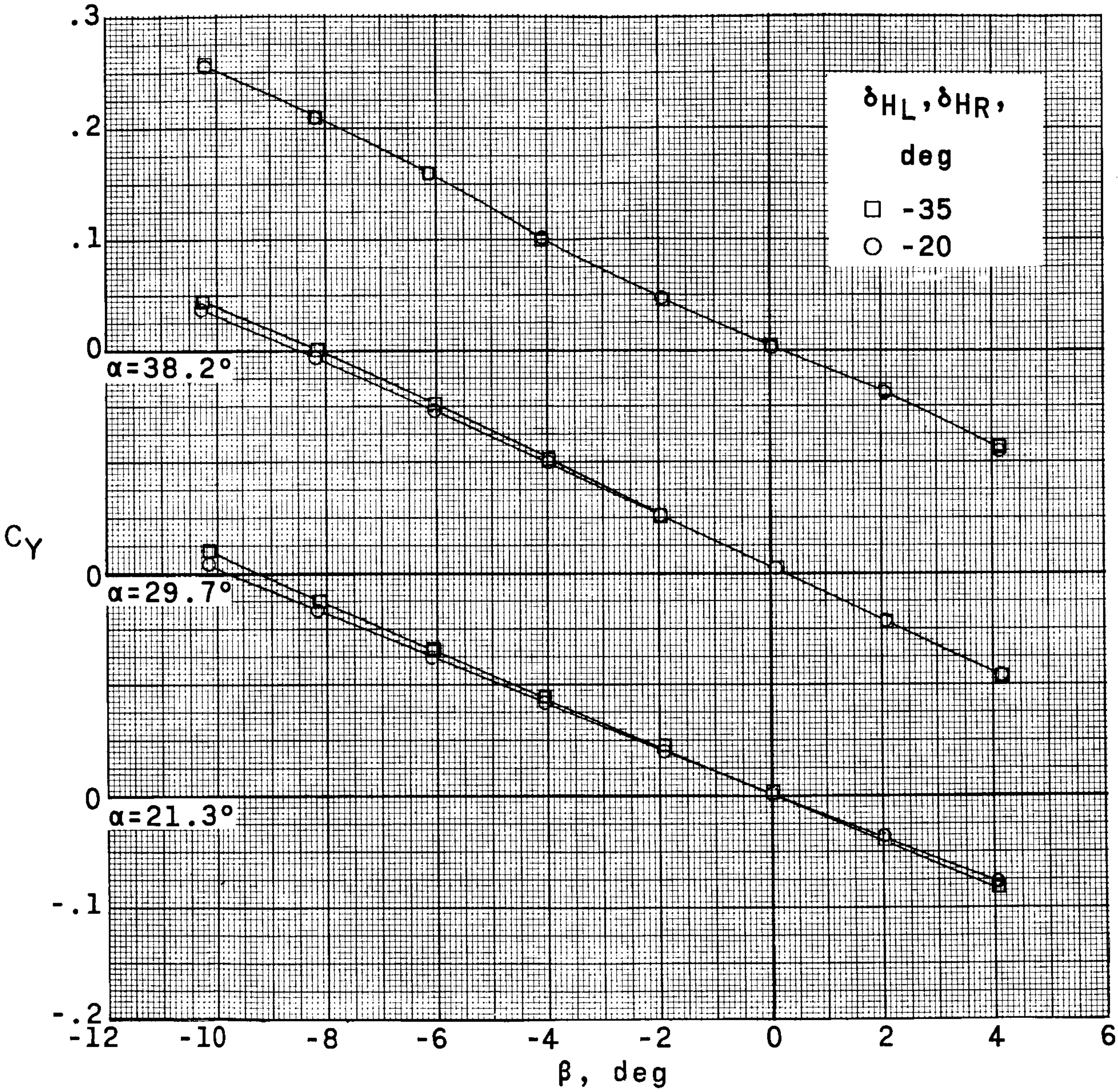

(b) Concluded.

Figure 25.- Concluded.

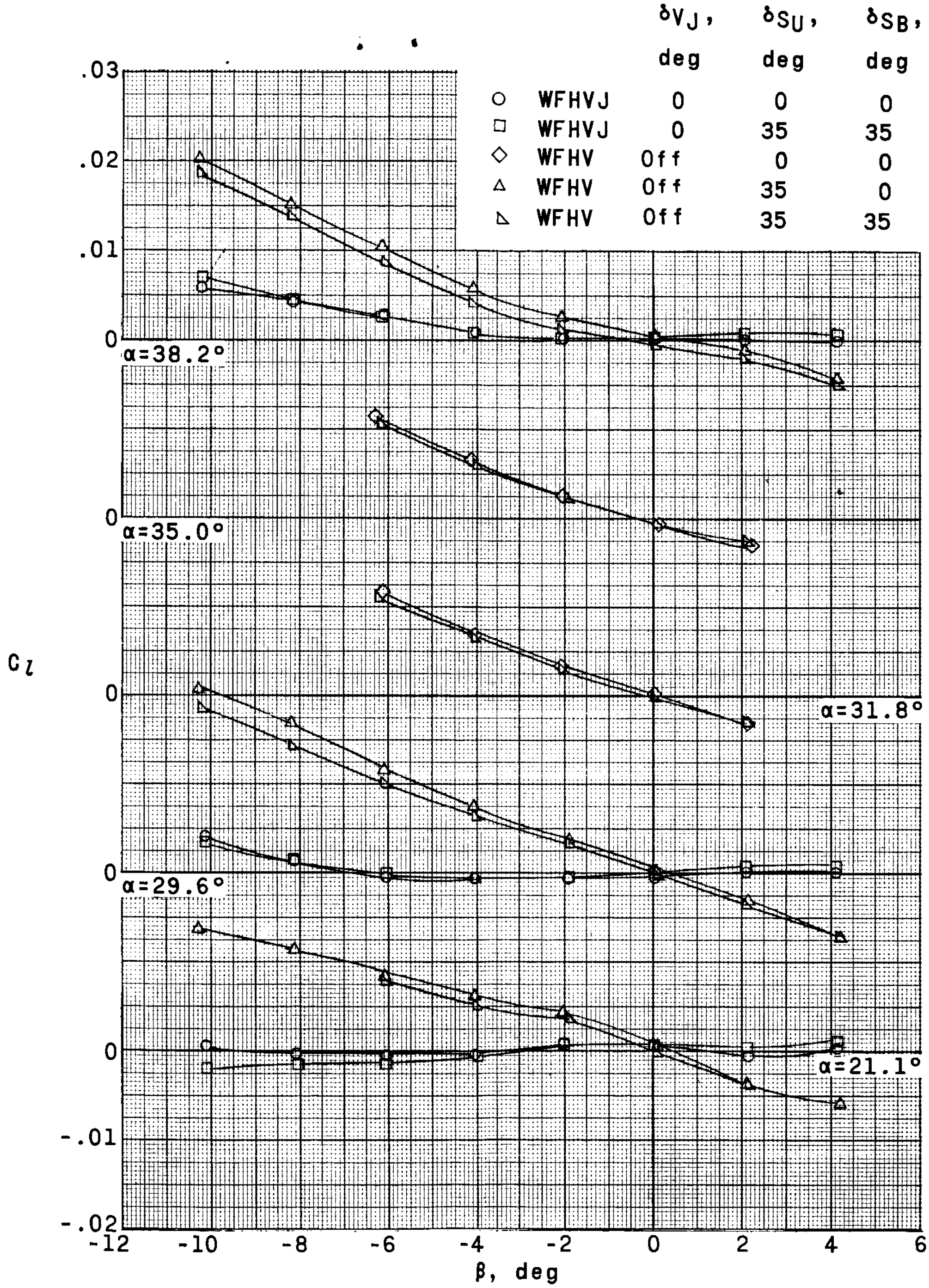

(a) M = 2.96.

Figure 26.- Effect of various configurations on aerodynamic characteristics in yaw at various angles of attack. $\delta_{H_L} = \delta_{H_R} = -35^{\circ}$; $\delta_{V_U} = 0^{\circ}$.

[redacted]

[redacted]

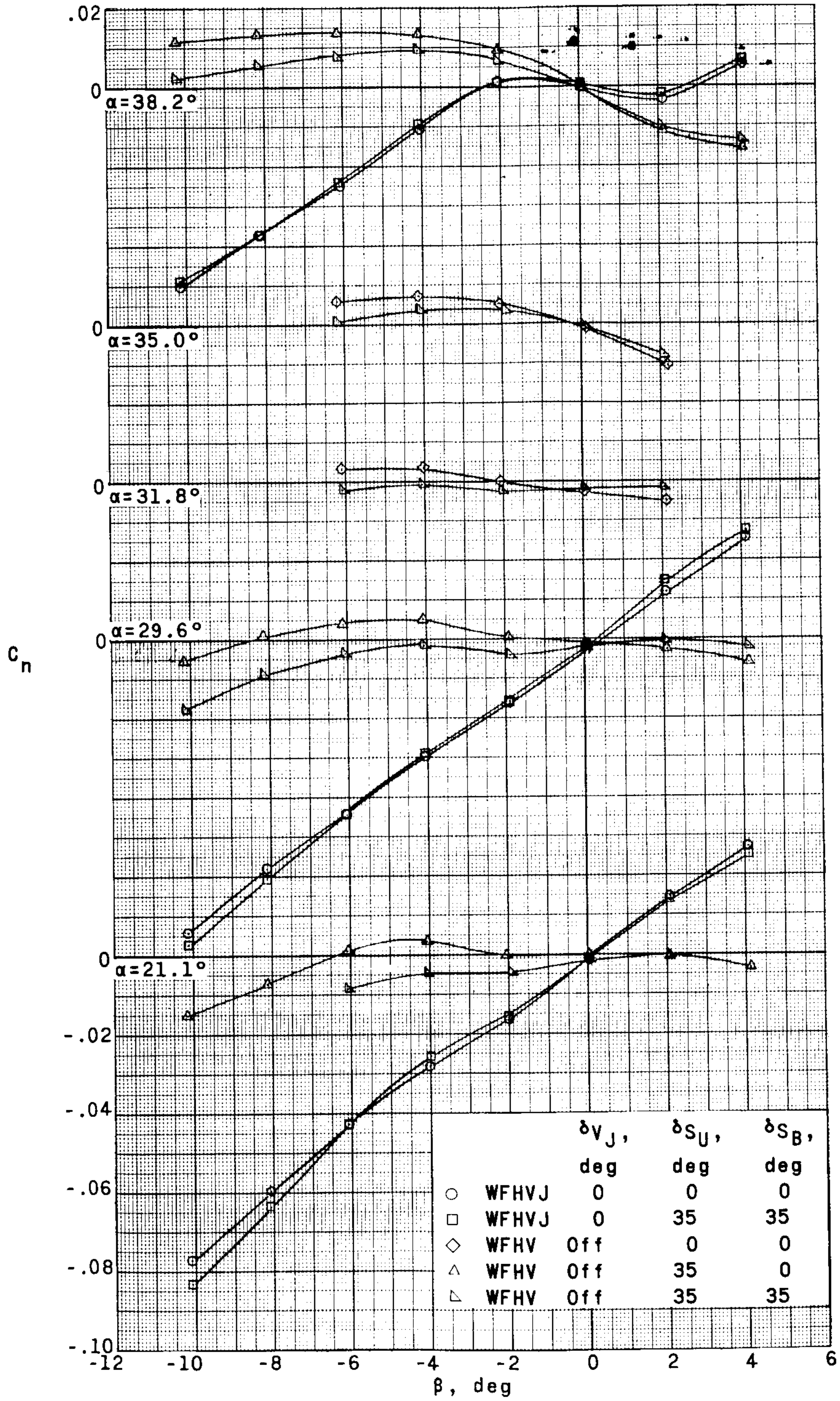

(a) Continued.

Figure 26.- Continued.

[redacted]

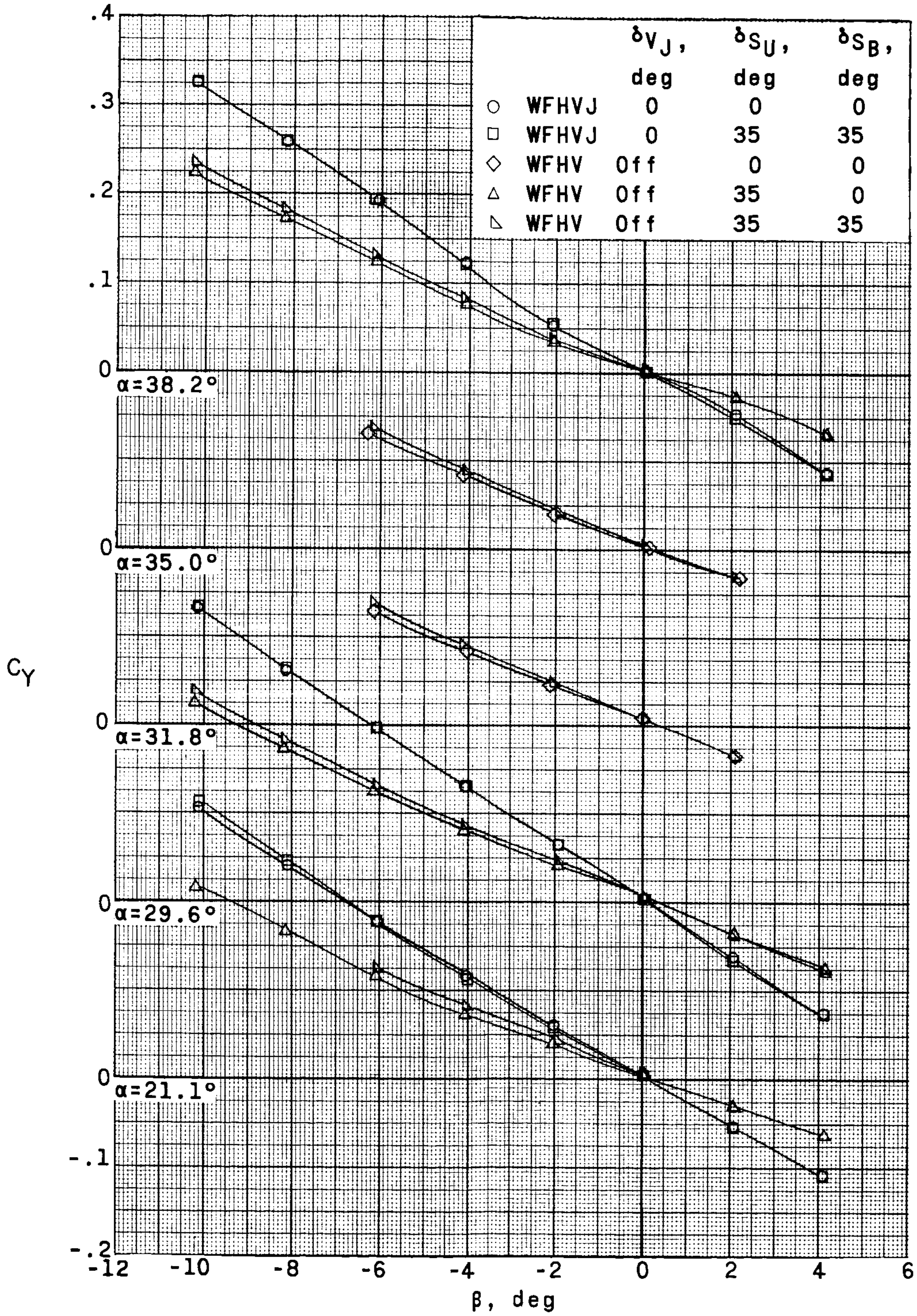

(a) Concluded.

Figure 26.- Continued.

[redacted]

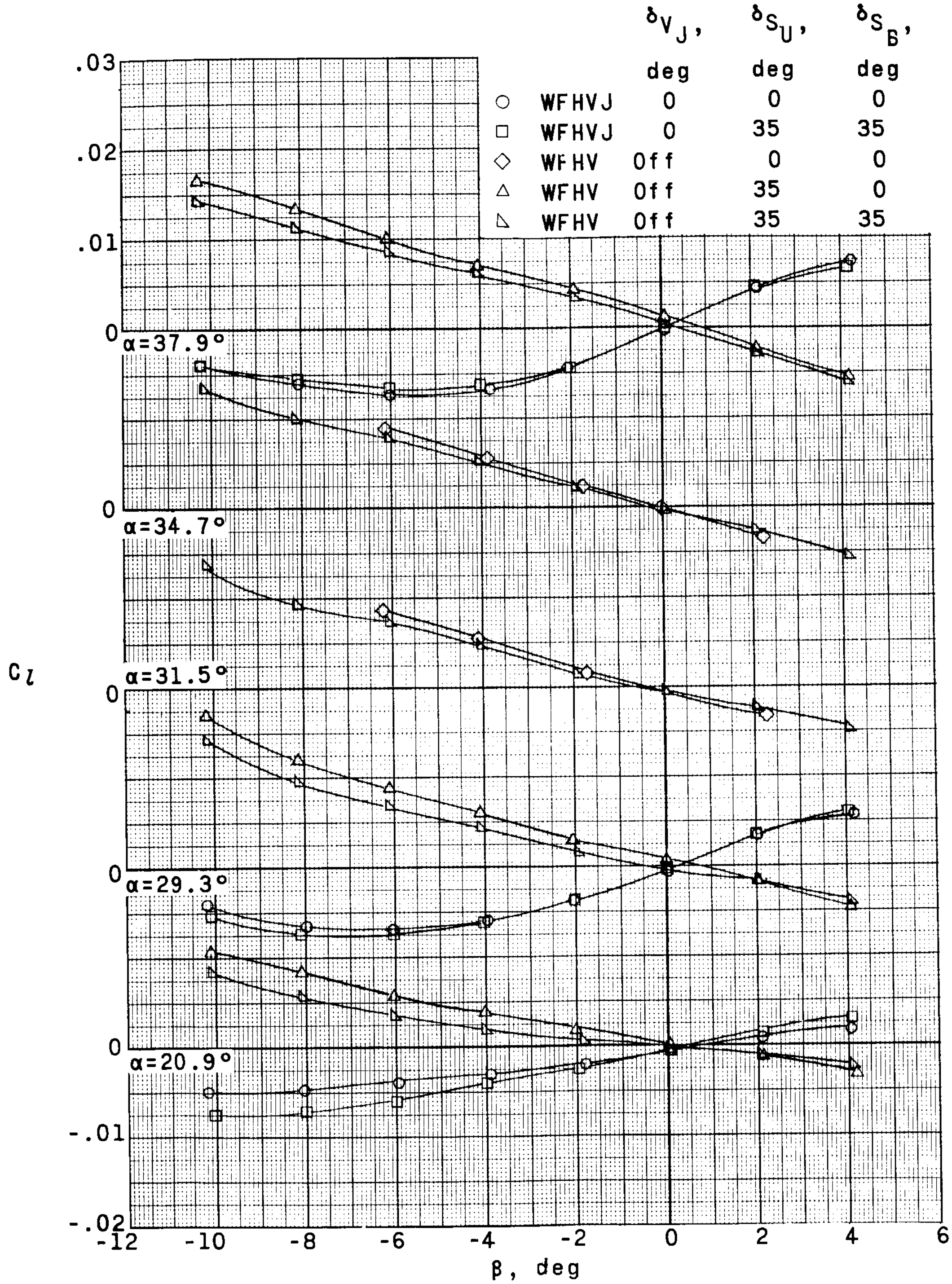

(b) M = 3.96.

Figure 26.- Continued.

[redacted]

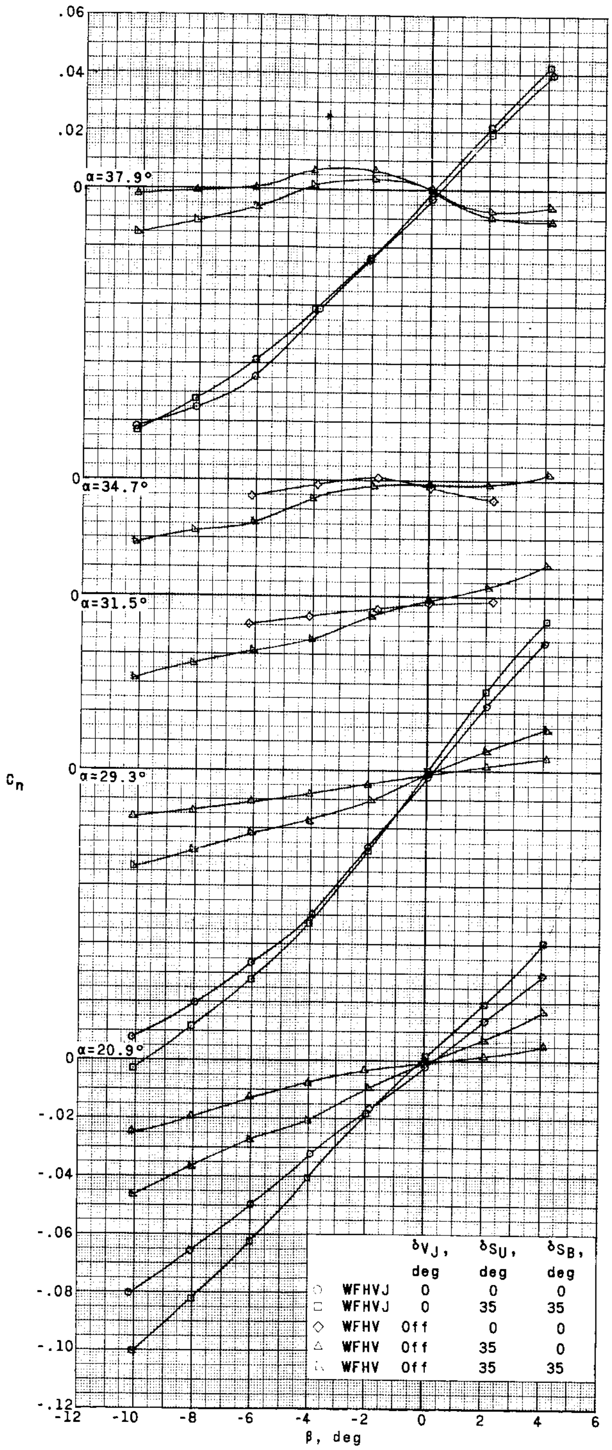

(b) Continued.

Figure 26.- Continued.

[redacted]

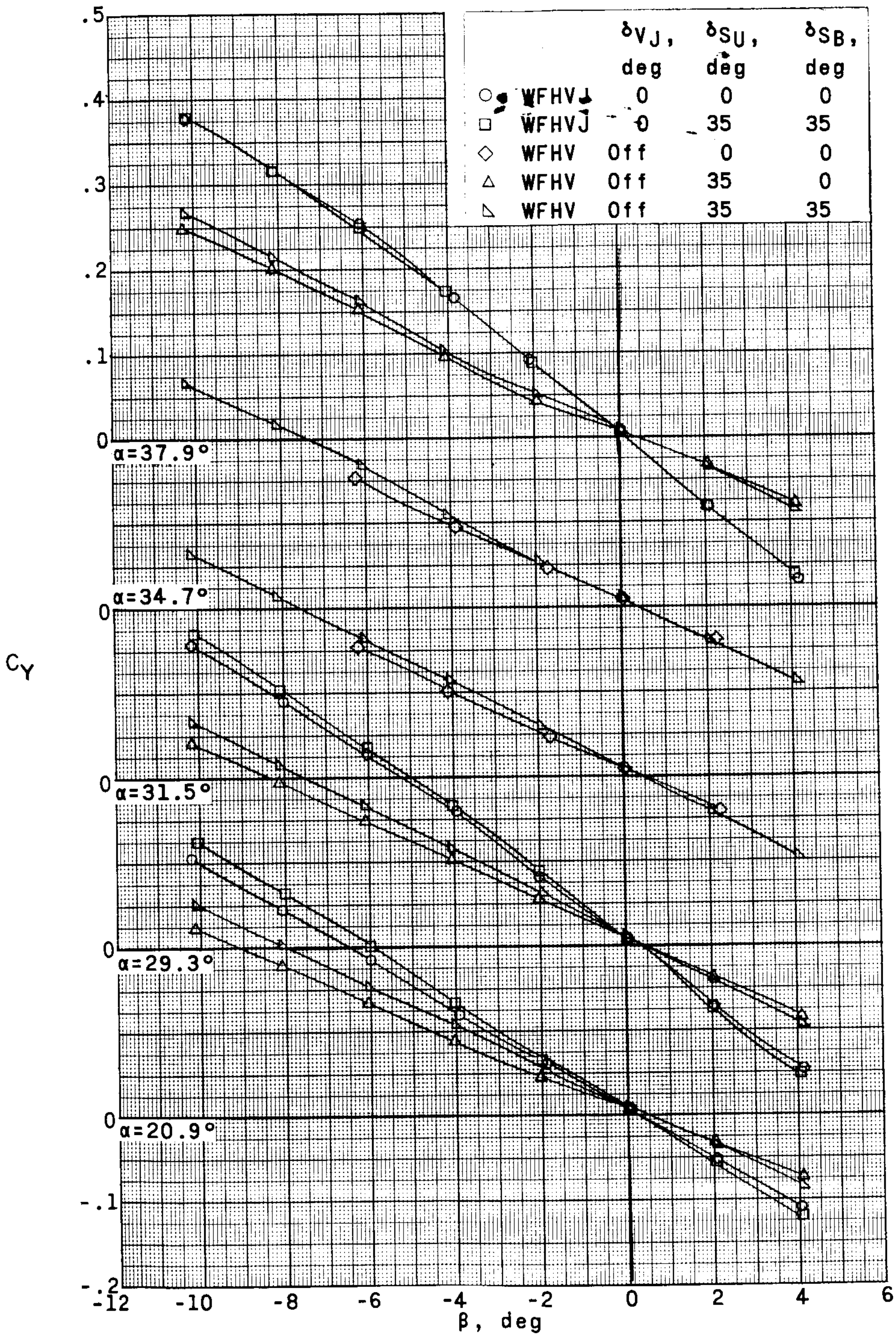

(b) Concluded.

Figure 26.- Continued.

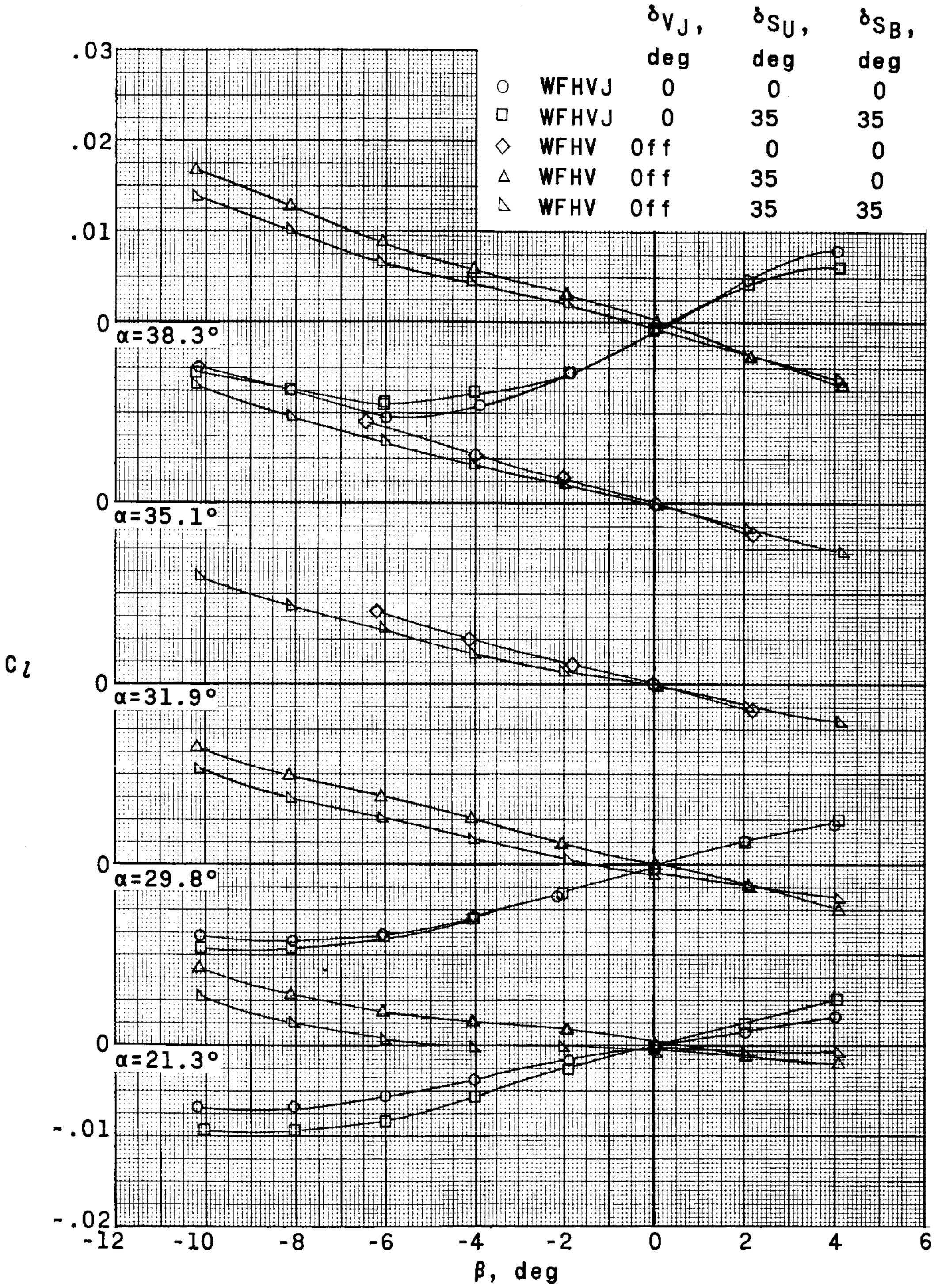

(c) M = 4.65.

Figure 26.- Continued.

[redacted]

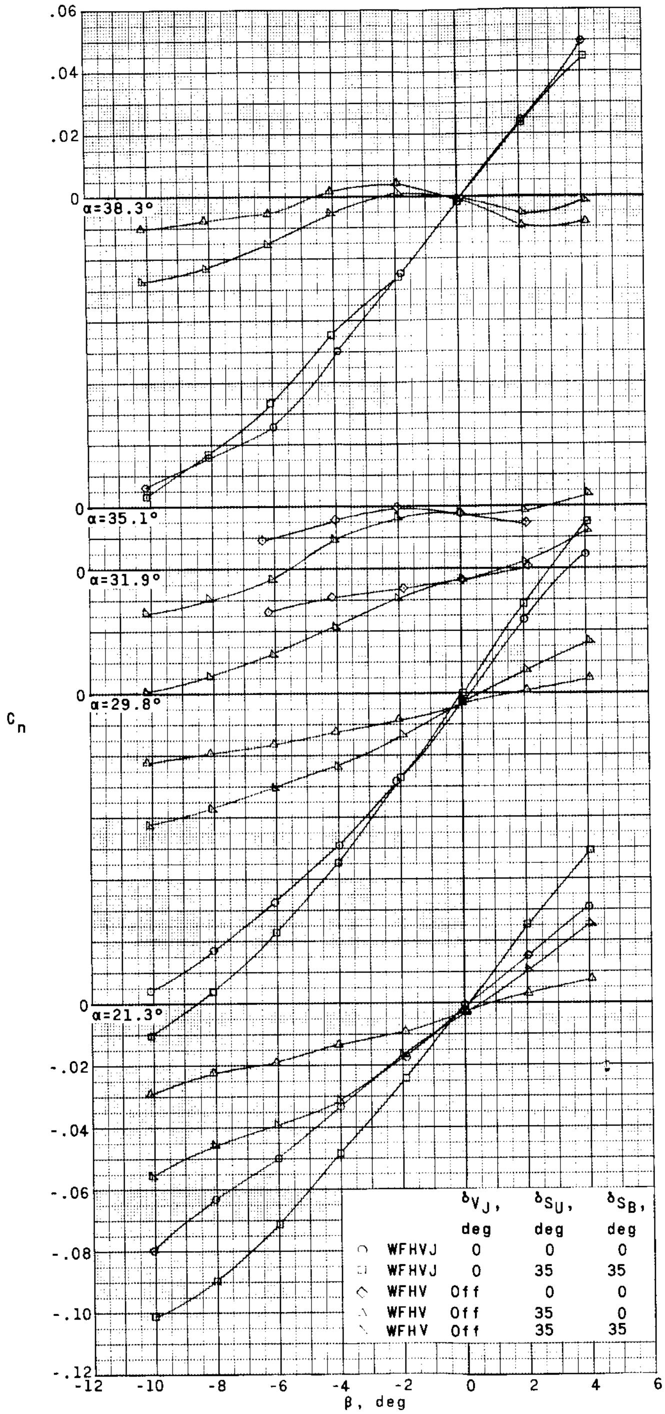

(c) Continued.

Figure 26.- Continued.

[redacted]

D[redacted]SSIFIED

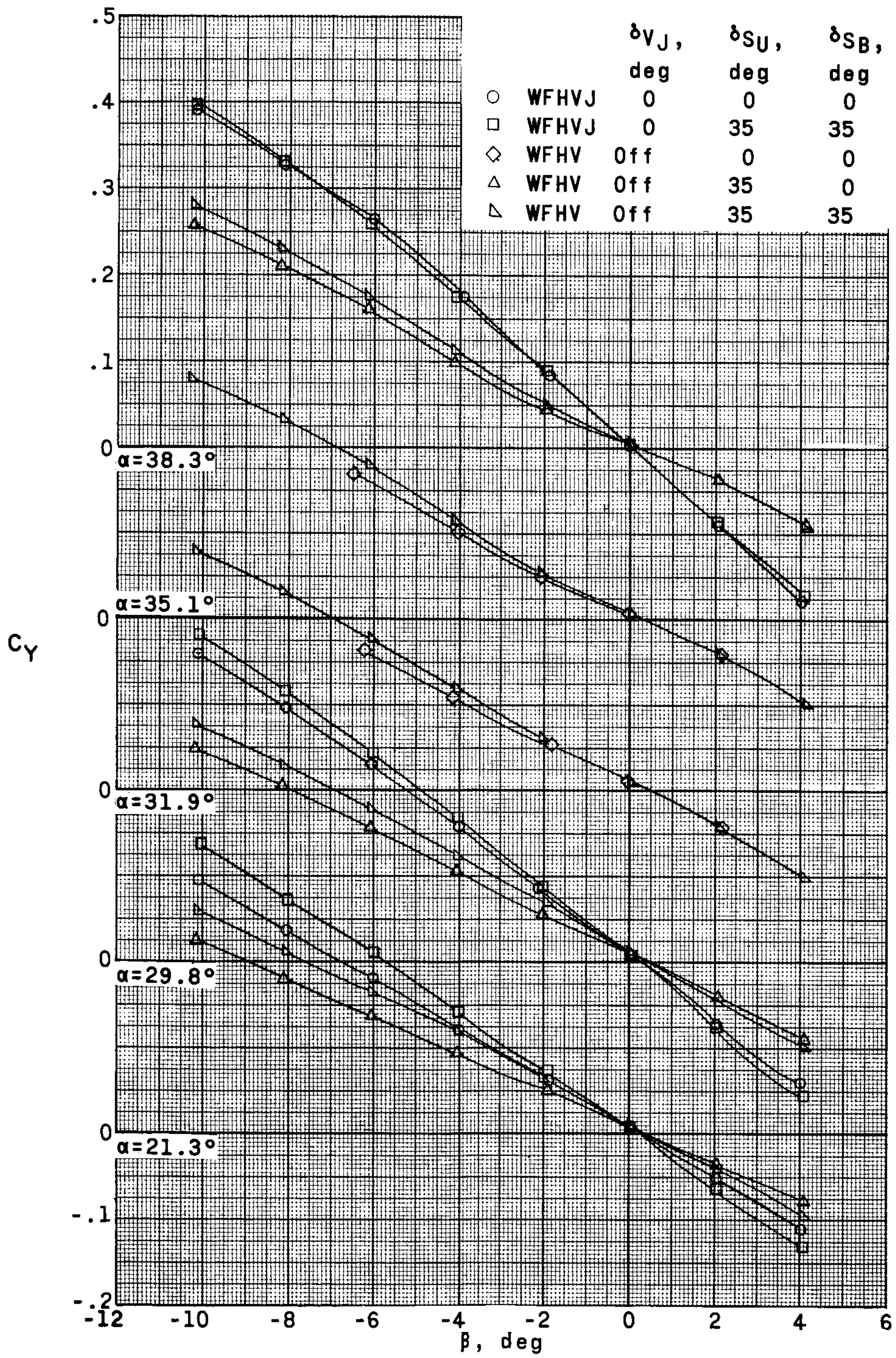

(c) Concluded.

Figure 26.- Concluded.

[redacted]

[redacted]

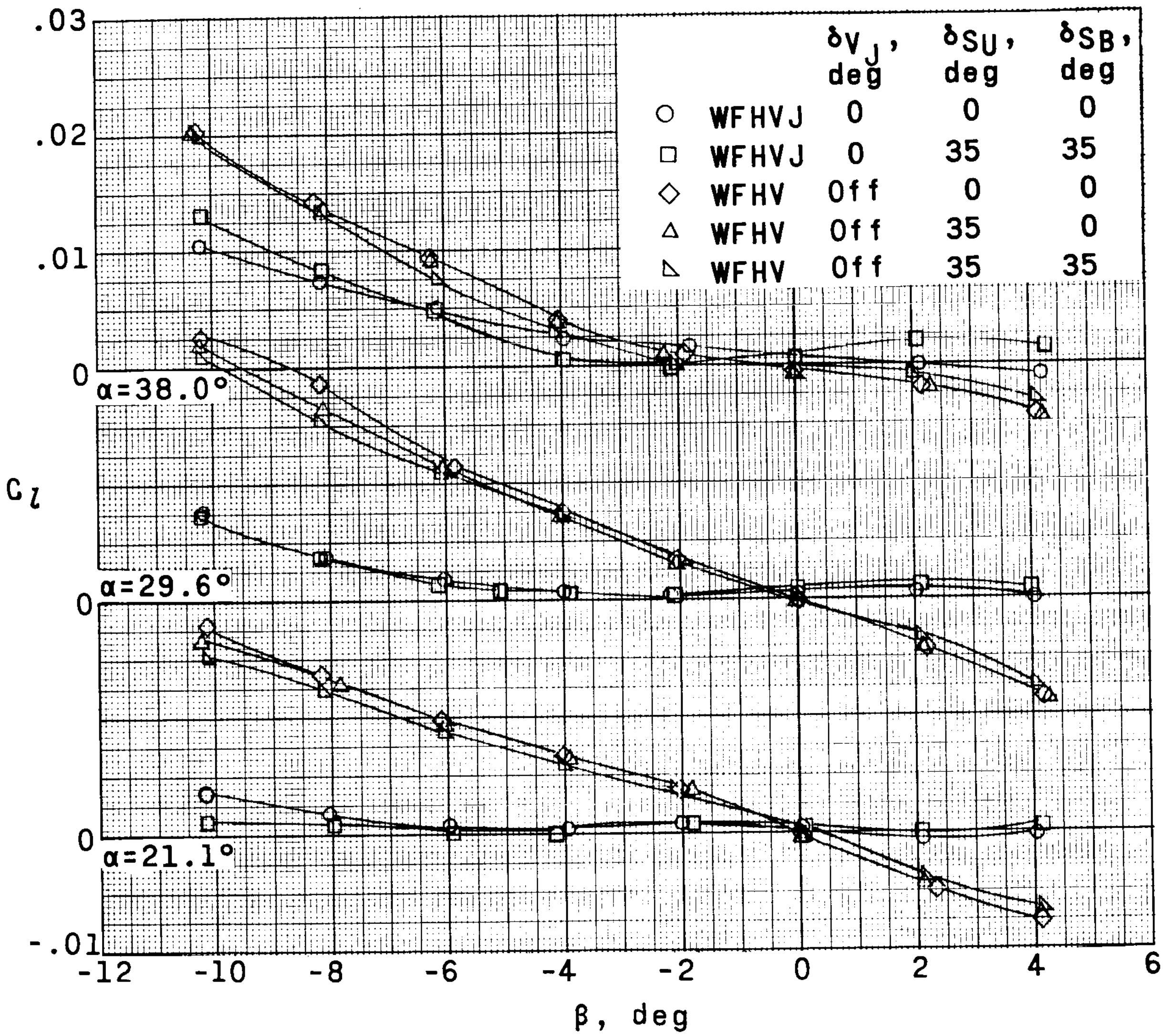

(a) M = 2.96.

Figure 27.- Effect of various configurations on aerodynamic characteristics in yaw at various angles of attack. $\delta_{H_L} = \delta_{H_R} = -20^{\circ}$; $\delta_{V_U} = 0^{\circ}$.

[redacted]

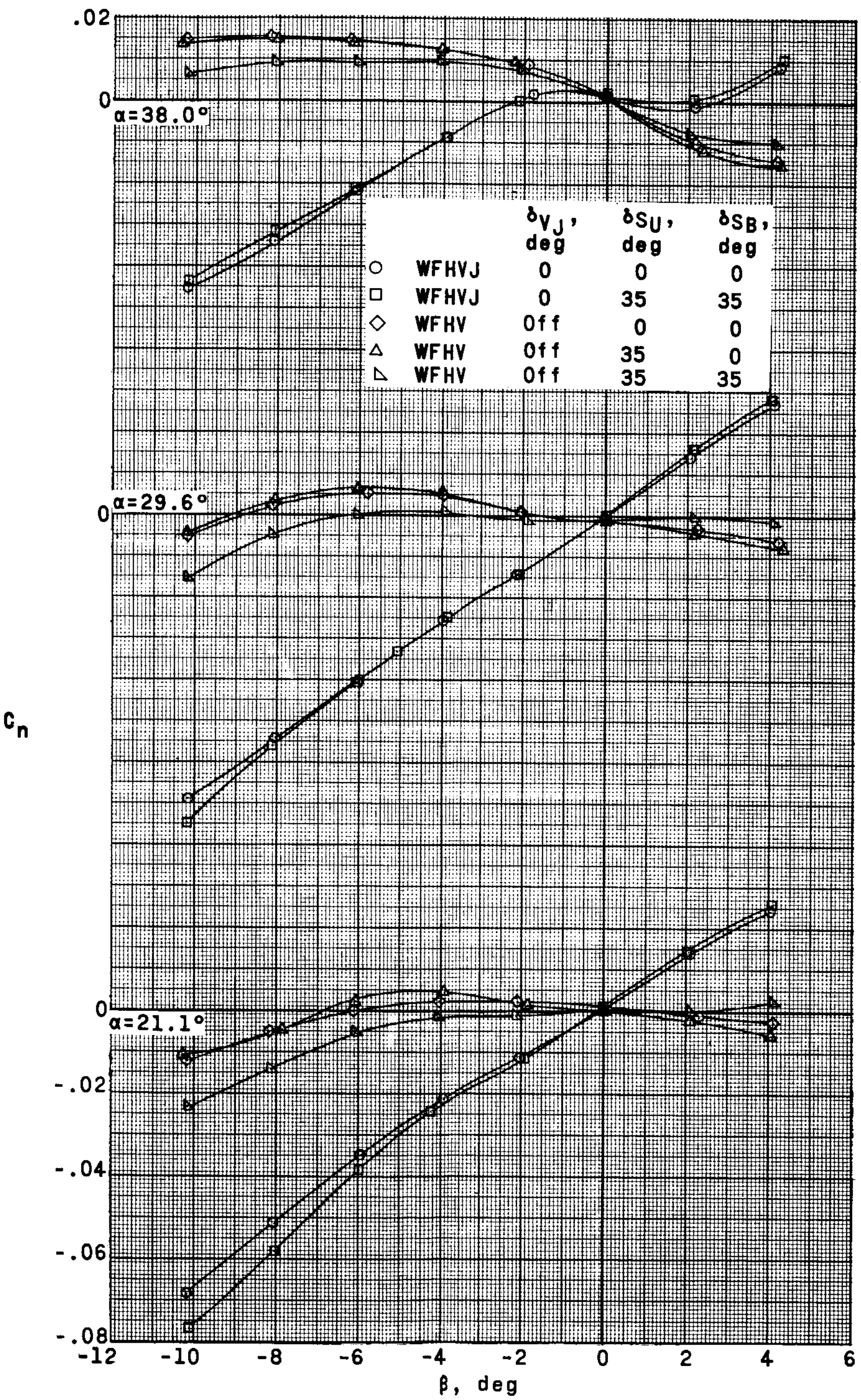

(a) Continued.

Figure 27.- Continued.

[redacted]

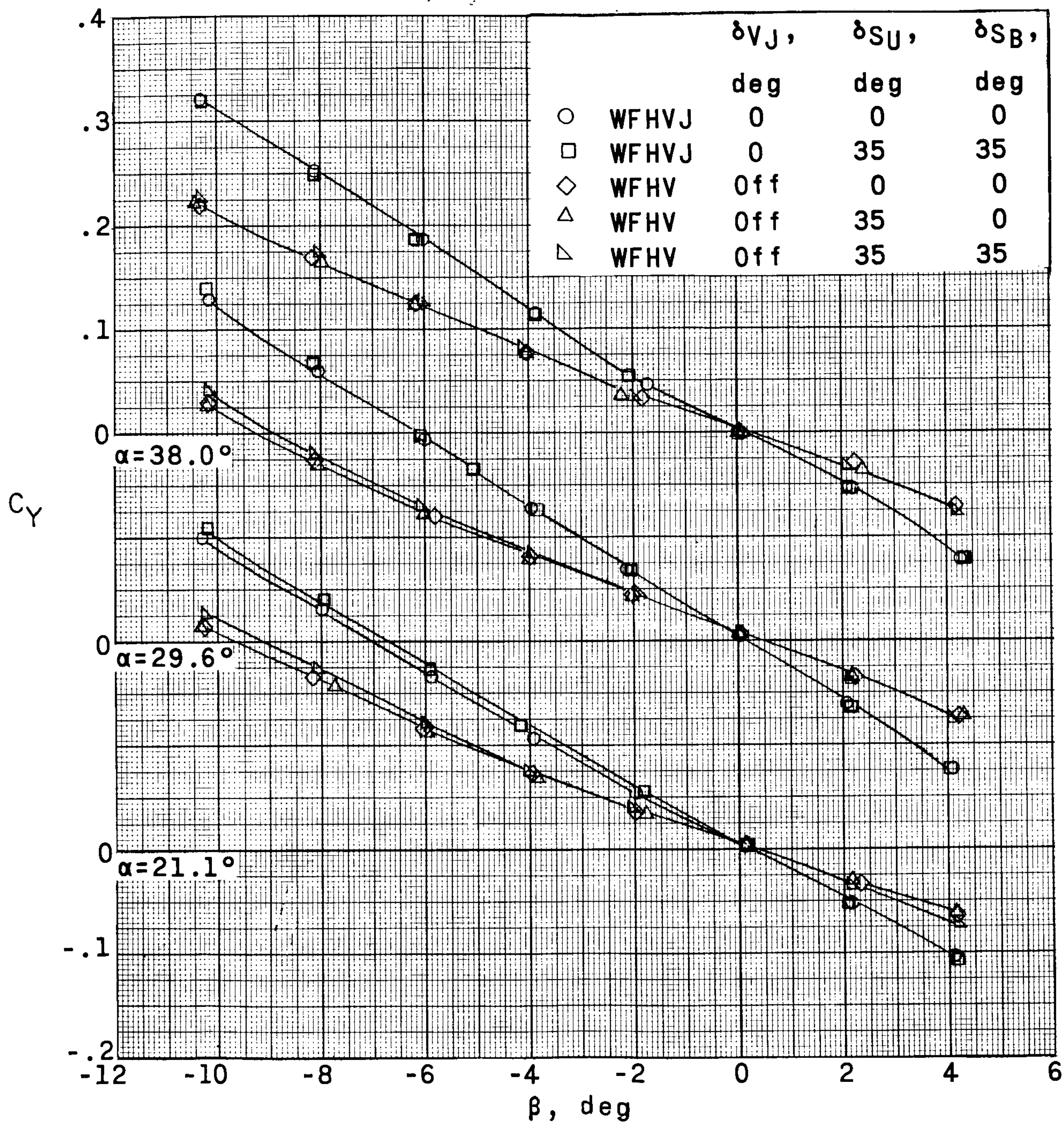

(a) Concluded.

Figure 27.- Continued.

[redacted]

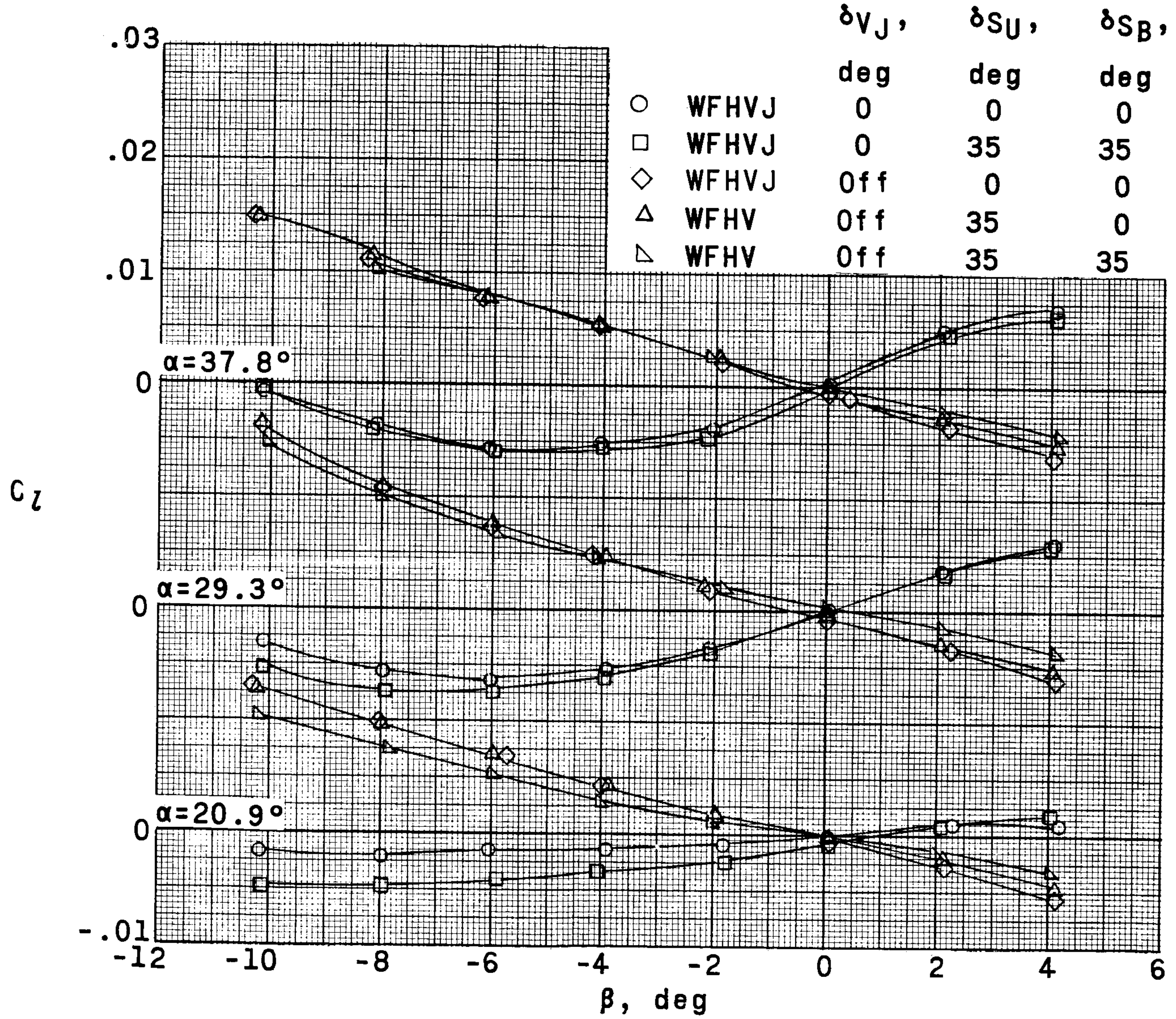

(b) M = 3.96.

Figure 27.- Continued.

[redacted]

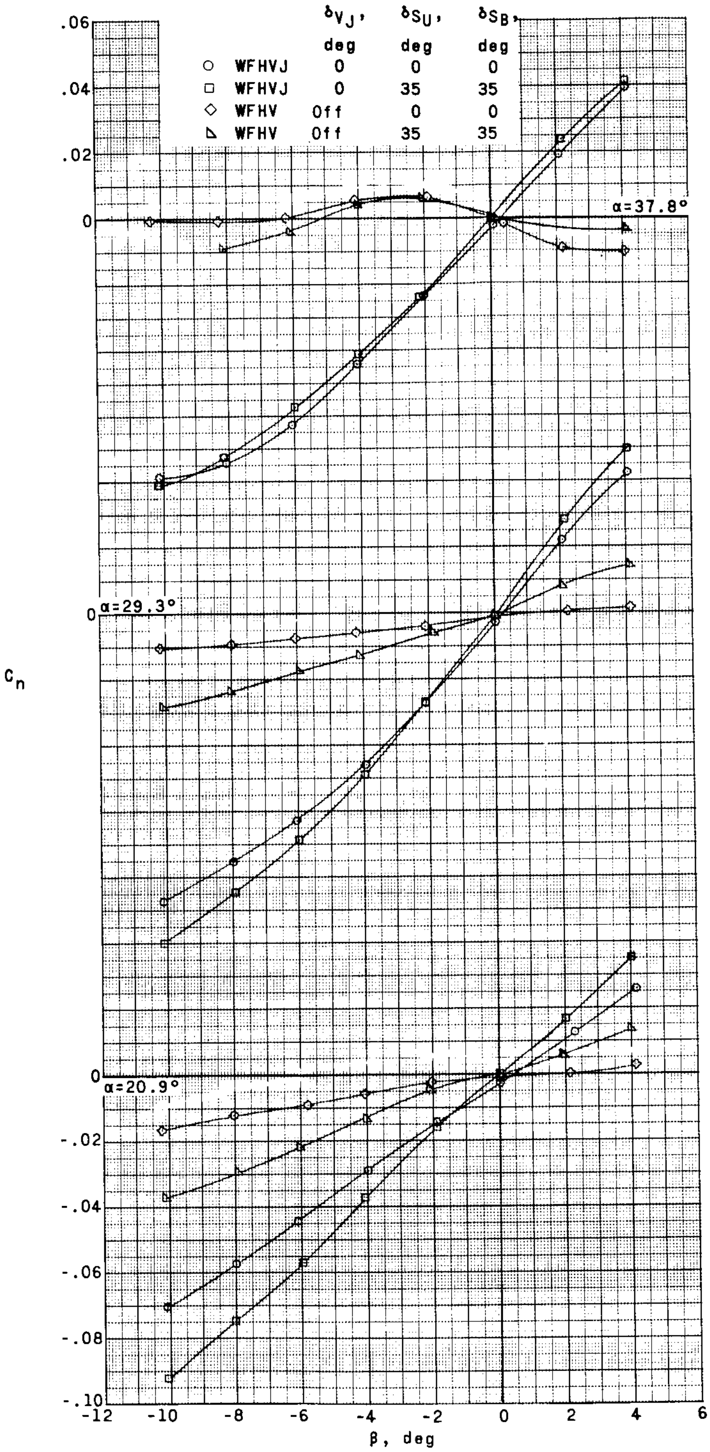

(b) Continued.

Figure 27.- Continued.

[redacted]

[redacted]

DECLASSIFIED

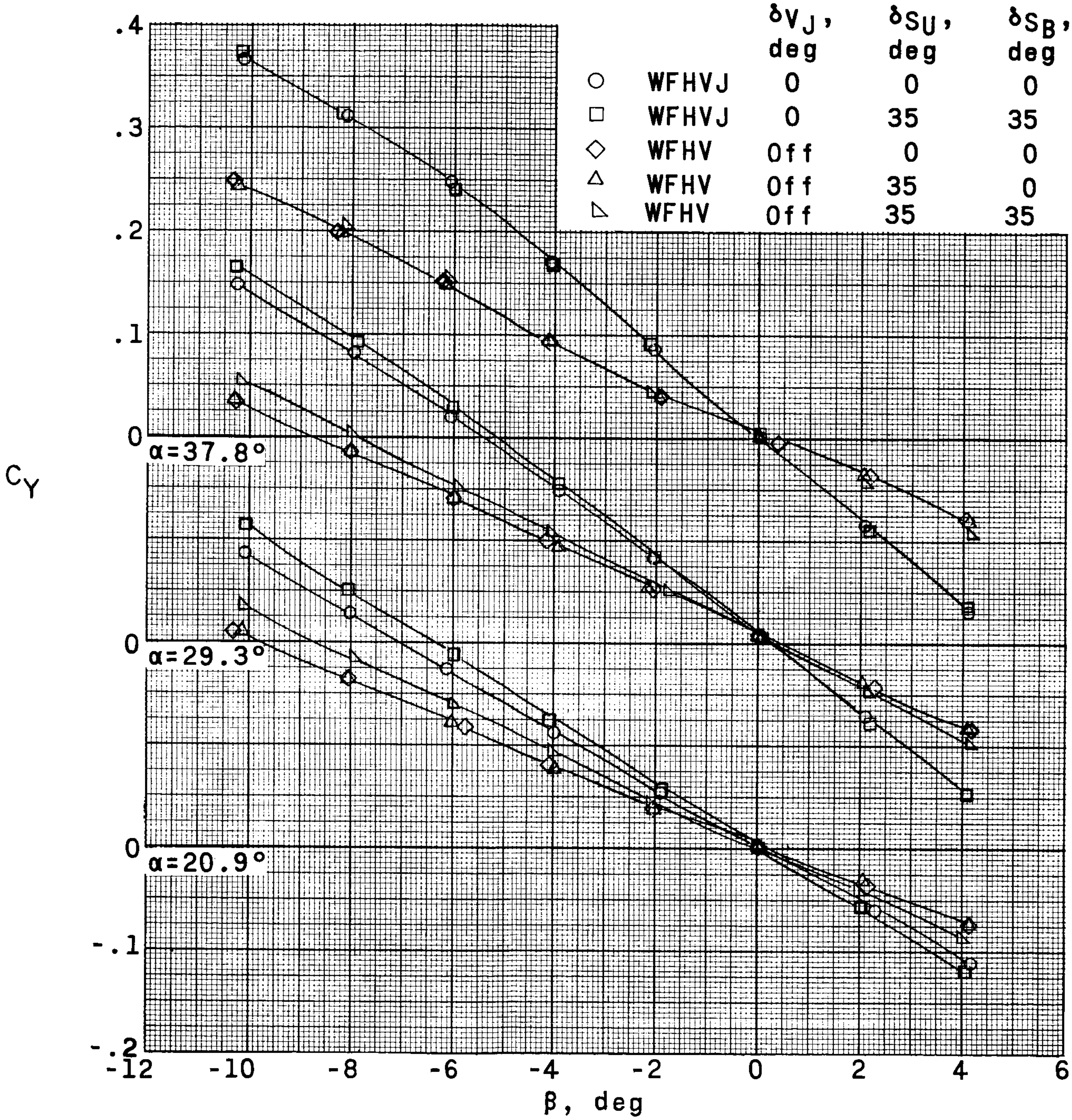

(b) Concluded.

Figure 27.- Continued.

[redacted]

[redacted]

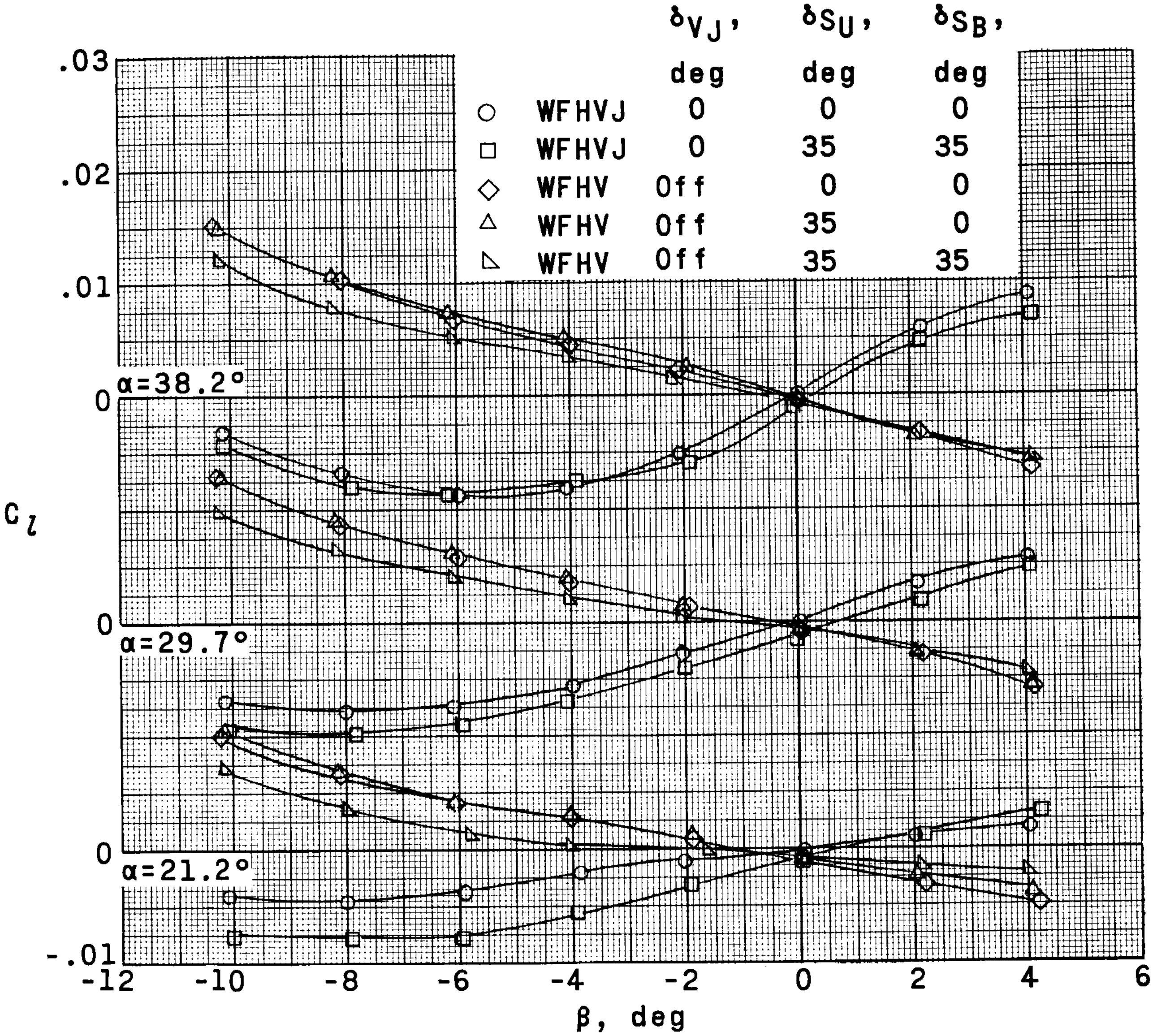

(c) M = 4.65.

Figure 27.- Continued.

[redacted]

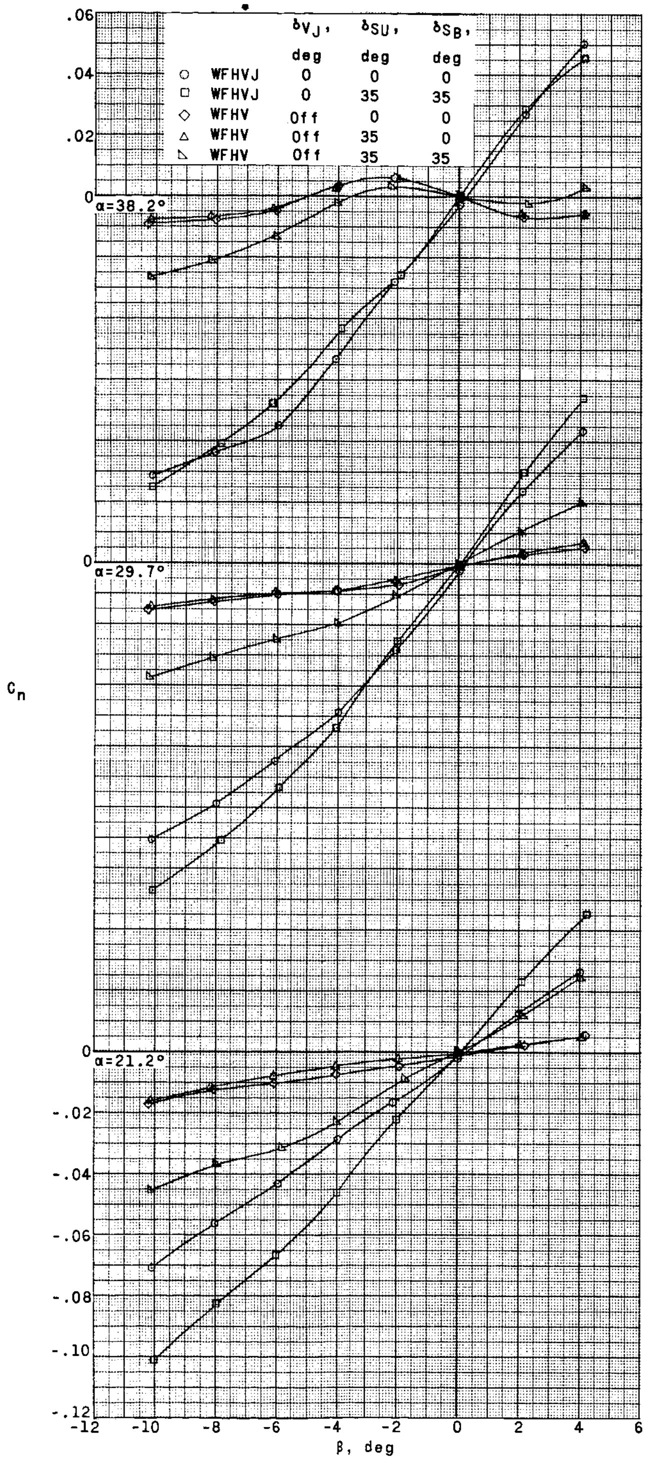

(c) Continued.

Figure 27.- Continued.

[redacted]

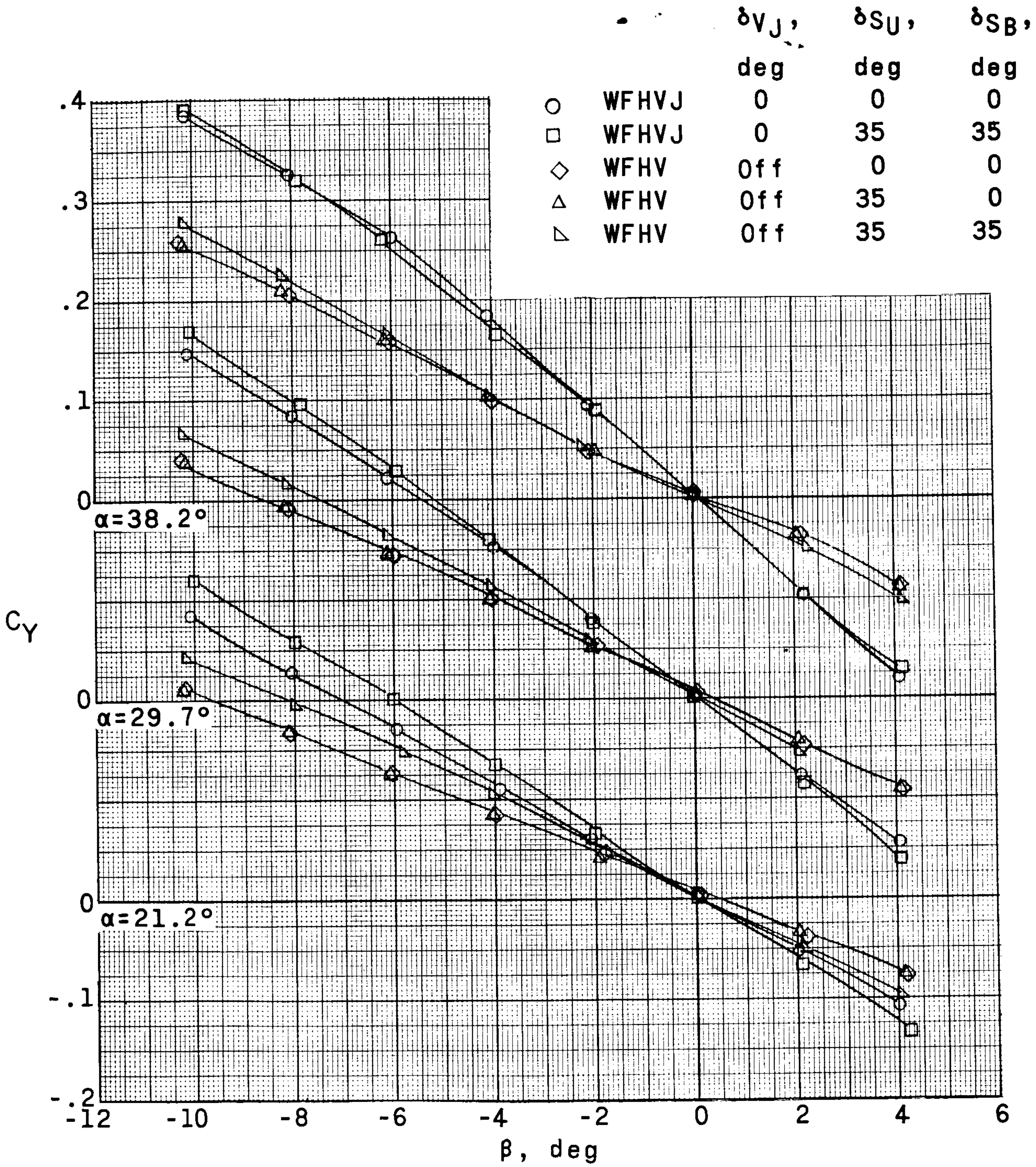

(c) Concluded.

Figure 27.- Concluded.

[redacted]

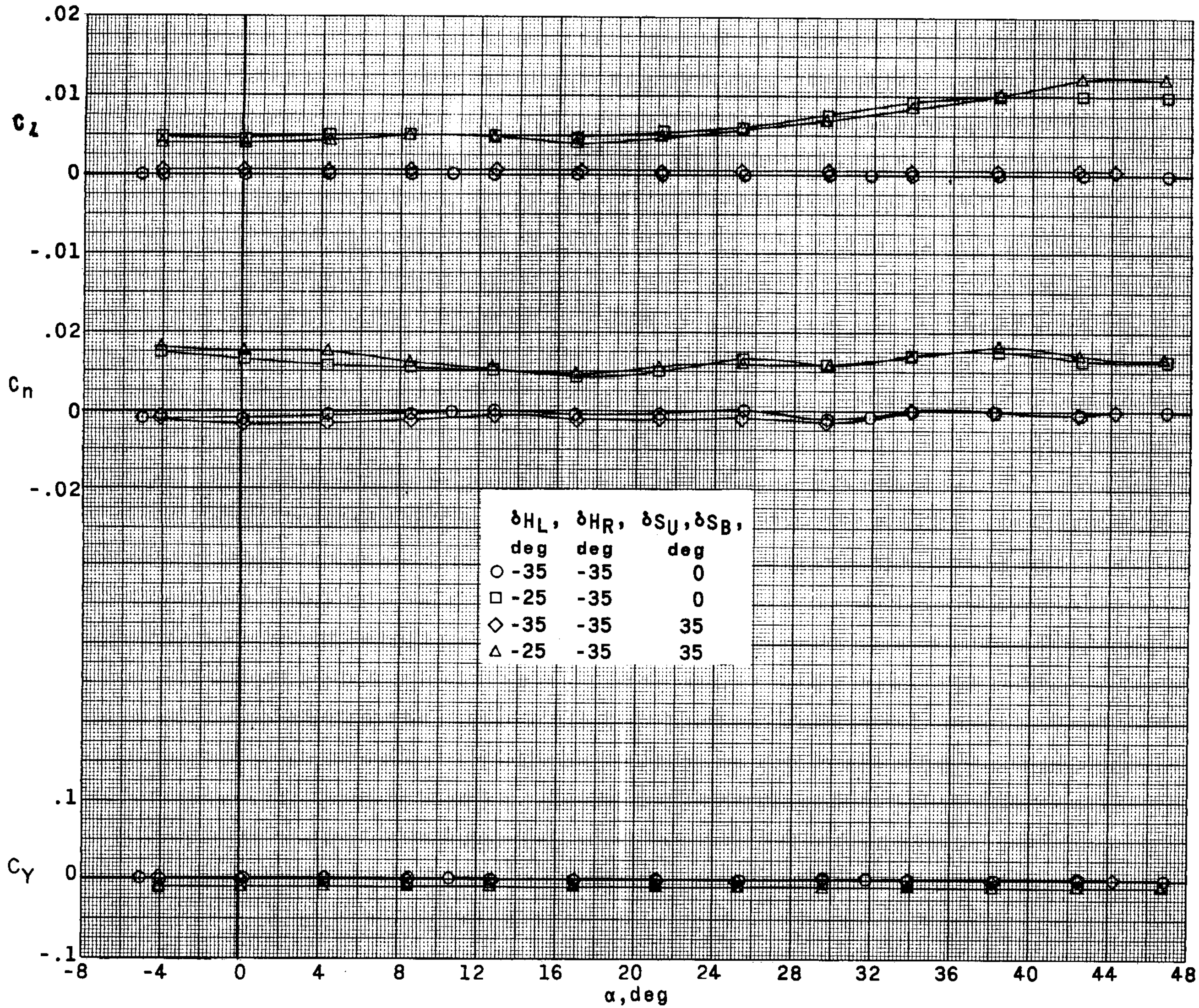

(a) M = 2.96.

Figure 28.- Effect of angle of attack and roll-control deflections on the lateral aerodynamic characteristics for various configurations. $\delta_{V_U} = \delta_{V_J} = 0^{\circ}$; $\beta = 0^{\circ}$.

[redacted]

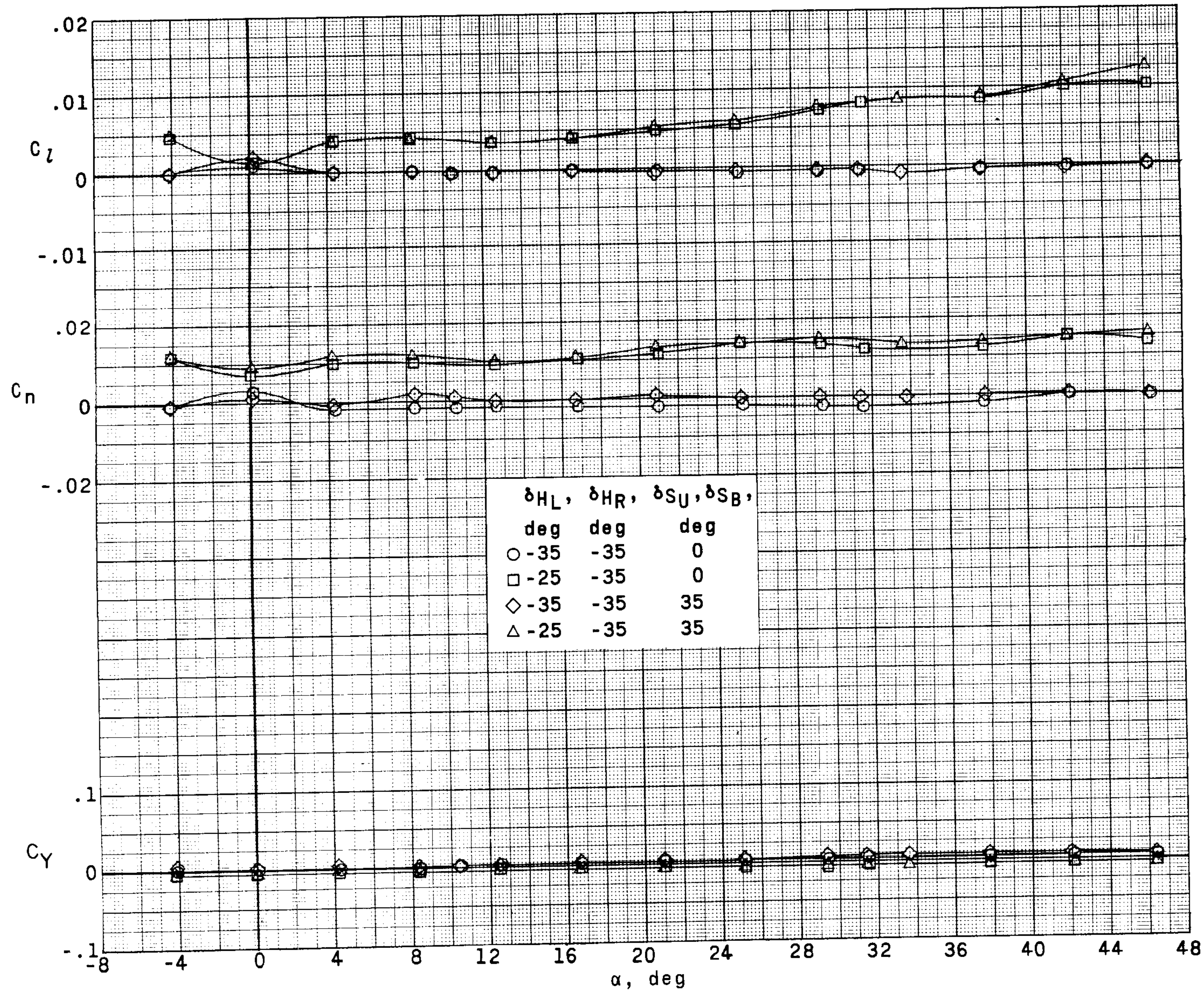

(b) M = 3.96.

Figure 28.- Continued.

[redacted]

[redacted]SIFIED

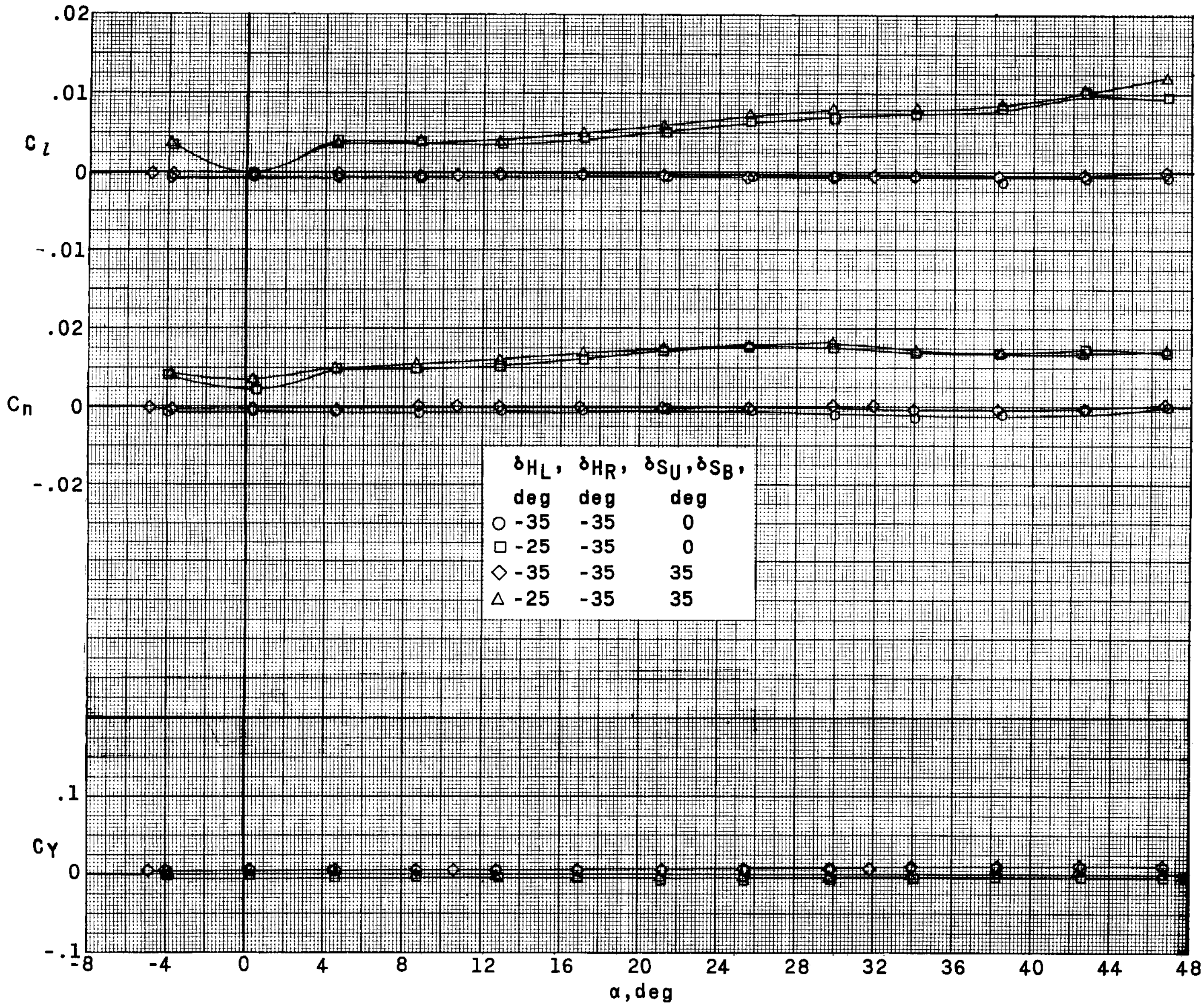

(c) M = 4.65.

Figure 28.- Concluded.

[redacted]

[redacted]

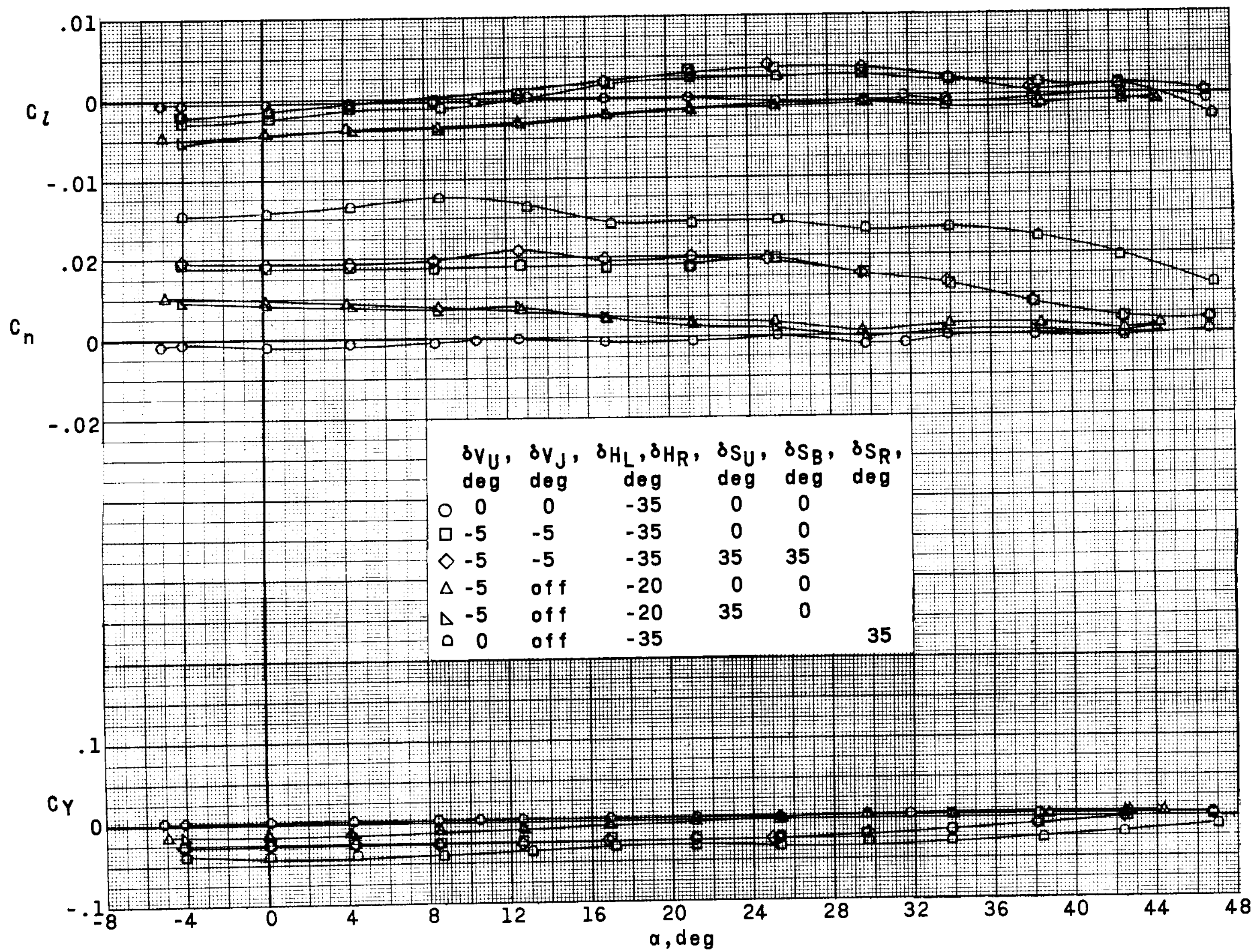

(a) M = 2.96.

Figure 29.- Effect of angle of attack and directional-control deflections on lateral aerodynamic characteristics for various configurations. $\beta = 0^{\circ}$.

[redacted]

[redacted]

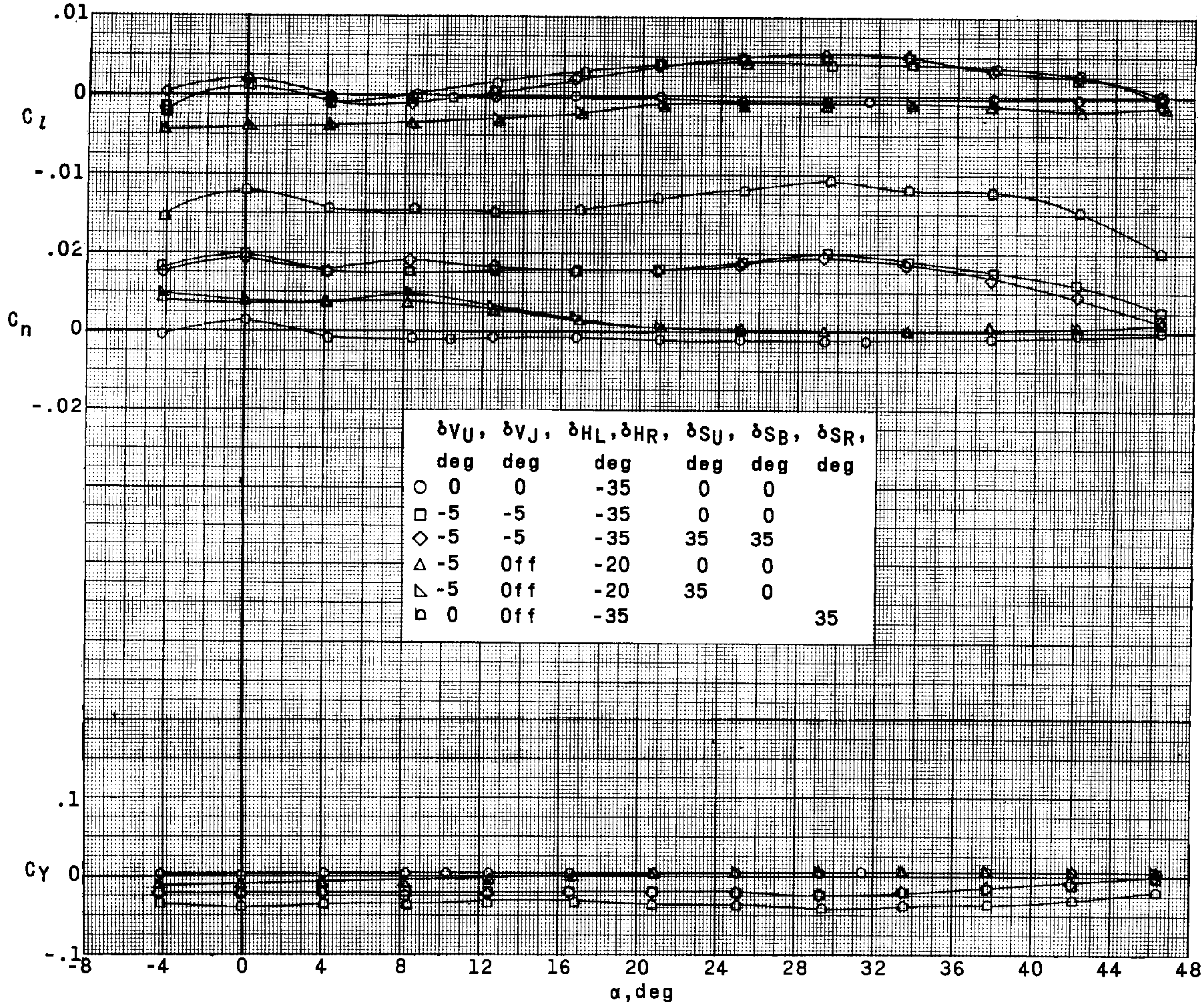

(b) M = 3.96.

Figure 29.- Continued.

[redacted]

[redacted]

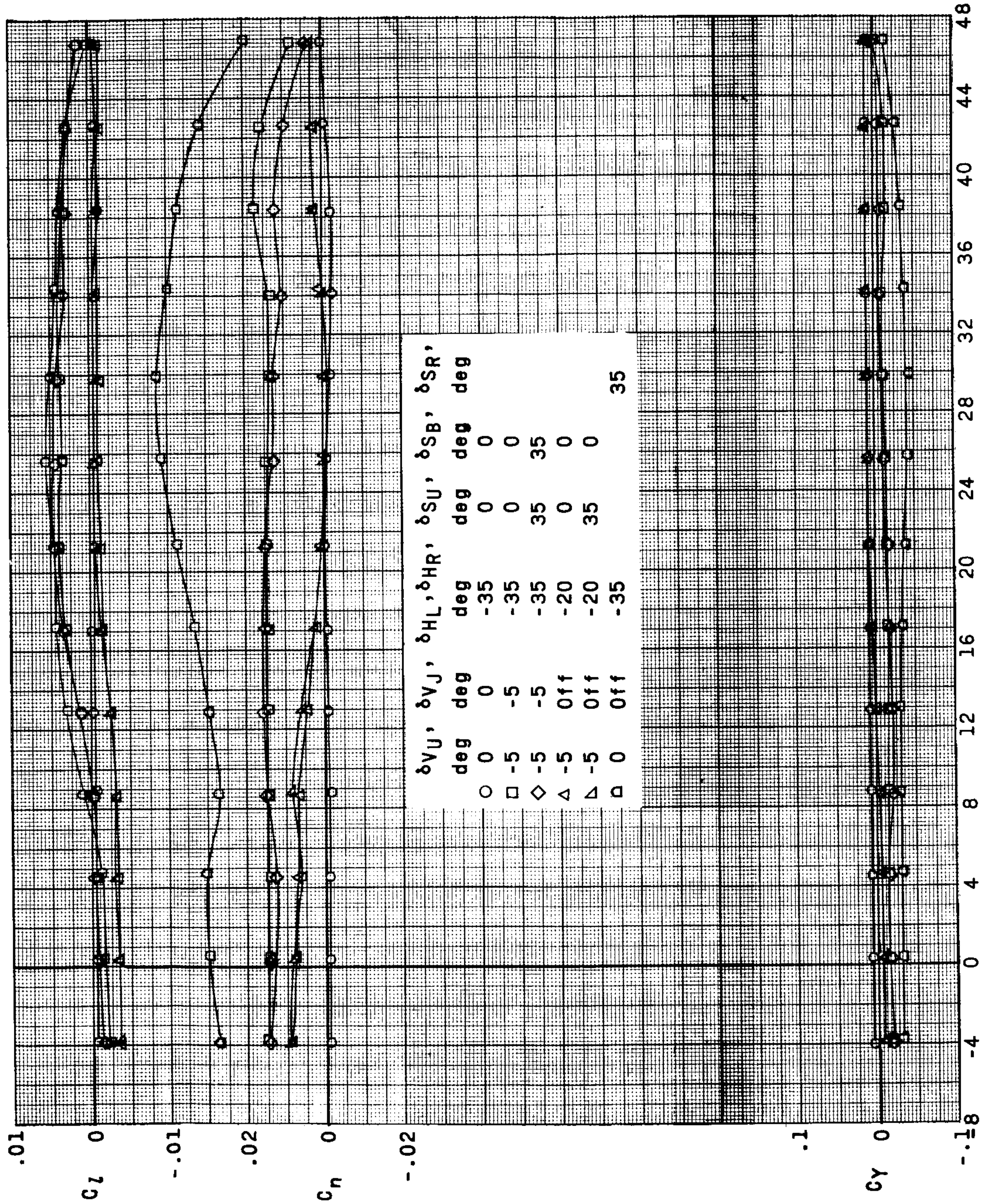

(c) M = 4.65.

Figure 29.- Concluded.

[redacted]

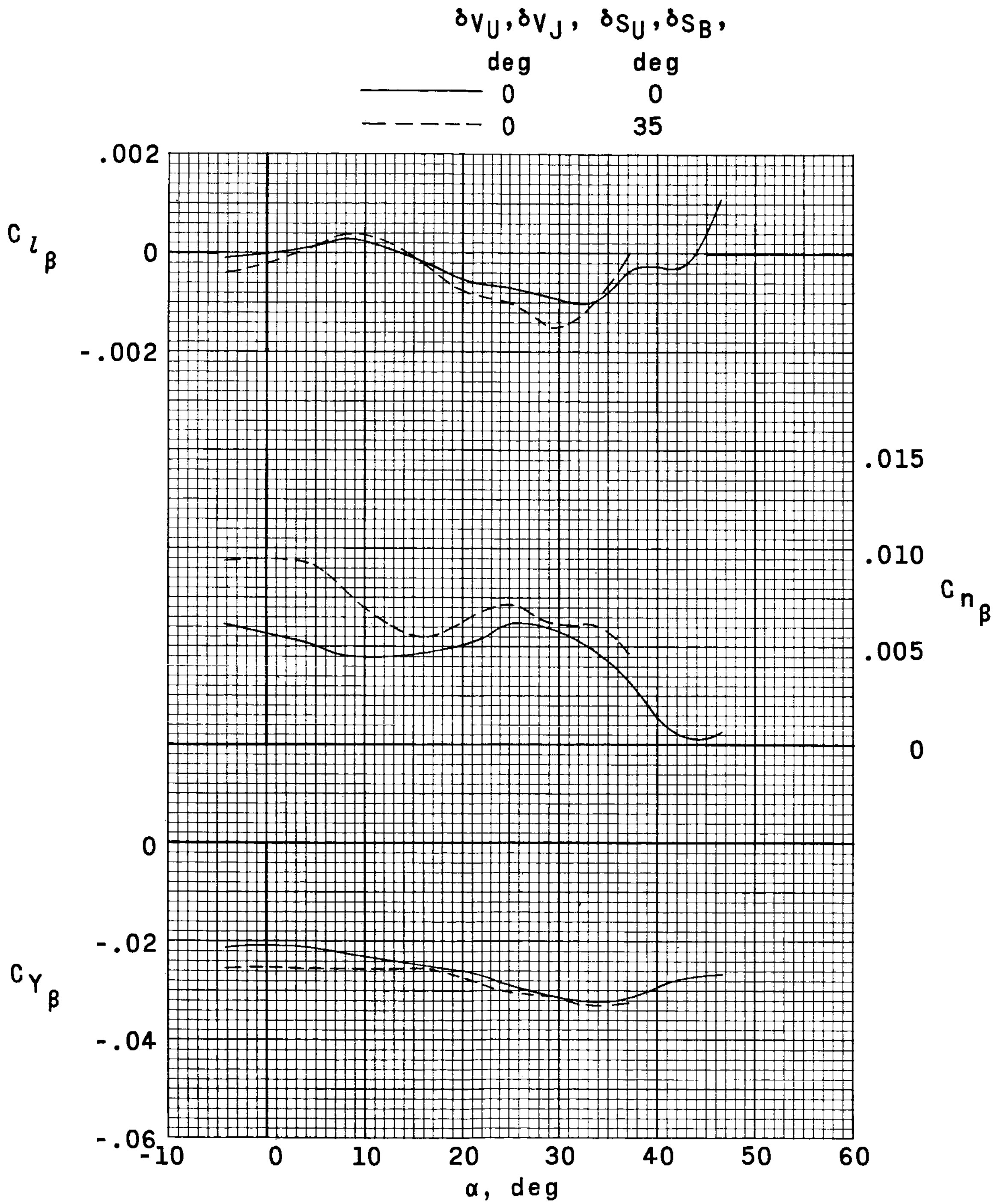

(a) M = 2.96.

Figure 30.- Effect of speed-brake deflections on lateral and directional stability characteristics of complete model. $\delta_{H_L} = \delta_{H_R} = 0^{\circ}$.

[redacted]

[redacted]

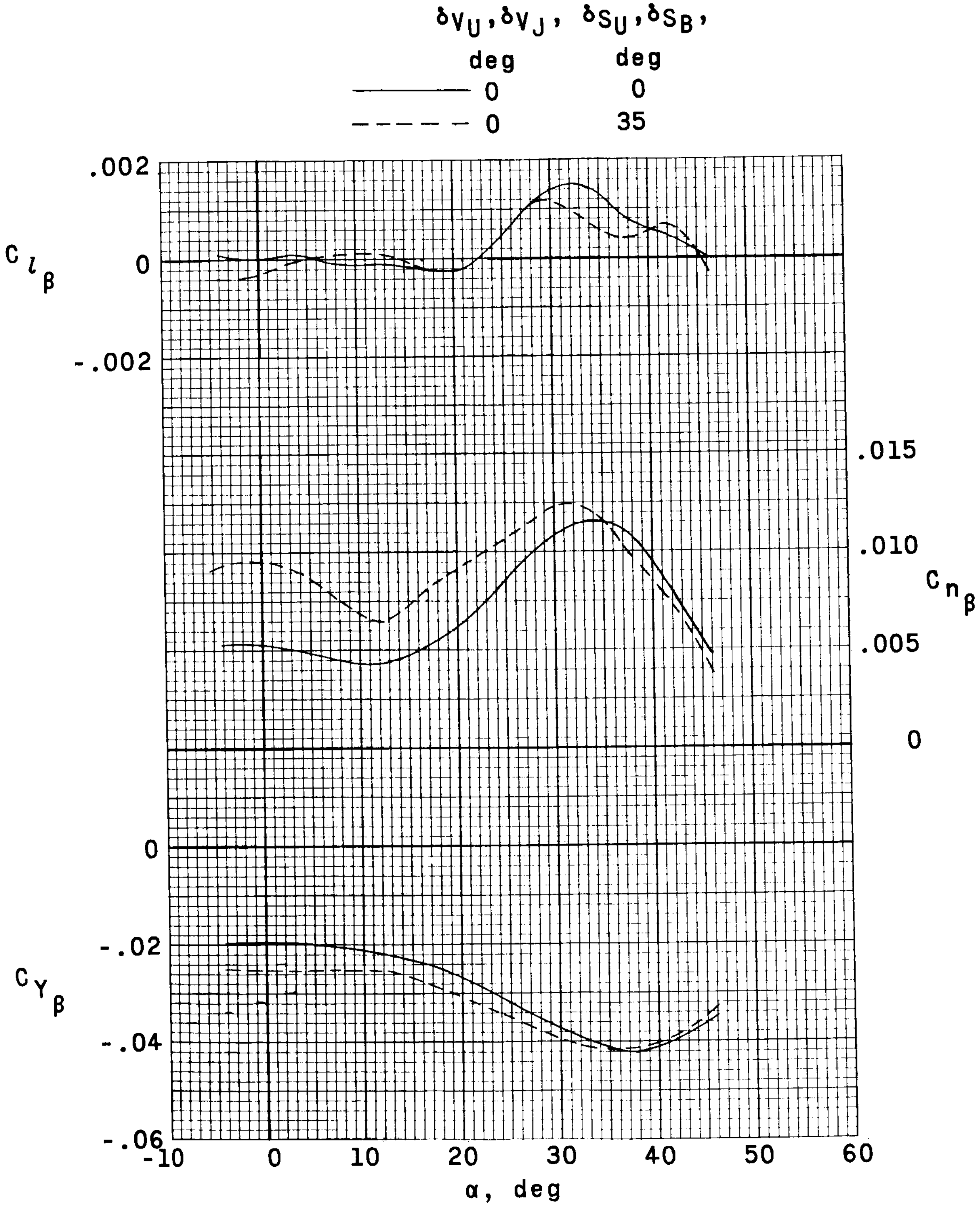

(b) M = 3.96.

Figure 30.- Continued.

[redacted]

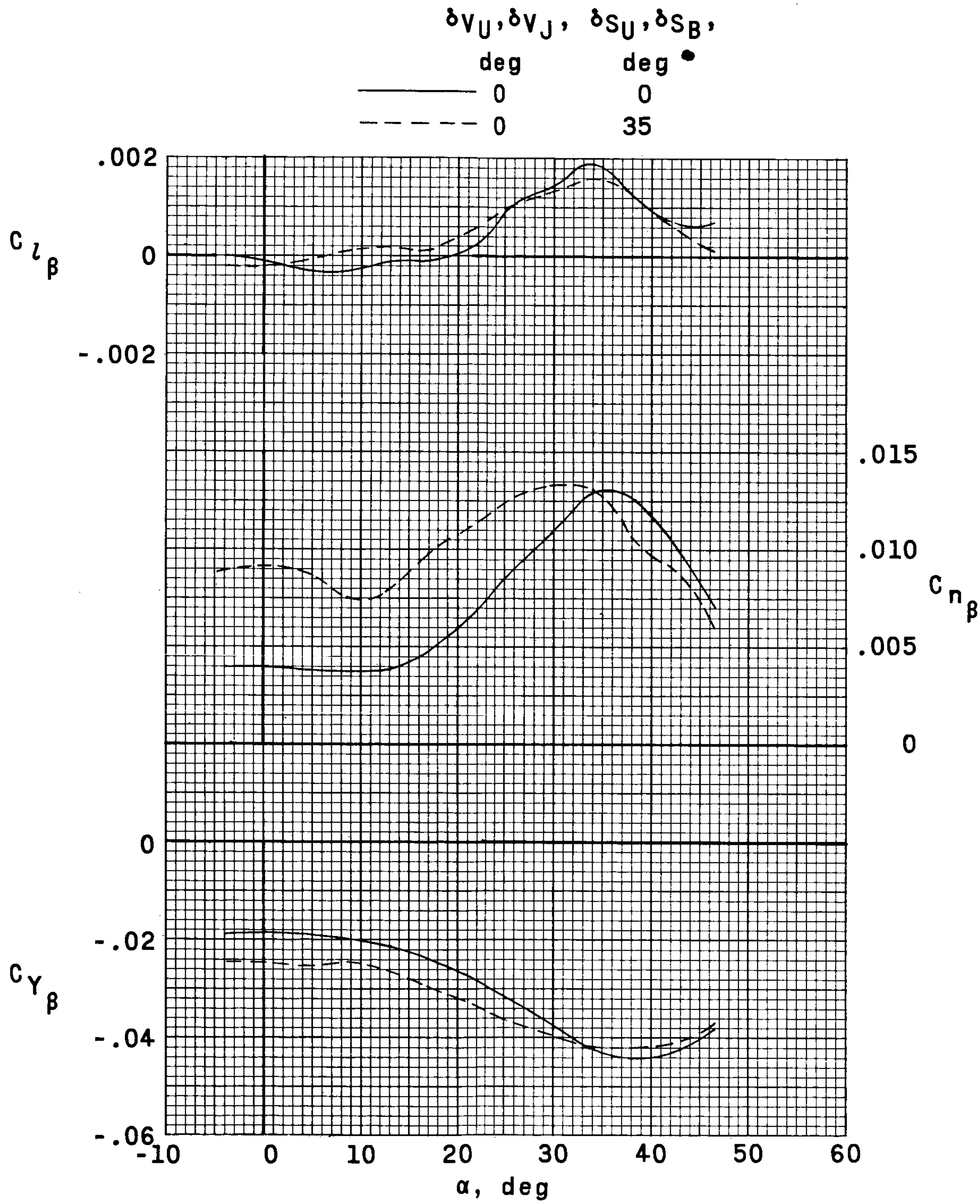

(c) M = 4.65.

Figure 30.- Concluded.

[redacted]

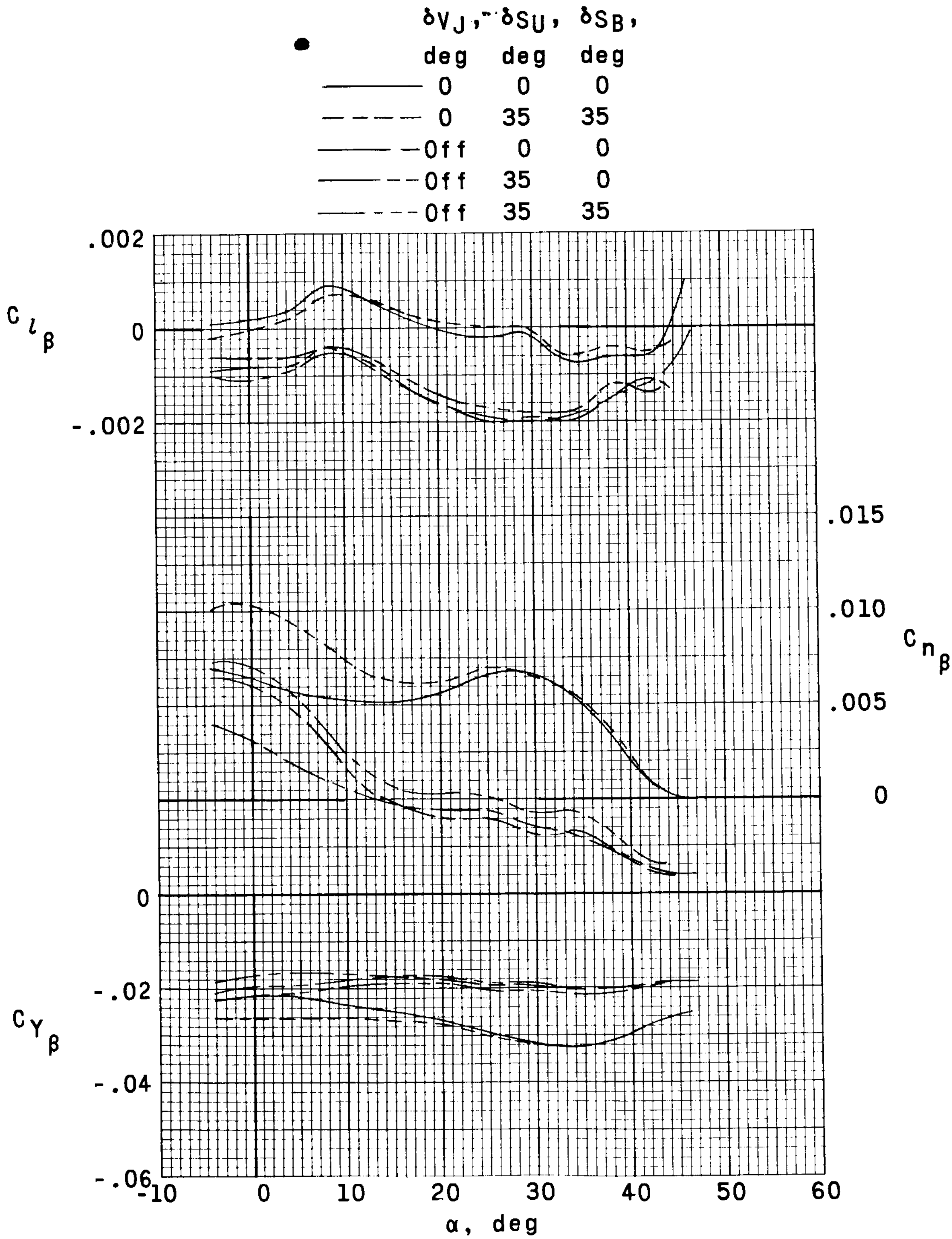

(a) M = 2.96.

Figure 31.- Effect of various configuration changes on lateral and directional stability characteristics. $\delta_{H_L} = \delta_{H_R} = -20^\circ$; $\delta_{V_U} = 0^\circ$.

[redacted]

[redacted]

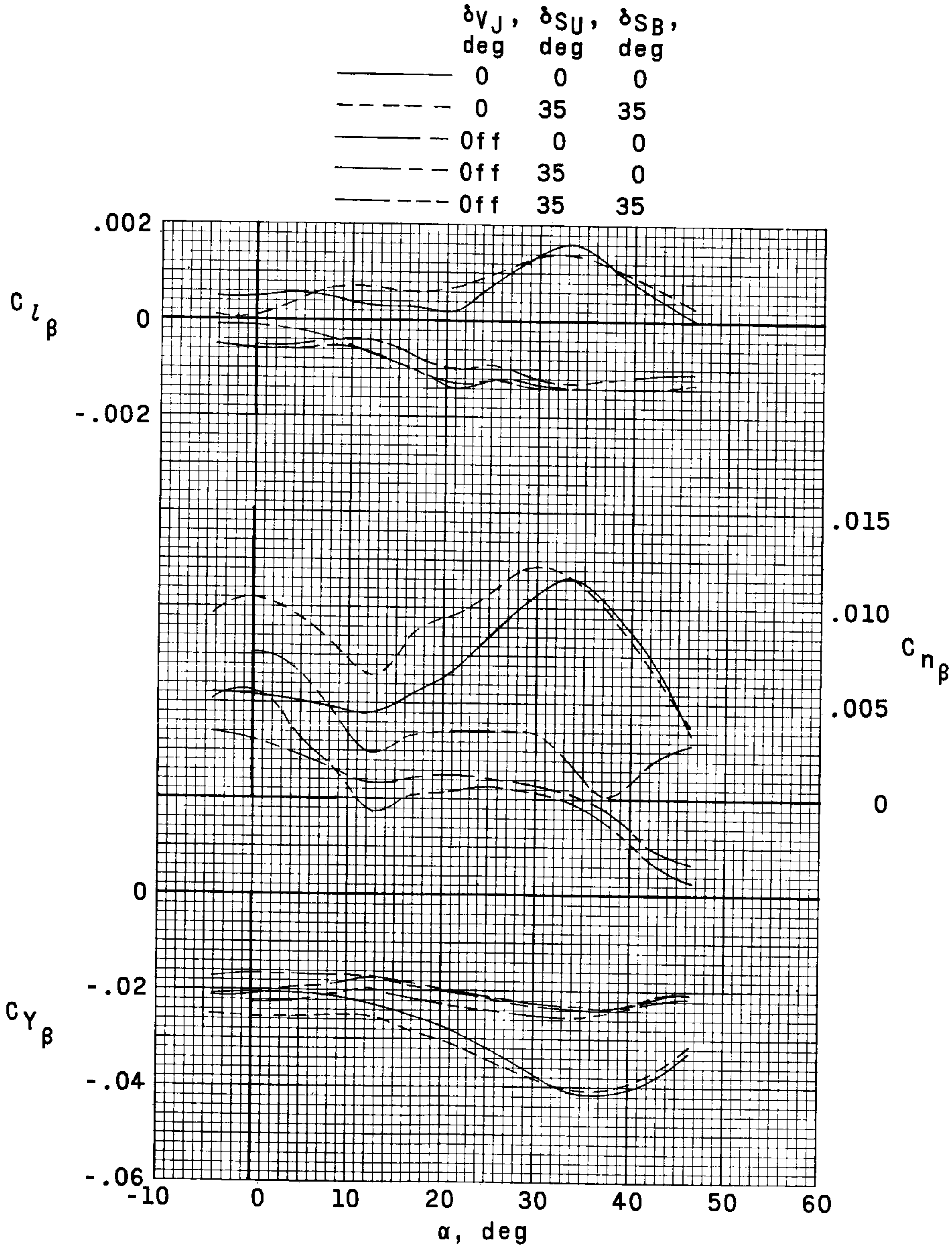

(b) M = 3.96.

Figure 31.- Continued.

[redacted]

[redacted]

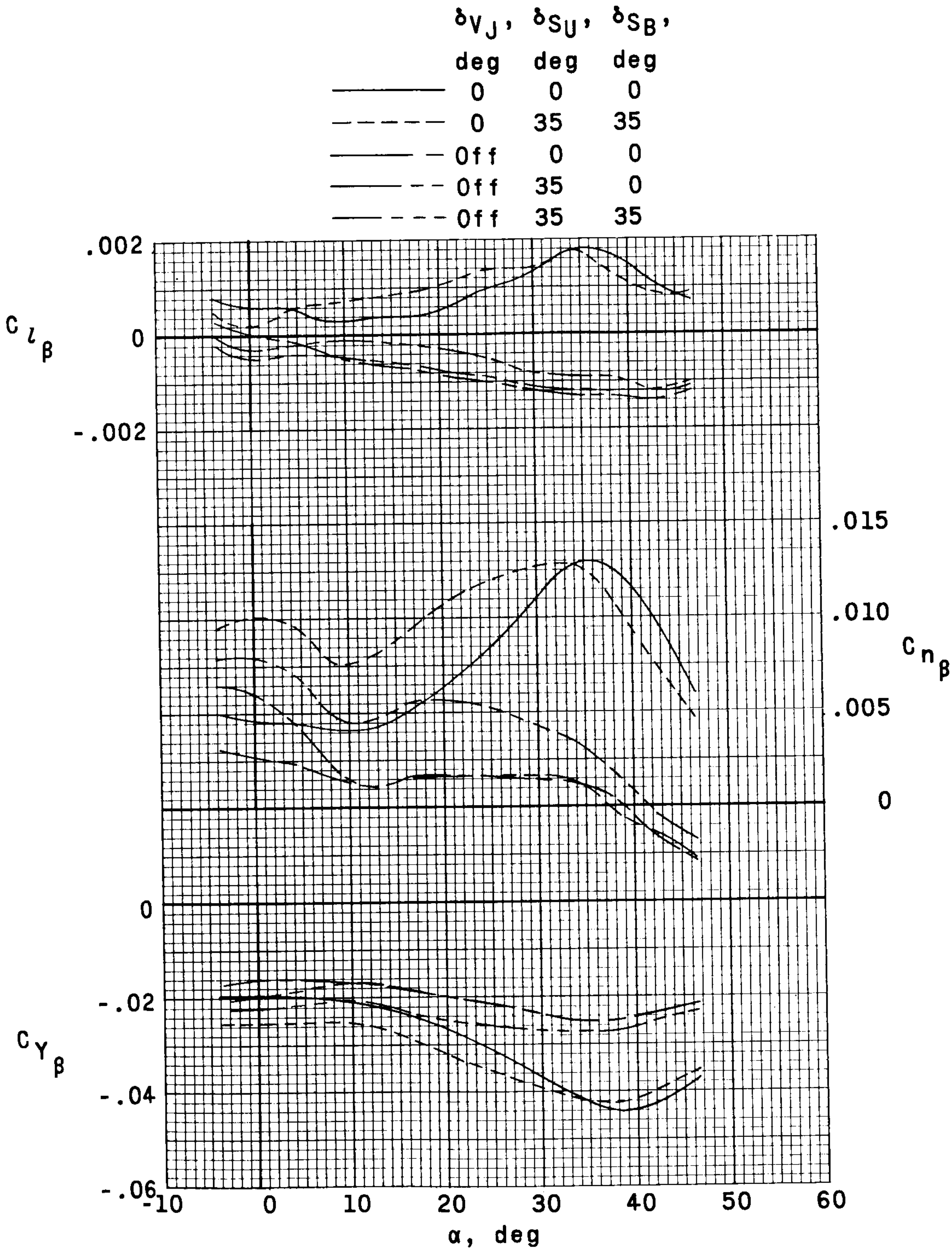

(c) M = 4.65.

Figure 31.- Concluded.

[redacted]

DE[redacted]IFIED

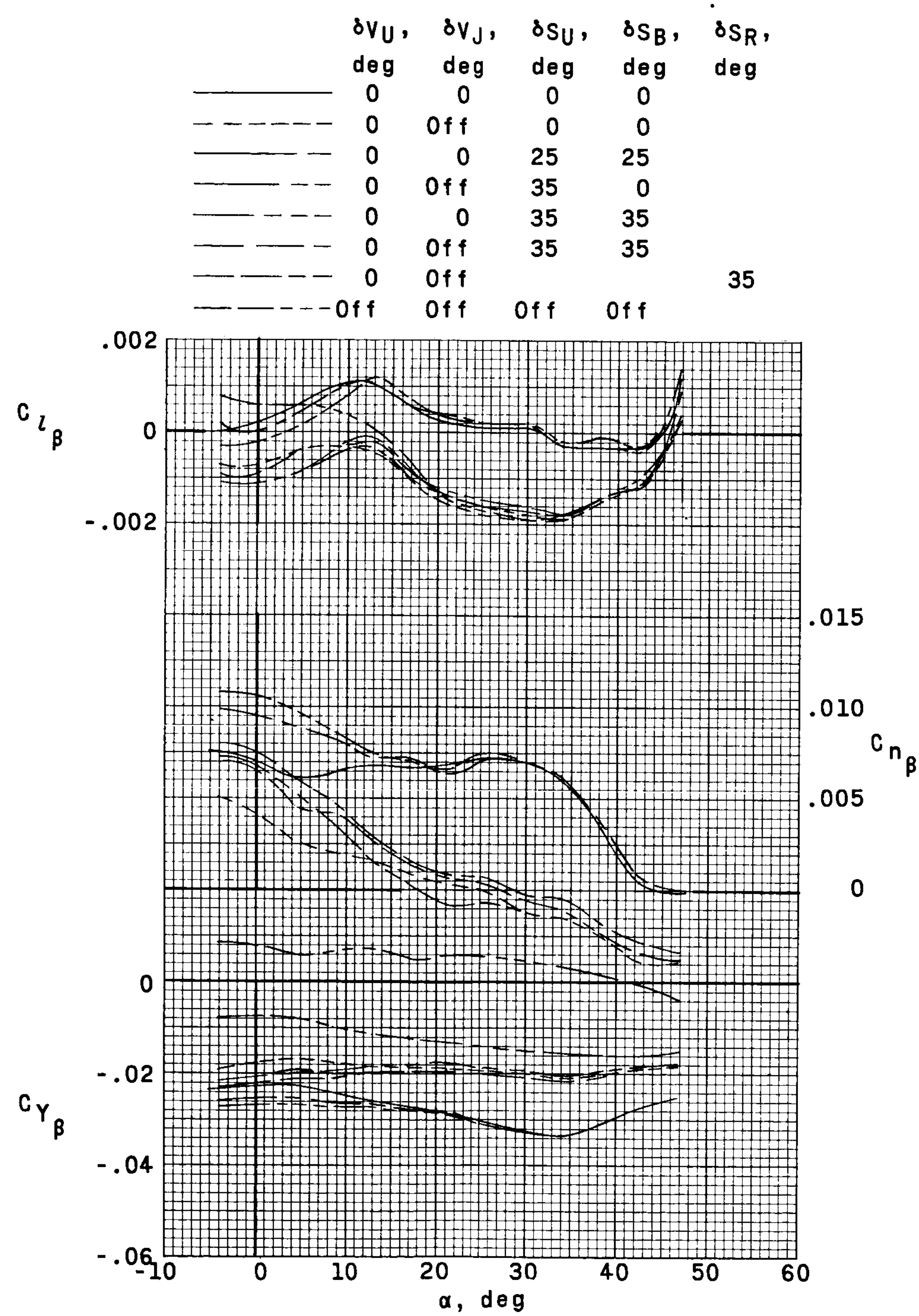

(a) M = 2.96.

Figure 32.- Effect of various configuration changes on lateral and directional stability characteristics. $\delta_{H_L} = \delta_{H_R} = -35^{\circ}$.

[redacted]

[redacted]

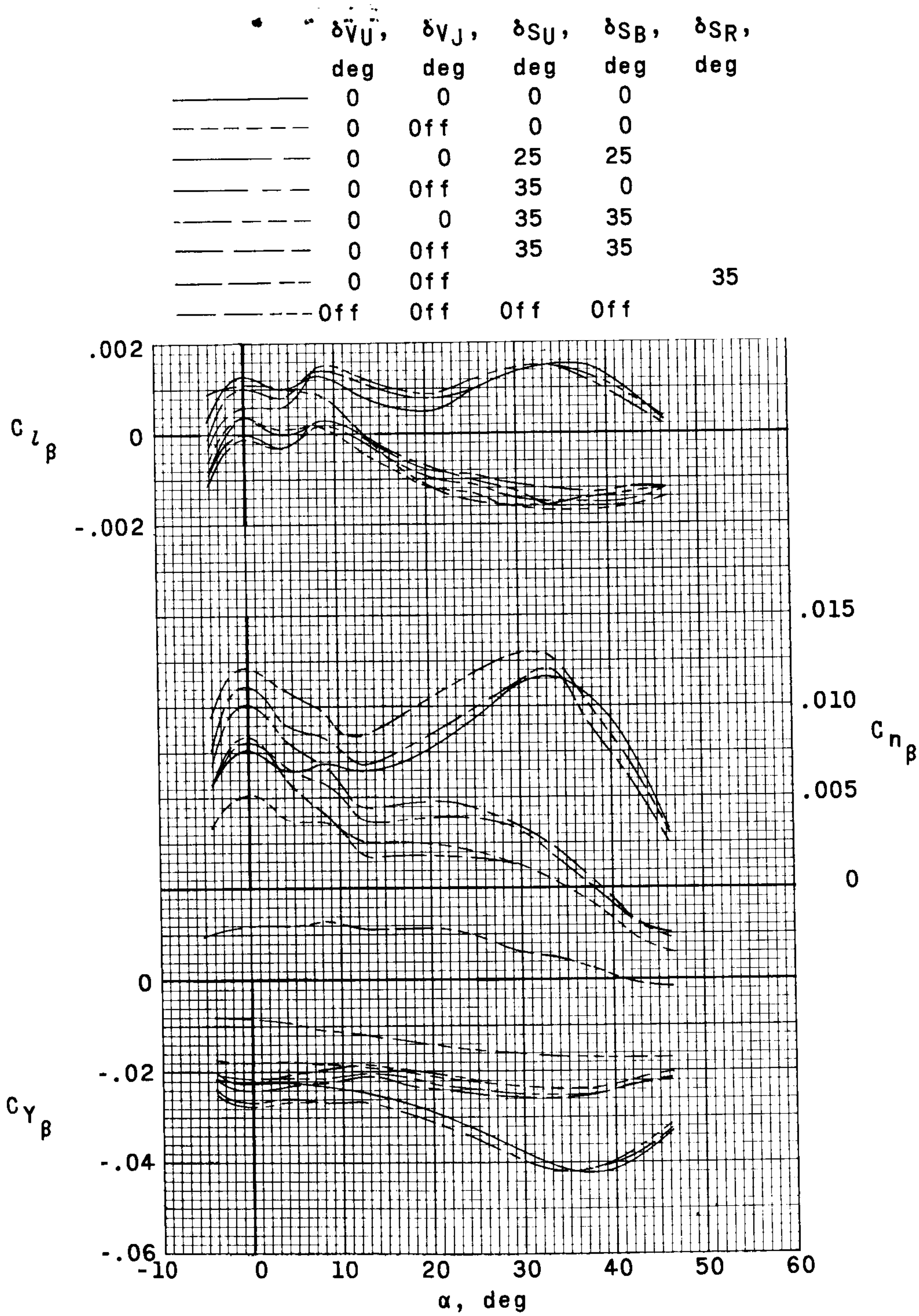

(b) M = 3.96.

Figure 32.- Continued.

[redacted]

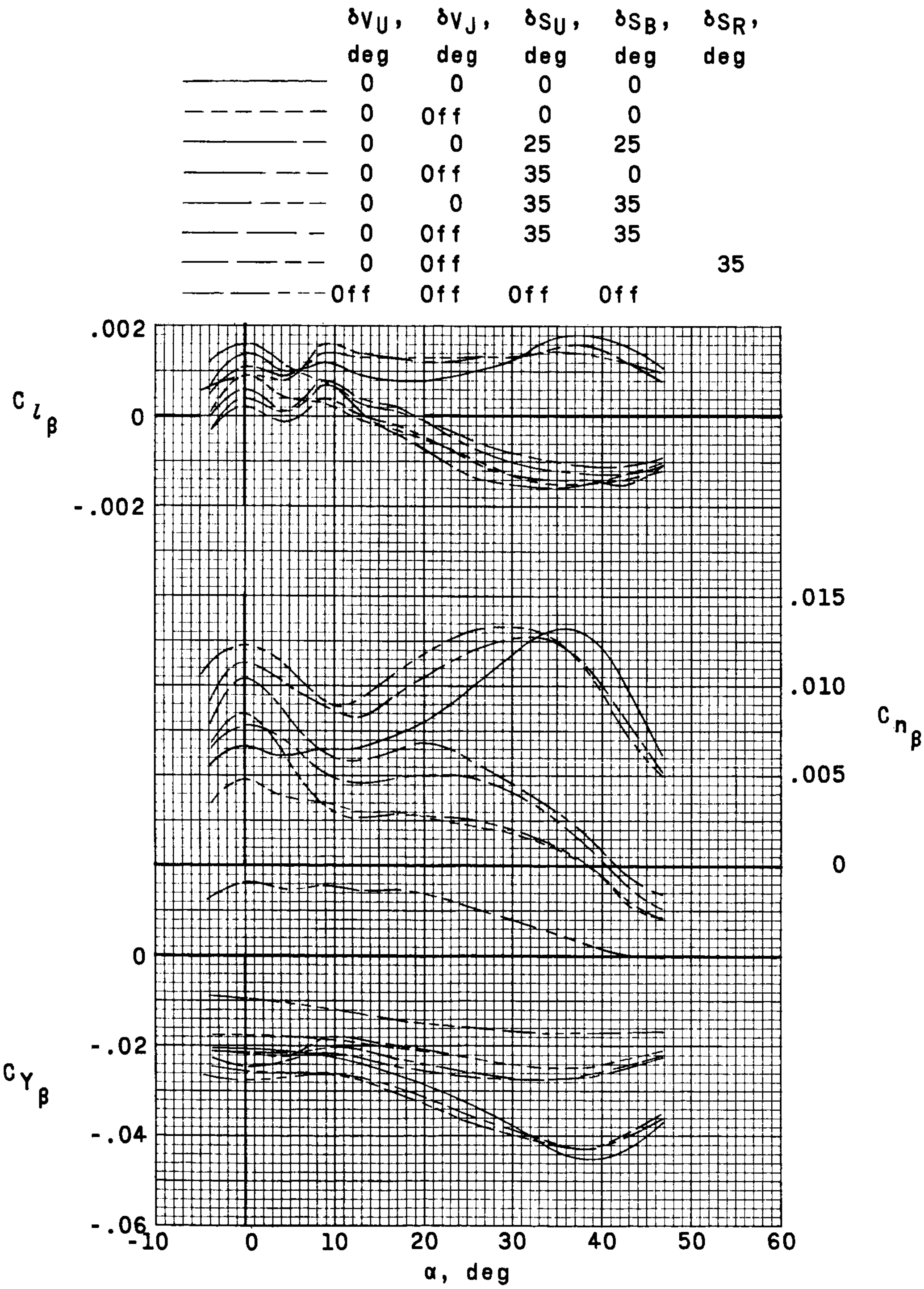

(c) M = 4.65.

Figure 32.- Concluded.

[redacted]

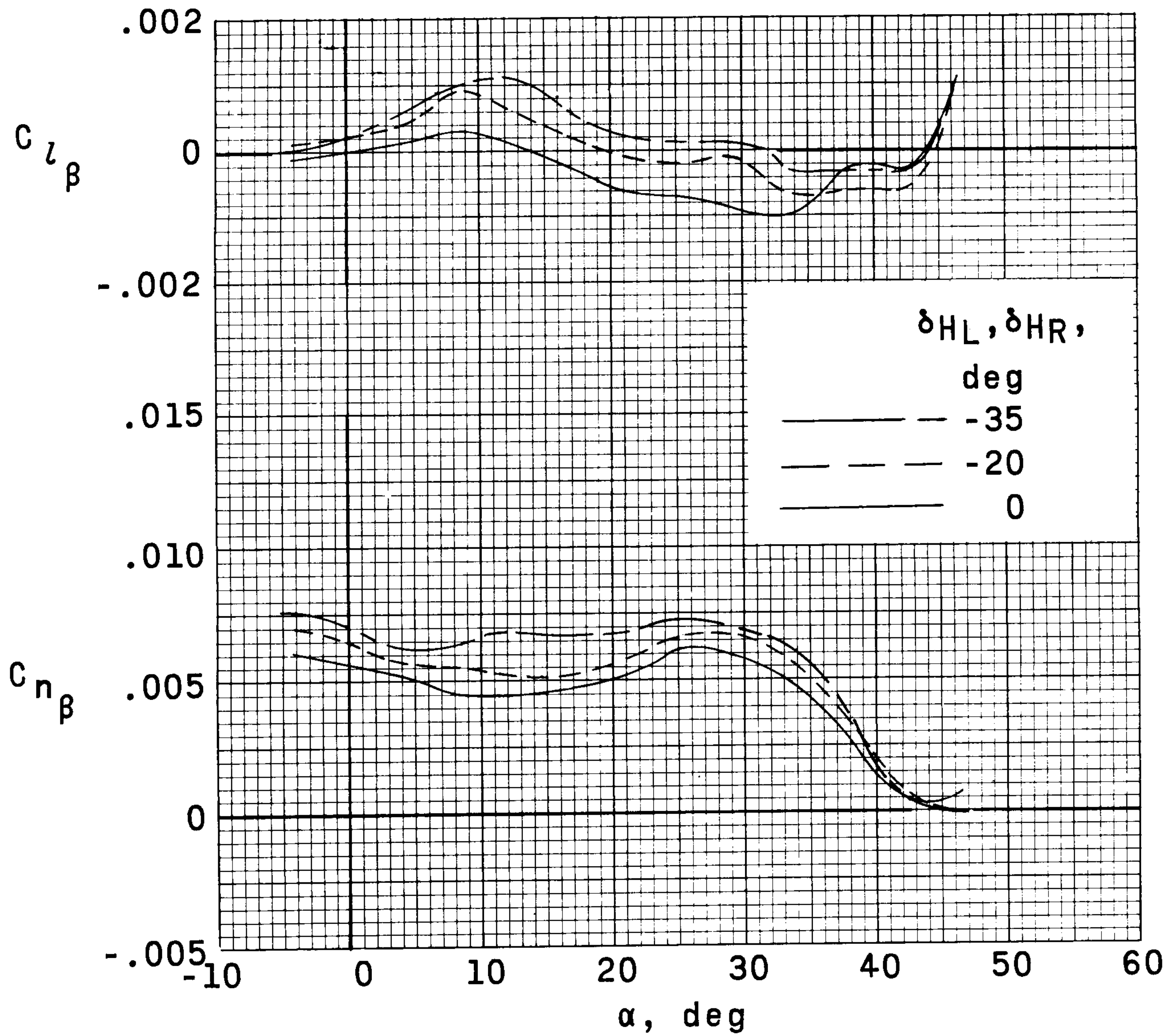

(a) M = 2.96.

Figure 33.- Effect of pitch-control deflections on lateral and directional stability characteristics with speed brakes retracted.

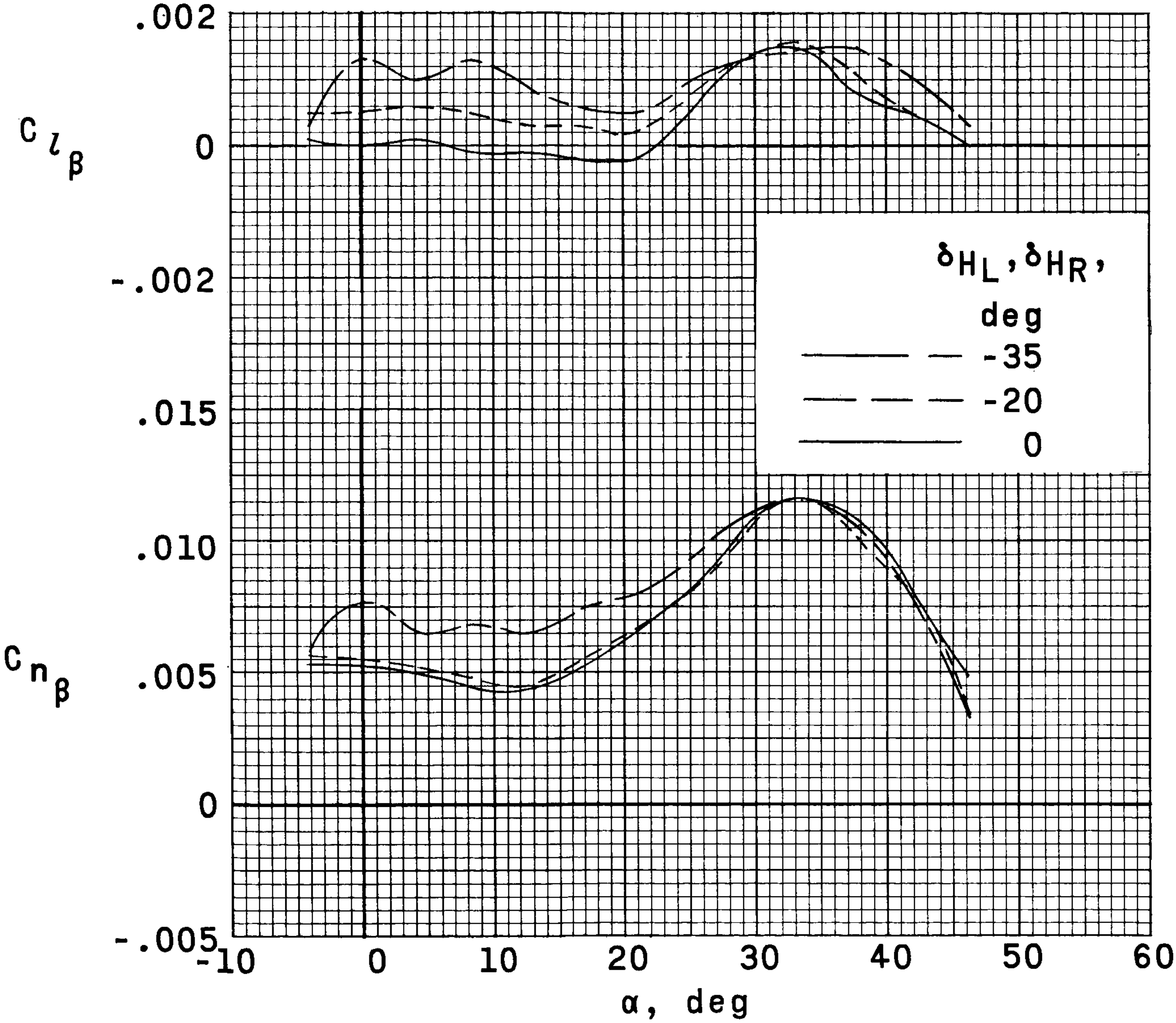

(b) M = 3.96.

Figure 33.- Continued.

[redacted]

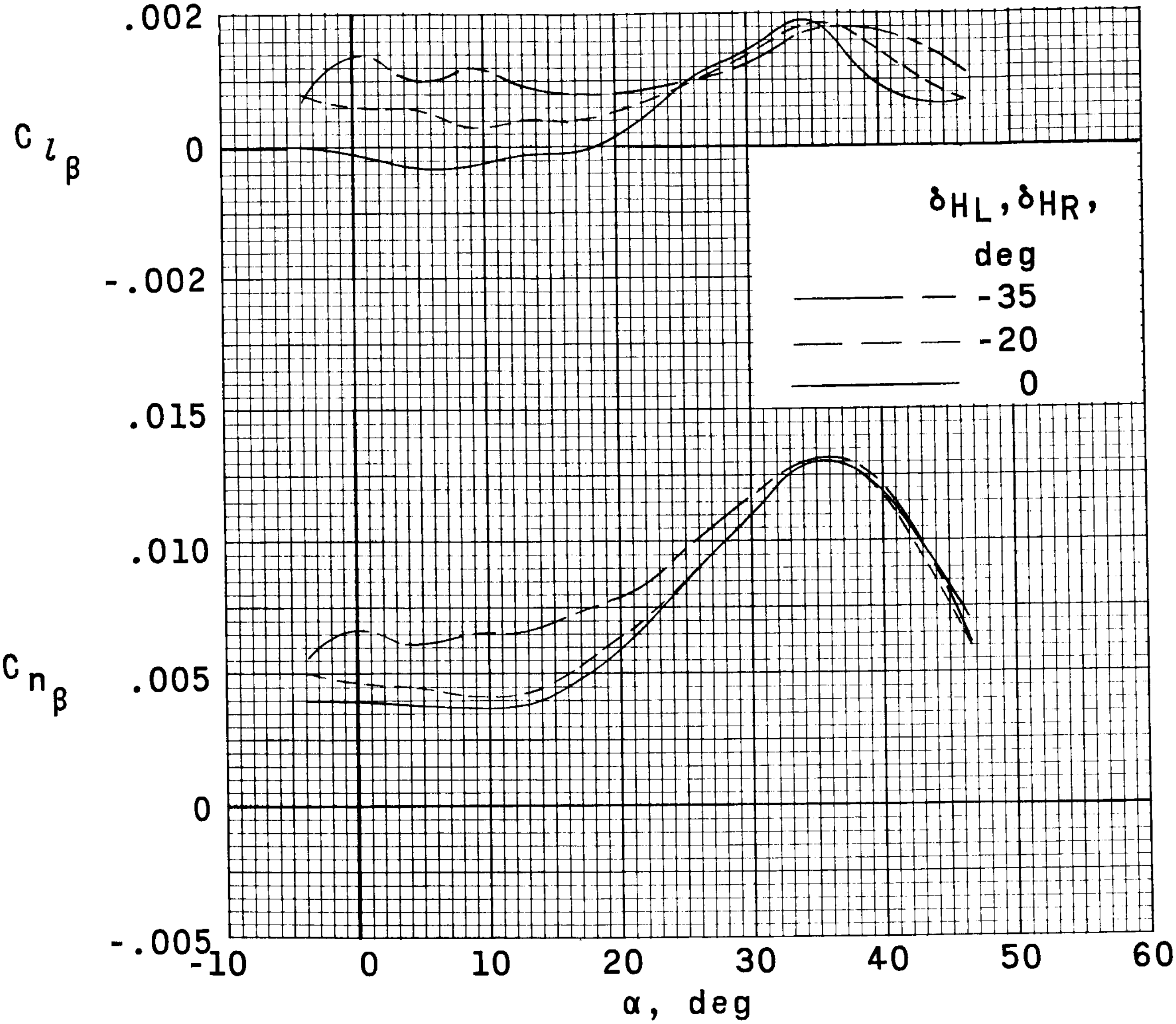

(c) M = 4.65.

Figure 33.- Concluded.

[redacted]

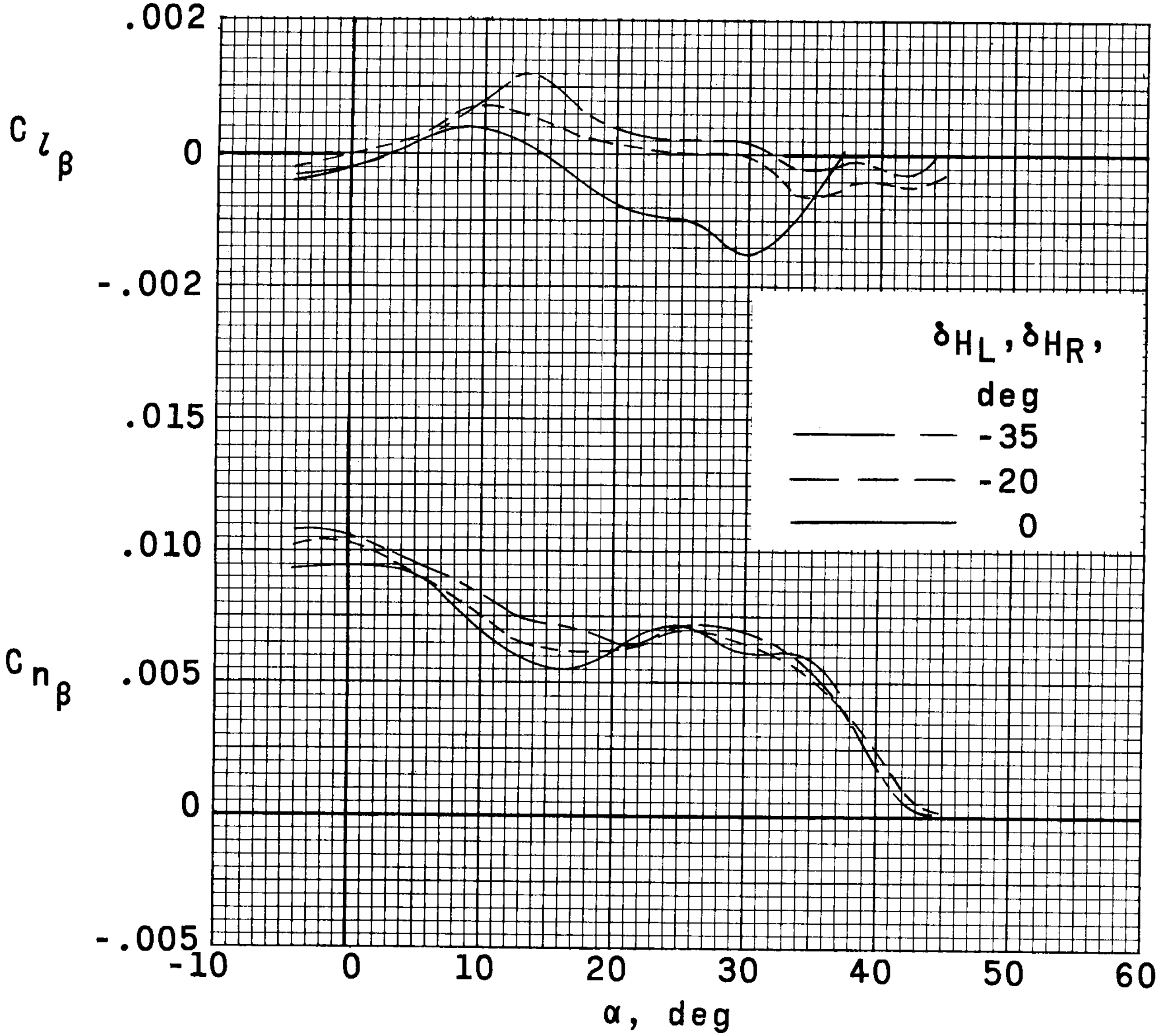

(a) M = 2.96.

Figure 34.- Effect of pitch-control deflections on lateral and directional stability characteristics with speed brakes deflected 35°.

[redacted]

[redacted]

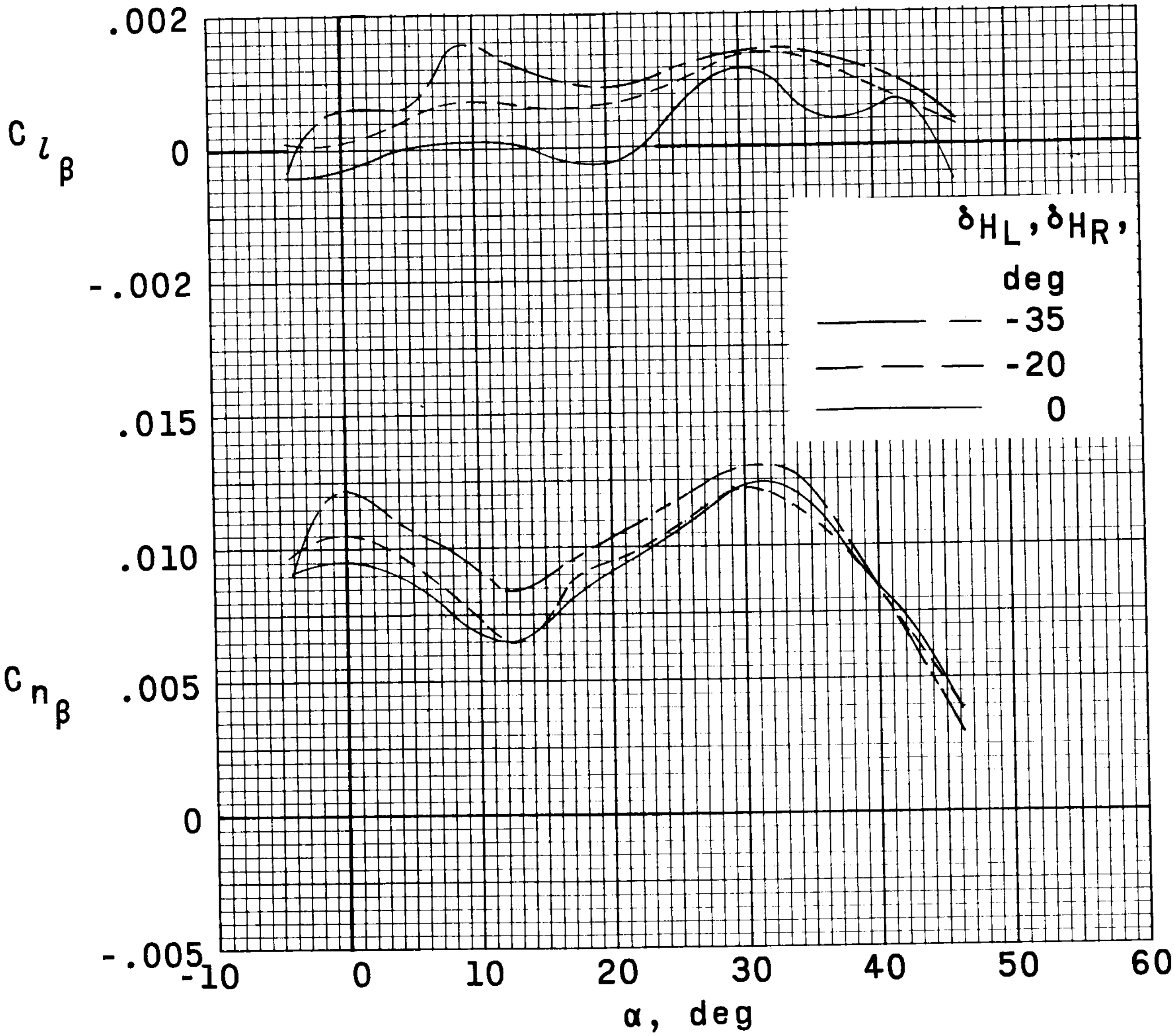

(b) M = 3.96.

Figure 34.- Continued.

[redacted]

D[redacted]IFIED

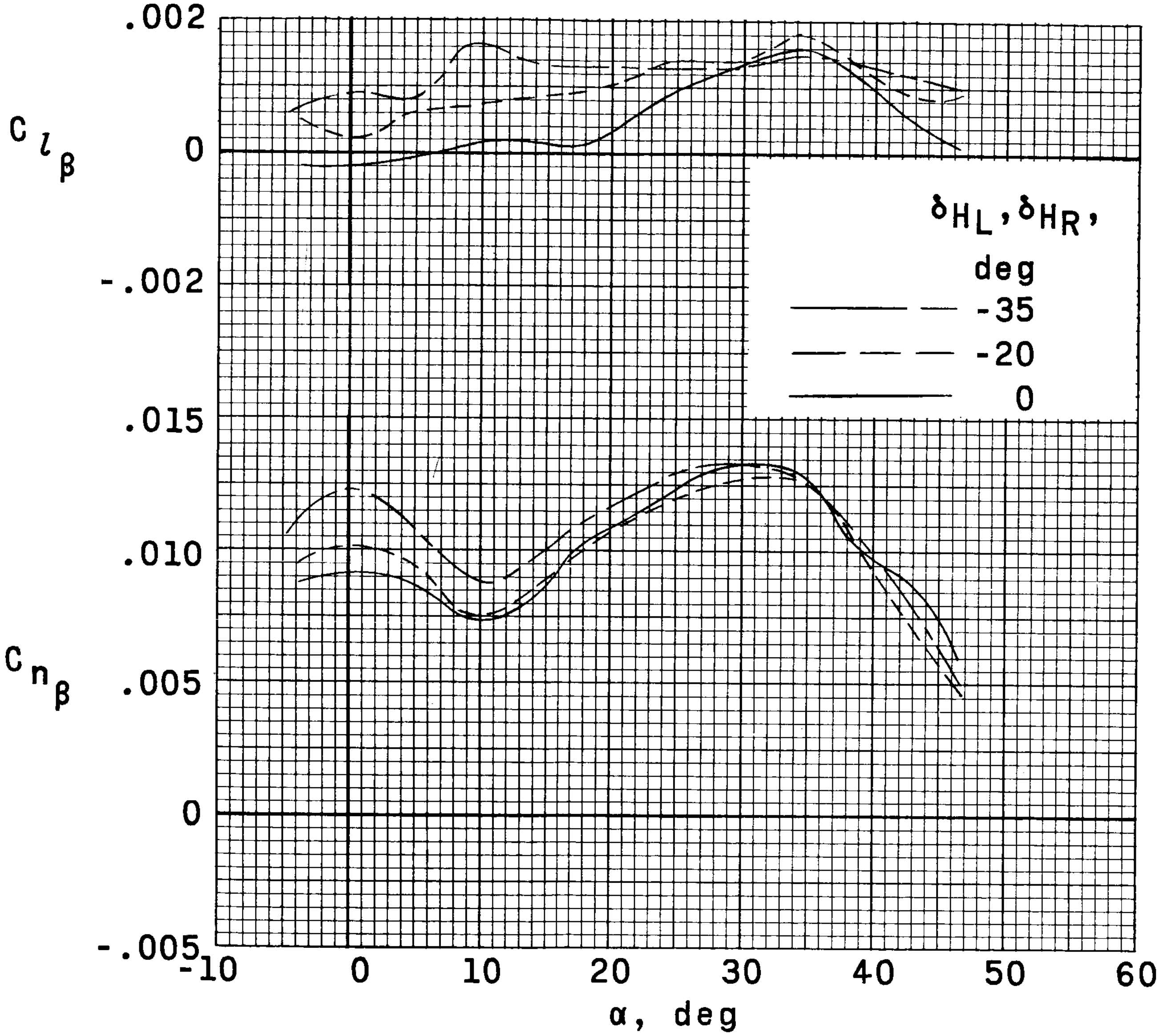

(c) M = 4.65.

Figure 34.- Concluded.